SEDIMENTOLOGICAL AND GEOCHEMICAL CHARACTERIZATION OF NEOPROTEROZOIC DEEP-MARINE LEVEE DEPOSITS

CELESTE CUNNINGHAM

Thesis submitted to the University of Ottawa
in partial Fulfillment of the requirements for the
PhD degree in Earth Sciences

Ottawa-Carleton Geoscience Centre
Faculty of Science
University of Ottawa

uOttawa

Abstract

Deep-marine levees are areally extensive features that border submarine channel systems. Compared to the adjacent channel, where episodes of erosion and bypass are commonplace, levees are mostly depositional features that experience little erosion, and therefore high preservation potential of individual beds, and presumably provide a nearly continuous depositional record of transport events down deep-marine slopes. Nevertheless, despite their size, volumetric prominence, and interpretive significance, deep-marine levees have received much less research attention compared to the adjacent channels. Accordingly, the spatial and temporal evolution of levee stratigraphy is much less well understood, in part because of the typically recessive nature of levee deposits exposed in outcrop in the ancient sedimentary record, and insufficient seismic resolution seismic in the modern. Also, although modern deep-marine levees have been shown to sequester a large proportion of the world's total buried organic carbon, few studies have attempted to assess carbon deposition and preservation in ancient deep-marine levee deposits.

In the Isaac Formation of the Windermere Supergroup (Neoproterozoic) of east-central British Columbia, Canada, well-exposed levee deposits display a systematic organization on several dimensional scales. Levee packages (decameter-scale) are interpreted to be due to cyclic changes in the granulometric makeup of sediment being supplied to the system, whereas bedsets (centimeter- to meter-scale) are interpreted to represent systematic and recurring pulses or surges during a single flow event. Furthermore, physical and geochemical characterization of levee strata at Castle Creek has shown that the unique depositional processes in levees can result in the concentration and enrichment of sedimentary marine organic matter (OM), which occurs mostly in banded, mud-rich sandstones deposited under oxic conditions. Organic carbon occurs

primarily as nano-scale coatings on clay particles and uncommon sand-sized organomineralic aggregates and discrete sand-sized amorphous grains. The distribution of this OM in levee strata is controlled by a combination of primary productivity, sea level, and rates of continental runoff and detrital terrigenous influx, which collectively are principally controlled by climate. Understanding the stacking patterns, geochemistry, and organic content of ancient levee deposits is important for assessing sedimentation patterns, depositional processes, event frequency and magnitude, paleoenvironmental conditions, and the evolution of ancient ocean and climate systems.

Résumé

Les levées de la mer profonde sont des éléments sédimentaires de grande superficie qui bordent les systèmes de chenaux sous-marins. Contrairement au chenal adjacent qui subit souvent de grands épisodes d'érosion et de contournement, les levées sont principalement les éléments dépositionnels qui ne subissent pas beaucoup d'érosion, et par conséquent ont une haute potentielle de préservation de lits individuels, et donc ils fournissent un record presque continu des événements de transport le long des pentes du marin profond. Néanmoins, malgré leur taille, importance volumétrique, et signifiance interprétative, les levées reçoivent beaucoup moins d'attention académique que les chenaux adjacents. Par conséquent, l'évolution spatiale et temporale de la stratigraphie des levées est beaucoup moins bien comprise, en partie à cause de la nature récessive des dépôts de levées dans le record sédimentaire ancien, et de l'insuffisance de la résolution sismique dans le record sédimentaire moderne. De plus, bien qu'il ait été démontré que les levées du marin profond moderne séquestrent une grande portion du carbone organique totale enfoui globalement, peu d'études ont tenté d'évaluer la déposition et préservation du carbone dans les anciens dépôts de levées du marin profond.

Dans la formation Isaac du supergroup Windermere (Néoprotérozoïque) à la Colombie-Britannique est-centrale, le Canada, des dépôts de levées bien-exposés présentent une organisation systématique dans plusieurs échelles dimensionnelles. Les paquets de levées (échelle de décamètres) sont interprétés d'être attribuées aux changements cycliques de la granulométrie du sédiment fourni au système, tandis que les ensembles de lits (échelle de centimètres à mètres) sont interprétés de représenter les impulsions systématiques et récurrentes pendant un seul événement de flux. De plus, la caractérisation physique et géochimique des strates de levées a montré que les processus de déposition uniques peuvent donner lieu à

l'enrichissement et à la concentration de la matière organique (OM) sédimentaire marins, qui se produit principalement dans les grès rubanés riches en boue, déposés dans les conditions oxiques. Le carbone organique se présente principalement dans la forme d'un revêtement à l'échelle nanométrique sur les particules d'argile, et rarement en forme d'agrégats organominéraux de taille de sable et de grains discrets amorphes de taille de sable. La distribution de cette OM dans les strates de levées est contrôlée par une combinaison de productivité primaire, le niveau de la mer, et les taux de ruissellement continental et d'afflux terrigène détritique, qui collectivement, sont contrôlés principalement par le climat. Une compréhension des motifs d'empilement, la géochimie, et le contenu organique des anciens dépôts de levées est important pour évaluer les processus dépositionels, la fréquence et magnitude d'événements, les conditions paléoenvironnementales, et l'évolution des anciens systèmes océaniques et climatiques.

Acknowledgments

This thesis would not have been possible without the support and collaboration of many people along the way. First, I would like to thank Dr. Bill Arnott for giving me the opportunity to work on an amazing project with an even more amazing group of people. Your passion and enthusiasm for geology is contagious and this project has been an incredible learning experience.

I would like to thank Dr. Justin Strauss, Dr. Clement Bataille, Dr. Don Cummings, and Dr. George Dix for taking the time to serve on my thesis committee.

To Patty Fraino, Simona Ruso, Mary Macquistan, and Jessie Kehew: I couldn't have done it without you. From our (mis)adventures in the field (special thanks to Mary for keeping me alive and in one piece) to our afternoon Tims runs to our many long discussions, y'all were an endless source of inspiration and fun.

To the rest of the Windy crew, past and present: Anika Bergen, Jag Ningthoujam, Omar Al-Mufti, Lilian Navarro, Liam Jasperse, Tyler Billington, Sean Ludzki, Nicole Miklovitch, Curran Wearmouth, and Genevieve Huyer, thank you for your friendship and insightful conversation.

Thank you to the McKirdy family and Matt Morison for your support in the field; with you handling logistics we were always happy, comfortable, and very well-fed.

I would like to thank Kerry Klassen, Paul Middlestead, Wendy Abdi, Patricia Wickham, and Erin Gomes-Reissmann in the Jan Veizer Laboratory, whose extensive knowledge and assistance in preparing and running my samples for geochemical analysis made this project possible, and to Glen Poirier for his help and training on the SEM. Thank you also to the support staff at uOttawa, especially Lisa Murphy, for always being there to answer my questions and help me out.

To my Western squad: Halima, Sarah, and Neera, I can't thank you enough for all the support and encouragement you've given me over the last few years.

Most importantly, to my family, especially my parents Monique and Mike, thank you for your unconditional love and support and for always encouraging me to pursue my passion.

Last but not least, I'd like to give a huge thanks to Shania Twain, whose music has kept me sane on this long journey. Let's go, girls.

Table of Contents

List of Figures

Chapter 1: Thesis Introduction

Chapter 2: Deep-marine Processes and Environments

List of Tables

Chapter 1: Thesis Introduction

1.1 Thesis Rationale

Deep-marine fan systems are unique geological environments that host the most significant accumulations of sediment on Earth. The main conduits for this sediment are channel-levee systems located on the continental slope. Channels can be up to hundreds of meters deep and several kilometers wide, and over time are commonly filled with sand-rich sediment. Bordering these channels are large, wedge-shaped levees that form from the overspill of sediment flows passing through the channel and in general tend to be finer grained than the adjacent channel deposits.

Understanding these systems and the flows that form them is an important task that can have many significant applications. The destructive nature of the flows, which principally are turbidity currents (Piper and Normark 2009), means that they pose a substantial risk to subsea infrastructure, such as the 400+ communication and internet cables currently in use, in addition to oil and gas pipelines (e.g., Carter et al. 2014). Knowing where, when, and how often these flows occur is therefore important for geohazard assessment and risk mitigation. These systems also host many high-quality hydrocarbon reservoirs, making them an important target for petroleum exploration (e.g., Clemenceau et al. 2000; Kendrick 2000; Leonard et al. 2000; Navarre et al. 2002; Sprague et al. 2002; Weimer and Slatt 2007). Turbidity currents also carry much more than just sediment, transporting substantial quantities of organic matter, nutrients, and pollutants (such as microplastics) into the deep sea. In fact, modern deep-marine levees have been shown to sequester a large proportion of the world's total buried organic carbon (Galy et al. 2007; Baudin et al. 2010) — a process that can significantly impact global carbon fluxes, and in

turn features like global climate and ocean chemistry. Because of this, studying the distribution and geochemistry of organic components in ancient channel-levee systems can help reconstruct environmental conditions in the Earth's past, and accordingly why much academic and economic attention has been focused on deep-marine channel-levee systems over the last few decades.

However, being located in the deep ocean, combined with their enormous spatial scale, has made studying these systems difficult, with the principal source of data being high-resolution seafloor imaging, seismic data, and widely-spaced drill-core. Although these methods have resulted in significant scientific advances, they cannot resolve small-scale sedimentological detail, which is essential to understanding depositional processes. Accordingly, investigation of ancient deep-marine systems exposed in outcrop is needed to examine small-scale sedimentology and internal strata attributes. However, although levees are generally thought to have near-continuous depositional records marked by high preservation potential of individual flow events (unlike the complex history of erosion, bypass, and deposition in channels), they have received much less research attention compared to the adjacent coeval channel fills, even in outcrop. Part of this disparity can be attributed to their generally fine-grained make-up, and as a consequence, generally poor exposure in outcrop.

Deep-marine slope and basin floor deposits of the Neoproterozoic Windermere Supergroup, however, are vertically dipping, glacially polished, and superbly well-exposed in a km-scale outcrop in the Cariboo Mountains of east-central British Columbia. This dissertation focuses on slope channel-levee complexes of the Isaac Formation in the Windermere turbidite system. In this outcrop, detailed sedimentological observations can be made at scales that range from millimetres to kilometres.

This thesis addresses several critical gaps in our knowledge of deep-marine levees by carefully documenting the sedimentological and geochemical attributes of ancient levee deposits in the Castle Creek study area. Doing so provides a more detailed understanding of the stratal make-up of levee deposits and the depositional processes that form them and elucidates what the geochemistry and organic carbon content of levee deposits can reveal about past climatic and oceanographic conditions, as well as the role they play in global carbon cycling.

1.2 Geological Background

1.2.1 Overview

The Windermere Supergroup (WSG) is an unconformity-bounded, 6-9 km-thick succession of Neoproterozoic (736 – 570 Ma) syn- and post-rift, mostly metasedimentary rocks (Figure 1.1). The deposition of the WSG is associated with the breakup of Rodinia and records the subsequent progradation of the Laurentian continental margin into the thermally subsiding proto-Pacific Ocean (Ross et al. 1995; Ross and Arnott 2007; Hadlari et al. 2021).

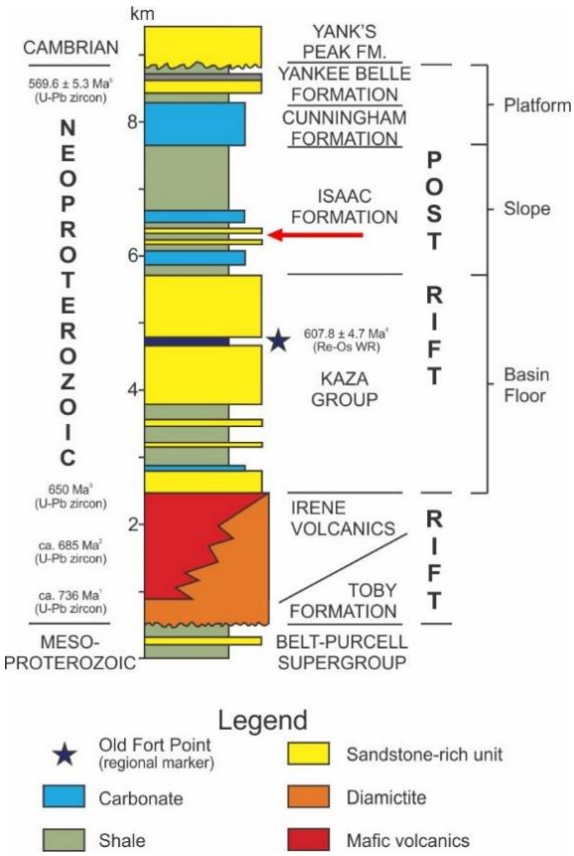

Figure 1.1. *Generalized stratigraphic log of the Windermere Supergroup in the southern Canadian Cordillera (modified from Ross et al. 1995). Geochronological dates are from [1]McDonough and Parrish (1991), [2]Lund et al. (2003), [3]Hadlari et al. (2021), [4]Kendall et al. (2004) and [5]Colpron et al. (2002). The stratigraphic position of strata described in this thesis is indicated by the red arrow.*

The WSG is exposed in an outcrop belt that stretches 4000 km from northwestern Mexico to the Alaska-Yukon border and is exceptionally well-exposed in the southern Canadian Cordillera, termed hereafter SCC (Figure 1.2) (Ross and Arnott 2007). Rocks of the WSG comprise siliciclastic continental, marginal-, and shallow-marine strata in Mexico and the southwestern United States, (Link et al. 1993), mixed siliciclastic and carbonate deep-marine strata in the SCC (Campbell et al. 1973; Ross et al. 1995; Ross and Arnott 2007), and carbonate-rich upper slope to shallow marine strata in the northern Canadian Cordillera.

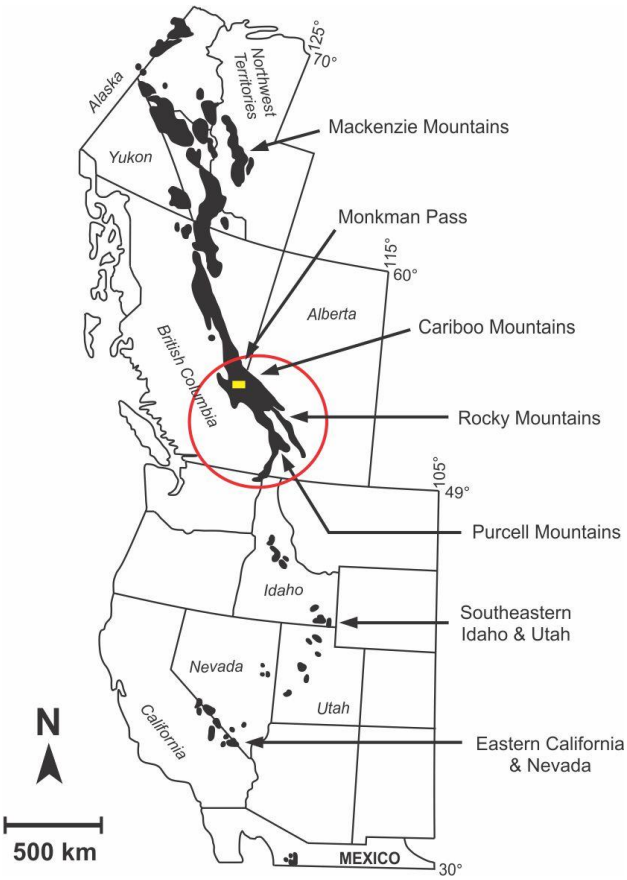

Figure 1.2. *Map showing the Windermere Supergroup outcrop belt in western North America (black polygon). The deep-water part is outlined by red circle, and the Castle Creek study site is shown with a yellow rectangle (after Ross 1991).*

1.2.2 Tectonic Setting and Metamorphism

The breakup of the supercontinent Rodinia occurred between ~780-580 Ma, with multiple phases of rifting (Li et al. 2013). Its disassembly resulted in the formation of an extensive passive continental margin system along the margins of the newly formed proto-Pacific Ocean and coincided with the onset of deposition of the WSG (Figure 1.3) (Ross 1991; Ross 1995). In the SCC initial sedimentation occurred during the early stages of rifting, depositing both glacial diamictites and volcanic rocks (see below). Deep-marine sedimentation occurred post-rift and was controlled by progressively diminishing rates of thermal subsidence (Ross 1991). Based on U/Pb dating of detrital zircons Hadlari et al. (2021) report a maximum

depositional age for the Windermere sedimentary pile of 650 Ma, thereby constraining the timing of continental separation.

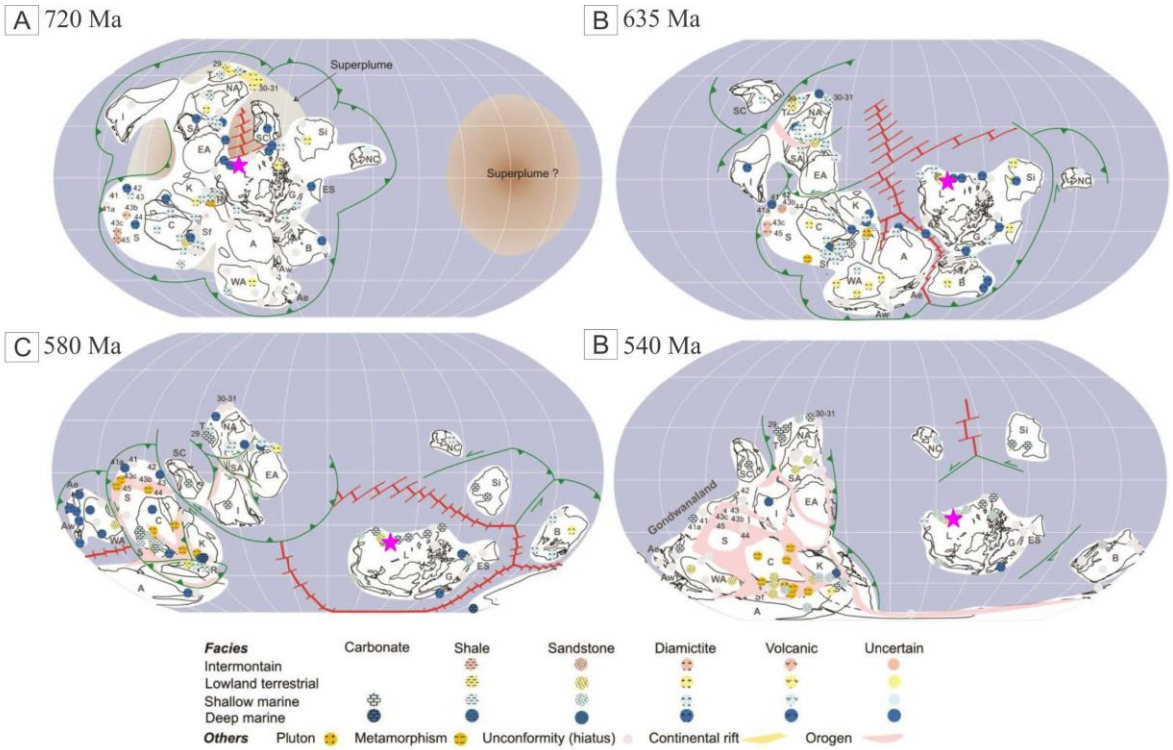

Figure 1.3. *Global paleogeographic reconstruction (modified from Li et al. 2013) showing the pattern of continent dispersal during the Neoproterozoic. (A) 720 Ma; ongoing breakup of the low-latitude Rodinia supercontinent. (B) 635 Ma; termination of the breakup of Rodinia and the onset of Marinoan glaciation. (C) 580 Ma; initiation of Gondwana and Gaskiers glaciation; (D) 540 Ma; formation of the Godwanaland supercontinent. Approximate location of the Windermere passive margin system is shown with a pink star.*

From the late Jurassic to the early Paleogene, collision and accretion of allochthonous terranes along the western coast of Laurentia formed the Canadian Cordillera (Price 2000). The orogen comprises five tectonic belts, which from west to east are Insular Belt, Coastal Belt, Intermontane Belt, Omineca Belt, and Fold and Thrust Belt (Figure 1.4). These belts have undergone a variety of deformational styles, including thrust and strike-slip faulting, and have significant tectonic discontinuities (Stewart 1972). In the SCC deep-marine rocks of the WSG are exposed over an area of 35,000 km^2, which if palinspastically restored, corresponds to an

area of at least 80,000 km^2, making it one of the largest turbidite systems in the ancient geological record (Figure 1.5) (Ross et al. 1995; Ross and Arnott 2007).

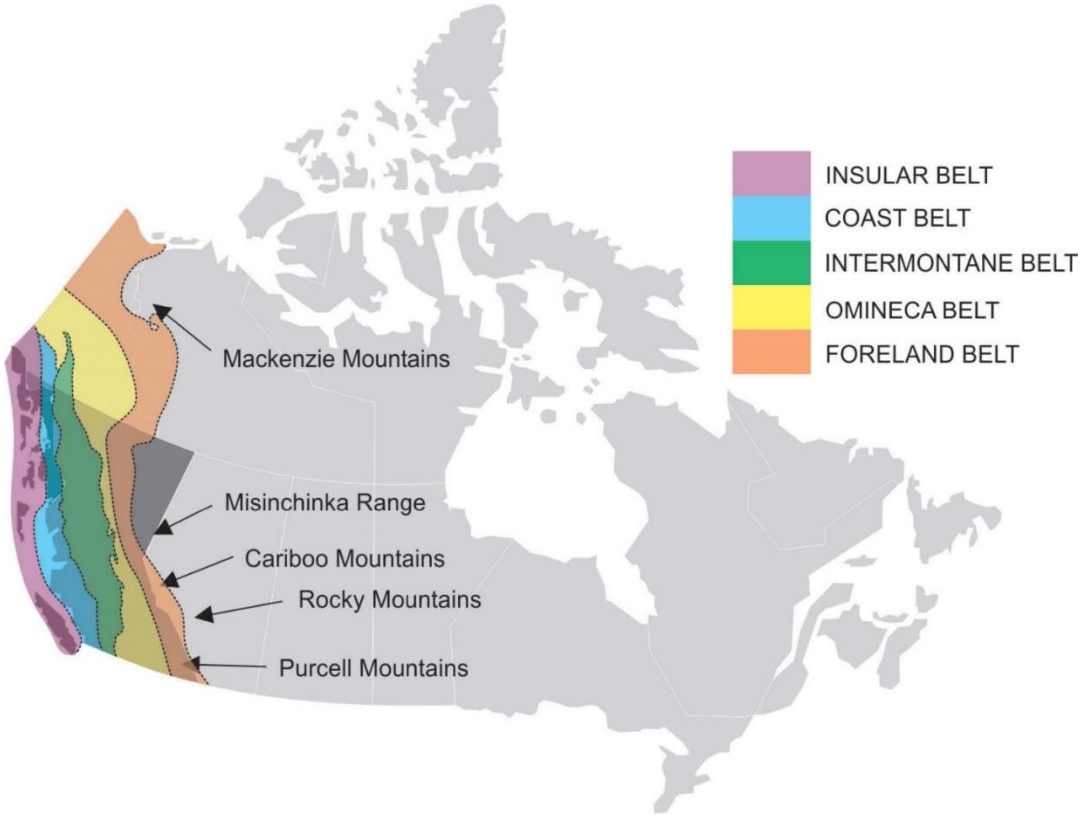

Figure 1.4. *Map of Canada showing the five tectonic belts that make up the Canadian Cordillera. The belts formed due to mountain building events related to collisional tectonism and accretion of allochthonous terranes along western Laurentia between 185-50 Ma, and from west to east are: the Insular Belt, the Coast Belt, the Intermontane Belt, the Omineca Belt and the Foreland Belt (modified from Davis 2011).*

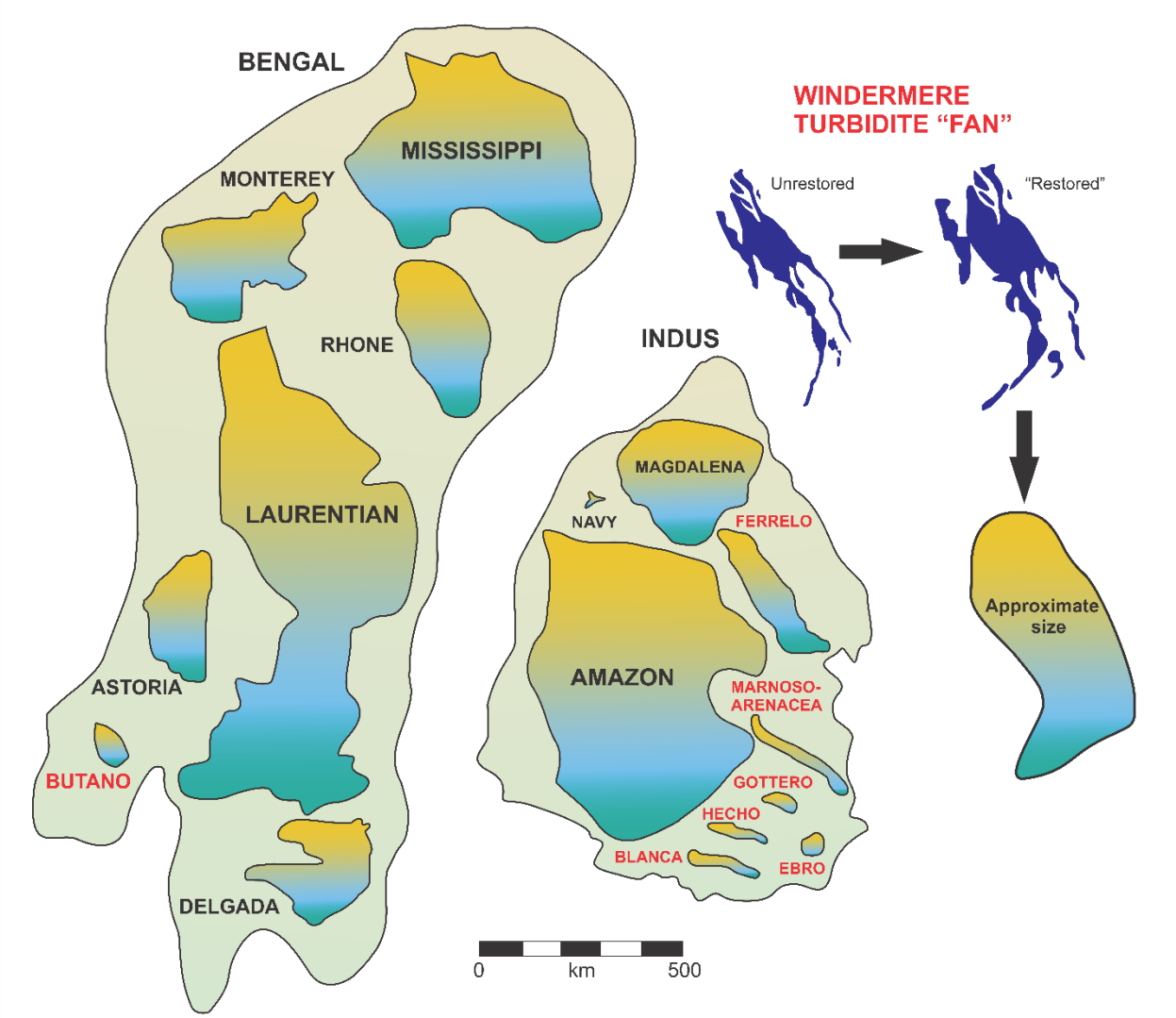

Figure 1.5. *Interpreted reconstruction of the Windermere turbidite system (Windermere turbidite "fan") in relation to other ancient (in red text) and modern (in black text) turbidite fan systems (redrawn from Ross 2000, modified from Barnes and Normark 1985).*

Strata in the Cariboo Mountains, which includes the Castle Creek study area, are part of the Omineca Belt and have undergone four phases of structural deformation (D1 – D4) and two phases of regional metamorphism (M1 and M2) (Murphy and Rees 1983; Murphy 1987a). Deformation and metamorphism are interpreted to be associated with collision and accretion of terranes along the western margin of North American from the Jurassic to the Tertiary (Murphy and Rees 1983; Murphy 1987a). The first phase of deformation (D1) produced northeast-verging

folds and bedding-parallel cleavage (Murphy 1987b), in addition to low-grade metamorphism (M1) that altered rocks to sub-greenschist facies (Murphy 1987b). This was followed by a second phase of deformation (D2) that produced km-scale southwest-verging folds and a prevalent axial planar crenulation cleavage (Murphy 1987a). A second episode of metamorphism (M2; up to greenschist facies) then overprinted earlier fabrics and structures (Murphy and Rees 1983). The third phase of deformation (D3) produced dextral strike-slip faults and refolded D1 and D2 structures to be northeast-verging. The final phase of deformation, D4, refolded previous deformation structures (D1 – D3) and formed meter- to decameter-scale, northeast-trending, steeply-inclined kink folds (Campbell et al. 1973; Ferguson 1994; Reid et al. 1997; Reid et al. 2002).

1.2.3 Regional Stratigraphy

In the southern Canadian Cordillera, rocks of the WGS unconformably overlie the Mesoproterozoic Belt-Purcell Supergroup (1.5 – 1.4 Ga) (Evans et al. 2000; Ross and Arnott 2007) and can be subdivided into syn-rift and overlying post-rift sequences (Figure 1.1, 1.6). The syn-rift succession is ~ 2.5 km thick and consists of glaciogenic diamictites, mudstones, sandstones, conglomerates, and limestones of the Toby Formation, intercalated with mafic volcanic rocks of the Irene Formation (Ross 1991; Ross et al. 1995). Diamictites of the Toby Formation are interpreted to have been deposited during the Sturtian (700-750) Ma glaciation (Aalto 1971; Ross et al. 1995), whereas mafic volcanics of the Irene Formation, which have been correlated to the 700-680 Ma Leola and Huckleberry volcanics in the northern Unites States (Lund et al. 2003; Keeley et al. 2013) and the 696-690 Ma Gataga volcanics in the northern Canadian Cordillera (Eyster et al. 2018), are interpreted to be associated with extensional

tectonism during the breakup of Rodinia and dated at 726-684 Ma (Ross et al. 1995; Lund et al. 2003; Ross and Arnott 2007).

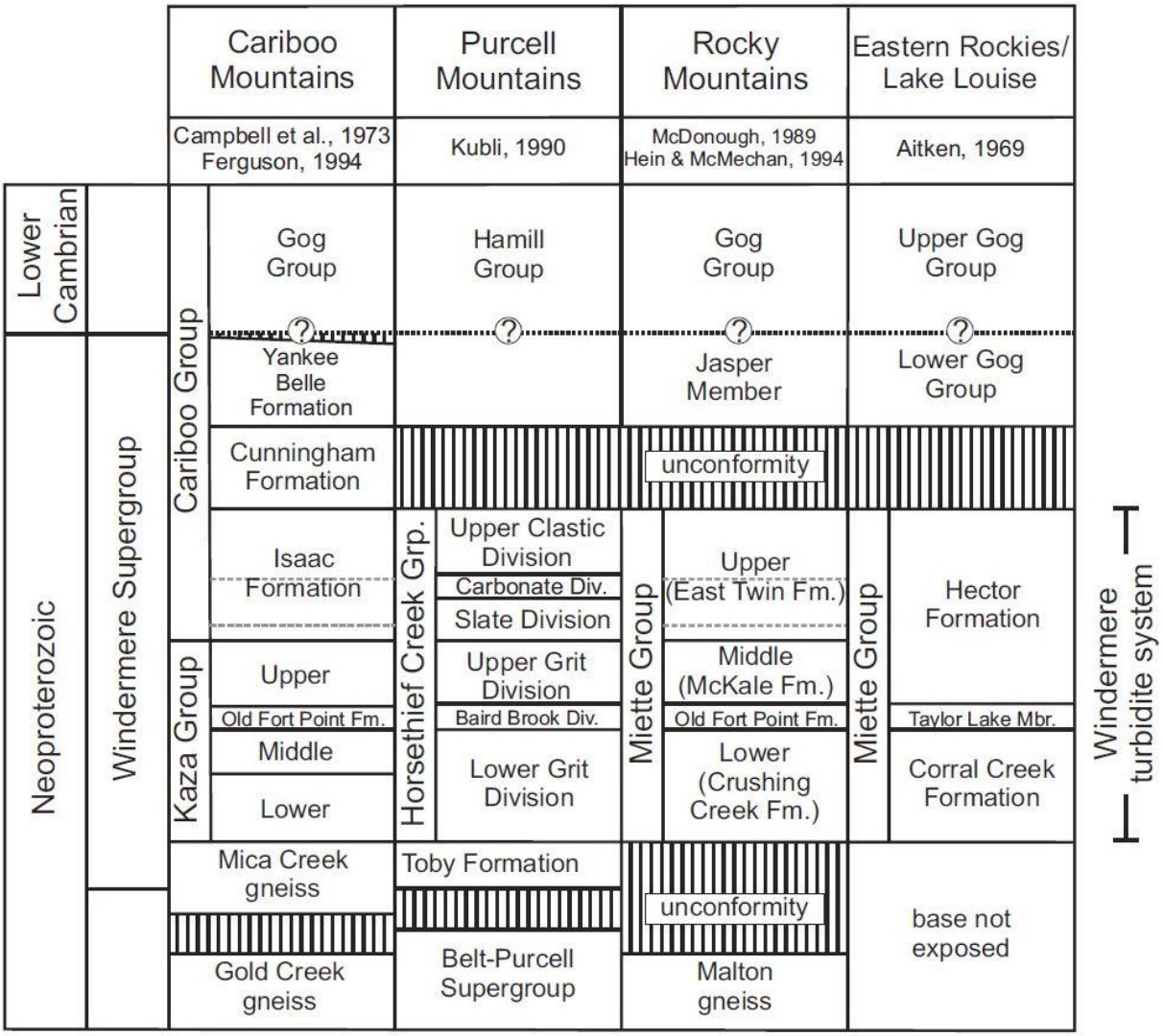

Figure 1.6*. Chart showing stratigraphic nomenclature of the Windermere Supergroup (WSG) throughout western Canada. Dashed lines in the Isaac Fm and Upper Twin Fm represent the first and second regional carbonate markers (Ross and Arnott 2007).*

Overlying these strata are marine sedimentary rocks of the post-rift sequence. This sequence consists of a 5-7 km-thick succession of sandstone, mudstone, conglomerate, and limestone. Deep-marine basin-floor deposits of the Kaza Group (termed the Lower Miette Group in the Rocky Mountains and Horsethief Creek Group in the Purcell Mountains) are conformably

overlain by slope, platform, and shelf deposits of the Cariboo Group (Ross 1995). The Kaza, which is ~ 3 km thick and dominated by sheet-like sandstones (Terlaky et al. 2016), is subdivided into the Lower, Middle, and Upper Kaza groups (Campbell et al. 1973). The overlying Cariboo Group is subdivided into three stratigraphic units: Isaac Formation (~ 2 km thick), consisting of mudstone-rich slope strata intercalated with laterally discontinuous, sandstone- and conglomerate-rich channel deposits; Cunningham Formation (up to 800 m thick), comprising carbonate platform oolitic intraclastic limestone; and the Yankee Belle Formation (~ 2 km thick), made-up of upper slope and shelf mixed siliciclastic-carbonate rocks (Gabrielse and Campbell 1991; Ross et al. 1995; Reid et al. 2002; Rowe 2003).

Unconformably overlying these WSG strata are Cambrian-age rocks of the Yank's Peak Formation. Much of the shallow-water strata in the southern Canadian Cordillera were removed by extensive regional erosion during post-depositional uplift. This erosion formed the sub-Cambrian unconformity that caps the WSG and is associated with a second phase of rifting at ~570 Ma that formed the economically important Western Canada Sedimentary Basin (Aitken 1969; Hadlari et al. 2021).

1.2.4 Geochronology

Due to a lack of datable markers and an absence of fossils, age control of the WSG in the southern Canadian Cordillera is generally poor. Although the dominantly siliciclastic rocks lack the material required for conventional radiometric dating, and exposed volcanic rocks lack sufficient datable zircons (Lund et al. 2003; Smith et al. 2011), maximum and minimum ages can be constrained by precise radiometric dates from below and above its bounding unconformities. A maximum depositional age of 728 ± 8 Ma was obtained from U-Pb zircon dates in granitic

rocks of the Deserters Range of northeastern British Columbia (Evenchick et al. 1984), which is supported by U-Pb zircon dates from crystalline basement rocks in the Monashee Mountains, dated at 740 ± 36 Ma (Parrish and Scammel 1988), and in the Malton Range, dated at 736 ± 23 Ma (McDonough and Parrish 1991).

At present a single rhenium-osmium isochron date of 607.8 ± 4.7 Ma from organic-rich mudrocks in the Old Fort Point Formation (OFP) dates deposition within the WSG (Kendall et al. 2004; Smith et al. 2014). However, zircons in volcanic rocks in Idaho and northern B.C., which are interpreted to be equivalent to rift-related rocks of the Irene Formation, yielded ages of ~ 685 Ma and 700-680 Ma, respectively (Lund et al. 2003; Keeley et al. 2013), and U-Pb dating of detrital zircons in continental slope deposits set a maximum depositional age for the WSG at 652 ± 9 Ma (Hadlari et al. 2021). Additionally, based on stable carbon isotope data, a 200-m-thick carbonate unit in the Isaac Formation, informally termed the first Isaac carbonate (FIC), has been correlated with deposition immediately preceding the Gaskiers glaciation at 580 Ma (Cochrane et al. 2019).

The minimum age of 570 ± 5 Ma for deposition the WSG is constrained by U-Pb zircon dates from syn-rift volcanics at the base of the overlying Hamill Group (Colpron et al. 2002). These constraints suggest that the Windermere turbidite system was active for a maximum of ~80-85 myr. and that the upper half of this succession (above the OFP) was deposited in ~ 40 myr.

1.2.5 Sediment Provenance

Studies of sediment provenance and paleocurrent of the WSG suggest that the deep-marine basin formed part of a longitudinal dispersal system that transported sediment from the east-southeast toward the northwest (Arnott and Hein 1986; Ross and Parrish 1991; Ross 2001; Ross and Arnott 2007). Uranium-lead dating on detrital zircons exhibits a distinctive bimodal distribution of 1950-1750 Ma (Paleoproterozoic) and > 2600 Ma (Archean) ages (Ross and Parrish 1991; Hadlari et al. 2021), suggesting that sediment was sourced from the southern Canadian Shield and eastern part of the Belt Basin in the northwestern United States. Paleocurrent data throughout the WSG also show general sediment transport toward the northwest, supporting the interpretation of an eastern to southeastern sediment source (Figure 1.7) (Arnott and Hein 1986; Ross and Arnott 2007).

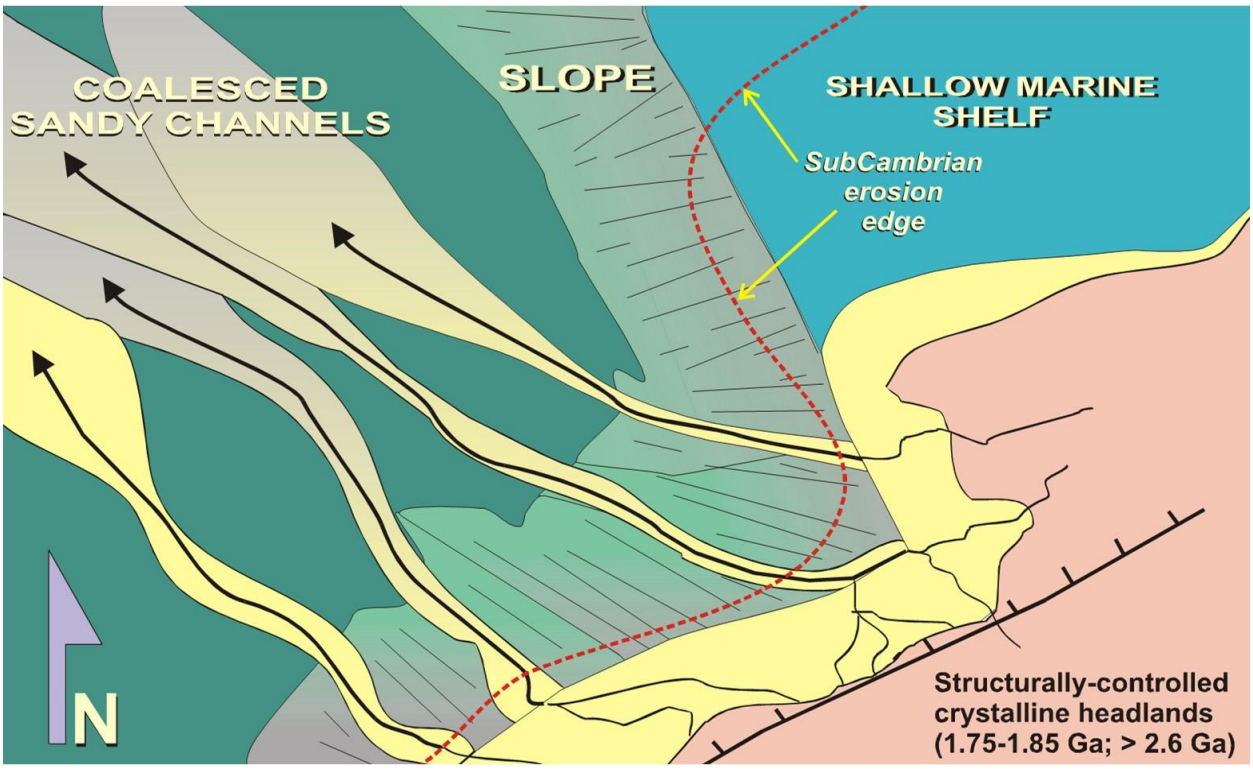

Figure 1.7. *Diagram illustrating the paleogeographic reconstruction of the Windermere turbidite system in the SCC. Paleoflow was from the southeast to the northwest (Ross, 2000).*

1.2.6 Regional Lithostratigraphic Markers

Because of the paucity of radiometric control and lack of biostratigraphy, regional correlation of the WSG in the SCC is based primarily on two distinctive, areally extensive lithostratigraphic markers: Old Fort Point Formation (OFP) and the first Isaac carbonate (FIC) (Ross et al. 1995; Ross and Arnott 2007).

The lowermost and most areally extensive is the lithologically and geochemically distinctive OFP that ranges from 60-450 m thick and comprises three members. The lowermost Temple Lake Member consists of fine-grained siliciclastic siltstone overlain by rhythmically bedded siltstone-limestone couplets and reflects sea level rise and transgression with increasing carbonate production on the shelf (Smith et al. 2014). The middle member is the Geikie Siding Member, comprising organic-rich siliciclastic mudstones that record sea level highstand and the shutdown of the carbonate platform. The intra-WSG date of 608 Ma (Kendall et al., 2004) is from the Geikie Siding Member. The Whitehorn Mountain Member forms the uppermost unit of the OFP and records a period of sea level lowstand, with deep scours from slope channel incision, followed by a period of sea level rise, with siliciclastic turbidites overlain by mixed siliciclastic-carbonate rocks as carbonate production on the shelf resumed (Smith et al. 2014). The Temple Lake and Geikie Siding members are interpreted to reflect rising sea level associated with a major deglacial event, whereas the sea level fall recorded in the Whitehorn Mountain Member has been attributed to rifting along the continental margin (Smith et al. 2011; Smith et al. 2014).

The FIC is up to 200 m thick and dominated by very thin- to thin-bedded calcareous turbidites interbedded with siliciclastic mud-dominated, thin-bedded turbidites. Cochrane et al.

(2019) conducted an inorganic carbon isotope analysis of the unit and showed that $\delta^{13}C_{carb}$ values rose from -5.2‰ at the base to 2-3‰ in the middle before decreasing again to -6.3‰ at the top. They interpreted this trend to correlate to the EN2 excursion in South China and a period of elevated sea level that flooded the continental shelf and promoted extensive carbonate platform production immediately before the Gaskiers glaciation at 580 Ma.

1.3 Castle Creek Study Site

The Castle Creek study area is located in the northern Cariboo Mountains of east-central British Columbia (Figure 1.8). At this location, a 2.5-km-thick succession of basin-floor to slope turbidite deposits is exposed for up to 8 km along strike (i.e., parallel to bedding). The lower 800 m of the succession makes up the Upper Kaza Group and consists predominantly of quasi-tabular, coarse-grained sandstone beds that comprise sand-rich distributary channel and terminal splay deposits intercalated with interlobe mudstones. Conformably overlying this is ~1.6 km of mudstone-dominated slope deposits of the Isaac Formation that are punctuated by several-decametre-thick, coarse-grained sandstone units interpreted to be slope channel-fill deposits.

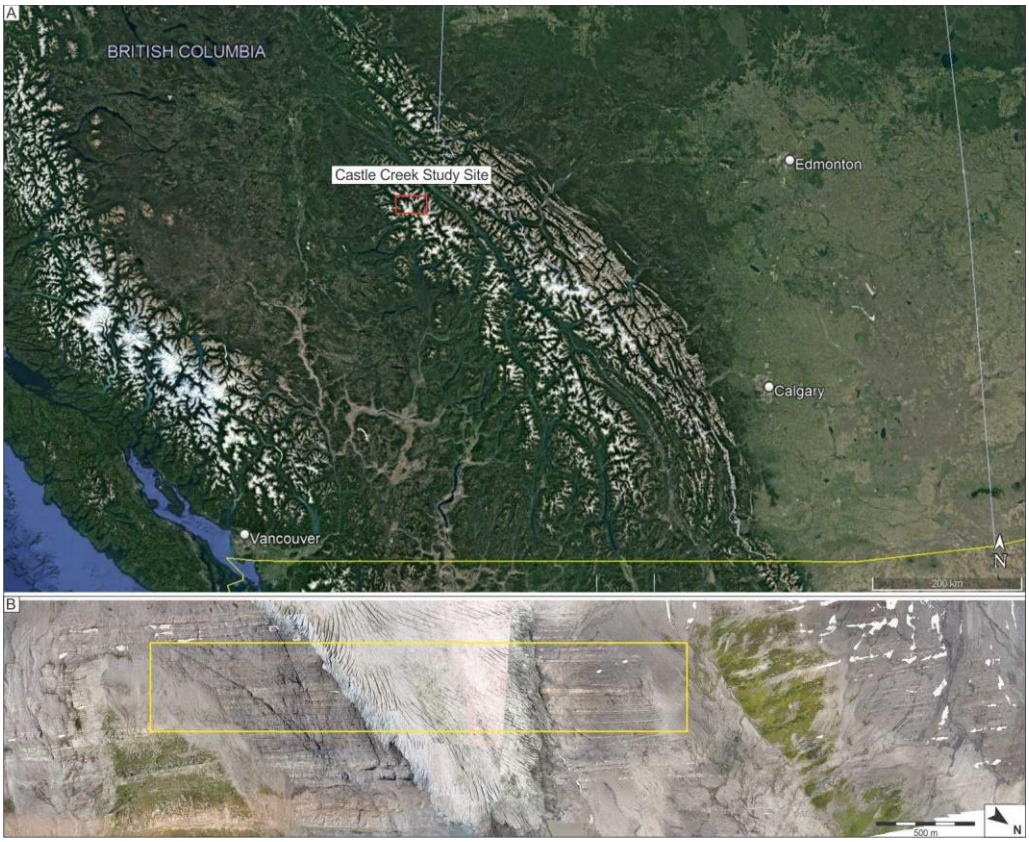

Figure 1.8. *A) Map of southern British Columbia with the Castle Creek study site indicated by a red box. B) Aerial photomosaic showing slope deposits of the Isaac Formation at Castle Creek. Levee deposits studied here are highlighted by a yellow box.*

Bedding at this site is near-vertical (~89°) due to its position on the steeply dipping limb of a southwest-verging anticline (Ross and Arnott 2007), and recent, rapid deglaciation has removed most surface debris and left the outcrop glacially polished and virtually vegetation free. This exposure allows for detailed field-based observation and measurement to be made from kilometre- down to millimetre-scale. Despite deformation and lower greenschist metamorphism, primary sedimentary structures and textures at Castle Creek are exceptionally well-preserved, with mm-scale features easily visible. However, detrital clay minerals, occurring principally in mudstones, have been recrystallized to metamorphic chlorite and muscovite, thereby obscuring their original composition (Terlaky 2014; Lee 2016).

1.4 Previous Studies

Regional mapping (1:250 000 scale) in the Castle Creek study area and surrounding region was first conducted by Campbell et al. (1973). This work also included detailed descriptions of the local stratigraphy, deformation, and metamorphism, as well as regional correlation of Proterozoic and Lower Paleozoic rocks. The area was later remapped at 1:50 000 scale by Ferguson and Ross (2003) and Ross and Ferguson (2003a, b) (Figure 1.9). The regional stratigraphy and structural geology have also been described in numerous other studies and reports (e.g., Murphy and Rees 1983; Murphy 1987a; Ross 1991; Gabrielse and Campbell 1991; Hein and McMechan 1994; Ross et al. 1995; Ross 2000; Reid et al. 2002; Reid 2003).

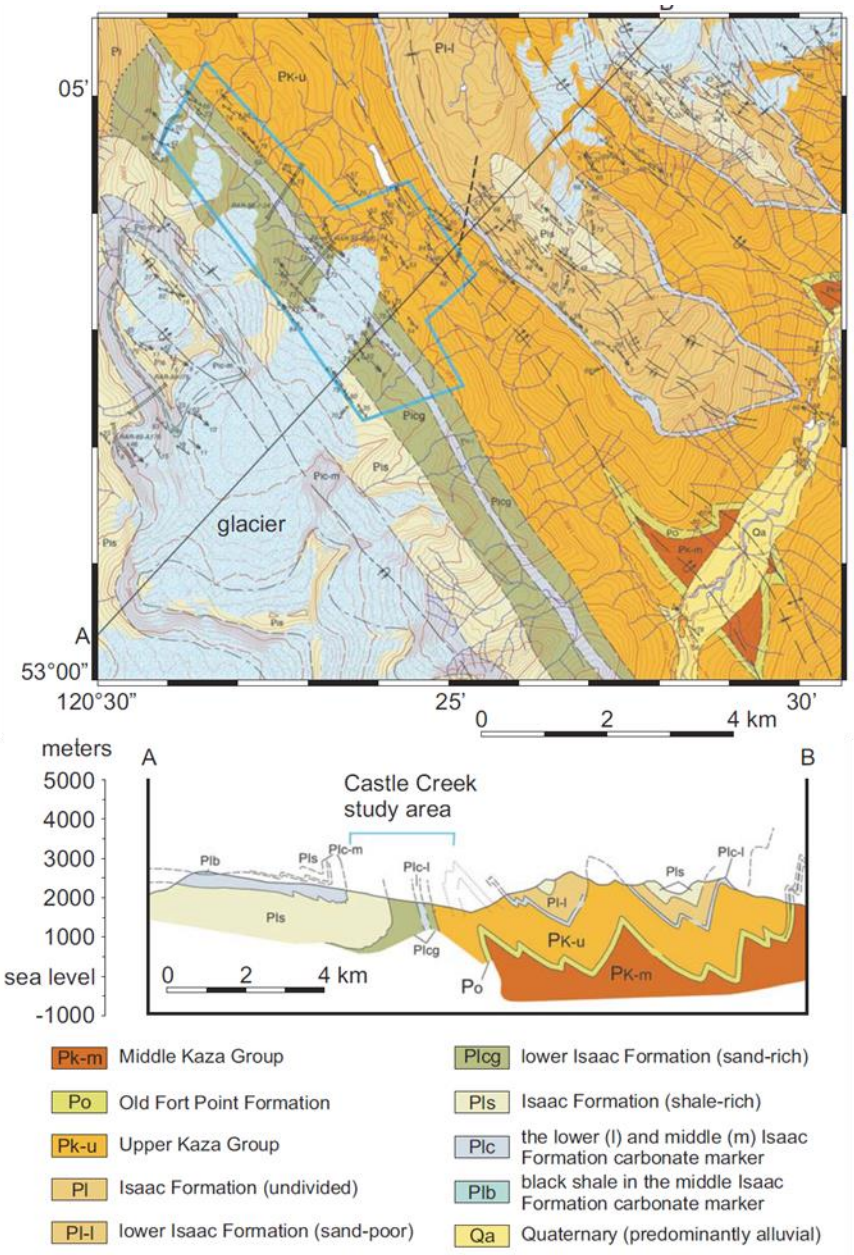

Figure 1.9. *Geology of the Castle Creek area (outlined in blue in the top diagram) and the surrounding region (Ross and Ferguson 2003a).*

More recently, detailed sedimentological, stratigraphic, architectural, and geochemical analyses of deep-marine strata at Castle Creek have been conducted by the Windermere Consortium, an industry-, government-, and academia-funded research initiative based at the University of Ottawa. Since its inception research in the consortium has focused on a wide range

of deep-marine depositional elements, such as basin-floor deposits (Meyer 2004; Meyer and Ross 2007; Rocheleau 2011; Terlaky 2014; Popović 2016; Terlaky et al. 2016), avulsion splay deposits (Angus 2016; Wearmouth 2018; Ningthoujam et al. 2022), slope channel deposits (Navarro et al. 2007; Arnott 2007; Gammon et al. 2007; O'Byrne et al. 2007; Schwarz and Arnott 2007a,b; Musa-Caleca 2008; Dumouchel 2015; Cochrane 2018; Cochrane et al. 2019; Fraino 2020; Arnott et al. 2021; Fraino et al. 2022), and mass-transport deposits (Laurin 2005; Arnott et al. 2011; Navarro and Arnott 2021). Although there have been several studies of levee complexes at Castle Creek (Khan and Arnott 2011; Khan et al. 2011; Khan 2012; Bergen 2017; Bergen et al. 2022), these have focused primarily on large-scale stratal architecture. This thesis expands on this work and provides an in-depth examination of smaller-scale sedimentological characteristics and processes, as well as an evaluation of geochemical attributes and trends.

1.5 Thesis Structure

This Ph.D. thesis is divided into seven chapters and presents a collection of four scientific articles. Two are published in peer-reviewed scientific journals, one is in the peer-review process, and one is in preparation for submission.

Chapter 1 is an introduction to the thesis and provides an overview of the thesis rationale and objectives, as well as a short review of previous work conducted at the study site.

Chapter 2 reviews deep-marine geological environments, processes, and deposits, with emphasis on those that are a focus of the thesis, in order to provide background and context for the thesis.

Chapter 3 focuses on the physical sedimentology and stratigraphic stacking patterns of deep-marine levee deposits. Detailed outcrop observation and description were used to model sedimentation patterns and depositional processes, thereby improving our understanding of deposition associated with single and successive flow events and culminating in a new depositional model that re-evaluates some of the fundamental assumptions regarding deep-marine sedimentology. This work is published in The Journal of Sedimentary Research:

Cunningham, C.M., and Arnott, R.W.C. (2021). Systematic organization of thin-bedded turbidites in ancient deep-marine levees: Possible evidence of rhythmic pulsing in turbidity currents: *Journal of Sedimentary Research*, v 91.11, p. 1257-1274.

Chapter 4 focuses on the physical and chemical characterization of organic carbon in ancient levee deposits. Outcrop description, optical and scanning electron microscopy, total organic carbon, and stable carbon isotope analyses were conducted to examine and interpret how organic matter is preserved and the effect of organic matter on the deposition and diagenesis of these ancient sediments. This work has been conditionally accepted in Sedimentology:

Cunningham, C.M., and Arnott, R.W.C. (accepted). Organic matter deposition and preservation in ancient deep-sea levee sediments: Implications for global trends in carbon burial: *Sedimentology*.

Chapter 5 focuses on the stratigraphic distribution of this organic matter throughout multiple levee successions at Castle Creek, and the factors that control this distribution. Outcrop observation is combined with X-Ray fluorescence (XRF) and total organic carbon analyses of samples taken every 5 – 10 m throughout the succession. Various proxies, based on XRF data, are used to reconstruct trends in primary productivity, ocean redox conditions, climate, and sea level, and the effect of each of these factors on organic carbon enrichment are outlined and

discussed. This is an expanded version of a manuscript in preparation for submission to *Marine and Petroleum Geology*

Cunningham, C.M., Ruso, S., and Arnott, R.W.C. (submitted). Controls on the stratigraphic distribution of organic carbon in ancient deep-marine levees: *Marine and Petroleum Geology*.

Chapter 6 focuses on the stratigraphic architecture of proximal levee deposits and its relationship to the density profiles of channelized flows, based on extensive outcrop measurement and description. This is an expanded version of a paper published in *The Journal of Sedimentary Research*:

Bergen, A.L., Cunningham, C.M., Terlaky, V., and Arnott, R.W.C. (2022). Influence of channelized-flow density structure on the stratal architecture of deep-marine levee deposits: *Journal of Sedimentary Research*, v. 92.4, p. 381-403.

Chapter 7 is a summary of the main findings of the research presented and combines the principal conclusions into a succinct depositional model. This chapter finishes with a discussion of areas for future research.

1.6 Contribution of Co-authors

Chapters 3 and 4 are based on fieldwork carried out by the author, with assistance in the field from Mary Macquistan, Jessie Kehew, Nicole Miklovitch, and Sean Ludzki. All data processing, analysis, and figure production was performed by the author, unless original figure sources are cited. The initial manuscript was written by the author and later revised through discussion with Dr. Bill Arnott (supervisor).

Chapter 5 is based on fieldwork carried out by the author, with assistance in the field from Mary Macquistan. XRF samples were processed by Simona Ruso, an M.Sc. student in the

research group, who also modelled tectonic setting, provenance, and continental supply proxies. All other field, petrographic, and geochemical analyses (including primary productivity and redox proxies, as well as total organic carbon) were performed by the author. Data discussion and interpretation was led by the author. The initial manuscript, as well as the figures, were written and produced by the author and later revised through discussion with Dr. Arnott and S. Ruso.

Chapter 6 is based on fieldwork carried out by Anika Bergen, Viktor Terlaky, and the author over multiple field seasons. Much of the data was collected and analyzed by A. Bergen for her M.Sc. dissertation, and as such she is first author on the resulting publication. Additional data collection, analysis and interpretation, figure production, and writing, as well as journal correspondence, was carried out by the author. V. Terlaky conducted outcrop measurement and analysis of the associated channel deposits. The manuscript was written and produced by A. Bergen and the author and later revised through discussion with Dr. Arnott.

1.7 References

AALTO, K. R., 1971, Glacial marine sedimentation and stratigraphy of the Toby conglomerate (upper Proterozoic), southeastern British Columbia, northwestern Idaho and northeastern Washington: Canadian Journal of Earth Sciences, v. 8, p. 753–787.

AITKEN, J. D., 1969, Documentation of the sub-Cambrian unconformity, Rocky Mountain Main Ranges, Alberta: Canadian Journal of Earth Sciences, v. 6, p. 193-200.

ANGUS, K., 2016, Lateral Facies Trends in Deep-Marine Slope and Basin Floor Matrix-Rich Beds, Neoproterozoic Windermere Supergroup, British Columbia, Canada. M.Sc. thesis, Université d'Ottawa/University of Ottawa, 167 p.

ARNOTT, R.W.C., 2007, Stratal architecture and origin of lateral accretion deposits (LADs) and conterminuous inner-bank levee deposits in a base-of-slope sinuous channel, lower Isaac Formation (Neoproterozoic), East-Central British Columbia, Canada: Marine and Petroleum Geology, v. 24, p. 515-528.

ARNOTT, R.W. AND HEIN, F.J., 1986, Submarine canyon fills of the Hector Formation, Lake Louise, Alberta: Late Precambrian syn-rift deposits of the proto-Pacific miogeocline: Bulletin of Canadian Petroleum Geology, v. 34, p. 395-407.

ARNOTT, R.W.C., WALLACE, K., AND LAURIN, J., 2011, Stratal architecture and temporal evolution of a passive margin mass-transport deposit, Neoproterozoic Isaac Formation, Cariboo Mountains, British Columbia, Canada. *In*: Mass-Transport Deposits in Deepwater Settings (Eds. R.C. Shipp, P. Weimer and H.W. Posamentier), SEPM Special Publications, v. 96, 532 pp. doi:10.2110/sepmsp.096.221

ARNOTT, R. W. C., TILSTON, M., FRAINO, P., NAVARRO, L., DUMOUCHEL, G., AND MIKLOVICH, N., 2021, Laterally accreting sinuous channels and their deposits: The Goldilocks of deep-water slope systems: Journal of Sedimentary Research, v. 91(5), p. 451-463.

BAUDIN, F., DISNAR, J.R., MARTINEZ, P., AND DENNIELOU, B., 2010, Distribution of the organic matter in the channel-levees systems of the Congo mud-rich deep-sea fan (West Africa): Implication for deep offshore petroleum source rocks and global carbon cycle: Marine Petroleum Geology, v. 27, p. 995-1010.

BARNES, N. E., AND W. R. NORMARK, 1985, Diagnostic parameters for comparing modern submarine fans and ancient turbidite systems. *In*: A. H. Bouma, W. R. Normark, and N. E. Barnes, eds., Submarine fans and related turbidite systems: New York, Springer-Verlag, p. 13–14 and back-pocket wall chart.

BERGEN, A.L., 2017, Vertical and lateral facies architecture of levees and their genetically-related channels, Isaac Formation, Neoproterozoic Windermere Supergroup, Cariboo Mountains, B.C. Unpublished M.Sc. thesis, Université d'Ottawa/University of Ottawa, 193 p.

BERGEN, A.L., CUNNINGHAM, C.M., TERLAKY, V., AND ARNOTT, R.W.C., 2022, Influence of channelized-flow density structure on the stratal architecture of deep-marine levee deposits: Journal of Sedimentary Research, v. 92.4, p. 381-403.

CAMPBELL, R. B., E. W. MOUNTJOY, AND F. G. YOUNG, 1973, Geology of McBride map-area, British Columbia: Geological Survey of Canada, Paper 72–35, 104 p.

CARTER, L., R. GAVEY, P.J. TALLING, AND J.T. LIU., 2014, Insights into submarine geohazards from breaks in subsea telecommunication cables: Oceanography, v. 27(2), p. 58–67.

CLEMENCEAU, G. R., J. COLBERT, AND D. EDENS, 2000, Production results from levee-overbank turbidite sands at Ram/Powell Field, deepwater Gulf of Mexico. *In*: P. Weimer, R. M. Slatt, J. Coleman, N. C. Rosen, H. Nelson, A. H. Bouma, M. J. Styzen, and D. T. Lawrence, eds., Deep-water reservoirs of the world: Gulf Coast Section, SEPM 20th Annual Research Conference, p. 241–251.

COCHRANE, D., 2018, Stratigraphic and Carbon Isotope Evolution of an Ediacaran Mixed Siliciclastic Deep-Marine Base-of-Slope System, First Isaac Carbonate, Windermere Supergroup, Canadian Cordillera, British Columbia. Unpublished M. Sc. thesis. University of Ottawa, Ottawa, ON.

COCHRANE, D. J., NAVARRO, L., AND ARNOTT, R. W. C., 2019, Sedimentological and geochemical evolution of an Ediacaran mixed carbonate-siliciclastic continental slope system, Windermere Supergroup, southern Canadian Cordillera, British Columbia, Canada: Precambrian Research, v. 327, p. 47-67.

COLPRON, M., J. M. LOGAN, AND J. K. MORTENSEN, 2002, U-Pb zircon age constraint for late Neoproterozoic rifting and initiation of the lower Paleozoic passive margin of western Laurentia: Canadian Journal of Earth Sciences, v. 39, p. 133–143.

DAVIS, L., 2011, Architecture of deep-marine interchannel deposits: Isaac Formation, Windermere Supergroup (Neoproterozoic), southern Canadian Cordillera. Unpublished M.Sc. thesis, University of Ottawa, Ottawa, 174 p.

DUMOUCHEL, I.G., 2015, Stratigraphic Architecture and Depositional History of Laterally-Accreted Channel Fills in the Lower Isaac Formation, Windermere Supergroup, British Columbia, Canada. Unpublished M.Sc. thesis, University of Ottawa, Ottawa, ON.

EVANS, K.V., ALEINIKOFF, J.N., OBRADOVICH, J.D., AND FANNING, C.M., 2000, SHRIMP U-Pb geochronology of volcanic rocks, Belt Supergroup, western Montana: evidence for rapid deposition of sedimentary strata: Canadian Journal of Earth Sciences, v. 37, p. 1287-1300.

EVENCHICK, C. A., PARRISH, R. R., AND GABRIELSE, H., 1984, Precambrian gneiss and late Proterozoic sedimentation in north-central British Columbia: Geology, v. 12, p. 233–237.

EYSTER, A., FERRI, F., SCHMITZ, M.D., AND MACDONALD, F.A., 2018, One diamictite and two rifts: Stratigraphy and geochronology of the Gataga Mountain of northern British Columbia: American Journal of Science, v. 318, p. 167-207.

FERGUSON, C.A., 1994, Structural geology and stratigraphy of the northern Cariboo Mountains between Isaac Lake and Fraser River, British Columbia: Map, University of Calgary, Calgary, AB,. (1997-047810) 157.

FERGUSON, C. A., AND ROSS, G. M., 2003, Geology and structure cross-sections, McBride, British Columbia: Geological Survey of Canada, "A" Series Map, 2004A, scale 1:50,000, 1 sheet.

FRAINO, P.E., 2020, Spatial and Temporal Stratal Evolution of an Ancient Deep-Marine Channel-Levee Complex, Neoproterozoic Isaac Formation, Windermere Supergroup, British Columbia, Canada. Unpublished M.Sc. thesis, University of Ottawa, 211 p.

Fraino, P.E., ARNOTT, R.W.C. AND NAVARRO, L. (2022) The influence of sediment supply on the stratigraphic evolution of an ancient passive margin deep-marine slope channel system, Windermere Supergroup, British Columbia, Canada: Journal of Sedimentary Research, v. 92, p. 232-256.

GABRIELSE, H., AND R. B. CAMPBELL, 1991, Upper Proterozoic assemblages, *in* H. Gabrielse, and C. J. Yorath, eds., Geology of the Cordilleran orogen in Canada: Geological Society of America, Geology of North America, v. G-2, p. 125–150.

GALY, V., FRANCE-LANORD, C., BEYSSAC, O., FAURE, P., KUDRASS, H., AND PALHOL, F., 2007, Efficient organic carbon burial in the Bengal fan sustained by the Himalayan erosional system: Nature, v. 450, p. 407-410. https://doi.org/10.1038/nature06273

GAMMON, P. R., R. W. C. ARNOTT, AND G. M. ROSS, 2007, Architectural relationship between channels, levees, and debris flows: Isaac Channel 6, Castle Creek South, lower Isaac Formation, Windermere Supergroup, British Columbia, Canada. *In:* T. H. Nilsen, R. D. Shew, G. S. Steffens, and J. R. J. Studlik, eds., Atlas of deep-water outcrops AAPG Studies in Geology 56, p. 102–105.

HADLARI, T., ARNOTT, R. W. C., MATTHEWS, W. A., POULTON, T. P., ROOT, K., MADRONICH, L. I. AND SIMMS, A. R., 2021, Provenance of the Incipient Passive Margin of NW Laurentia (Neoproterozoic): Detrital Zircon from Continental Slope and Basin Floor Deposits of the Windermere Supergroup, Southern Canadian Cordillera: Lithosphere, 10 pp. doi:10.2113/2021/8356327.

HEIN, F. J., AND M. E. MCMECHAN, 1994, Proterozoic-Lower Cambrian strata of the Western Canada Sedimentary Basin. *In:* G. D. Mossop, and I. Shestsen, eds., Geological atlas of the western Canada sedimentary basin: Calgary, Canadian Society of Petroleum Geologists and Alberta Geological Survey, p. 57–68.

KEELEY, J. A., LINK, P. K., FANNING, C. M., AND SCHMITZ, M. D., 2013, Pre-to synglacial rift-related volcanism in the Neoproterozoic (Cryogenian) Pocatello Formation, SE Idaho: New SHRIMP and CA-ID-TIMS constraints: Lithosphere, v. 5(1), p. 128-150.

KENDALL, B. S., R. A. CREASAR, G. M. ROSS, AND D. S. SELBY, 2004, Constraints on the timing of Marinoan "Snowball Earth" glaciation by 187Re–187Os dating of a Neoproterozoic, post-glacial black shale in western Canada: Earth and Planetary Science Letters, v. 222, p. 729–740.

KENDRICK, J. W., 2000, Turbidite reservoir architecture in the northern Gulf of Mexico deepwater: insights from the development of Auger, Tahoe, and Ram/Powell Fields. *In:* P. Weimer, R. M. Slatt, J. Coleman, N. C. Rosen, H. Nelson, A. H. Bouma, M. J. Styzen, and D. T. Lawrence, eds., Deep-water Reservoirs of the world: Gulf Coast Section, SEPM 20th Annual Research Conference, p. 450–468.

KHAN, Z. A., AND R. W. C. ARNOTT, 2011, Stratal attributes and evolution of asymmetric inner and outer-bend levee deposits associated with an ancient deep-water channel-levee complex within the Isaac Formation, southern Canada: Marine and Petroleum Geology, v. 28, p. 824–842.

KHAN, Z. A., R. W. C. ARNOTT, AND A. PUGIN, 2011, An alternative model of producing topography in the crest region of deep-water levees: AAPG Bulletin, v. 95, p. 2085–2106.

LAURIN, J., 2005, Depositional history and sequence stratigraphic context of a Neoproterozoic mass transport deposit, Isaac Formation, east-central B.C.. Unpublished B.Sc. thesis, University of Ottawa, Ottawa, ON.

LEE, S.L., 2016, Microstructural and external characterization of a low-grade metaturbidite succession in the Windermere Supergroup, British Columbia, Canada. Unpublished B.Sc. thesis, University of Ottawa, Ottawa, ON.

LEONARD, A., JOLLEY, E., CARTER, A., MILLS, C., JONES, N., AND BOWMAN, M., 2000, Lessons learned from the Management of basin floor submarine fan reservoirs in the UKCS. *In:* P. Weimer, R. M. Slatt, J. L. Coleman, N. Rosen, C. H. Nelson, A. H. Bouma, M. Styzen, and D. T. Lawrence, eds., Global deepwater reservoirs: Gulf Coast Section SEPM Foundation 20th Annual Research Conference, p. 478–501.

LI, Z.X., EVANS, D.A.D., AND HALVERSON, G.P., 2013, Neoproterozoic glaciations in a revised global palaeogeography from the breakup of Rodinia to the assembly of Gondwanaland: Sedimentary Geology, v. 294, p. 219-232.

LINK, P. K., 1993, Middle and late Proterozoic stratified rocks of the western U.S. Cordillera, Colorado Plateau, and Basin and Range Province. *In:* J. C. Reed, Jr., M. E. Bickford, R. S. Houston, P. K. Link, D. W. Rankin, P. K. Sims, and W. R. Van Schmus, eds., Precambrian: Conterminous U. S., The Geology of North America: Geological Society of America Decade of North American Geology Series, v. c-3, p. 474–690.

LUND, K., J. N. ALEINIKOFF, K. V. EVANS, AND C. M. FANNING, 2003, SHRIMP U-Pb geochronology of Neoproterozoic Windermere Supergroup, central Idaho: Implications for rifting of western Laurentia and synchroneity of Sturtian glacial deposits: Geological Society of America Bulletin, v. 115, p. 349–372.

MCDONOUGH, M.R. AND PARRISH, R.R., 1991, Proterozoic gneisses of the Malton Complex, near Valemount, British Columbia: U-Pb ages and Nd isotopic signatures: Canadian Journal of Earth Sciences, v. 28, p. 1202-1216.

MEYER, L., 2004, Internal architecture of an ancient deep-water, passive margin, basin-floor fan system, Upper Kaza Group, Windermere Supergroup, Castle Creek, British Columbia. Unpublished M.Sc. thesis, University of Calgary, Calgary, 175 p.

MEYER, L., AND G. M. ROSS, 2007, Channelized lobe and sheet sandstones of the Upper Kaza Group basin-floor turbidite system, British Columbia, Canada. *In:* T. H. Nilsen, R. D. Shew, G. S. Steffens, and J. R. J. Studlik, eds., Atlas of deep-water outcrops AAPG Studies in Geology, v. 56, p. 85–88.

MURPHY, D. C., 1987a, Suprastructure/infrastructure transition, east-central Cariboo Mountains, British Columbia; geometry, kinematics and tectonic implications: Journal of Structural Geology, v. 9, p. 13–29.

MURPHY, D. C., 1987b, Kaza Group, eastern Wells Gray Park, British Columbia: Geological Survey of Canada Paper 87–1A, p. 735–742.

MURPHY, D. C., AND C. J. REES, 1983, Structural transition and stratigraphy in the Cariboo Mountains, British Columbia: Geological Survey of Canada Paper 83–1A, p. 245–252.

MUSSA-CALECA, M., 2008, Architecture and depositional history of a Neoproterozoic deepwater slope channel complex in a passive margin setting: Isaac Formation, Windermere Supergroup, southern Canadian Cordillera. Unpublished M.Sc. thesis, University of Ottawa, Ottawa, 128 p.

NAVARRE, J.C., CLAUDE, D., LIBRELLE, E., SAFA, P., VILLON, G., AND KESKES, N., 2002, Deepwater turbidite system analysis, West Africa: Sedimentary model and implications for reservoir model construction: The Leading Edge, v. 21, p. 1132–1139.

NAVARRO, L. AND ARNOTT, R.W.C., 2020, Stratigraphic record in the transition from basin floor to continental slope sedimentation in the ancient passive-margin Windermere turbidite system: Sedimentology, v. 67, p. 1710-1749. https://doi.org/10.1111/sed.12676

NAVARRO, L., Z. KHAN, AND R. W. C. ARNOTT, 2007, Architecture of a deep-water channel levee complex: Channel 3, Castle Creek South, Isaac Formation, Windermere Supergroup, Bristish Columbia, Canada. *In:* T. H. Nilsen, R. D. Shew, G. S. Steffens, and J. R. J. Studlik, eds., Atlas of deep-water outcrops: AAPG Studies in Geology v. 56, p. 93–96.

NINGTHOUJAM, J., WEARMOUTH, C., AND ARNOTT, R.W.C., 2022, Stratal characteristic and depositional origin of two-part (Mud-poor overlain by mud-rich) and associated deep-water strata: Components in a lateral depositional continuum related to particle settling in negligibly sheared mud-rich suspensions: Journal of Sedimentary Research v. 92(6): p. 503–529. doi: https://doi.org/10.2110/jsr.2021.053

O'BYRNE, C. J., M. D. BARTON, G. S. STEFFENS, C. PIRMEZ, AND B. HEINZ, 2007, Architecture of a laterally migrating channel complex: Channel 4, Isaac Formation, Windermere Supergroup, Castle Creek North, British Columbia, Canada. *In:* T. H. Nilsen, R. D. Shew, G. S. Steffens, and J. R. J. Studlik, eds., Atlas of deep-water outcrops: AAPG Studies in Geology v. 56, p. 115–118.

PARRISH, R.R., AND SCAMMELL, R.J., 1988, The age of the Mount Copeland syenite gneiss and its metamorphic zircons, Monashee Complex, southeastern British Columbia. *In:* Radiogenic age and isotopic studies: Report 2, Geological Survey of Canada Paper 88-2, 21-28.

PIPER, D. J. W., AND W. R. NORMARK, 2009, Processes that initiate turbidity currents and their influence on turbidites; a marine geology perspective: Journal of Sedimentary Research, v. 79, p. 347–362.

POPOVIĆ, N., 2016, Sedimentology and stratigraphy of a matrix-poor to matrix-rich depositional continuum in proximal basin floor strata, upper Kaza Group, Windermere Supergroup, B.C., Canada. Unpublished M.Sc. thesis, University of Ottawa, Ottawa, ON.

PRICE, R. A., 2000, The southern Canadian Rockies: evolution of a foreland thrust and fold belt: GeoCanada 2000, Field Trip Guidebook 13, 244 p.

REID, L. F., 2003, Stratigraphy, structure, petrology, geochronology and geochemistry of the Hobson Lake area (Cariboo Mountains, British Columbia) in relation to the tectonic evolution of the southern Canadian Cordillera: Unpublished Ph.D. thesis, University of Calgary, Calgary, 221 p.

REID, L.F., COOK, F.A., AND ERDMER, P., 1997, Structural correlation across the suprastructure infrastructure transition (Cariboo Mountains, British Columbia); possible, impossible or work in progress?, lithoprobe slave Northern cordillera lithospheric evolution (SNORCLE) and cordilleran tectonics workshop; report of the 1997 combined meeting. Lithoprobe Report, v. 56, p. 181-182.

REID, L. F., SIMONY, P.S., AND ROSS, G.M., 2002, Dextral strike-slip faulting in the Cariboo Mountains, British Columbia: a natural example of wrench tectonics in relation to Cordilleran tectonics: Canadian Journal of Earth Sciences, v. 39, p. 953–970.

ROCHELEAU, J., 2011, Depositional architecture of a near-slope turbidite succession: Upper Kaza Group, Windermerer Supergroup, Castle Creek, British Columbia, Canada. Unpublished M.Sc. thesis, University of Ottawa, Ottawa, 94 p.

ROSS, G. M., 1991, Tectonic setting of the Windermere Supergroup revisited: Geology, v. 19, p. 1125–1128.

ROSS, G. M., 2000, The Neoproterozoic Windermere Supergroup: An on-land continental margin turbidite system: Geological Survey of Canada Open File 3932, 2 sheets.

ROSS, G. M., AND ARNOTT, R.W.C., 2007, Regional geology of the Windermere Supergroup, southern Canadian Cordillera and stratigraphic setting of the Castle Creek study area, Canada. *In:* T. H. Nilsen, R. D. Shew, G. S. Steffens, and J. R. J. Studlik, eds., Atlas of deep-water outcrops: AAPG Studies in Geology 56 (CD-ROM), 16 p.

ROSS, G. M., AND FERGUSON, C.A., 2003a, Geology and structure cross-sections, Eddy, British Columbia: Geological Survey of Canada, "A" Series Map, 1967A, scale 1:50,000, 1 sheet.

ROSS, G. M., AND FERGUSON, C.A., 2003b, Geology and structure cross-sections, Goat River, British Columbia: Geological Survey of Canada, "A" series Map, 2003A, scale 1:50,000, 1 Sheet.

ROSS, G. M., AND PARRISH, R.R., 1991, Detrital zircon geochronology of metasedimentary rocks in the southern Omineca Belt, Canadian Cordillera: Canadian Journal of Earth Sciences, v. 28, p. 1254–1270.

ROSS, G. M., BLOCH, J.D., AND KROUSE, H.R., 1995, Neoproterozoic strata of the southern Canadian Cordillera and the isotopic evolution of seawater sulfate: Precambrian Research, v. 73, p. 71–99.

ROWE, C.E., 2003, The Cunningham formation: a ramp to platform carbonate in the terminal Proterozoic of the Cariboo Mountains, British Columbia. Unpublished M.Sc. thesis, University of Calgary, Calgary, AB.

SCHWARZ, E., AND ARNOTT, R.W.C., 2007a, Anatomy and evolution of a slope channel complex set (Neoproterozoic Isaac Formation, Windermere Supergroup, southern Canadian Cordillera): implications for reservoir characterization: Journal of Sedimentary Research, v. 77, p. 89–109.

SCHWARZ, E., AND ARNOTT, R.W.C., 2007b, Outcrop characterization of a passive-margin channel-complex set: Isaac Channel 5, Neoproterozoic Isaac Formation, British Columbia, Canada. *In:* T. H. Nilsen, R. D. Shew, G. S. Steffens, and J. R. J. Studlik, eds., Atlas of deep-water outcrops AAPG Studies in Geology 56 (CD-ROM), 15 p.

SMITH, M. D., ARNAUD, E., ARNOTT, R. W. C., AND ROSS, G. M., 2011, The record of Neoproterozoic glaciations in the Windermere Supergroup, southern Canadian Cordillera: Geological Society, London, Memoirs, v. 36, p. 413-424.

SMITH, M.D., ARNOTT, R.W.C., AND ROSS, G.M., 2014, Physical and geochemical controls on sedimentation along an ancient continental margin: The deep-marine Old Fort Point Formation (Ediacaran), southern Canadian Cordillera: Bulletin of Canadian Petroleum Geology, v. 62, p. 14-36.

SPRAGUE, A. R., SULLIVAN, M.D., CAMPION, K.M., JENSEN, G.N., GOULDING, F.J., SICKAFOOSE, D.K., AND JENNETTE, D.C., 2002, The physical stratigraphy of deep-water stratal a hierarchical approach to the analysis of genetically–related stratigraphic elements for improved reservoir prediction: AAPG Annual Convention Abstracts, Houston, TX, p. 10–13.

STEWART, J. H., 1972, Initial Deposits in the Cordilleran Geosyncline: evidence of a Late Precambrian (<850 m.y.) Continental Separation: Geological Society of America Bulletin, v. 83, p. 1345–1360.

TERLAKY, V., 2014, Sedimentology, stratigraphy, architecture and origin of deep-water, basin-floor deposits: Middle and upper Kaza Group, Windermere Supergroup, B.C., Canada. Unpublished Ph.D. thesis, University of Ottawa, Ottawa, ON.

TERLAKY, V., ROCHELEAU, J., AND ARNOTT, R.W.C., 2016, Stratal composition and stratigraphic organization of stratal elements in an ancient deep-marine basin-floor succession, Neoproterozoic Windermere Supergroup, British Columbia, Canada: Sedimentology, v. 63, p. 136-175.

WEARMOUTH, C., AND ARNOTT, R.W.C., 2018, Spatial, Temporal and Physical Origin of Matrix-Poor to Matrix-Rich Sandstones, Neoproterozoic, Windermere Supergroup, British Columbia, Canada. Unpublished M.Sc. thesis, University of Ottawa.

WEIMER, P., AND SLATT, R.M., 2007, Introduction to the petroleum geology of deepwater settings: AAPG Studies in Geology 57 (CD-ROM), 816 p.

Chapter 2: Deep-marine Processes and Environments

2.1 Deep-marine Processes

Large quantities of sediment are transported into deep-water environments by sediment-gravity flows and, less importantly, mass movements. These subaqueous flows build up some of the thickest and most areally extensive sediment accumulations on Earth and can be highly destructive events that pose a significant risk to undersea infrastructure (e.g., Kneller and Buckee 2000; Carter et al. 2014). Most of these flows are sediment-gravity flows, in which a density gradient formed by the difference in density between fluid rich in suspended sediment and the surrounding ambient fluid is acted up by gravity and initiates movement (Middleton and Hampton 1973).

Sediment-gravity flows generally originate near the continental shelf break or on the continental slope and can be triggered by various mechanisms, including earthquakes, high sedimentation rates, slope instability, and high hyperpycnal river outflows (Shanmugam 2006). A single sediment-gravity flow can transport more than 180 km^3 of sediment and travel 100s to 1000s of kilometres, at speeds of up to 100 km/hr (Talling et al. 2012; Talling 2014). Because of their powerful and destructive nature it is difficult to directly observe them in modern systems (monitoring instruments are often completely destroyed), and so much of our knowledge comes from descriptions in the ancient geological record, laboratory experiments, and seafloor imaging and seismic from modern oceans.

2.1.1 Sediment-gravity Flows

Sediment-gravity flows are sediment-laden flows in which gravitational forces act on the suspended sediment particles, driving both the particles and adjacent interstitial fluid downslope (Middleton and Hampton 1973). This differs from fluid gravity flows, like rivers, where the fluid is moved by gravity, which then moves the sediment.

In this thesis, sediment-gravity flows are classified according to the scheme of Mulder and Alexander (2001), which uses particle cohesivity, particle support mechanisms, and sediment concentration to differentiate types of sediment-gravity flows (Figure 2.1; see below). This system has two end-member types: cohesive and frictional (non-cohesive) flows. Cohesive flows are dominated by matrix strength from particle-particle bonding, whereas in frictional flows particles are dispersed in a fluid (Mulder and Alexander 2001).

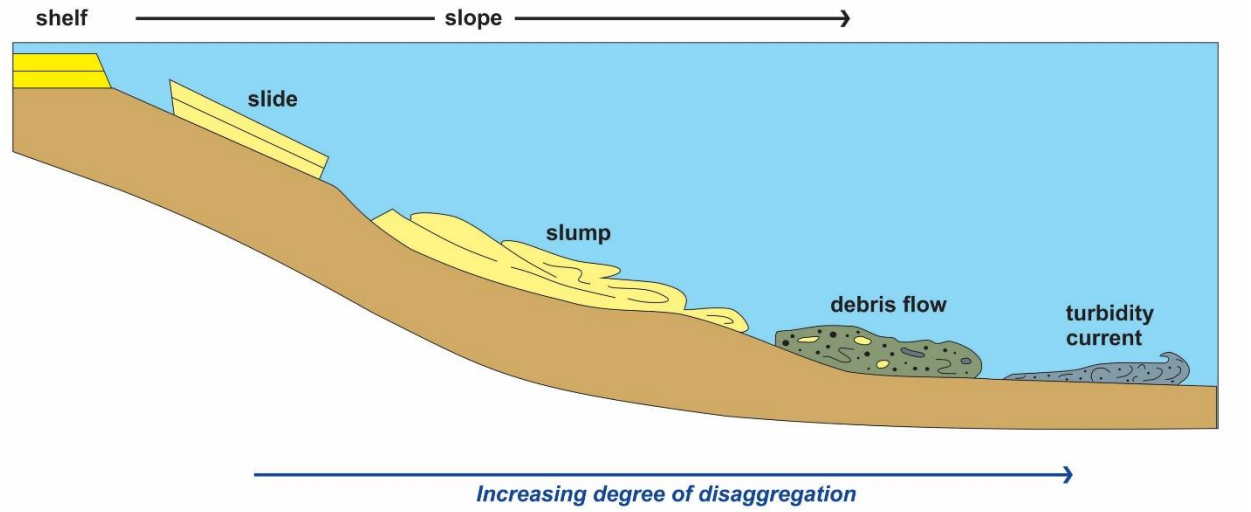

Figure 2.1. *Schematic showing the types of sediment-gravity flows and their typical downslope evolution from coherent slides to cohesionless water-sediment flows. Slides result from the failure of unstable material that moves downslope under gravitational forces. Internal deformation associated with slides is minimal and typically increases downslope where slides evolve into slumps. Incorporation of water during downslope transport may result in the transformation of slumps to debris flows. Further increasing fluid content causes debris flows to evolve into turbidity currents. Gravity-driven sediment failures do not always evolve in this manner and any one of these gravity-driven mass movements or sediment flows may evolve directly from sediment failure near the shelf edge, on the slope, or in the distal basin (from Khan 2012, after Shanmugam et al., 1994).*

Name	Sediment support mechanism
Fluid Turbulence	Coherent movement of fluid masses at an angle to the main axis of flow in order to minimize a momentum gradient. Turbulence intensity increases with the velocity gradient and is capable of suspending sediment if the strength of the upward component of turbulent motion equals or exceeds the downward settling velocity of the particle due to gravity (Middleton and Hampton, 1973).
Hindered Settling	Reduced particle settling velocity due to increased drag imposed by upward moving fluid/sediment mixture that increases with sediment concentration (Davies, 1968).
Buoyancy	Displacement of a fluid by a moving particle generates an upward force on the particle that is equal to the mass of the displaced fluid volume (Lowe, 1979).
Dispersive Pressure	Collision between solid particles generates a dispersive force that helps maintain the particles in suspension, but also causes the flow to dilate. Grain-to-grain interactions become increasingly important as sediment concentration increases (Bagnold, 1962).
Matrix Strength (cohesive strength)	Ionic surface charges and large surface area:volume ratio of clay particles cause them to become aggregated into larger masses by weak van der Waal's forces. At sufficiently high concentration, the aggregated clay minerals form a sufficiently strong particle network capable of supporting the weight of larger grains (Mulder and Alexander, 2001)

Table 2.1. *List of particle support mechanisms that individually or in combination act in sediment gravity flows. Adapted from Dumouchel (2012).*

2.1.1.1 Cohesive Flows

Cohesive flows have a pseudoplastic rheology in which cohesive forces suspend sediment (Nardin et al. 1979; Mulder and Alexander 2001; Shanmugam 2006). Cohesive forces arise from the interaction between adjacent clay-size clay mineral particles in the flow, which carry a weakly negative electrostatic surface-charge that allows them to form weak electrostatic bonds and build an aggregated particle network. This aggregation increases the fluid viscosity, which, in addition to buoyancy, particle-particle interaction, hindered settling, elevated fluid turbulence, and pore pressure, permits particles ranging from clay to boulders to be suspended

(Rodine and Johnson 1976; Lowe 1982; Leigh and Hartley 1992; Van Weering et al. 1998; Mulder and Alexander 2001).

Cohesive flows are subdivided into mud flows and debris flows based on sediment size and sorting: mud flows have < 5% gravel by volume and a mud to sand ratio > 1, whereas debris flows have > 5% gravel by volume and can transport boulder-sized clasts and decametre-scale blocks (Mulder and Alexander 2001).

Debris flows have runout distances of up to several hundreds of kilometres and can be > 100 m thick (Gardner and Kidd 1983). Their deposits, termed debrites, are sheetlike to lobate and often have planar, non-erosive basal contacts due to both turbulence dampening by the cohesive matrix and the process of hydroplaning, where a layer of water becomes trapped between the base of the flow and the underlying bed. This dramatically reduces basal friction and allows the flow to travel over long distances (Mohrig et al. 1998; Mulder and Alexander 2001).

Deposition from cohesive flows occurs by en-masse freezing when the forces resisting shear (fluid viscosity and grain-to-grain friction) overcome the driving gravitational force (Alexander and Mulder 2001; Arnott 2010), causing the flow to freeze from the area of lowest shear, which is at the top of the flow, to the area of highest shear, at the base. Alternatively, cohesive flows may transform through mixing and dilution along their leading edge in addition to entrainment along the upper boundary into non-cohesive sediment-gravity flows (Hampton 1972; Fisher 1983; Weirich 1988), termed frictional flows by Mulder and Alexander (2001) (see next).

2.1.1.2 Frictional Flows

Frictional (non-cohesive) flows are subdivided into three kinds based on sediment concentration: hyperconcentrated density flows (most concentrated), concentrated density flows, and turbidity currents (least concentrated) (Mulder and Alexander 2001). The different kinds are based on the dominant sediment-supporting mechanism, which include grain-to grain interaction, buoyancy, fluid turbulence, and matrix support (Figure 2.2, Table 2.1) (Mulder and Alexander 2001). These mechanisms, in turn, are influenced by factors like sediment concentration, flow conditions, sediment type, and grain size distribution.

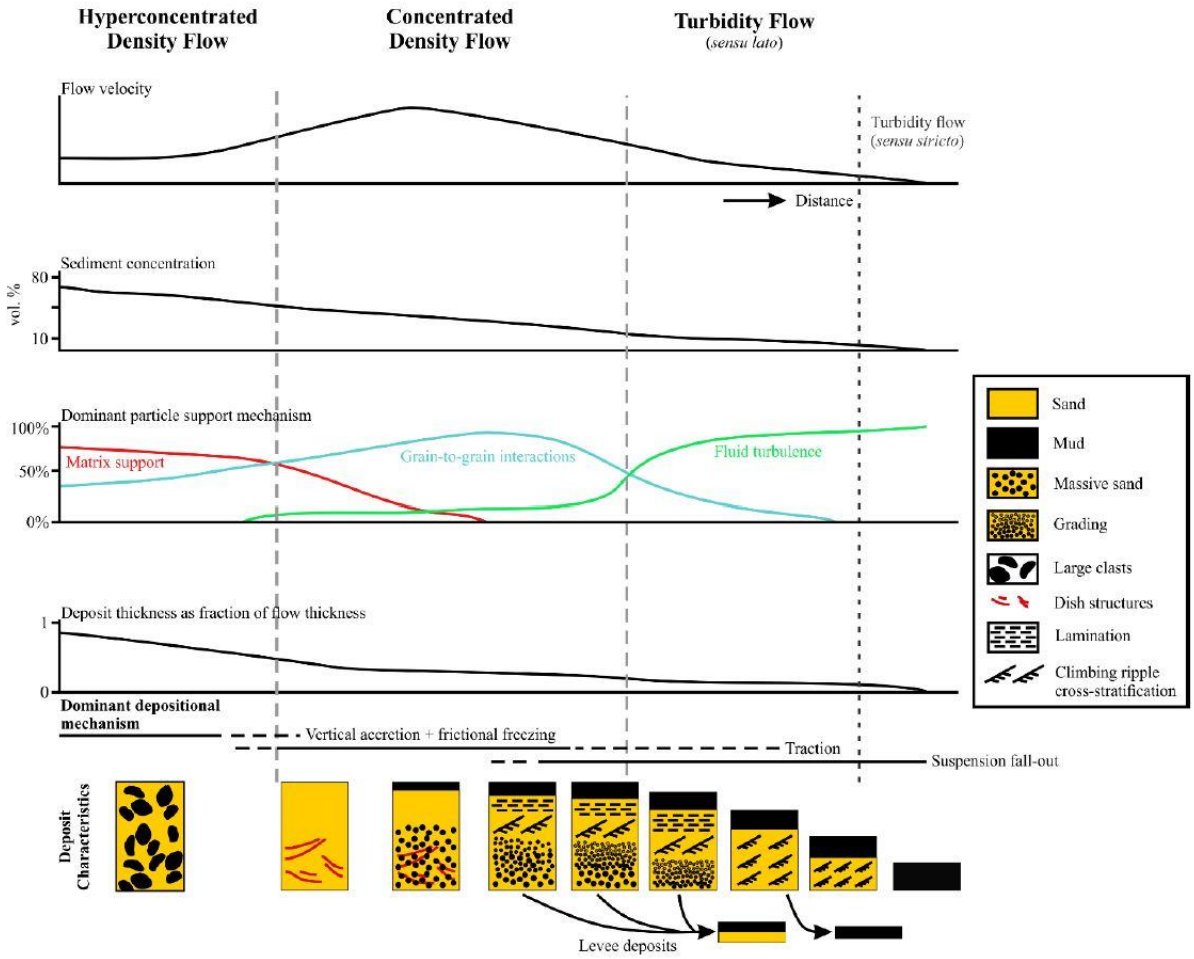

Figure 2.2. *Diagram illustrating the changes in flow characteristics of frictional flows across the different subdivisions. Flow types are differentiated based on differences in sediment concentration, which results in differences in flow behaviour and depositional characteristics (redrawn by Billington (2019) from Mulder and Alexander (2001)).*

2.1.1.2.1 Hyperconcentrated Density Flows

Although hyperconcentrated density flows are similar in sediment-to-fluid ratio to cohesive flows, they contain less clay and/or have higher velocity with stronger internal shear (Mulder and Alexander 2001). In these flows the high sediment concentration (> 25% volume sediment concentration) make grain-grain collisions the most significant mechanism for maintaining sediment in suspension. Hyperconcentrated flows typically have limited runout distance due to high internal friction, which causes particle interlocking (frictional freezing) and rapid deposition of structureless, ungraded or locally inversely graded beds (Mulder and Alexander 2001). If flows become sufficiently diluted by fluid entrainment and turbulence increases, hyperconcentrated flows may transition into concentrated flows downflow.

2.1.1.2.2 Concentrated Density Flows

Concentrated density flows have lower sediment concentration than hyperconcentrated flows (10-25% volume sediment concentration), and therefore reduced grain-grain interaction. The transition from hyperconcentrated to concentrated flow occurs when there is sufficient flow dilution to allow the upper part of the flow to become fully turbulent and become the dominant support mechanism (Mulder and Alexander 2001).

Under these conditions differential grain settling occurs, resulting in the deposition of large, dense particles first and the formation of massive or normally graded beds. The near-bed region in concentrated flows behaves similar to hyperconcentrated flows, which may result in the

development of a traction carpet at the base of the flow and an associated inversely graded unit (Lowe 1982).

Lowe (1982) developed a six-part (R_1, R_2, R_3, S_1, S_2, S_3) classification for concentrated density flow deposits with gravel-rich (R) and sand-rich (S) end members (Figure 2.3), where R_1 consists of structureless gravel, R_2 – inversely graded gravel, and R_3 – normally graded gravel. In sand-rich strata, S_1 consists of planar- or cross-stratified sandstone, S_2 – inversely graded sandstone, and S_3 – massive or normally graded sandstone (Lowe 1982). Physical sedimentary structures, grading, and sorting are better developed in concentrated density flows compared to hyperconcentrated density flows (Mulder and Alexander 2001).

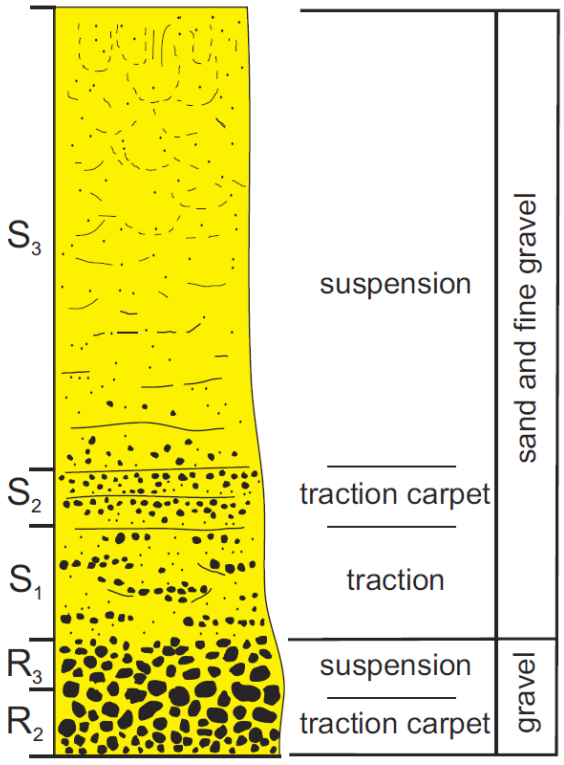

Figure 2.3. *Sequence of sedimentary textures and structures deposited by high-density, coarse-grained turbidity currents (redrawn from Lowe 1982).*

2.1.1.2.3 Turbidity Currents

The most common type of frictional flows are turbidity currents, which are sediment-gravity flows in which sediment is supported mainly by the upward component of fluid turbulence (Mulder and Alexander 2001). These flows are the principal agent of sediment transport into the deep sea and form deposits called turbidites, which are ubiquitous in the deep-marine sedimentary record (Arnott 2010).

Lowe (1982) subdivided turbidity currents into low- and high-density end members. Low-density turbidity currents contain < 9% sediment by volume, termed the Bagnold limit (Bagnold 1954), and fluid turbulence is the only particle support mechanism. Once sediment exceeds this concentration (high-density turbidity currents) mechanisms such as dispersive pressure, hindered settling, and buoyancy provide additional support (Arnott 2010).

Turbidity currents have a longitudinal structure with three distinct parts: head, body, and tail (Figure 2.4). The head is the sediment-rich, most erosive-part of the flow, and is where most of the mixing with ambient seawater occurs (Kneller and Buckee 2000; Arnott 2010). The head is characterized by a sharp overhanging nose that slopes back upstream due to fluid resistance along its margin and carries sediment-laden fluid back towards the body. To make up for this loss the body, which moves 30-40 % faster than the head, must continuously supply sediment to the head in order to sustain it (Kneller and Buckee 2000; Arnott 2010). With time, the flow becomes longitudinally stratified in terms of grain size, such that each of the three parts consist of different sediment populations: coarse sediment accumulates in the lower part of the head and finer sediment is swept upward and then backwards into the body, eventually forming a fine-grained, low-density, slower-moving dispersion that makes up the tail of the flow (Kneller and Buckee 2000; Arnott 2010).

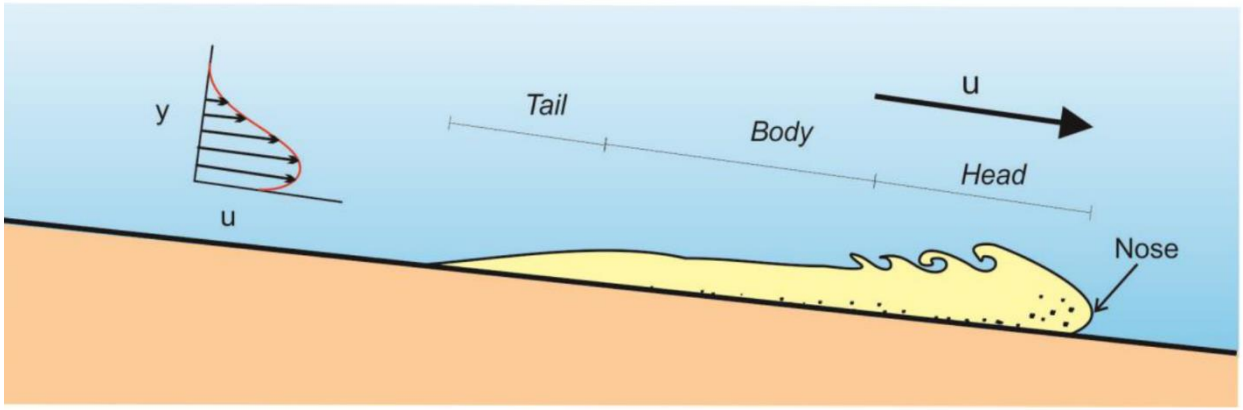

Figure 2.4. *Diagram of a turbidity current showing the head, body, and tail regions. Note the overhanging nose at the front of the head that forms in response to frictional forces between the lower boundary of the flow and the static bed and the upper boundary of the flow and ambient fluid. The flow head accelerates downslope, commonly eroding the substrate in the process. Eroded sediments become incorporated into the flow, which in turn in turn increase the density contrast between the flow and the ambient fluid. Behind the head is the thinner but faster moving body, which continuously feeds sediment to the head. The tail is a dilute suspension that trails more slowly behind the main flow. From Navarro (2016).*

Turbidity currents are vertically density-stratified, with grain concentration highest near the base (Mulder and Alexander 2001). Deposition from turbidity currents occurs as the flow decelerates, forming a deposit called a turbidite. In 1962 Arnold Bouma described the idealized vertical succession, generally termed the Bouma Sequence, which later was interpreted to represent deposition from decelerating, low-density turbidity currents. This succession fines upward with a characteristic suite of sedimentary structures and comprises five divisions labelled T_a to T_e (Figure 2.5).

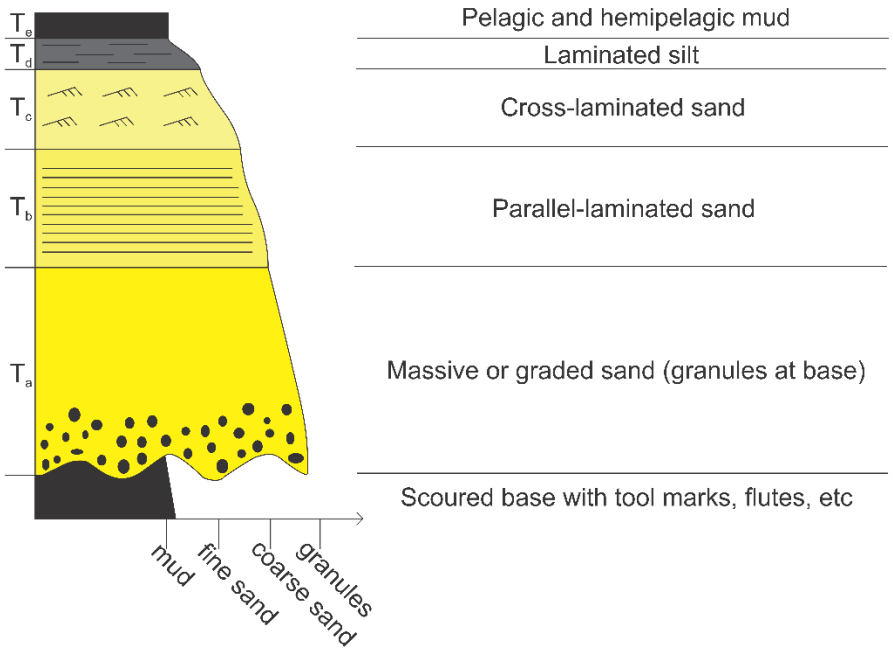

Figure 2.5. *Complete Bouma sequence showing grain size and sedimentary structures observed in each division. Note that the full succession is rarely preserved in turbidites (redrawn and modified from Bouma, 1962).*

The T_a division is characterized by coarse-grained, structureless, massive or normally graded sandstone interpreted to have been deposited rapidly from suspension, with the high rates of fallout inhibiting the development of tractional sedimentary structures (Arnott and Hand 1989). The T_b division consists of medium- to fine-grained, distinctively planar-laminated sandstone indicative of reduced rates of sediment fallout. Bed-surface sediment transport was more or less spatially uniform, with planar lamination formed by traction transport on a surface that lacked the requisite bed defects needed to initiate the development of angular bedforms like ripples or dunes (Tilston et al. 2015). The T_c division consists of fine- to very fine-grained, cross-stratified sandstone interpreted to form from the downflow migration current ripples. The T_d division consists of planar interlaminated siltstone and mudstone deposited by rhythmic alternation of bedload traction and suspension fallout (Stow and Bowen 1980). Finally, the

uppermost T_e division consists of massive mudstone deposited by fine-grained suspension fallout.

2.1.2 Mass-Movement Deposits

The term mass-movement is used to describe the dislodgement and downslope movement of coherent to semi-coherent masses of sediment due to gravity (Shanmugam 2006; Arnott 2010). Movement occurs when gravitational forces exceed the tensile strength of the sediment mass, at which point it moves downslope along discrete failure planes until the resisting forces, principally friction along the base, exceed the force of gravity and deposition occurs en-masse. Mass-movement deposits are subdivided into two end-members based on the degree of internal deformation: slides, being coherent masses of sediment that move along planar glide planes with negligible internal deformation; and slumps, which move along concave-upwards glide planes and develop a wide range of internal deformation structures exhibiting rotational movement and contortion (Shanmugam 1996; Shanmugam 2006; Arnott 2010). Mass-movements can travel hundreds of kilometres downslope and form deposits hundreds of meters thick. Importantly mass-movements can also disaggregate during movement, which aided by mixing with ambient fluid, can evolve into a sediment-gravity flow (Figure 2.1) (Shanmugam 2006; Arnott 2010).

2.1.3. Bottom Currents

Contour currents are thermohaline-induced bottom currents that generally flow along continental slopes (parallel to bathymetric contours) and rework deep-marine sediments on the ocean floor (Heezen et al. 1966; Flood and Hollister 1974; Stow et al. 1998). These currents

form elongate, slope-parallel sediment bodies that can be 10 – 100 km long, 10s of kilometres wide, and over 1 km thick (Stow and Piper 1984a; Arnott 2010). Because these currents continually rework and redeposit sediment that was originally deposited by sediment-gravity flows (Shanmugam 1997; Shanmugam 2000), the differentiation between the two can be problematic (Stow 1979; Arnott 2010; Shanmugam 2017). However, there are several characteristics that can be used to identify contourites. Contourites typically display inverse grading in silt and fine sand, internal erosion surfaces, well-sorted sediment due to winnowing of fines, rhythmicity of sand and mud layers, and a lack of a distinct vertical facies succession (i.e., lack the systematic organization of the Bouma Sequence) (e.g., Stow 1979; Shanmugam 2000; Arnott 2010; Shanmugam 2017). Contourites are also typically intensely bioturbated, reflecting the low instantaneous sedimentation rate and extended periods of exposure on the sea floor (Stow 1979; Shanmugam 2017).

2.2 Deep-marine Environments

2.2.1 Overview

Sediment-gravity flows transport enormous volumes of sediment from the shelf and upper slope to the ocean floor, where it is deposited in large-scale depositional systems called submarine fans (Menard 1955; Mutti and Normark 1987, 1991). Submarine fans are complex systems with origins and characteristics controlled by many factors, including sea level, tectonics, salinity, sediment composition and size distribution, and organic supply (Reading 1996; Arnott 2010). Since the 1960s numerous depositional models and classification schemes have been proposed to describe and interpret the depositional processes, nature of sediment

transport, and sediment distribution in these deep-water systems (e.g., Normark 1970; Haner 1971; Reading and Richards 1994; Meiburg and Kneller 2010).

Reading and Richards (1994) classified submarine fan systems according to both the nature of the supply system (point-source, multiple-source, and linear-source) and sediment grain size (gravel-rich, sand-rich, mud-rich, and mixed sand-mud), resulting in 12 distinct classes (Figure 2.6). Coarser-grained (i.e., gravel-rich) systems were generally small, ranging in size from ~ 1-50 km in radius, whereas finer-grained systems had radii of up to ~ 100-300 km. According to this classification scheme, the Windermere turbidite system would be considered a mixed sand-mud system, although interestingly, it is comparable in size to modern mud-rich systems, such as the Amazon (330,000 km^2) and Mississippi (300,000 km^2) fans, which are typically larger than mixed sand-mud systems.

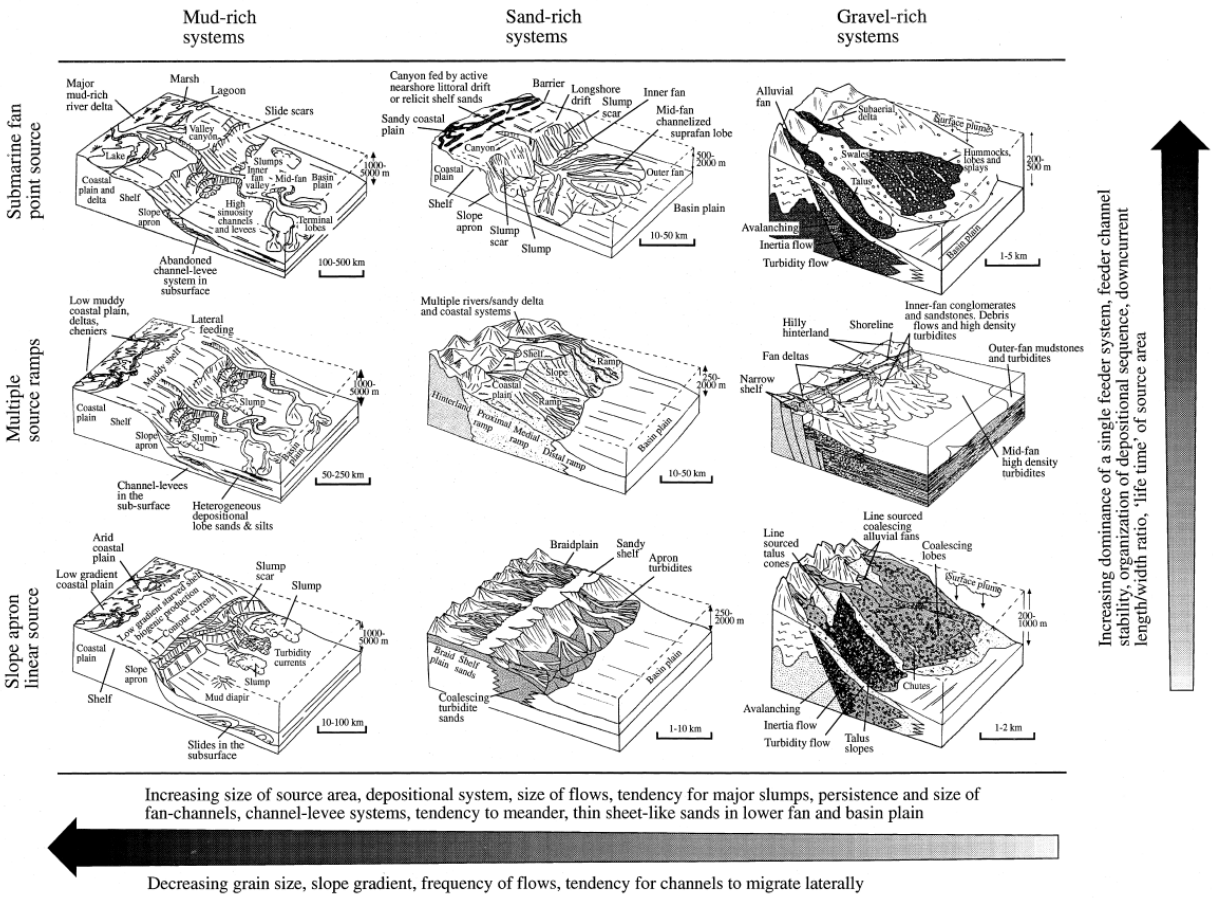

Figure 2.6. *Classification of deep-water systems based on grain size (mud-rich, sand-rich, and gravel-rich) and nature of sediment supply (single point, multiple sources, or linear source) (from Stow and Mayall 2000; after Reading and Richards 1994).*

Submarine fans are commonly divided into an upper, middle, and lower fan region (Figure 2.7), with each region having unique sub-environments and architectural elements. Together, these comprise the deep-marine sediment transport system.

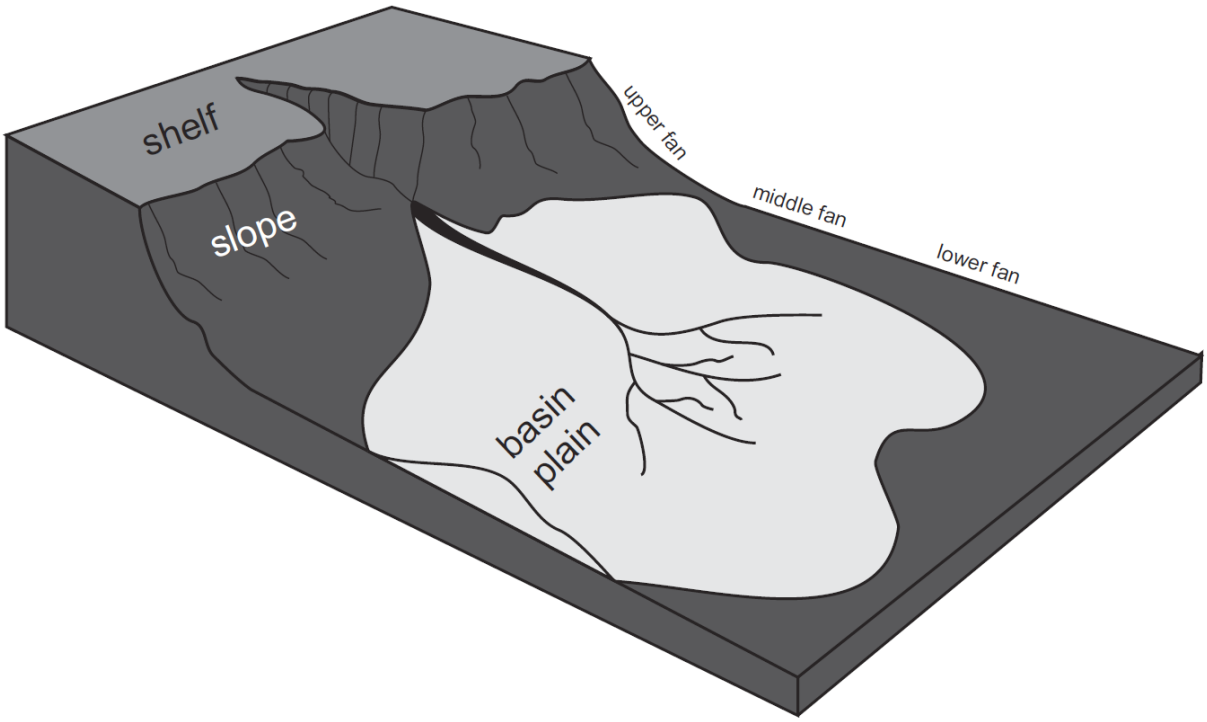

Figure 2.7. *Diagram illustrating the upper, middle, and lower parts of a typical submarine fan system (Khan 2012).*

2.2.2 Architectural Elements

Architectural elements are the basic geomorphic components of both ancient and modern submarine fans and individually consist of distinct facies assemblages (Mutti and Normark 1991; Posamentier and Kolla 2003). In deep-marine turbidite systems, the main architectural elements include canyons, channels, levees, splays, and terminal lobes (Figure 2.8) (Posamentier and Kolla 2003).

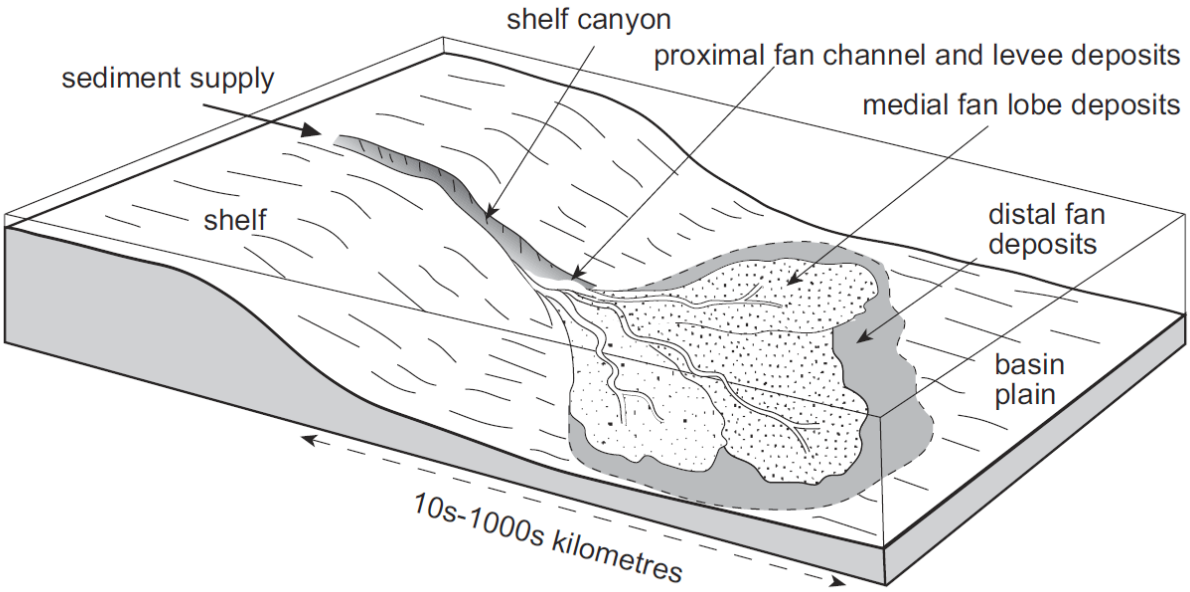

Figure 2.8. *Diagram showing the various depositional environments found in submarine fan systems (Nichols 2009).*

Submarine canyons are large-scale erosional features located in the upper fan region. They incise the shelf and upper slope and act as the main upflow conduit for sediment being transported to the basin floor. Canyons range in size from tens to thousands of kilometres in length and tens to hundred of kilometres in width, with an average depth of 900 m (Shepard and Dill 1966; Shepard 1973; Carlson and Karl 1988).

Downslope in the middle fan region canyons narrow and shallow, transitioning into large, sinuous channels confined by well-developed levees. In this region, the lower, sand-rich part of turbidity currents generally remains confined to the channel, whereas the upper, finer-grained, more dilute part of the flow overspills the channel and contributes to the construction of levees. Because so much sediment is lost in this way on the slope, levee topography becomes progressively reduced towards the lower fan region, eventually resulting in a loss of channel confinement (Posamentier and Kolla 2003). This promotes channel bifurcation in the lower fan

and the development of a network of narrow, shallow distributary channels. Distributary channels continue to shallow downslope until they can no longer confine throughgoing flows, at which point the deposition of large, unconfined sand lobes (called terminal lobes) occurs (Posamentier and Kolla 2003).

Because channel-bounding levee systems and their deposits are the main focus of this paper, the characteristics and formative processes of channels and levees are described in greater detail next.

2.2.2.1 Channels

Submarine channels are negative topographical elements that act as long-term conduits for the transport of sediment basinwards (Mutti and Normark 1991; Arnott 2007). Channels are large features that can be hundreds of meters deep, several kilometres wide, and thousands of kilometres long (e.g., Chough and Hesse 1976; Hesse and Chough 1980; Kolla and Coumes 1984; Clark and Pickering 1996; Torres et al. 1997; Babonneau et al. 2002, Wyn et al. 2007; Fraino et al. 2022). In the ancient sedimentary record channel-fill deposits typically consist of coarse-grained sand and gravel, making them more resistant to weathering than adjacent fine-grained overbank deposits. As such, channels are well-represented in outcrop and well-documented in the deep-marine literature.

Deep-water channels, like fluvial channels, have a concave-up profile with a decrease in gradient downslope (Pirmez et al. 2000; Kneller 2003). Submarine channels, like fluvial channels, will either erode or aggrade in order to achieve an equilibrium profile that maximizes basinward sediment transport (Figure 2.9), with base level being the lowest point a turbidity

current can reach in the basin (Pirmez et al. 2000). Channel equilibrium profile is controlled by a number of intrinsic and extrinsic factors, including sediment calibre, flow magnitude, lobe deposition and position, sea level, and tectonics, and like in fluvial systems, is constantly being adjusted. Erosional channels reflect conditions where slope of the channel floor exceeds its equilibrium profile, or aggradational, where the channel slope is below its equilibrium profile. As implied in its name, erosional channels are erosionally confined, whereas aggradational channels, also termed depositional channels (Normark 1970), create their own confinement through the deposition of channel-bounding levees that typically aggrade as fast or faster than the channel floor.

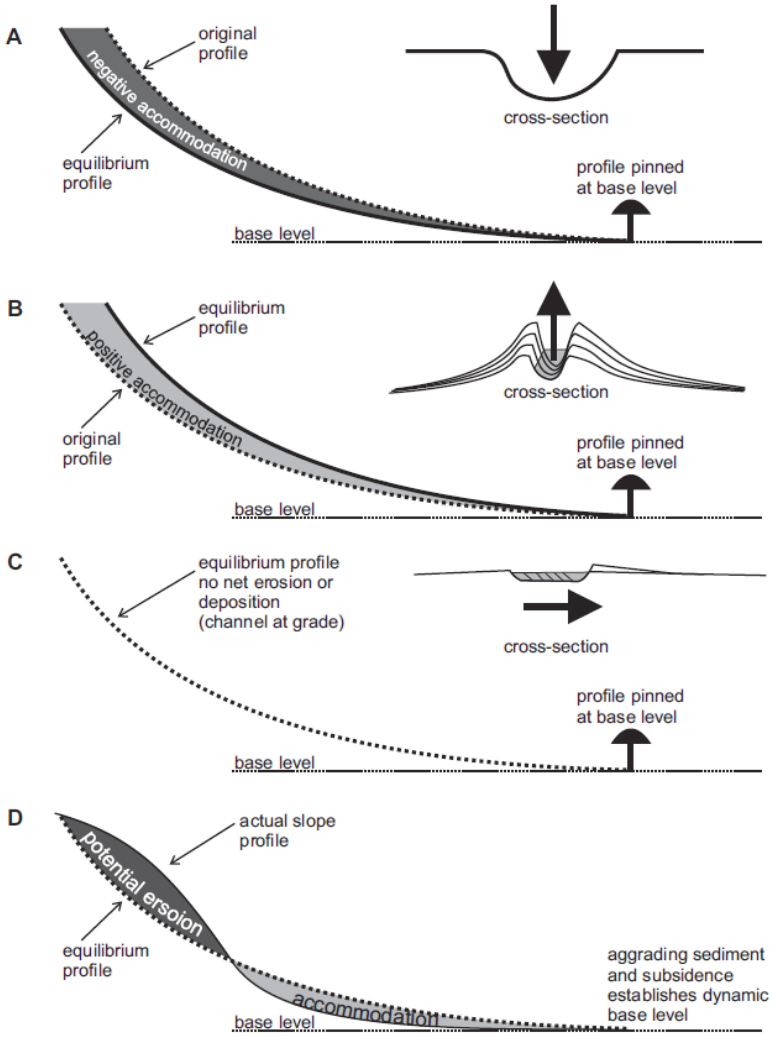

Figure 2.9. *Diagram showing how channel profiles adjust to attain transport equilibrium. A) Channels positioned above equilibrium erode to flatten their profile; B) channels positioned below equilibrium aggrade to steepen their profile; C) channels at grade show no net aggradation or erosion but can instead shift laterally and bypass sediment basinward; D) channels may be both erosional and aggradational at different locations along their length in order to achieve equilibrium (redrawn from Kneller 2003; after Samuel et al. 2003).*

2.2.2.2 Levees

Submarine levees are interpreted to form from the deposition of throughgoing channelized flows that spill out of the channel and deposit sediment along its margins (Buffington 1952; Hay 1987a, b; Hiscott et al. 1997; Skene et al. 2002). Levees typically display a gullwing-shaped geometry in cross-section (Figure 2.10), which is a result of lateral thinning

and fining of beds away from the channel (Skene et al. 2002; Beaubouef 2004; Arnott 2010; Kane et al. 2011; Morris et al. 2014). Because the density contrast between the overspilling flow and the ambient fluid is considerably less in submarine systems than fluvial systems, overspilling flows can travel for tens of kilometres laterally, and as such levees are commonly an order of magnitude or more wider than their associated channels (Posamentier and Kolla 2003).

Modern levees range from tens to several hundreds of meters high, and as such act to partly to completely confine the flows to the channel (Emmel and Curray 1981a, b, 1984, 1985; Bouma et al. 1984, 1985; Bouma and Coleman 1985; Kolla and Coumes 1984, 1987; Droz and Bellaiche 1985; Kastens and Shor 1985, 1986; Pickering et al. 1986; Pirmez et al. 1997; Piper and Normark 2001; Deptuck et al. 2003; Curray et al. 2003, Wynn et al. 2007; Morris et al. 2014). Their expansive areal extent and significant thickness make deep-marine levees the most significant element, in terms of volume, in middle fan environments (Emmel and Curray 1981a, b, 1984, 1985; Bouma et al. 1984, 1985; Bouma and Coleman 1985; Kolla and Coumes 1984, 1987; Droz and Bellaiche 1985; Kastens and Shor 1985, 1986; Pickering et al. 1986; Pirmez et al. 1997; Piper and Normark 2001; Deptuck et al. 2003; Curray et al. 2003).

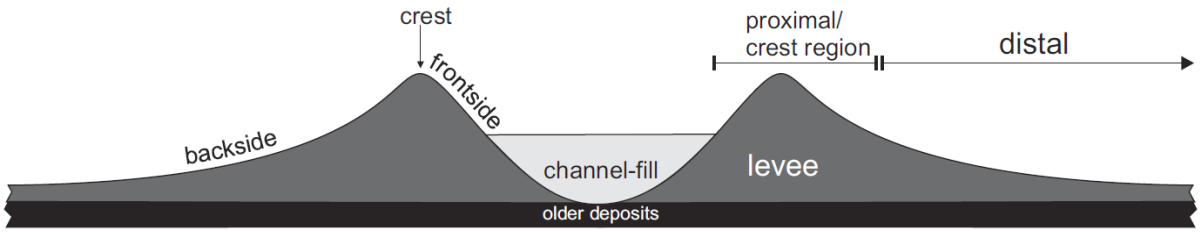

Figure 2.10. *Cross-section of an idealized channel-levee system, showing the wedge-shaped morphology and general levee terminology (Khan 2012).*

Three types of overspill build up submarine levees: flow stripping, inertial overspill, and continuous overspill. Flow stripping occurs along the outer bend of channels where momentum

causes the upper, more dilute part of the flow to detach from the lower, more concentrated part of the flow (Figure 2.11) (Piper and Normark 1983; Fildani et al. 2006; Arnott 2010). The fine-grained upper part then spills out of the channel and moves over the levee while the coarser-grained lower part of the flow remains confined to the channel and continues downslope. Superelevation along the outer channel bend, amplified by the reduced density between the flow and ambient fluid, amplifies this effect by increasing the thickness of the flow along outer bends, which causes the surface of the flow to slope towards the inner bend (Posamentier 2003; Posamentier and Kolla 2003; Khan and Arnott 2011). Because the density difference between the flow and ambient fluid in submarine systems is greatly reduced compared to fluvial systems, the superelevation of the flow is significantly larger, resulting in submarine levees much greater in size and height than their fluvial counterparts.

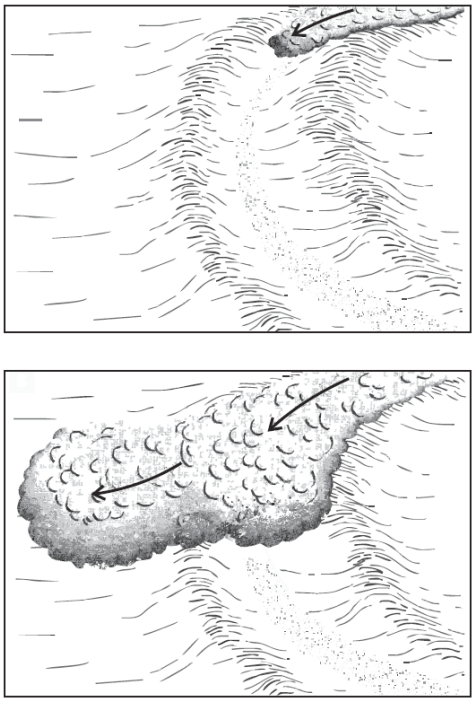

Figure 2.11. *Diagram showing the process of flow stripping, where the upper, dilute part of the flow preferentially overspills along the outer-bend of the channel while the coarser-grained, lower part of the flows remains confined within the channel (Khan 2012; redrawn from Peakall et al. 2000).*

Like flow stripping, inertial overspill occurs mostly along the outer bend of channels, but in this process it is the inertia of the throughgoing channelized flow that enables more than just the dilute upper part of the flow to ride up and overspill the channel bank (Figure 2.12) (Hay et al. 1983; Hay 1987b). Being processes that preferentially occur on the outer bends of channels, both flow stripping and inertial overspill result in asymmetric levees, with thicker, more sand-rich levee deposits on the outer bend compared to the inner bend.

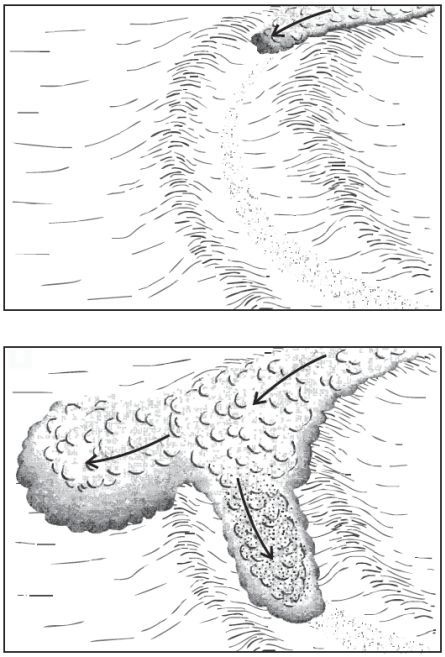

Figure 2.12. *Diagram showing the process of inertial overspill, where the flow along the outer bend rides up and over the side of the channel due to fluid inertia (Khan 2012; after Kane et al. 2007).*

Finally, continuous overspill occurs where the throughgoing flow is thicker than the depth of the channel (Figure 2.13), and the part of the flow above the levee crest continuously overspills, building up levees equally on both sides of the channel (Peakall et al. 2000; Kane et al. 2007; Arnott 2010).

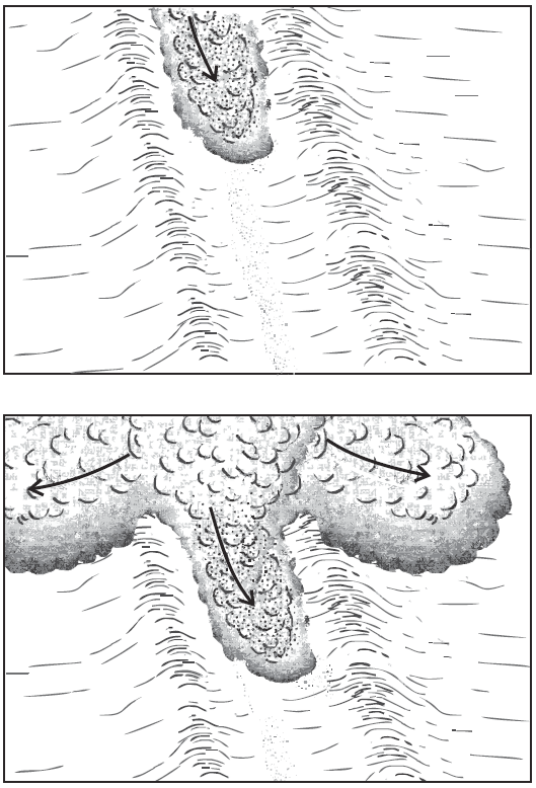

Figure 2.13. *Diagram showing the process of continuous overspill wherein the upper, dilute part of throughgoing channel flows deposit along both sides of the channel (Khan 2012; after Peakall et al. 2000 and Kane et al. 2007).*

As the upper, lower density part of the flow overspills onto the levees and loses connection with the high-density, channel-confined part of the flow, flow velocity and related transport capacity wane rapidly. Accordingly, the lower, channel-proximal parts of levees are generally the coarsest-grained and the thickest bedded (e.g., Hiscott et al. 1997; Eschard et al. 2003; Beaubouef 2004; Khan and Arnott 2011; Bergen et al. 2022) and contain complete or near-complete Bouma sequences. However, as the levee aggrades and relief between channel floor and levee crest increases, only the higher, even more dilute, finer-grained part of the flow overspills, resulting in the deposition of more thinly-bedded, finer-grained, mostly upper division (T_{cde}) turbidites (Walker 1985; Hiscott et al. 1997; Kane et al. 2007; Khan and Arnott 2011; Cunningham and Arnott 2021; Bergen et al. 2022).

Most levee beds also thin away from the channel, with thicker-bedded strata thinning more rapidly than thinner-bedded strata (DeVries and Lindholm 1994; Beaubouef 2004; Kane et al. 2007; Khan and Arnott 2011; Bergen et al. 2022). This lateral thinning corresponds to a decrease in the sand-to-mud ratio that can occur rapidly over distances of only a few hundred meters (Khan and Arnott 2011; Cunningham and Arnott 2021; Bergen et al. 2022), or over several kilometres (e.g., Clemenceau et al. 2000). Notably also, lateral thinning and fining occurs more gradually in the thinner, finer, inner-bend levee deposits than in outer-bend levee deposits (Khan and Arnott 2011; Khan et al. 2011). Levee strata can also exhibit characteristic thickening and then thinning trends away from their adjacent channels (Kane et al. 2007; Khan and Arnott 2011). This trend has been interpreted to result from particle inertia as flows overspill the channel margin, which can result in the location of maximum sedimentation to be displaced several hundreds of meters outward from the channel margin. Beyond this point, as flows become depleted of coarse-grained sediment they rapidly wane and beds accordingly fine and thin with further distance.

2.3 References

ARNOTT, R.W.C., 2007, Stratal architecture and origin of lateral accretion deposits (LADs) and conterminuous inner-bank levee deposits in a base-of-slope sinuous channel, lower Isaac Formation (Neoproterozoic), East-Central British Columbia, Canada: Marine and Petroleum Geology, v. 24, p. 515-528.

ARNOTT, R. W. C., 2010, Deep-marine sediments and sedimentary systems. *In*: Facies models 4, p.295-322. Geological Association of Canada, St. John's, Newfoundland and Labrador.

ARNOTT, R.W.C., AND HAND, B.M., 1989, Bedforms, primary structures and grain fabric in the presence of suspended sediment rain: Journal of Sedimentary Petrology, v. 59, p. 1062–1069.

BABONNEAU, N., SAVOYE, B., CREMER, M., AND KLEIN, B., 2002, Morphology and architecture of the present canyon and channel system of the Zaire deep-sea fan: Marine and Petroleum Geology, v. 19, p. 445–467.

BAGNOLD, R. A., 1954, The physics of blown sand and desert dunes: London, Methuen, 265 p.

BEAUBOUEF, R.T., 2004, Deep-water leveed-channel complexes of the Cerro Toro Formation, upper Cretaceous, southern Chile: American Association of Petroleum Geologists, Bulletin, v. 88, p. 1471–1500.

BERGEN, A.L., CUNNINGHAM, C.M., TERLAKY, V., AND ARNOTT, R.W.C., 2022, Influence of channelized-flow density structure on the stratal architecture of deep-marine levee deposits: Journal of Sedimentary Research, v. 92.4, p. 381-403.

BILLINGTON, T., 2019, Sedimentologic and Petrographic Evidence of Flow Confinement in a Passive Continental Margin Slope Channel Complex, Isaac Formation, Windermere

Supergroup, British Columbia, Canada. Unpublished M.Sc. thesis, University of Ottawa, Ottawa, ON

BOUMA, A. H., 1962, Sedimentology of some Flysch deposits: a graphic approach to facies interpretation: Amsterdam, Elsevier, 168 p.

BOUMA, A. H., AND COLEMAN, J.M., 1985, Mississippi Fan: Leg 96 program and principal Results. *In:* A. H. Bouma, W. R. Normark, and N. E. Barnes, eds., Submarine Fans and Related Turbidite Systems: New York, Springer, p. 247–252.

BOUMA, A. H., STELTING, C.E., AND COLEMAN, J.M., 1984, Mississippi Fan: internal structure and depositional processes: Geo-Marine Letters, v. 3, p. 147–153.

BOUMA, A. H., STELTING, C.E., AND COLEMAN, J.M., 1985, Mississippi Fan: Gulf of Mexico. *In:* A. H. Bouma, N. E. Barnes, and W. R. Normark, eds., Submarine Fans and Related Turbidite Sequences: Berlin, Springer, p. 143–150.

BUFFINGTON, E. C., 1952, Submarine natural levees: Geology, v. 60, p. 473–479.

CARLSON, P. R., AND KARL, H.A., 1988, Development of large submarine canyons in the Bering Sea indicated by morphologic, seismic, and sedimentologic characteristics: Geological Society of America Bulletin, v. 100, p. 1594–1615.

CARTER, L., GAVEY, R., TALLING, P.J., AND LIU., J.T., 2014, Insights into submarine geohazards from breaks in subsea telecommunication cables: Oceanography, v. 27(2), p. 58–67.

CHOUGH, S., AND HESSE, R. 1976, Submarine meandering talweg and turbidity currents flowing for 4000 km in the Northwest Atlantic Mid-Ocean Channel: Geology, v. 4, p. 529–533.

CLARK, J. D., AND PICKERING, K.T., 1996, Architectural elements and growth patterns of submarine channels: application to hydrocarbon exploration: AAPG Bulletin, v. 80, p. 194–221.

CLEMENCEAU, G. R., COLBERT, J., AND EDENS, D., 2000, Production results from levee-overbank turbidite sands at Ram/Powell Field, deepwater Gulf of Mexico. *In*: P. Weimer, R. M. Slatt, J. Coleman, N. C. Rosen, H. Nelson, A. H. Bouma, M. J. Styzen, and D. T. Lawrence, eds., Deep-water reservoirs of the world: Gulf Coast Section, SEPM 20th Annual Research Conference, p. 241–251.

CUNNINGHAM, C.M., AND ARNOTT, R.W.C., 2021, Systematic organization of thin-bedded turbidites in ancient deep-marine levees: Possible evidence of rhythmic pulsing in turbidity currents: Journal of Sedimentary Research, v 91.11, p. 1257-1274.

CURRAY, J. R., EMMEL, F.J., AND MOORE, D.G., 2003, The Bengal Fan: morphology, geometry, stratigraphy, history and processes: Marine and Petroleum Geology, v. 19, p. 1191–1223.

DEPTUCK, M. E., STEFFENS, G.S., BARTON, M., PIRMEZ, C., AND MUTTI, E., 2003, Architecture and evolution of upper fan channel-belts on the Niger Delta slope and in the Arabian Sea: Marine and Petroleum Geology, v. 20, p. 649–676.

DEVRIES, M. B., AND LINDHOLM, R.M., 1994, Internal architecture of a channel-levee complex, Cerro Toro Formation, southern Chile. *In* P. Weimer, A. H. Bouma, and B. F. Perkins, eds., Submarine fans and turbidite systems: Sequence stratigraphy, reservoir architecture and production characteristics: Gulf Coast Section, SEPM 15th Annual Research Conference, p. 105–114.

DROZ, L., AND BELLAICHE, G., 1985, Rhone Deep-Sea Fan: morphostructure and growth pattern: AAPG Bulletin, v. 69, p. 460–479.

DUMOUCHEL, I.W., 2012, Effects of relative sea-level change on the stratigraphic architecture of a passive margin deep-marine channel fill complex, Windermere Supergroup, British Columbia, Canada. Unpublished B.Sc. thesis, University of Ottawa.

EMMEL, F. J., AND CURRAY, J.R., 1981a, Channel piracy on the lower Bengal Fan: Geo-Marine Letters, v. 1, p. 123–127.

EMMEL, F. J., AND CURRAY, J.R., 1981b, Dynamic events near the upper and mid-fan boundary of the Bengal Fan: Geo-Marine Letters, v. 1, p. 201–205.

EMMEL, F. J., AND CURRAY, J.R., 1984, The Bengal submarine fan, northeastern Indian Ocean: Geo-Marine Letters, v. 3, p. 119–124.

EMMEL, F. J., AND CURRAY, J.R., 1985, Bengal Fan, Indian Ocean. *In:* A. H. Bouma, W. R. Normark, and N. E. Barnes, eds., Submarine Fans and Related Turbidite Systems: New York, Springer, p. 107–112.

ESCHARD, R., E. ALBOUY, R. DESCHAMPS, T. EUZEN, A. AYUB, AND E. MUTTI, 2003, Downstream evolution of turbiditic channel complexes in the Pab Range outcrops; Maastrichtian, Pakistan: Marine and Petroleum Geology, v. 20, p. 691–710.

FILDANI, A., W. NORMARK, S. KOSTIC, AND G. PARKER, 2006, Channel formation by flow stripping: large-scale scour features along the Monterey East Channel and their relation to sediment waves: Sedimentology, v. 53, p. 1265–1287.

FISHER, R.V., 1983, Flow transformation in sediment gravity flows: Geology, v. 11, p. 273-274.

FLOOD, R. D., AND HOLLISTER, C. D., 1974, Current-controlled topography on the continental margin off the eastern United States. *In*: C. A. Burke, C. L. Drake (Eds.), The geology of Continental Margins. New York: Springer-Verlag.

Fraino, P.E., ARNOTT, R.W.C. AND NAVARRO, L., 2022, The influence of sediment supply on the stratigraphic evolution of an ancient passive margin deep-marine slope channel system,

Windermere Supergroup, British Columbia, Canada: Journal of Sedimentary Research, v. 92, p. 232-256.

GARDNER, J. V., AND KIDD, R. B., 1983, Sedimentary processes on the iberian continental-margin viewed by long-range side-can sonar: Oceanologica Acta, v. 6(3), p. 245-254.

HAMPTON, M. A., 1972, The role of subaqueous debris flows in generating turbidity currents: Journal of Sedimentary Petrology, v. 42, p. 775–793.

HANER, B. E., 1971, Morphology and sediments of Redondo submarine fan, southern California: Geological Society of America Bulletin, v. 82, p. 2413–2432.

HAY, A. E., 1987a, Turbidity currents and submarine channel formation in Rupert Inlet, British Columbia 1. Surge observations: Journal of Geophysical Research, v. 92, p. 2875–2881.

HAY, A. E., 1987b, Turbidity currents and submarine channel formation in Rupert Inlet, British Columbia 2. The roles of continuous and surge-type flow: Journal of Geophysical Research, v. 92, p. 2883–2900.

HEEZEN, B. C., HOLLISTER, C. D., AND RUDDIMAN, W. F., 1966, Shaping of the continental rise by deep geostrophic contour currents: Science, v. 152, p. 502-508.

HAY, A. E., J. W. MURRAY, AND R. W. BURLING, 1983, Submarine channels in Rupert Inlet, British Columbia: I. morphology: Sedimentary Geology, v. 36, p. 289–315.

HESSE, R., AND S. CHOUGH, 1980, The Northwest Atlantic Mid-Ocean Channel of the Labrador Sea: II. Deposition of parallel laminated levee-muds from the viscous sublayer of low-density turbidity currents: Sedimentology, v. 27, p. 697–711.

HISCOTT, R. N., F. R. HALL, AND C. PIRMEZ, 1997, Turbidity-current overspill from the Amazon Channel; texture of the silt/sand load, paleoflow from anisotropy of magnetic susceptibility and implications for flow processes: Proceedings of the Ocean Drilling Program, Scientific Results, v. 155, p. 53–78.

KANE, I. A., B. C. KNELLER, M. DYKSTRA, A. KASSEM, AND W. D. MCCAFFREY, 2007, Anatomy of a submarine channel-levee: An example from Upper Cretaceous slope sediments, Rosario Formation, Baja California, Mexico: Marine and Petroleum Geology, v. 24, p. 540–563.

KANE, I. A., AND D. M. HODGSON, 2011, Sedimentological criteria to differentiate submarine channel levee subenvironments: Exhumed examples from the Rosario Fm. (Upper Cretaceous) of Baja California, Mexico, and the Fort Brown Fm. (Permian), Karoo Basin, S. Africa Marine and Petroleum Geology, v. 28, p. 807–823.

KASTENS, K. A., AND A. N. SHOR, 1985, Depositional processes of a meandering channel on Mississippi Fan: AAPG Bulletin, v. 69, p. 190–202.

KASTENS, K. A., AND A. N. SHOR, 1986, Evolution of a channel meander on the Mississippi Deep-Sea Fan: AAPG Bulletin, v. 71, p. 165–175.

KHAN, Z. 2012. Origin and architecture of deep-water level deposits: Insight from the ancient rock record and experiments. Unpublished Ph.D. thesis, University of Ottawa, Ottawa, ON.

KHAN, Z. A., AND R. W. C. ARNOTT, 2011, Stratal attributes and evolution of asymmetric inner and outer-bend levee deposits associated with an ancient deep-water channel-levee complex within the Isaac Formation, southern Canada: Marine and Petroleum Geology, v. 28, p. 824–842.

KHAN, Z. A., R. W. C. ARNOTT, AND A. PUGIN, 2011, An alternative model of producing topography in the crest region of deep-water levees: AAPG Bulletin, v. 95, p. 2085–2106.

KNELLER, B. C., 2003, The influence of flow parameters on turbidite channel slope architecture: Marine and Petroleum Geology, v. 20, p. 901–910.

KNELLER, B., AND BUCKEE, C., 2000, The structure and fluid mechanics of turbidity currents: a review of some recent studies and their geological implications: Sedimentology, v. 47, v. 1, p. 62–94.

KOLLA, V., AND COUMES, F., 1984, Morpho-acoustic and sedimentologic characteristics of the Indus Fan: Geo-Marine Letters, v. 3, p. 133–139.

KOLLA, V., AND COUMES, F., 1987, Morphology, internal structure, seismic stratigraphy and sedimentation of Indus Fan: AAPG Bulletin, v. 71, p. 650–677.

LEIGH, S., AND HARTLEY, A. J., 1992, Mega-debris flow deposits from the Oligo-Miocene Pindos foreland basin, western mainland Greece: implications for transport mechanisms in ancient deep marine basins. Sedimentology, v. 39, p. 1003-1012.

LOWE, D. R., 1982, Sediment gravity flows: II. depositional models with special reference to the deposits of high-density turbidity currents: Journal of Sedimentary Petrology, v. 52, p. 279–297.

MEIBURG, E., & KNELLER, B., 2010, Turbidity currents and their deposits: Annual Review of Fluid Mechanics, v. 42, p. 135-156.

MENARD, H.W., 1955, Deep-sea channels, topography, and sedimentation: AAPG Bulletin, v. 39, p. 236–255.

MIDDLETON, G.V., AND HAMPTON, M.A., 1973, Sediment gravity flows: mechanics of flow and Deposition. *In:* G. V., Middleton, A. H., Bouma, Eds., Turbidites and Deep-water Sedimentation: SEPM Pacific section Short Course, Anaheim, California, p. 1–38.

MOHRIG, D., ELLIS, C., PARKER, G., WHIPPLE, K. X., & HONDZO, M., 1998, Hydroplaning of subaqueous debris flows: Geological Society of America Bulletin, v. 110, p. 387-394.

MORRIS, E. A., HODGSON, D. M., BRUNT, R. L., AND FLINT, S. S., 2014, Origin, evolution and anatomy of silt-prone submarine external levées: Sedimentology, v.61(6), p. 1734-1763.

MULDER, T., AND ALEXANDER, J., 2001, The physical character of subaqueous sedimentary density flows and their deposits: Sedimentology, v. 48, p. 269-299.

MUTTI, E., AND NORMARK, W.R., 1987, Comparing examples of modern and ancient turbidite systems: problems and concepts, *in* J. R. Leggett, and G. G. Zuffa, eds., Marine Clastic Sedimentology: Concepts and Case Studies: London, Graham and Trotman, p. 1–37.

MUTTI, E., AND NORMARK, W.R., 1991, An integrated approach to the study of turbidite Systems. *In:* P. Weimer, and M. H. Link, eds., Seismic facies and sedimentary processes of submarine fans and turbidite systems: New York, Springer-Verlag, p. 75–106.

NARDIN, T. R., HEIN, F. J., GORSLINE, D. S., AND EDWARDS, B. D., 1979, A review of mass movement processes, sediment and acoustic characteristics and contrasts in slope and base-of-slope systems versus canyon-fan-basin-floor basins. *In:* L. J. Doyle, and O. H. Pilkey (Eds.), Geology of Continental Slopes. Society of Economic Paleontologists and Mineralogists, Special Publication, v. 27, p. 61–73.

NAVARRO, L., 2016, Stratigraphic architecture depositional processes and reservoir implications of the basin floor to slope transition, Neoproterozoic Windermere turbidite system, Canada. Unpublished Ph.D. thesis, University of Ottawa, Ottawa, ON.

NICHOLS, G., 2009, Sedimentology and Stratigraphy, 2nd Edition: Blackwell, Oxford, 411 p.

NORMARK, W. R., 1970, Growth Patterns of Deep-Sea Fans: AAPG Bulletin, v. 54, p. 2170–2195.

PEAKALL, J., W. D. MCCAFFREY, AND B. C. KNELLER, 2000, A process model for the evolution, morphology, and architecture of sinuous submarine channels: Journal of Sedimentary Research, v. 70, p. 434–448.

PICKERING, K. T., J. COLEMAN, M. CREMER, L. DROZ, B. KOHL, W. NORMARK, S. O'CONNELL, D. STOW, AND A. MEYER-WRIGHT, 1986, A high sinuosity, laterally migrating submarine fan channel–levee-overbank: results from DSDP Leg 96 on the Mississippi Fan, Gulf of Mexico: Marine and Petroleum Geology, v. 3, p. 3–18.

PIPER, D. J. W., AND W. R. NORMARK, 1983, Turbidite depositional patterns and flow characteristics, Navy submarine fan, California Borderland: Sedimentology, v. 30, p. 681–694.

PIPER, D. J. W., AND W. R. NORMARK, 2001, Sandy fans; from Amazon to Hueneme and beyond: AAPG Bulletin, v. 85, p. 1407–1438.

PIRMEZ, C., R. N. HISCOTT, AND J. D. KRONEN, JR., 1997, Sandy turbidite successions at the base of channel-levee systems of the Amazon Fan revealed by FMS logs and cores; unraveling the facies architecture of large submarine fans: Proceedings of the Ocean Drilling Program, Scientific Results, v. 155, p. 7–33.

PIRMEZ, C., R. T. BEAUBOUEF, S. J. FRIEDMANN, AND D. C. MOHRIG, 2000, Equilibrium profile and baselevel in submarine channels; examples from late Pleistocene systems and implications for the architecture of deepwater reservoirs. *In:* P. Weimer, R. M. Slatt, J. Coleman, N. C. Rosen, H. Nelson, A. H. Bouma, M. J. Styzen, and D. T. Lawrence, eds., Deep-water reservoirs of the world: Gulf Coast Section, SEPM 20th Annual Research Conference, p. 782–805.

POSAMENTIER, H. W., 2003, Depositional elements associated with a basin floor channel-levee system: case study from the Gulf of Mexico: Marine and Petroleum Geology, v. 20, p. 677–690.

POSAMENTIER, H. W., AND KOLLA, V., 2003, Seismic geomorphology and stratigraphy of depositional elements in deep-water settings: Journal of Sedimentary Research, v. 73, p. 367–388.

READING, H. G., 1996, Sedimentary Environments: process, facies and stratigraphy: Cambridge, Blackwell Science, 688 p.

READING, H. G., AND RICHARDS, M., 1994, Turbidite systems in deep-water basin margins classified by grain size and feeder system: AAPG Bulletin, v. 78, p. 792–822.

RODINE, J. D., AND JOHNSON, A. M., 1976, The ability of debris, heavily freighted with coarse clastic materials, to flow on gentle slopes: Sedimentology, v. 23(2), p. 213-234.

SAMUEL, A., B. KNELLER, S. RASLAN, A. SHARP, AND C. PARSONS, 2003, Prolific deep-marine slope channels of the Nile Delta, Egypt: AAPG Bulletin, v. 87, p. 541–560.

SHANMUGAM, G., 1996, High-density turbidity currents: are they sandy debris flows?: Journal of Sedimentary Research, v. 66, p. 2-10.

SHANMUGAM, G., 1997, The Bouma sequence and the turbidite mind set: Earth-Science Reviews, v. 42, p. 201-229.

SHANMUGAM, G., 2000, 50 years of the turbidite paradigm (1950s–1990s): deep-water processes and facies models – a critical perspective: Marine and Petroleum Geology, v. 17, p. 285–342.

SHANMUGAM, G., 2006, Deep-water processes and facies models: Implications for sandstone petroleum reservoirs: New York, Elsevier, 476 p.

SHANMUGAM, G., 2017, The contourite problem. *In*: Sediment provenance (pp. 183-254). Elsevier.

SHANMUGAM, G., LEHTONEN, L. R., STRAUME, T., SYVERTSEN, S. E., HODGKINSON, R. J., AND SKIBELI, M., 1994, Slump and debris-flow dominated upper slope facies in the Cretaceous of the Norwegian and northern North Seas (61-67 N): Implications for sand distribution: AAPG bulletin, v. 78(6), p. 910-937.

SHEPARD, F. P., 1973, Submarine geology: New York, Harper & Row Publishers, 517 p.

SHEPARD, F. P., AND R. F. DILL, 1966, Submarine canyons and other sea valleys: Chicago, Rand McNally & Co., 382 p.

SKENE, K. I., D. J. W. PIPER, AND P. S. HILL, 2002, Quantitative analysis of variations in depositional sequence thickness from submarine channel levees: Sedimentology, v. 49, p. 1411–1430.

STOW, D. A. V., 1979, Distinguishing between fine-grained turbidites and contourites off Nova Scotia: Sedimentology, p. 371–387.

STOW, D. A. V., AND A. J. BOWEN, 1980, A physical model for the transport and sorting of fine-grained sediment by turbidity currents: Sedimentology, v. 27, p. 31–46.

STOW, D. A. V., AND M. MAYALL, 2000, Deep-water sedimentary systems: new models for the 21st century: Marine and Petroleum Geology, v. 17, p. 125–135.

STOW, D. A., AND PIPER, D. J., 1984, Deep-water fine-grained sediments: facies models: Geological Society of London, Special Publications, v. 15, p. 611-646.

STOW, D. A., FAUGÈRES, J. C., VIANA, A., AND GONTHIER, E., 1998, Fossil contourites: a critical review: Sedimentary Geology, v. 115, p. 3-31.

TALLING, P. J., 2014, On the triggers, resulting flow types and frequencies of subaqueous sediment density flows in different settings: Marine Geology, v. 352, p. 155-182.

TALLING, P. J., D. G. MASSON, E. J. SUMNET, AND G. MALGESINI, 2012, Subaqueous sediment density flows: Depositional processes and deposit types: Sedimentology, v. 59, p. 1937-2003.

TILSTON, M., ARNOTT, R.W.C., RENNIE, C.D., AND LONG, B., 2015, The influence of grain size on the velocity and sediment concentration profiles and depositional record of turbidity currents: Geology, v. 43, p. 839-842.

TORRES, J., L. DROZ, B. SAVOYE, E. TERENTIEVA, P. COCHONAT, N. H. KENYON, AND M. CANALS, 1997, Deep-sea avulsion and morphosedimentary evolution of the Rhone Fan Valley and Neofan during the Late Quaternary (north-western Mediterranean Sea): Sedimentology, v. 44, p. 457–477.

VAN WEERING, T. C., NIELSEN, T., KENYON, N. H., AKENTIEVA, K., AND KUIJPERS, A. H., 1998, Large submarine slides on the NE Faeroe continental margin: Geological Society of London, Special Publications, v. 129(1), p. 5-17.

WALKER, R. G., 1985, Mudstones and thin-bedded turbidites associated with the Upper Cretaceous Wheeler Gorge conglomerates, California; a possible channel-levee complex: Journal of Sedimentary Petrology, v. 55, p. 279–290.

WEIRICH, F.H., 1988, Field evidence for hydraulic jumps in subaqueous sediment gravity flows: Nature, v. 332, p. 626-629

WYNN, R. B., B. T. CRONIN, AND J. PEAKALL, 2007, Sinuous deep-water channels: Genesis, geometry and architecture: Marine and Petroleum Geology, v. 24, p. 341–387.

Chapter 3: Systematic Organization of Thin-bedded Turbidites in Ancient Deep-marine Levees: Possible Evidence of Rhythmic Pulsing in Turbidity Currents

3.1 Introduction

Channel-levee slope complexes are prominent features in deep marine turbidite systems, but to date considerably more research has been devoted to the channels compared to the adjacent levees. In part this disparity can be attributed to the comparative economic importance of channel strata as hydrocarbon reservoirs, but also the generally fine-grained nature of levee deposits and hence their typically poor exposure in the ancient rock record, or one-dimensionality and widely spaced control in subsurface cores, which collectively makes deciphering the stratigraphic architecture and interpreting the formative processes problematic. Similarly, various seismic techniques are unable to resolve centimetric stratigraphic details in stratigraphic intervals of substantial thickness, and as a result these sub-seismic-scale attributes to the larger-scale depositional evolution of levee deposits remain poorly known.

Deep-marine levees are areally extensive and volumetrically significant stratal elements that experience less erosion and bypass compared to the adjacent channels, and, therefore, preserve a more or less continuous record of sedimentation. Many previous studies that have examined levee systems in modern (e.g., Prior et al. 1983; Damuth et al. 1988; Hiscott et al. 1997; Piper et al. 1999; Skene et al. 2002; Deptuck et al. 2003; Babonneau et al. 2004; Wynn et al. 2007) and ancient (e.g. Hesse and Dalton 1995; Beaubouef 2004; Hodgson et al. 2011; Englert et al. 2018) systems have focused on identifying and classifying large-scale architectural elements and levee morphology in order to better understand the entire channel-levee system, and/or improving hydrocarbon reservoir modelling (e.g., Clemenceau et al. 2000; Kendrick

2000; Weimer et al. 2000). These studies have clearly shown that deep-marine levee deposits exhibit a characteristic gull-wing or wedge-shaped morphology related to turbidity-current overspill from the adjacent channel, augmented locally by flow stripping (Piper and Normark 1983) and inertial run-up (Hay 1987a, 1987b; Straub et al. 2008), that builds positive (depositional) topography and serves to confine subsequent flows (Clark and Pickering 1996; Kane and Hodgson 2011; Posamentier and Kolla 2003).

In contrast, a much smaller number of studies (e.g., Kane et al. 2007; Kane and Hodgson 2011; Khan and Arnott 2011; Khan et al. 2011; Hansen et al. 2015; Hansen et al. 2017, Bergen et al. 2022) have described levees at the bed-by-bed scale, but it is this level of detail that is needed to understand flow processes not only in overbank environments, but anywhere along the whole transport system. In general, these studies have shown that irrespective of the overspilling process, or combination thereof, once detached from the dense channelized part of the flow, the more dilute overspill rapidly wanes and deposits its coarsest grained sediment immediately adjacent to the channel followed by a reduction in both sedimentation rate and grain size. In addition, systematic decameter-thick, upward-thinning and/or -thickening trends have been documented (e.g., Walker 1985; Hiscott et al. 1997; Manley et al. 1997; Normark and Damuth 1997; Cronin et al. 2000; Beaubouef 2004; Kane et al. 2007; Khan and Arnott 2011; Khan et al. 2011; Bergen et al. 2022) and related to autogenic processes, such as increases or decreases in the height of the levee crest versus some aspect of the channelized flow, or allogenic processes, like the increase or decrease in the magnitude and/or frequency of flows with time. However, irrespective of the interpreted influence and comparative importance of various intrinsic and extrinsic sedimentological variables, it is generally assumed that each turbidite correlates with deposition from a single channelized flow event (e.g., Bouma 1962; Walker 1965; Middleton and

Hampton 1973, 1976). Here, however, we attempt to provide a more detailed understanding of deposition associated with single and successive flow events by describing the systematic organization of decameter- to meter-scale sharp-based bedsets composed of multiple self-similar beds in well exposed ancient levee deposits in the Neoproterozoic Windermere Supergroup. Significantly, the data presented challenge the notion of the one-bed, one-flow-event model, and in turn the interpretation of per-event sedimentation and event frequency in parts of the deep-marine sedimentary record, prompting a re-evaluation of some common assumptions regarding deep-marine sedimentation patterns.

3.2 Geological Setting

3.2.1 Geological Background

The Neoproterozoic Windermere Supergroup (WSG) is an unconformity-bounded succession of mostly metasedimentary rocks deposited on the passive continental margin of Laurentia (ancestral North America) during the breakup of the supercontinent Rodinia (Fig. 1B). In outcrop the WSG forms a linear belt that stretches from northwestern Mexico through the western United States and Canada and northward to the Yukon-Alaska border (Ross and Arnott 2007) (Fig. 1B). In the southern Canadian Cordillera (SCC) rocks of the WSG are particularly well exposed and form a succession that ranges up to about 7 – 9 km thick. The base of the succession consists of a few-kilometer-thick assemblage of intercalated glacial diamictites and mafic volcanics related to an early phase of continental rifting. This is then overlain by a 5 – 7-km-thick post-rift succession, which in ascending stratigraphic order consists of deep-marine basin floor (Kaza Group), continental slope (Isaac Formation), to upper continental slope and shelf (Cunningham and Yankee Belle formations) deposits (Campbell et al. 1973) representing

progradation of the Laurentian continent margin into the thermally subsiding proto-Pacific Ocean (Ross and Arnott 2007). Due to a paucity of datable markers and absence of macroscopic fossils, age control of the WSG in the SCC is generally poor and largely constrained by radiometric dates from rocks below and above its bounding unconformities, respectively, 736-728 Ma (Evenchick et al. 1984; McDonough and Parrish 1991; Eyster et al. 2018) and 570 ± 5 Ma (Colpron, et al. 2002). Dates in the Windermere sedimentary pile are confined to a single Re-Os isochron date of 607.8 +/- 4.7 Ma from organic rich mudrocks of the Geike Siding Member, Old Fort Point Formation (Kendall et al. 2004; Smith et al. 2014), and the interpreted correlation of a mixed carbonate-siliciclastic succession with deposition immediately before the Gaskiers glaciation at 580 Ma (Cochrane et al. 2019). Later, during the Mesozoic to early Cenozoic, collision and accretion of allochthonous terranes along the western margin of Laurentia formed the Canadian Cordillera, which incorporated rocks of the WSG into the Omineca orogenic belt of the southern Canadian Cordillera that locally underwent multiple phases of deformation and low-grade regional metamorphism (Price 2000; Reid et al. 2002).

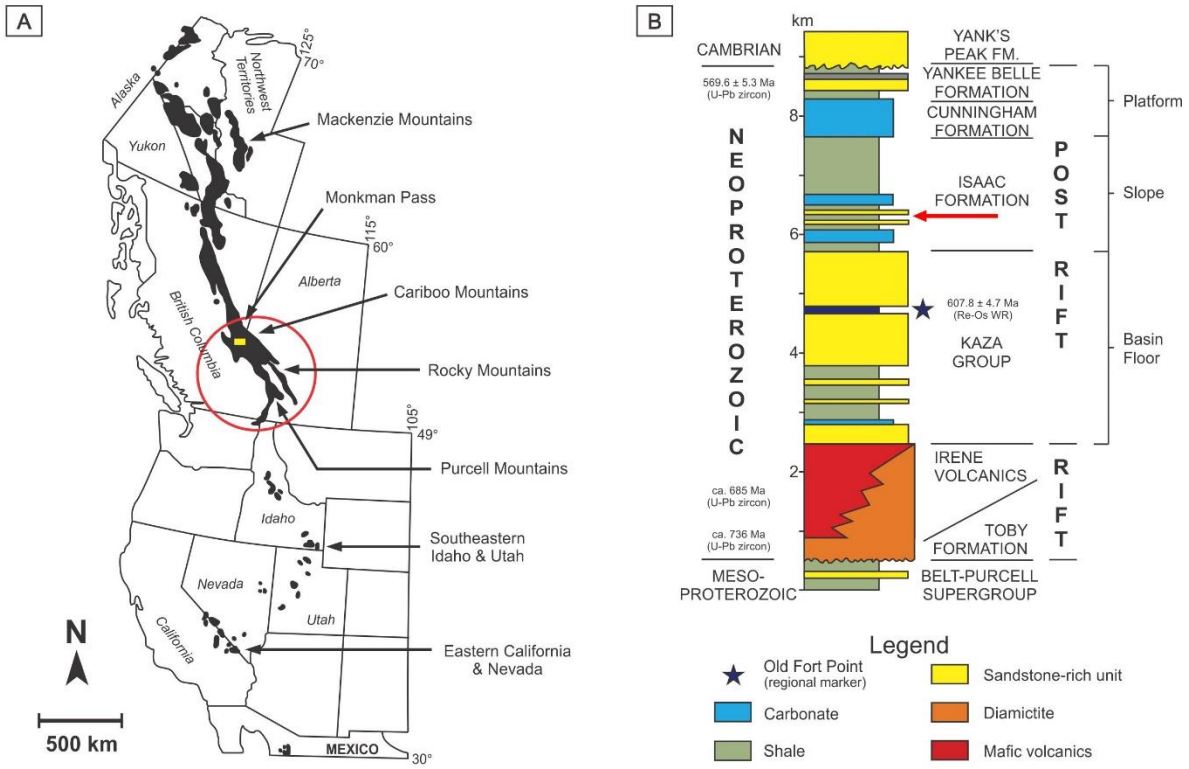

Figure 3.1. *A) Distribution of exposed rocks of the Windermere Supergroup (black polygons) in western North America – a linear belt that extends for approximately 4000 km along strike. Red circle indicates deep-marine strata of the Windermere turbidite system cropping out in the southern Canadian Cordillera; yellow rectangle indicates the location of the Castle Creek study area. B) Regional stratigraphy of the WSG, southern Canadian Cordillera (Khan 2012). Rocks exposed at the Castle Creek study area consist of basin-floor strata of the Upper Kaza Group overlain conformably by slope deposits of the Isaac Formation. Red arrow indicates the location of strata described here.*

3.2.2 Study Area

At the Castle Creek study area (Cariboo Mountains, east-central British Columbia, Canada), continental-slope strata of the Isaac Formation gradationally overlie basin-floor deposits of the Upper Kaza Group and together form a superbly well-exposed section approximately 2.6 km thick and up to 8 km wide (Terlaky et al. 2016; Navarro and Arnott 2020). Bedding is nearly vertical due to its location on the upright limb of a regionally extensive, southwest-verging

anticline (Ross and Arnott 2007) and despite lower-greenschist-facies metamorphism, but also the absence of the disruptive effects of bioturbation, primary sedimentary structures and textures are exceptionally well-preserved. Additionally, the ongoing retreat of the Castle Creek glacier has resulted in a glacially polished, vegetation-free outcrop that allows layers, even down to centimeter thick, to be easily measured vertically but more significantly traced continuously along strike for several hundreds of meters.

3.2.3 Previous Work

The Isaac Formation comprises at least seven laterally discontinuous, coarse-grained sandstone and conglomerate units that range up to over 200 m in thickness. These strata are interpreted to be slope-channel complexes bounded by finer-grained, genetically related levees (Fig. 2). Previous work on levee deposits at Castle Creek has identified seven discrete levee units associated with two channel complexes and documented their stratigraphic architecture in detail (Navarro et al. 2007; Khan and Arnott 2011; Khan et al. 2011; Bergen 2017; Bergen et al. 2022).

Both Isaac Channel 3 and Isaac Channel 4.2 are bounded by finer-grained strata that have previously been interpreted to be genetically related levee deposits (Fig. 3) (Navarro et al. 2007; Khan and Arnott 2011; Khan et al. 20011; Bergen 2017; Bergen et al. 2022). Isaac Channel 3 is up to 90 m thick and 1.6 km wide and consists mostly of aggradationally filled channel-fill units that laterally offset-stack toward the northwest (Navarro et al. 2007). Each channel unit comprises multiple channel fills that consist principally of erosionally-based, thick-bedded, structureless, coarse-grained sandstone that fine and thin upward to medium-bedded, medium-grained sandstone. Each channel unit is bounded on both sides by genetically related levee deposits. There are three outer-bend levee units associated with Isaac Channel 3 (Khan et al. 2011; Khan and

Arnott 2011). Proximal levee deposits are in contact with channel-fill deposits and are relatively sand-rich. Grain size and bed thickness of levee strata decrease away from the channel over hundreds of meters laterally, resulting in a wedge-shaped geometry as the levee succession thins. Away from the channel unit margins, the outer-bend levee succession thins from 100 m to 60 m over ~ 2 km, compared with thinning from 40 m to 20 m over a distance of 600 m for the inner-bend levee succession.

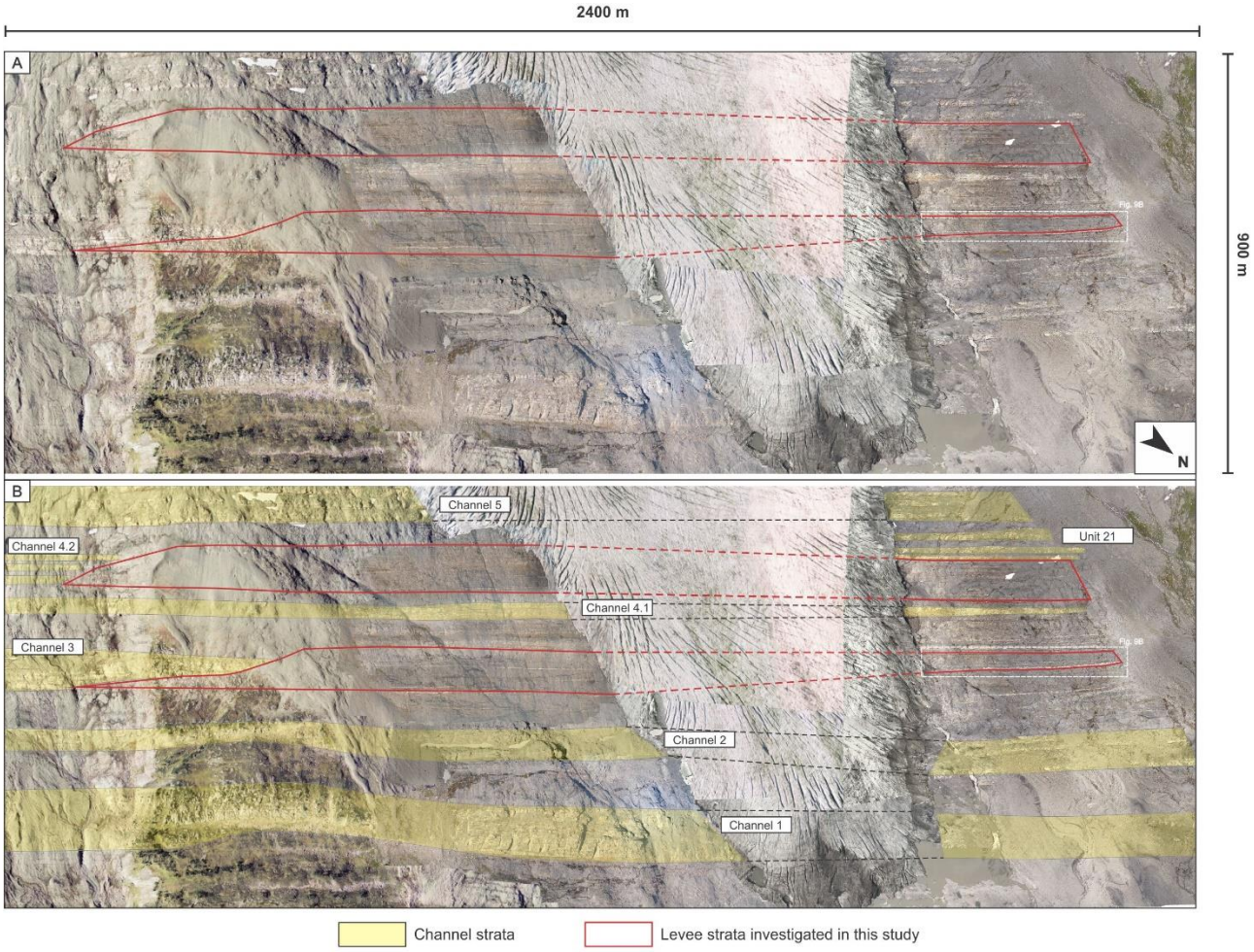

Figure 3.2. *A) Uninterpreted photomosaic showing slope deposits of the Isaac Formation in part of the Castle Creek study area. Note that stratigraphy is vertically dipping. Levee deposits analyzed in this study are highlighted in red boxes. Dashed white box indicates location of Figure 9B. B) Interpreted photomosaic showing the distribution of slope channel and associated levee deposits.*

Similar to Isaac Channel 3, Isaac Channel 4.2 comprises at least three channel-fill units that laterally offset-stack towards the northwest. The exposed part of Isaac Channel 4.2 is 85 m thick and 860 m wide, and strata consist principally of amalgamated, medium- to thick-bedded, massive or graded coarse- to medium-grained sandstone (Bergen 2017; Bergen et al. 2022). Levee deposits are exposed only on one side of the four stacked units and terminate abruptly against the coarser-grained channel-fill deposits in one direction but in the opposite direction extend for over 1.5 km along-strike, where they thin from 130 m to 90 m (Bergen 2017; Bergen et al. 2022). Paleoflow data measured in levee strata associated with Isaac Channels 3 and 4.2 indicate that the overspilling flows were directed towards the northwest (mean paleoflow from 30 measurements = 305°), and therefore at a high angle to paleoflow direction in the adjacent channel fill. For further details on channel and levee sedimentology and stratigraphic architecture see Navarro et al. (2007), Khan et al. (2011), and Khan and Arnott (2011) for Isaac Channel Complex 3, and Bergen (2017) and Bergen et al. (2022) for Isaac Channel Complex 4.2.

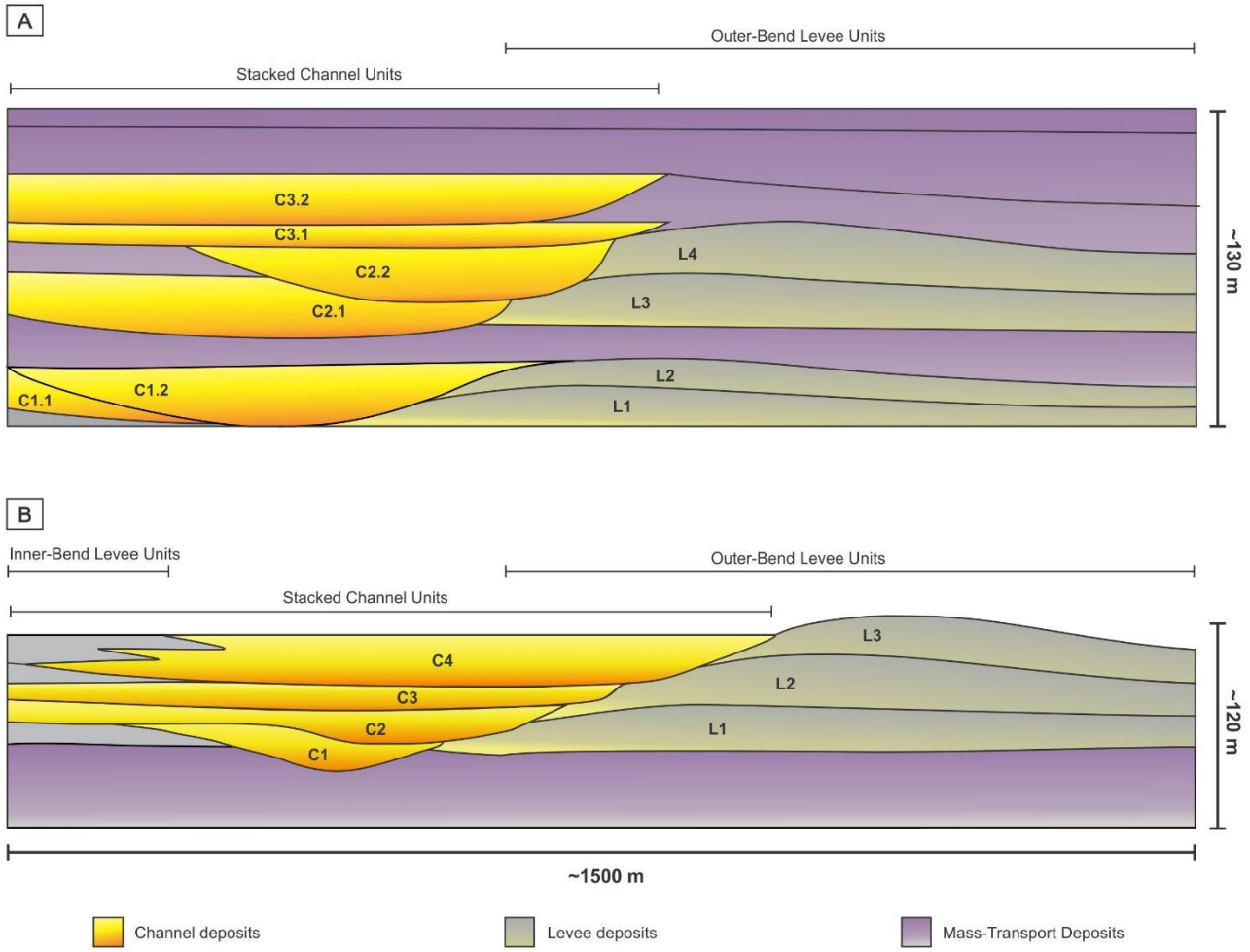

Figure 3.3. *A) Schematic illustrating the generalized stratigraphy of Isaac Channel Complex 4.2 and associated levees (modified from Bergen et al. 2022). Channel units are labelled C1 – C3, with individual channel fills designated 1.1, 1.2, etc. Levee units are numbered L1 – L4. Note the common intercalated mass-transport complexes. B) Schematic illustrating the generalized stratigraphy of Isaac Channel Complex 3 that consists of channel units C1 – C4, and associated levee units L1 – L3 (modified from Navarro et al. 2007).*

3.3 Methods and Terminology

3.3.1 Methods

Results presented here are based on observations of levee units from four sites in the Castle Creek study area, encompassing over 250 m of stratigraphy vertically and ~ 2 km along strike (Fig. 2). Deposits are associated with two different Isaac channel complexes and include

both channel-proximal and channel-distal deposits. Levee deposits were measured in bed-by-bed (cm-scale) detail; each bed was then traced physically along strike for 400 – 500 m and supplemented with high-resolution aerial drone photos. Lateral spacing between stratigraphic logs ranged from 40 to 70 m.

3.3.2 Terminology

For clarity, a summary of the terminology that is used in this paper is first outlined. Descriptions of bed thickness are given using the classification scheme of Ingram (1954): very thick-bedded (> 100 cm), thick-bedded (30 – 100 cm), medium-bedded (10 – 30 cm), thin-bedded (3 – 10 cm), and very thin-bedded (1 – 3 cm). Grain sizes are categorized using the Wentworth grain-size classification scale (Wentworth, 1922).

Turbidites are described according to the terminology of Bouma (1962) and are divided into the five divisions that make up the Bouma Sequence:

T_a: poorly sorted, structureless sandstone, often with a scoured base. The term *structureless* describes strata that lack evidence of traction-transport deposition (see discussion of traction transport below)

T_b: planar-laminated sandstone, typically finer-grained than the Ta division

T_c: ripple cross-laminated sandstone, finer-grained than T_b

T_d: silt, often planar-laminated

T_e: pelagic and hemipelagic mud

Collectively, these divisions record the progressive waning of the turbidity current that deposited them. It is important to note that turbidites rarely contain all five divisions and instead typically comprise only part of this sequence. *Lower division* turbidites consist of the bottom two Bouma divisions (T_a and T_b), whereas *upper division* turbidites comprise only the upper two or three divisions (T_c, T_d, and T_e).

The term *bedset* is used to describe a conformable succession of genetically related beds. A *flow event* refers to a single channelized turbidity current travelling downslope. A *depositional episode* is a discrete period of deposition associated with a single flow event. Because deposition can occur in one or more locations, but at different times during a flow event, there may be multiple depositional episodes associated with a single flow event. An *event deposit* refers to the cumulative sediment deposited from a flow event at any one location and includes the deposit(s) of one or more depositional episodes.

3.4 Results

3.4.1 Facies

Levee deposits in the Isaac Formation comprise three facies: (F1) very thin- to medium-bedded upper-division turbidites, (F2) medium- to very thick-bedded lower-division turbidites, and (F3) mass-transport deposits. Due to the difficulty of differentiating T_d from T_e divisions in the field, both are considered here as a single $T_{d/e}$ division. Levee deposits are dominated by strata of F1 and F2, which collectively constitute 90% of the measured stratigraphy, and are described in more detail below. The percent occurrence of complete and partial classical Bouma turbidites in F1 and F2 strata is summarized in Table 3.1.

3.4.1.1 Facies 1: Very Thin- to Medium-Bedded Upper-Division Turbidites

Facies 1 (F1) beds dominate levee strata and constitute 68% of the measured stratigraphy in this study. Beds range in thickness from < 1 – 28 cm but generally are 2 – 15 cm thick and consist of $T_{cd/e}$ and $T_{d/e}$ turbidites. Basal contacts are typically sharp and planar, but small-scale load and flame structures are common. Grain size in the basal T_c part of these beds typically ranges from very fine to fine sand with common dispersed grains of medium and rare coarse sand in thicker beds. T_c divisions are then overlain either gradationally or more commonly abruptly by siltstone and mudstone of the $T_{d/e}$ division. T_c divisions range from < 1 – 20 cm thick and contain 1 – 10 sets of ripple cross-lamination that in the field typically show very low to no detectible angle of climb. $T_{cd/e}$ turbidites can be subdivided into three types based on the number and type of component sets of ripple cross-lamination: (1) multi-set, (2) single-set, and (3) starved (Fig. 4); each is described next. Where present, $T_{d/e}$ divisions range from 0.1 to 8 cm thick and are either thinly laminated or massive. Where laminated, layers consist of alternating < 1 – 3 mm thick, parallel bands of light-gray coarse siltstone or clayey siltstone and dark gray or black bands of fine siltstone, claystone, or silty claystone. In thicker beds, the basal part of the $T_{d/e}$ division commonly contains plane parallel or wavy-stratified very fine sandstone and coarse siltstone (laminae are 0.1 – 0.8 cm thick) that grade upwards into the laminated siltstone and mudstone described above.

Bouma divisions	Percent occurrence
$T_{abcd/e}$	2%
$T_{abd/e}$	< 0.5%
$T_{acd/e}$	< 0.5%
$T_{ad/e}$	2%
$T_{bcd/e}$	16%
$T_{bd/e}$	4%
$T_{cd/e}$	69%
$T_{d/e}$	6%

Table 3.1: *Percent occurrence of complete and partial classical Bouma turbidites in F1 and F2 strata. Percentage refers to the total number of beds counted (n = 4200).*

Multiple Set - Beds composed of multiple sets of ripple cross-lamination are thin- to medium-bedded. Bed thickness ranges from 2 to 28 cm with an average thickness of 10 cm. The thickness of the lower sandstone part in these beds is directly related to the number of component sets of ripple cross-lamination (i.e., cosets with more sets of ripple cross-lamination are typically thicker). Coset thickness ranges from 1 to 20 cm, with an average thickness of 5 cm. Multi-set ripple cross-laminated beds are composed of 2 – 10 ripple sets, but most commonly 2 – 4 sets with individual sets being 0.5 – 5 cm thick and usually separated by a thin (< 1 cm) silt drape. Fading ripple cross-lamination (*sensu* Jopling and Walker 1968; Stow and Shanmugan 1980) is rare but where observed typically form the uppermost set. Multi-set ripple cross-laminated beds are observed in both channel-proximal and channel-distal levee deposits, but generally are thicker and more common in channel-proximal regions – average bed thickness is 11.5 cm in proximal levees (T_c part is 6 cm) compared to 9 cm in distal levees (T_c part is 4 cm). Multi-set ripple cross-laminated sandstone consists of moderately well-sorted, fine to medium sand, and uncommonly very fine- or coarse-grained sand. Typically, this is then overlain by laminated or massive siltstone and mudstone, or commonly by plane parallel- or wavy-stratified very fine to fine sand and silt that then grades upward to laminated silt. On average the thickness of the

lower T_c and upper $T_{d/e}$ parts of individual beds is subequal, specifically 55% versus 45%, although where there is a disparity the sandstone is typically thicker and can make up to 95% of the total bed thickness.

Single Set - Beds consisting of a single set of ripple cross-lamination range from 1 to 17 cm thick (average of 5 cm). Sets range from 0.5 to 4 cm thick and consist of moderately well-sorted, fine-grained sandstone, although sets of very fine- and medium-grained sandstone are common, and coarse-grained sandstone is rare. Like beds of multi-set ripple cross-laminated sandstone, single-set ripple cross-laminated beds are usually overlain by parallel stratified, very fine-grained sandstone and siltstone that drapes the underlying ripple formset, and in turn is overlain by laminated or massive siltstone and mudstone ($T_{d/e}$). The lower sandstone (T_c) part of single-set ripple cross-laminated beds typically constitutes only about one third of the total bed thickness, with the rest made up of the overlying siltstone part ($T_{d/e}$). In both channel-proximal and channel-distal levee deposits, single-set ripple cross-laminated beds are of similar abundance, with average bed thickness and sandstone content equal to 5.2 cm (sandstone part 1.7 cm), and 4.7 cm (sandstone part 1.5 cm), respectively.

Starved Set - Starved-ripple sets consist of laterally discontinuous single-ripple-formset trains that lack discernible internal cross-stratification and have crests typically spaced 1 – 8 cm apart (see also Shanmugam et al. 1993; Kane et al. 2007; Barton et al. 2010). Strata are well-sorted and consist of very fine- to fine-grained sandstone, but rarely are composed of medium-grained sandstone. Starved-ripple sets range in thickness from 0.1 to 2 cm (0.6 cm average) and are overlain by a thick siltstone cap. Beds range from 0.5 to 10 cm (3.2 cm average) thick, with the lower sandstone part (T_c) making up about 24% of the bed thickness. Additionally, although starved ripples occur in both channel-proximal and channel-distal levee deposits, they are more

common but thinner in distal levees – in proximal levees average bed thickness is 4.1 cm and sets are 0.7 cm thick, compared to 2.2 cm thick with 0.5-cm-thick sets in distal deposits.

Interpretation: Very thin- to medium-bedded upper division turbidites of F1 are interpreted to represent incomplete Bouma sequences deposited from the more dilute, finer-grained upper part of turbidity currents that overspilled the adjacent channel and decelerated (Walker, 1965; Allen, 1970; Middleton and Hampton, 1976; Lowe, 1982). These strata would form both from larger flows when levee relief was high, and from small flows when channel relief was low. The lack of erosional basal contacts indicates that these flows became depositional immediately upon overspilling the channel margins (e.g., Khan and Arnott 2010), although the typical lack of an appreciable angle of ripple-cross-lamination climb suggests that sedimentation rates were never high (Walker, 1985). Multi-set ripple cross-laminated sandstones were likely to have been deposited by sustained, sand-rich flows that experienced only low to moderate rates of sediment fallout and related bed aggradation (Khan, 2012). Turbidity currents that deposited single-set ripple cross-lamination were probably little different hydraulically, but net sedimentation rate was reduced to zero with general transport bypass and bed-surface reworking (Shanmugam et al. 1993). In contrast, starved ripples were probably deposited by very dilute flows with even lower rates of sediment fallout (Stanley 1993). The apparent lack of internal cross-stratification is likely a consequence of the very well-sorted nature of the sediment, which in the field makes the sediment appear massive. The upward transition from ripple cross-stratified sandstone to laminated sandstone and mudstone in all ripple types records flow deceleration and associated decrease in flow competence (Walker 1965; Komar 1985).

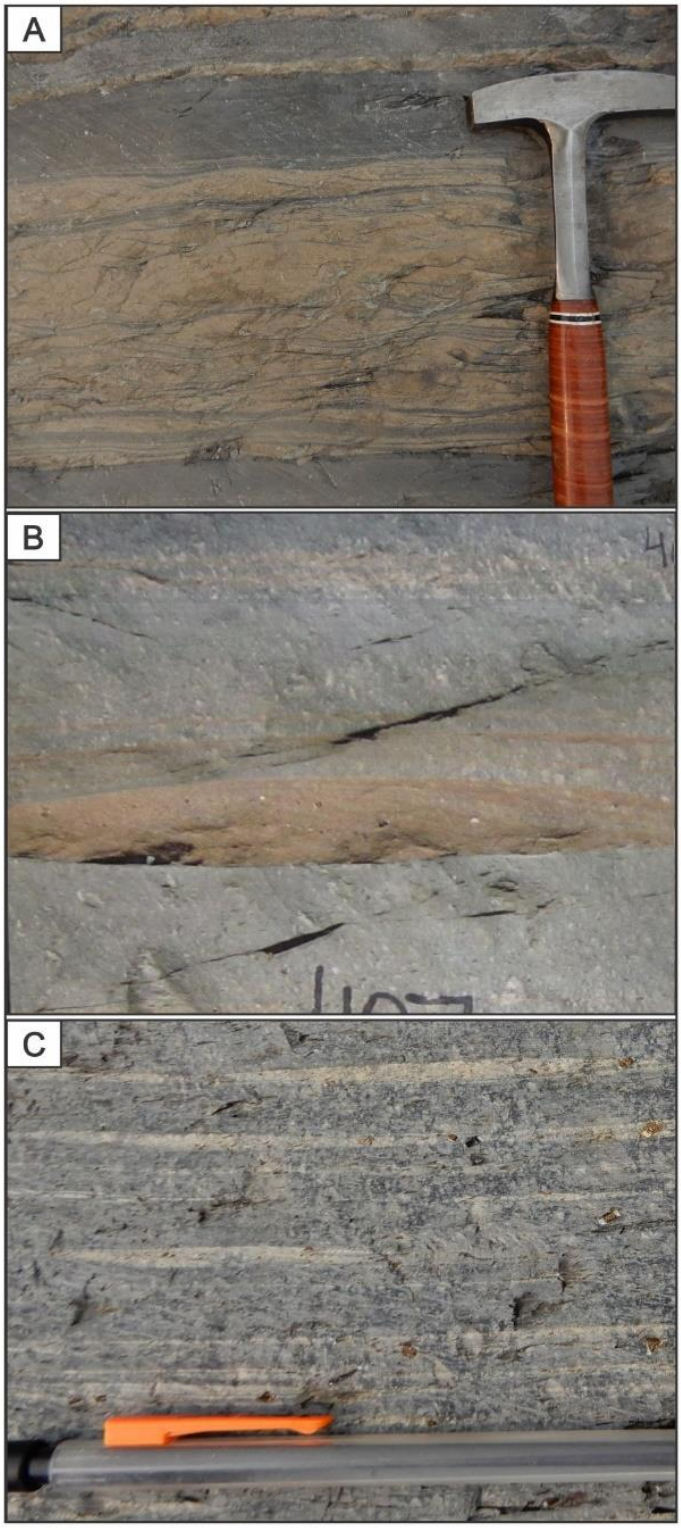

Figure 3.4. *A) Multi-set ripple-cross-laminated T_c; B) Single-set ripple-cross-laminated T_c; and C) Starved-ripple T_c.*

3.4.1.2 Facies 2: Medium- to Very Thick-bedded Lower Division Turbidites

Facies 2 (F2) beds occur in both proximal and distal levees but are more common in channel-proximal regions. These beds constitute 22% of the cumulative thickness of the measured levee section. Beds range from 14 to 180 cm thick but generally are 25 – 80 cm thick with either a T_a (structureless) or T_b (planar-stratified) division at their base. Rarely, beds form 2 – 5-m-thick amalgamated units where the finer, upper division part (T_c, $T_{d/e}$) of individual beds is typically scoured by younger events. Basal structureless T_a divisions are uncommon and occur only in 17% of F2 beds; most F2 beds (83%) are $T_{bcd/e}$ turbidites (i.e., are planar stratified at their base). Beds are typically moderately to well-sorted and grade from coarse- or upper-medium-grained sandstone to lower-medium- or fine-grained sandstone in the T_{a-c} divisions, which then are capped by laminated or massive siltstone and mudstone of the $T_{d/e}$ division. $T_{d/e}$ divisions of F2 beds are lithologically similar to those in F1 beds except that they are generally thinner, typically ranging in thickness from 0.5 to 3 cm. Although siltstone and mudstone laminae do not differ from those described in F1, parallel-stratified, very fine sandstone and siltstone that is common in the basal part of F1 T_d divisions is absent in F2 strata, and the contact between T_c and $T_{d/e}$ divisions is instead sharp and marked by an abrupt decrease in grain size. Basal contacts are generally sharp and planar, although local scours and undulatory bases are common in beds with a basal T_a layer. Moreover, mudstone intraclasts are common and range from 1 cm x 1.5 cm to 5 cm x 30 cm and typically occur in the lower 5 – 20 cm of the bed. Flame structures are also common.

Interpretation: Medium- to very thick-bedded lower division turbidites of F2 are interpreted to represent complete to partly complete Bouma sequences deposited from decelerating turbidity currents composed of sediment ranging from coarse sand to clay (Lowe, 1982). At the time of

deposition it is likely that there was little relief between the levee crest and channel base, such that the dense, coarser-grained lower part of the channelized turbidity current was able to at least partially overspill onto the levee. These beds could also be the result of anomalously large flows that overtopped the channel margin despite the levee relief. The paucity of mud intraclasts and erosional basal contacts indicates that most flows became immediately depositional upon overspilling the channel margins, and only rarely were able to erode the underlying seafloor (Khan and Arnott 2011). The dominance of tractional structures, typically with insignificant angle of climb, suggests generally low rates of sediment fallout and bed aggradation (e.g., Arnott and Hand 1989) with the exception being uncommon basal T_a division sandstones in which the structureless nature suggests higher rates of suspension fallout from denser, most probably highly stratified flows with suppressed near-bed turbulence (e.g., Cantero et al. 2011). The upward transition from structureless sandstone (T_a division) to planar-stratified (traction-structured) sandstone (T_b division) and the fining and succession of sedimentary structures that makeup the $T_{b-d/e}$ divisions records continued deceleration of the flow and decreasing rates of sediment fallout relative to bed-surface transport (Bouma 1962).

3.4.1.3 Facies 3: Mass-Transport Deposits

F3 strata, although anomalously thick and making up a significant volumetric part of levee stratigraphy, are, in terms of abundance, comparatively rare and also formed by mechanisms unrelated to those more typical of overbank sediment transport and deposition. Strata consist of gray to black, structureless, poorly sorted mudstone with dispersed granule- to pebble-size quartz clasts and/or cobble- to boulder-size intraclasts of sandstone or mudstone. Thickness of these deposits ranges from 0.5 to 11 m.

Interpretation: These beds are interpreted to have been deposited by cohesive sediment gravity flows (debris flows) due to an upflow failure of the seabed (Middleton and Hampton, 1973; Lowe, 1979).

3.4.2 Stacking Patterns

Levee strata are dominated by stacked very thin- to medium-bedded T_{cde} turbidites that exhibit a systematic organization on several dimensional scales. At the smallest scale, lithologically and dimensionally similar beds, here termed "self-similar" beds, stack to form sharply bounded bedsets that comprise 2 – 45 individual beds and range from 5 to 290 cm thick. Within a bedset the component beds exhibit similar lithological attributes, including ripple cross-lamination type (multi-set, single-set, or starved), bed thickness, sandstone (T_c) and siltstone-mudstone ($T_{d/e}$) division thickness, and grain size (Fig. 5). More specifically, grain size changes negligibly in a single bedset and bed thickness varies only by several millimeters to at most several centimeters – rarely by more than half the average bed thickness in a given bedset. Additionally, ripple-cross-lamination type does not change and ripple-cross-lamination set thickness and length varies little. The base of a bedset is almost always sharp and planar whereas load and flame structures are common along the bases of the overlying component beds (Fig. 6).

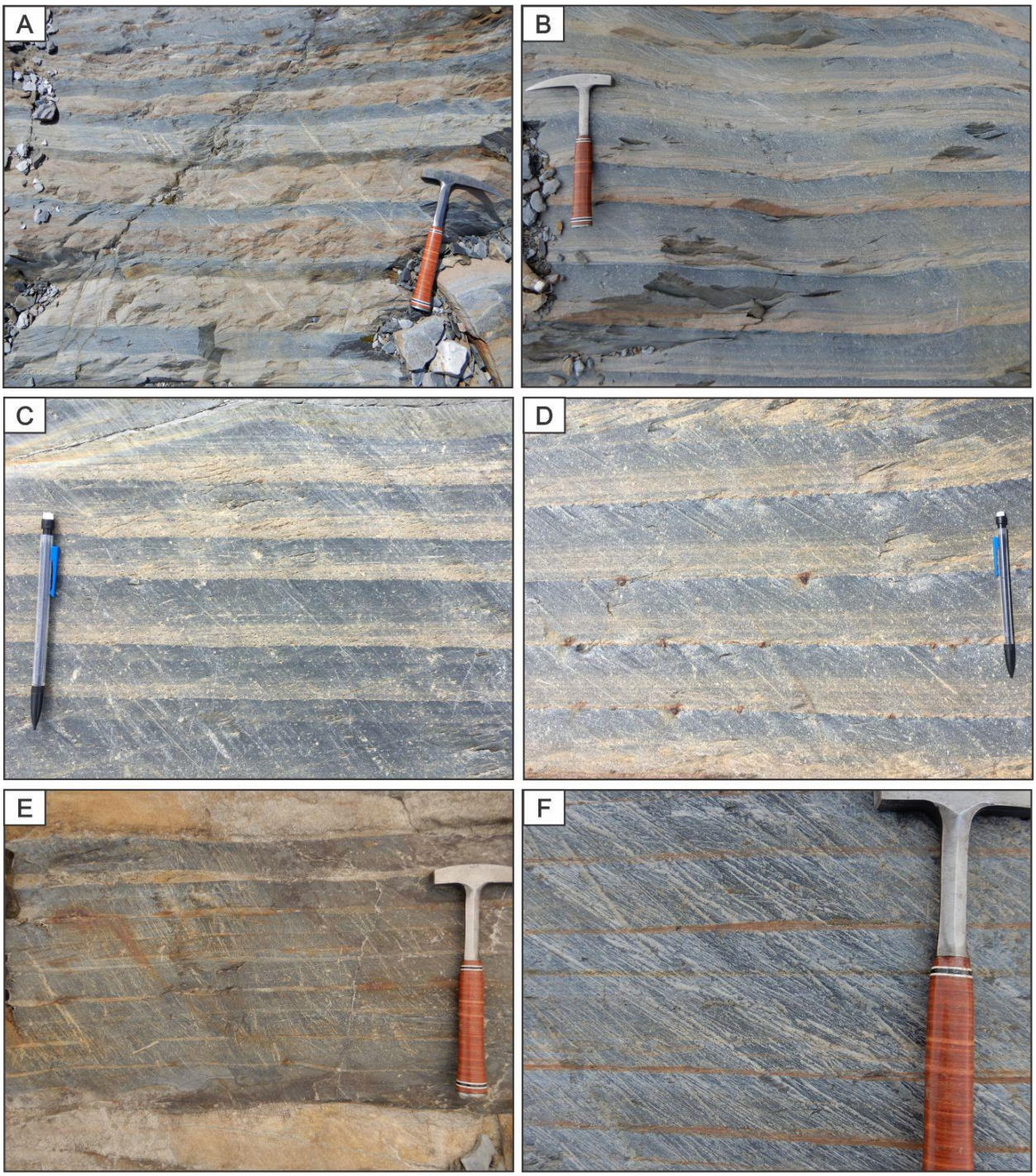

Figure 3.5. *Bedsets composed of stacked self-similar beds. Beds in each bedset have similar thickness, grain size, and sandstone proportion, and all are of a single ripple type. A) Multi-set ripple-cross-laminated bedset; beds have 3 – 6 ripple sets. B) Multi-set ripple cross-laminated bedset; beds have 2 or 3 ripple sets. C) Single-set ripple-cross-laminated bedset; fading ripples are common in the upper part of each set of ripple cross-lamination that are then draped by plane parallel- or wavy-stratified very fine sandstone and siltstone. D) Single-set ripple-cross-laminated bedset; ripples are overlain by plane parallel- or wavy-stratified, very fine sandstone and siltstone. E) Starved-ripple bedset; formsets have spacings of 0.5 – 3 cm. F) Starved-ripple bedset; formsets have spacings of 1 – 8 cm.*

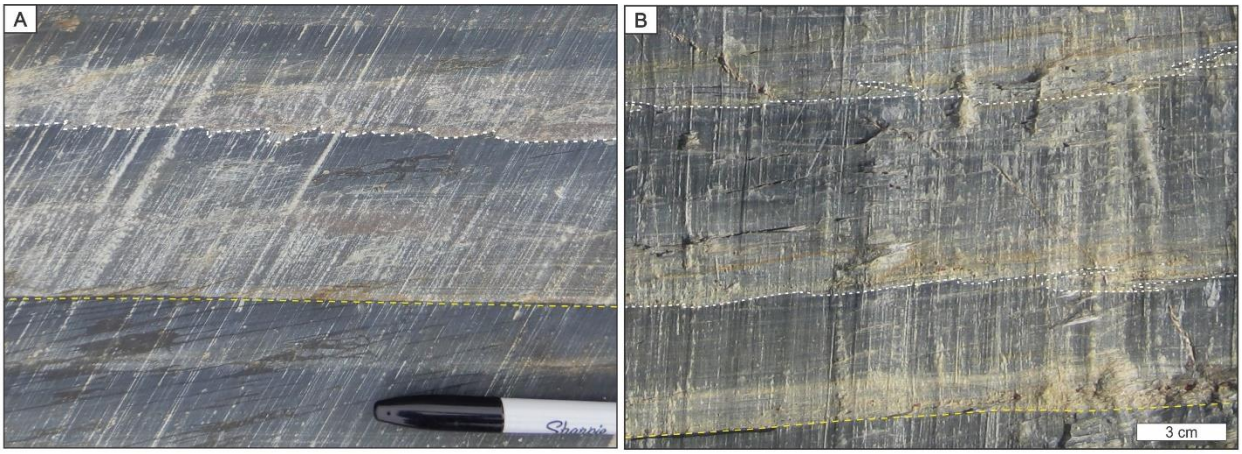

Figure 3.6. *Bottommost beds in bedsets commonly have sharp, planar basal contacts (dashed yellow lines) whereas overlying beds have irregular basal contacts caused by loading (dashed white lines).*

Bedset boundaries are marked by abrupt changes in ripple-cross-lamination type, bed thickness, T_c division thickness, and/or grain size (Figs. 7, 8). Although it is common for several of these characteristics to change between adjacent bedsets, an abrupt change in any one of them constitutes a new bedset (Fig. 8). Data from 253 bedsets consisting of approximately 4200 individual beds is presented here. Bedsets are categorized according to ripple-cross-lamination type, which typically correlates with other lithological properties (see summary in Table 3.2). Irrespective of ripple-cross-lamination type, bedsets generally contain 4 – 20 beds, and rarely up to 45. Bedsets range in thickness from 5 to 288 cm but typically are 10 – 90 cm thick. Bedset thickness correlates closely with ripple-cross-lamination type; multi-set ripple-cross-laminated bedsets range in thickness from 15 to 288 cm (average 85 cm), single-set ripple-cross-laminated bedsets are 9 – 219 cm thick (average 64 cm), and starved ripple bedsets are 5 – 216 cm thick (average 53 cm). Differences in the average bedset thickness is consistent with the thickness of the constituent beds, as multi-set-ripple cross-laminated beds are generally thicker and coarser-grained than single-set cross-laminated or starved-ripple beds, and starved-ripple bedsets thinner and finer than single-set ripple-cross-laminated bedsets.

Count: 253 bedsets 4200 beds		**Ripple Type**		
		Multi-Set	**Single-Set**	**Starved**
Bedset Thickness (cm)	Min	15.1	8.6	5.4
	Max	287.6	219.3	216.1
	Average	85	64	53
Bed Thickness (cm)	Min	2	1	0.5
	Max	28	17	10
	Average	9	5	3.2
Number of Beds	Min	2	2	2
	Max	17	20	45
	Average	6	10	12
Grain Size (Tc division)	Min	vf	vf	vf
	Max	c	c	m
	Average	f - m	f	vf - f
Tc Thickness (cm)	Min	1	0.5	0.2
	Max	20	4	2
	Average	5.2	1.7	0.6
Tc % of Total Bed Thickness	Min	8	4	3
	Max	95	78	60
	Average	53	36	24

Table 3.2: *Summary of minimum, maximum, and average values of bed and bedset characteristics for each of the three ripple types. Grain size of sand: c – coarse; m – medium; f – fine; vf – very fine.*

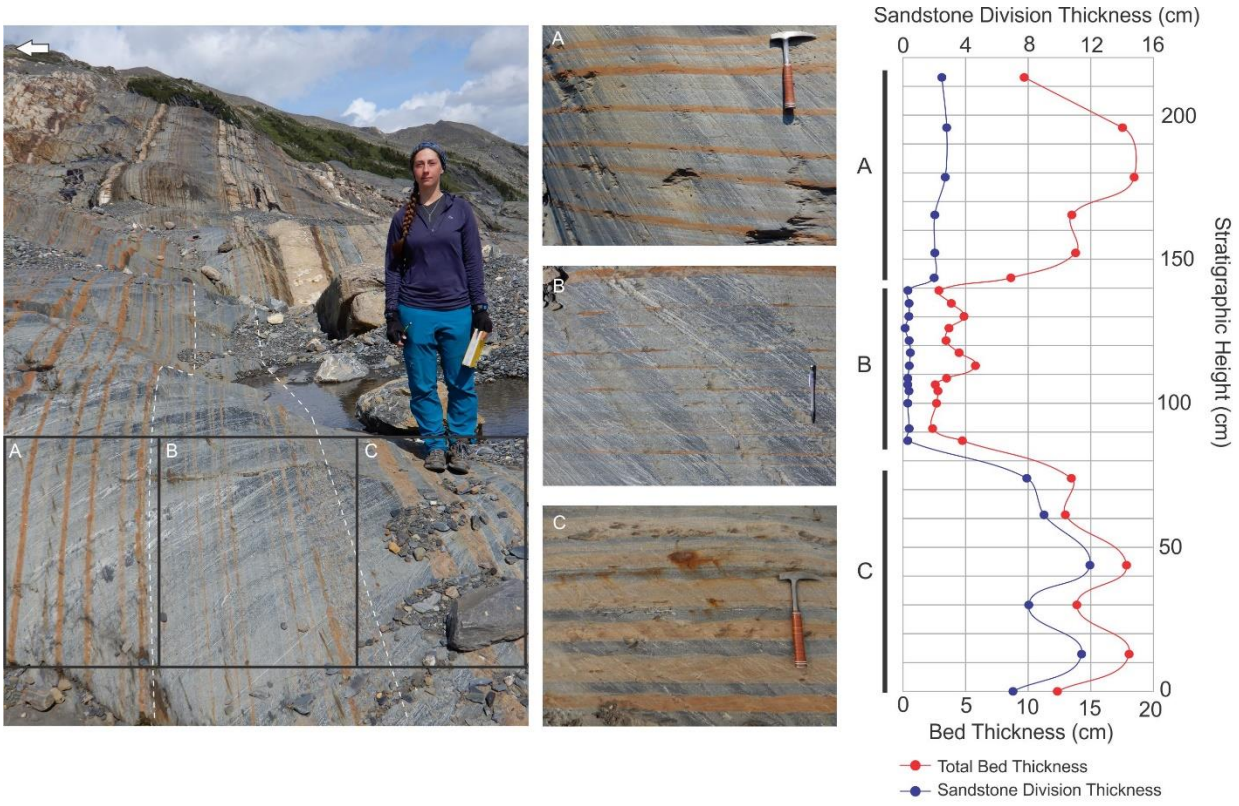

Figure 3.7. *A stack of three sharp-based bedsets – bases are indicated by white dashed lines and marked by abrupt changes in ripple type, bed thickness, and/or sandstone thickness. Here a bedset composed of multi-set ripple-cross-laminated beds (C) is abruptly overlain by a starved-ripple bedset (B), which in turn is overlain by a single-set ripple-cross-laminated bedset (A). White arrow indicates stratigraphic up direction. The graph (right) demonstrates the abrupt change in total bed thickness (red) and sandstone/T_c division thickness (blue) between the three bedsets. Each point on the graph represents an individual bed plotted relative to its stratigraphic position in the succession.*

Strata in each bedset fine and thin slightly laterally away from their genetically related channel on scales of tens to hundreds of meters. Also, these lateral changes occur gradationally and uniformly in all beds in a single bedset so that vertically the self-similarity of all component beds is maintained at all positions along strike (Fig. 9). Significantly also, as beds fine and thin laterally in some bedsets there also is a consistent change from multi-set ripple-cross-lamination to single-set and then starved ripple T_c units, or single-set to starved-ripple T_c units, and these transitions occur on horizontal scales of hundreds of meters. Thinning of individual beds is principally caused by thinning of the ripple-cross-stratified (T_c) part of the turbidite whereas the

overlying $T_{d/e}$ part changes little or uncommonly thickens slightly. Bedsets also thin laterally due to the thinning and fining of their component beds, but thinning is typically only several centimeters to a few tens of centimeters over lateral distances of several hundred meters.

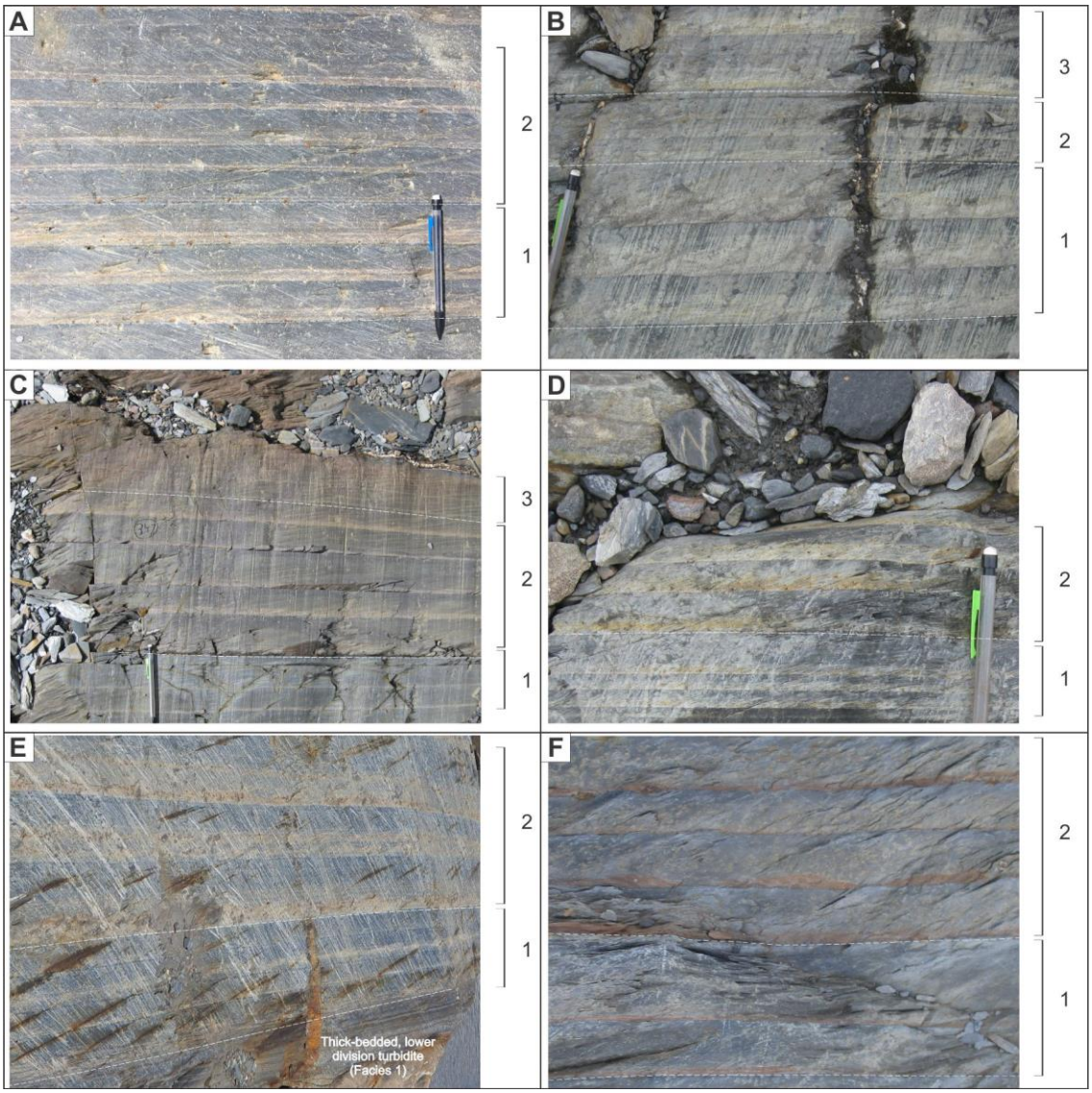

Figure 3.8. *Photos showing typical lithological changes across bedset boundaries. Boundaries indicated by dashed white lines. A) Bedset of single-set ripple-cross-stratified beds with thicker T_c divisions overlain abruptly by a starved-ripple bedset. B) Three bedsets: multi-set ripple-cross-stratified bedset overlain by a single-set ripple-cross-stratified bedset overlain by another multi-set ripple-cross-stratified bedset. C) Three bedsets: starved-ripple bedset overlain by a single-set ripple-cross-stratified bedset capped by another starved-ripple bedset. D) Two stacked single-set ripple-cross-stratified bedsets. Although both bedsets consist of single-set ripple-cross-stratified beds, beds in the lower bedset are thinner than those in the overlying bedset. E) Two bedsets: lower, single-set ripple-cross-stratified bedset overlain by a multi-set ripple-cross-stratified bedset. Bedsets overlie a thick-bedded, lower-division Facies 1 turbidite. F) Two stacked starved-ripple bedsets. Both bedsets consist of starved-ripple beds, but the T_c divisions in the lower bedset are thinner.*

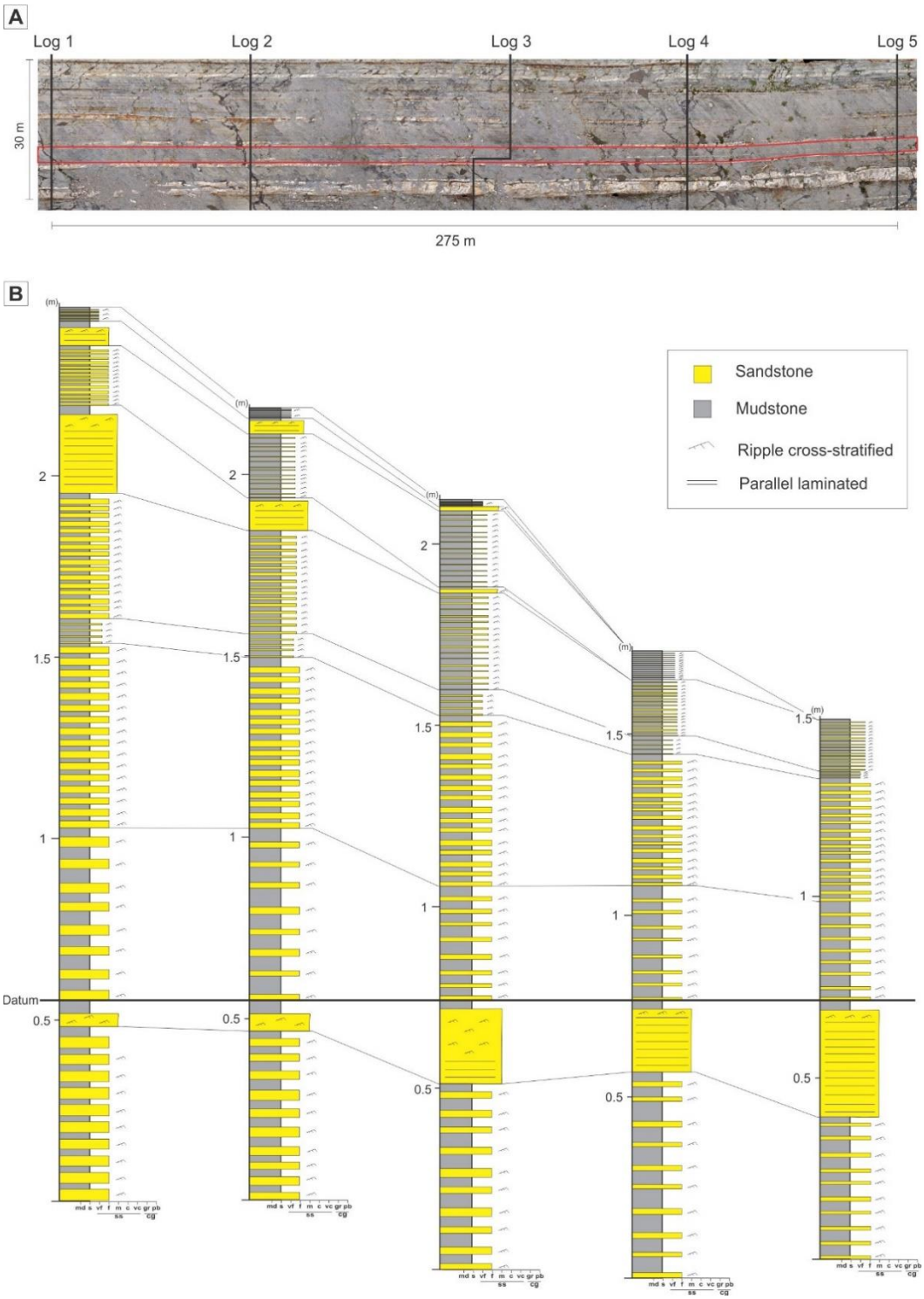

Figure 3.9. *A) Photomosaic of distal Isaac Channel Complex 3 levee strata (see Figure 2 for location) showing the location of each log in Part B. The stratigraphic interval illustrated in Part B is indicated by the red box. B) Detailed measured sections of levee strata spaced 50 – 75 m apart. Correlation lines (solid black lines) bound individual bedsets. Note the lateral thinning of bedsets that is caused by the lateral thinning, and also fining, of their composite beds.*

3.5 Discussion

3.5.1 Long-Duration Pulsing Flows

The lithological and dimensional similarity, or simply self-similarity, of beds in each sharply bounded bedset suggests that each bed was deposited under similar flow conditions, and that these conditions were repeated several times before changing abruptly with deposition of the next bedset. Assuming that each bed in a bedset was deposited by a single flow event, in order to be self-similar the channelized flows that fed the overspill must have been similar in height, duration, structure, and sediment composition, and then changed abruptly with deposition of the overlying bedset. Because flow characteristics are generally controlled by a complex combination of long-term autocyclic and allocyclic controls (e.g., Walker 1985; Hiscott et al. 1997; Cronin et al. 2000), it is unlikely that flow conditions would change so abruptly or so frequently, but also remain so consistent during deposition of an individual bedset. Although autoregulation processes such as flow tuning (see Kelly et al. 2019) could result in increased homogeneity of overbank deposits and the stacking of self-similar beds, they cannot account for the significant variation between stacked bedsets. Instead, an alternative explanation involves the systematic and recurring pulses or surges during a single flow event that multiply overspilled the channel margin and spread over the levee.

In this model the coarse-grained, sand-rich lower part of flows traveling downslope remains mostly confined to the channel, with only the dilute upper silt- and mud-rich part of the flow escaping the channel. Episodic, high-energy pulses temporarily increase the height of the flow such that the coarse-grained part rises above the height of the levee crest, resulting in overspill and discrete depositional episodes on the levee (Fig. 10A). For this to occur, flows must exceed some minimum thickness that depends on the relief between channel floor and levee

crest; otherwise they remain confined to the channel with no overspill. Later waning stages of the flow may not be recorded in levee strata for this same reason - as the flow decreases in size the sand-rich lower part is no longer able to overspill the channel margins even during pulses, and final, smaller pulses may therefore remain confined. Depending on the duration of the channelized flow, multiple such pulses may occur, with each pulse or surge depositing a single bed – each bedset, then, is an event deposit and represents deposition from a single flow event. In order for the beds deposited from each pulse to be self-similar, the pulses themselves must also be approximately hydraulically and texturally similar.

Moreover, pulses must have been of sufficiently low frequency to allow the accumulation of the $T_{d/e}$ layer at the top of each bed. Additionally, the lack of flame and load structures at the base of the lowermost bed in each bedset, but their commonality in overlying beds (Figs. 6, 10B) suggests a longer period of time, and therefore greater bed consolidation, between bedsets, and underconsolidated conditions during deposition of an individual bedset. It is important to note that although rare bedsets contain up to 45 beds, most bedsets contain fewer than 15 beds. Significantly, the bedsets that contain a large number of beds are almost always made up of starved-ripple bedsets in which the narrow range of textural properties could make it difficult to separate individual bedsets, and as a result two or more starved-ripple bedsets were logged as one. Accordingly, irrespective of bedset type, the number of pulses per flow would therefore be expected to range from ~ 2 to 15.

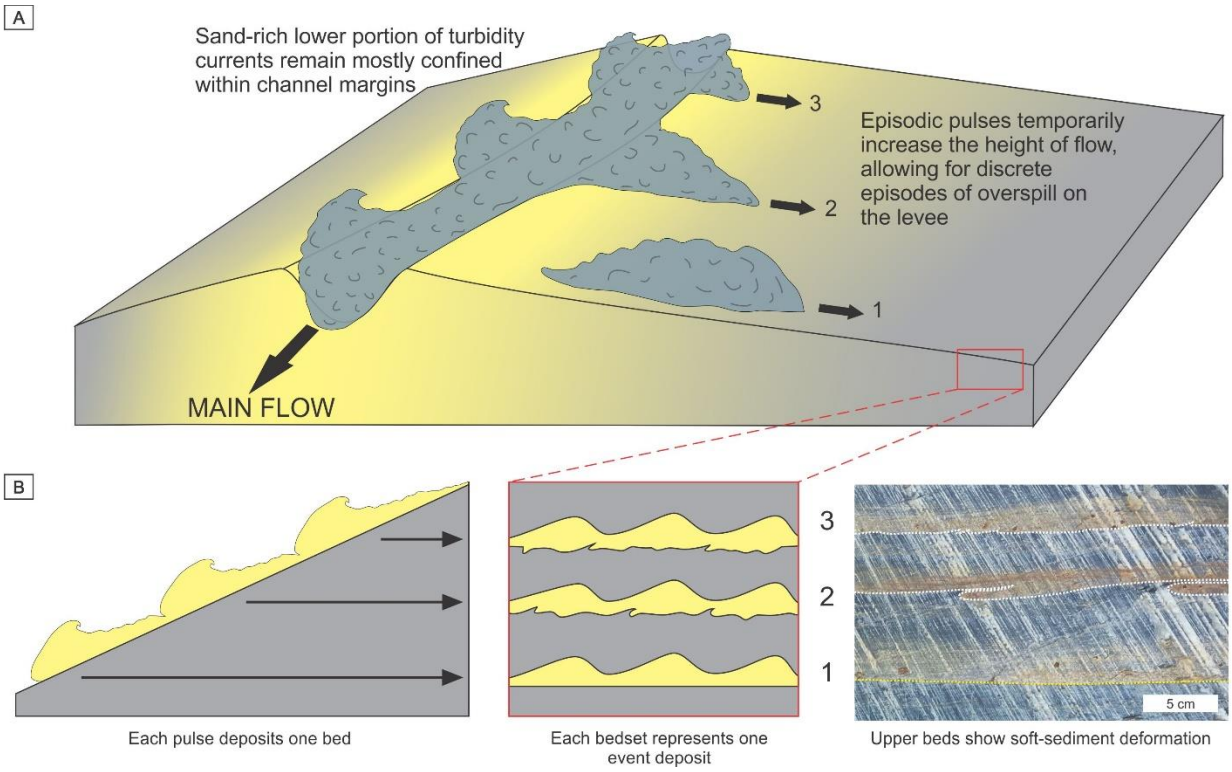

Figure 3.10. *A) Flows traveling downslope remain mostly confined within the channel margins, except for high-energy pulses whose height temporarily exceeds the height of the levee crest allowing overspill onto the levee. In this schematic, multiple pulses are shown originating from one flow event, with each pulse resulting in a depositional episode on the levee (depositional episodes numbered 1 to 3). B) Each depositional episode on the levee results in one turbidite bed, which then stack to form a bedset of self-similar beds. Together, the three beds make up a bedset (shown in red box) representing an event deposit. The upper beds in the bedset show soft-sediment deformation such as loading and flame structures (indicated by the dotted white lines in the photo on the right), indicating that the underlying bed was only partly consolidated at the time of deposition, whereas the bottommost bed in the bedset has a sharp, planar contact (shown by a dotted yellow line in the photo), indicating greater bed consolidation that likely reflects a longer period of time between successive bedsets.*

The exact cause of these pulses remains unclear, although evidence for such a phenomenon has previously been reported from both outcrop interpretation and live turbidity-current monitoring (Gennesseaux et al. 1971; Lambert et al. 1976; Normark and Dickson 1976; Pickering 1979; Lowe 1982; Larue and Provine 1988; Duringer et al. 1991; Best et al. 2005; Kostachuk et al. 2018; Normandeau et al. 2020; Simmons et al. 2020). Live monitoring of natural, continuous turbidity currents driven by sediment-laden density underflows at river mouths has documented the ubiquitous presence of distinct velocity pulsations, generally

characterized by sharp accelerations followed by slower decelerations, with accordant variations in sediment concentration and bed shear stress (Lambert et al. 1976; Best et al. 2005; Kostachuk et al. 2018). It was theorized that these pulsations could be related to the supercritical nature of the flow (Lambert et al. 1976), or the result of instabilities created by shifting surface lobes along the plunge line where the river meets the basin (Best et al. 2005; Kostachuk et al. 2018). Pulsing or surging flows with multiple velocity peaks have also been observed from live monitoring in the Var submarine canyon (Gennesseaux et al. 1971), Lake Superior (Normark and Dickson 1976), the Laurentian Channel of the St. Lawrence Estuary (Normandeau et al. 2020), and the Congo Canyon (Simmons et al. 2020).

In each of these systems, pulsing was observed only in flows with long durations (generally several hours to many days). Also, Normark and Dickson (1976) recorded velocity oscillations with periods ranging from 0.5 to ~ 2.5 hours and noted that in some cases the oscillations appeared to have a regular one-hour cycle. Similarly, Normandeau et al. (2020) observed a turbidity current in the Laurentian Channel with three distinct velocity pulses of ~ one hour duration and 1 – 2 hour spacing, and another turbidity current that lasted only 70 minutes but had three distinct pulses. Although not explicitly discussed in the text, the velocity and backscatter data presented by Simmons et al. (2020) also appear to show several turbidity currents, each lasting 5 – 10 days, with two or more distinct velocity pulses.

Of these publications, Normark and Dickson (1976) alone proposed a mechanism for the generation of the pulses, suggesting that loose packing caused by rapid sedimentation on the upper slope could cause periodic repacking (under the weight of new sediment), which would expel excess pore water and carry fine sediment back into suspension. This elutriation of sediment back into the overriding flow increased sediment concentration in discrete episodes,

creating pulses in the flow. Alternatively, these same authors suggested that "pulsing" may instead be related to the development of turbulent eddies in the upper part of the flow, which later separated completely from the main flow. Although Normandeau et al. (2020) did not discuss a mechanism for pulsing, they noted that all such currents were initiated during large storm events with prolonged periods of sustained high winds and wave height, and interpreted the turbidity currents to have been trigged by the remobilization of shelf sediment.

Despite the observation of pulsing or surging flows from live monitoring, relatively few studies have described evidence of this in outcrop. The repetitive stacking of successions composed of similar Bouma turbidite divisions within a single bed, and lacking evidence of intervening erosion, has previously been reported by Lowe (1982) and Larue and Provine (1988), both of whom attribute the alternations to discrete pulses or surges in flow velocity – Lowe (1982) noted that "surging undoubtedly characterized many sediment flows". Although Lowe suggested that successive surges should show an overall reduction in size, Larue and Provine (1988) found little textural evidence to suggest a progressive velocity decline and instead hypothesized that successive surges were of similar magnitude. Duringer et al. (1991) interpreted Oligocene and Carboniferous arenite-pelite turbidites (equivalent to the $T_{cd/e}$ divisions of the Bouma sequence) in Eastern France to be the result of variations in sediment concentration in a single continuous flow event rather than successive turbidity currents separated by periods of quiescence. In this model the flow was predominantly silt and mud interrupted episodically by higher-energy pulses that delivered sand to form the intervening ripple-cross-stratified Tc intervals; however, the origin of the higher-energy pulses was not discussed.

Pickering (1979) described three "sequences" from the Kongsfjord Formation, Norway that are not unlike the bedsets described here: each sequence ranged in thickness from 1.8 to 4.8

m and contained at least five beds, most of which were upper-division turbidites. Similar to the interpretation presented here for the deposition of bedsets, Pickering interpreted the deposition of individual beds to be separated by a short hiatus, and that each bed was genetically related to the previous one and together were part of a single flow event. However, unlike the bedsets described here, beds in the Kongsfjord Formation sequences fine and thin upward, suggesting progressive flow waning. This was attributed to upslope retrogressive slumping as discrete volumes of sediment collapsed successively from the same slump scarp and transformed downslope into turbidity currents (Pickering 1979).

3.5.2 Enhanced Deposition of Turbiditic Mud Caps

Although the sandy T_c division of each bed may be deposited relatively quickly, there must be sufficient time between pulses to allow the relatively slow deposition of the up to 8-cm-thick mudstone that caps the bed, and its partial consolidation. This suggests that the pulses cannot be due to local billows or small-scale, high-frequency Kelvin-Helmholtz instabilities. However, it is consistent with the general observation that pulsing occurs only in events of long duration. The long duration, and also the long intervals between successive pulses, could allow the deposition and semiconsolidation of the silt- and mud-rich $T_{d/e}$ division at the top of each bed. Because the settling rate of silt and particularly clay is several orders of magnitude slower than that of sand, it is generally assumed that their deposition would take much longer and occur only once the flow had all but waned (e.g., Nichols 2009; Boggs 2006). However, this does not consider physicochemical or biological effects on clay minerals in natural environments. Clay surfaces are chemically active, and so they can interact with dissolved ions in seawater as well as organic matter. Because of this, clay particles often exist in a flocculated state in natural saline

waters, where the presence of cations like Ca^{2+}, Na^{+}, and Mg^{2+} increase the rate of flocculation and floc strength (Packman and Jerolmack 2004; Winterwerp and Van Kesteren 2004; Zbik et al. 2008; Van Leussen 2011; Tan et al. 2014). For example, laboratory experiments show that the settling of kaolinite flocs, which is believed to have been the dominant clay mineral in the Isaac Formation at the time of deposition, is several orders of magnitude higher than that of individual clay particles, and that initial bed formation can occur in minutes (Wolanski et al. 1992; Lau and Krishnappan 1992; Packman and Jerolmack 2004; Zbik et al. 2008; Van Leussen 2011; Sutherland et al. 2015).

Additionally, biologically synthesized organic substances like extracellular polymeric substances (EPSs) can also significantly affect the transport and deposition of clay particles. EPSs are dominated by high-molecular-weight polysaccharides and are a major fraction of primary productivity in marine environments (Bhaskar and Bhosle 2005). Clay particles can interact with EPSs via a number of processes, including polymer bridging, ion-dipole interaction, polymer intercalation into interlayer spaces of swelling clays, and hydrogen bonding, all of which act to facilitate flocculation by increasing the volume of the existing network of cohesive clay grains and enhancing floc strength (Dade et al. 1996; Winterwerp and Van Kesteren 2004; Bhaskar and Bhosle 2005; Van Leussen 2011; Tan et al. 2014). Because floc breakup in turbulent flows is a function of the ratio of turbulence-induced stress to floc strength, the increased floc strength provided by the presence of salt and EPSs in seawater is critical in enabling mass deposition of mud from turbidity currents and could allow the rapid deposition of the $T_{d/e}$ layers of each bed in a bedset.

3.5.3 Alternative Interpretations

Although pulsing in natural turbidity currents has been observed in modern settings and postulated to explain depositional patterns in ancient outcrops, recent experiments by Ho et al. (2018) on multi-pulsed turbidity currents found that secondary pulses accelerated faster than the first pulse (or turbidity current head), and so pulses inevitably merged at some distance from the source. Additionally, recent work by Kelly et al. (2019) on flow behavior in partially confined turbidity currents found that as flows travel downslope, the mechanisms of overspill and ambient entrainment act to balance each other and push the flow towards a quasi-equilibrium state, which would intuitively act to suppress any intrinsic pulsing or surging in the flow. Although it is possible that these effects would occur only significantly downslope of the source and that levees higher upslope could still experience multiple overspill episodes from pulsing flows, their work emphasizes the need to consider interpretations alternative to that presented above.

Autoregulation processes such as flow tuning, as described by Kelly et al. (2019), can result in increased uniformity in overbank deposition, particularly in downflow parts of the channel-levee system where there has been sufficient time (i.e., distance) for the flow to reach a quasi-equilibrium state. Although this process can cause the stacking of self-similar beds as observed in this study, it cannot account for the significant and sudden changes between successive bedsets, which indicate multiple dramatic changes in conditions of channelized flow. One possible mechanism leading to such sudden changes could be local autogenic channel avulsion. Avulsion could be the result of anomalously large, erosive flows that breach the channel wall and reset flow conditions in the new channel. Although observed in modern deep-sea systems like the Amazon (Damuth et al. 1983, 1988; Flood et al. 1991; Dorrell et al. 2015), avulsion in continental slope environments is insufficiently frequent to account for the large

number of observed bedsets. Additionally, channel avulsion has been attributed to the deposition of distinctively matrix-rich sandstones, which is a lithology that is absent in strata described here (Terlaky and Arnott 2014; Angus et al. 2019). Conversely, anomalously large, depositional flows, in addition to mass-transport deposits, may locally alter the channel gradient or geometry, and therefore the structure and properties of subsequent channelized turbidity currents. However, the lack of any systematic trends in bed thickness or sand content in stacked bedsets suggests more significant and irregular changes in flow structure than would be caused by shifting channel gradient due to aggradation of the channel floor.

Other autogenic factors such as lateral channel migration and shifting meander bends could also contribute to a change in bed properties between bedsets, which has the potential to be accentuated by the two-dimensional nature of the outcrop. The planform geometry of sinuous channels evolves with time, resulting in changes to meander amplitude and location. This makes it possible for vertically juxtaposed levee beds to have been deposited at significantly different distances from the channel margin. Assuming that flow tuning acts to regulate overspilling flows and increase the self-similarity of levee beds, a sudden change in bed characteristics could reflect a shift in the channel's local planform geometry. Stacked bedsets could therefore be a result of flow tuning combined with shifting meander patterns. Although plausible, the decameter- to meter-scale thickness of individual sharp-based bedsets would require frequent punctuated lateral shifts of the channel. Also, the lack of a systematic upward stacking of bedsets indicating deposition closer to versus farther from the channel suggests that systematic lateral channel migration is an unlikely cause.

3.5.4 Implications for Event Recurrence and Levee Development

A significant implication of the proposed model is that if single flow events deposit multiple beds, the total number of events recorded in each levee is considerably less than traditional estimates. By considering each bedset as an event deposit the number of recorded events is reduced by up to an order of magnitude, and accordingly impacts our current understanding of flow frequency and preservation. Studies of modern and recent deep-sea levees such as those in the Bengal, Amazon, and Congo fan systems have shown that individual channel-levee systems typically form over ~ 3 – 20 ky (although systems in the Amazon Fan can form in as little as 1 ky) and channel complexes over several tens of thousands of years (Flood et al. 1991; Flood and Piper 1997; Mikkelsen et al. 1997; Manley and Flood 1988; Droz et al. 2003; Pirmez and Imran 2003; Savoye et al. 2009; Dorrell et al. 2015; Jobe et al. 2015). Additionally, sedimentation rates on the levees of these systems, as well as those of the Niger, have been found to generally range from 25 to 800 cm/ky (Damuth et al. 1983; Mikkelsen et al. 1997; Weber et al. 1997; Savoye et al. 2009; Pouderoux et al. 2012; Jobe et al. 2015). If the sedimentation rates on the levees of the Isaac Formation were similar, this confirms that levee units in the Castle Creek study area would have formed over 1 – 20 ky. By combining this estimate of the lifespan of each levee unit with the number of individual beds or bedsets they comprise, it is possible to estimate the frequency of overbank depositional events. In each levee unit at Castle Creek, for example, there are between 10 and 45 event deposits, which suggests an average event recurrence of several hundred years, and a range from as short as 22 years to as long as 2000 years.

Although there have been several studies that documented recurrence intervals of several hundreds of years (Savoye et al. 1990; Johnson et al. 2006), many studies, in particular those

using direct monitoring, report much more frequent turbidity-current activity. Relatively small, river-fed systems, such as in fjords or lakes, commonly experience small turbidity currents every 2 – 4 days with higher-energy flows every several months (Prior et al. 1987; Clare et al. 2016), and larger systems such as the Amazon, Congo, and Laurentian observe events with a recurrence of several weeks to several years (Piper and Deptuck 1997; Savoye et al. 2009; Azpiroz-Zabala et al. 2017; Normandeau et al. 2020; Simmons et al. 2020). This frequency would far exceed what we would expect to observe based on the number of beds and bedsets in each levee unit at Castle Creek, even if individual beds were counted as event deposits rather than bedsets, and suggests that the majority of flows were either not sufficiently energetic to travel far enough downstream to leave a record on the slope, or too thin to result in any appreciable deposition on the levee.

In the case of the latter, flows would remain mostly confined to the channel with only the dilute, mud-rich sediment cloud overspilling onto the levee and deposit thin silt and mud laminae, which in the ancient sedimentary record would most likely not be recognized as discrete events. Indeed, several studies based on live observation of turbidity currents reported that most flows do not reach the terminal fan, instead ending much farther upslope (Prior et al. 1987; Savoye et al. 2009; Clare et al. 2016). It is unlikely that these flows would contribute significantly to levee aggradation, which results in long periods of nondeposition (or pelagic sedimentation only) on the channel-bounding levees. When larger flows with sufficient energy to reach the fan occur, they probably act to flush out the channel, eroding previously deposited sediment from smaller flows and transporting it downslope. These high-energy, long-duration flows probably also result in significant deposition on the levee – if the thickness of the coarse-grained, sand-rich lower part of the flow exceeds the height of the levee crest, medium to very

thick, coarse-grained sandy turbidites (Facies 2) may form from continuous overspill, but if the coarse-grained, sand-rich lower part of flows remain mostly confined to the channel with the exception of short-lived overspill episodes associated with each passing pulse (as is more common based on the observations in this study), a bedset comprising multiple self-similar, thin-bedded, finer-grained turbidites (Facies 1) will form.

The bulk of levee strata is therefore interpreted to be deposited rapidly by anomalously large, pulsing flows that deposit several beds over a relatively short period of time but may occur only once every several hundred years. Separating these large events are long periods of comparative quiescence on levees, characterized by hemipelagic fallout and minor sedimentation from only the dilute, silt- and mud-rich upper parts of smaller flows traversing the channel.

3.6 Conclusions

Observations from well-exposed slope deposits of the Windermere Supergroup have shown that levee deposits are dominated by thin-bedded, upper-division turbidites that stack to form bedsets composed of self-similar beds. This suggests that each individual bedset represents deposition from a single channelized flow event that had multiple, episodic pulses, with each pulse depositing one bed in the bedset. Most gravity flows that travel downslope therefore either do not travel far enough or are of insufficient thickness to escape confinement and result in appreciable levee deposition. Instead, the bulk of levee strata is interpreted to be deposited by anomalously large, pulsing flows that deposit several beds over a relatively short period of time, but which may only occur every several hundred years.

3.7 References

ALLEN, J.R.L., 1970, The sequence of sedimentary structures in turbidites with special reference to dunes: Scottish Journal of Geology, v. 6, p. 146–161.

ANGUS, K., ARNOTT, R.W.C., AND TERLAKY, V., 2019, Lateral and vertical juxtaposition of matrix-rich and matrix-poor lithologies caused by particle settling in mixed mud-sand deep-marine sediment suspensions: Sedimentology, v. 66, p. 940-962.

ARNOTT, R.W.C., AND HAND, B.M., 1989, Bedforms, primary structures and grain fabric in the presence of suspended sediment rain: Journal of Sedimentary Petrology, v. 59, p. 1062–1069.

AZPIROZ-ZABALA, M., CARTIGNY, M.J., TALLING, P.J., PARSONS, D.R., SUMNER, E.J., CLARE, M.A., SIMMONS, S.M., COOPER, C., AND POPE, E.L., 2017, Newly recognized turbidity current structure can explain prolonged flushing of submarine canyons: Science advances, v. 3.10, e1700200.

BABONNEAU, N., SAVOYE, B., CREMER, M., AND BEZ, M, 2004, Multiple terraces within the deep incised Zaire Valley (ZaïAngo Project): are they confined levees?, *in* Lomas, S.A., and Joseph, P., eds., Turbidite Sedimentation in Confined Systems; Geological Society, London, Special Publications, v. 222, p. 91-114.

BARTON, M., O'BYRNE, C., PIRMEZ, C., PRATHER, B., VAN DER VLUGT, F., ALPAK, F.O., AND SYLVESTER, Z. 2010, Turbidite channel architecture: Recognizing and quantifying the distribution of channel-base drapes using core and dipmeter data, *in* Pöppelreiter, M., García-Carballido, C., and Kraaijveld, M.A., eds., Dipmeter and Borehole Image-Log Technology: American Association of Petroleum Geologists, Memoir 92, p. 195–211.

BEAUBOUEF, R.T., 2004, Deep-water leveed-channel complexes of the Cerro Toro Formation, upper Cretaceous, southern Chile: American Association of Petroleum Geologists, Bulletin, v. 88, p. 1471–1500.

BERGEN, A.L., 2017, Vertical and lateral facies architecture of levees and their genetically-related channels, Isaac Formation, Neoproterozoic Windermere Supergroup, Cariboo Mountains, B.C.: Unpublished M.Sc. thesis, Université d'Ottawa/University of Ottawa, 193 p.

BERGEN, A.L., CUNNINGHAM, C.M., TERLAKY, V., AND ARNOTT, R.W.C., 2022, Influence of sediment supply and related channelized-flow density structure on the timing and stratal architecture of deep-marine levee sedimentation: Journal of Sedimentary Research, v. 92, p. 381-403.

BEST, J. L., KOSTASCHUK, R.A., PEAKALL, J., VILLARD, P.V., AND FRANKLIN, M., 2005, Whole flow field dynamics and velocity pulsing within natural sediment-laden underflows: Geology, v. 33, p. 765-768.

BHASKAR, P.V., AND BHOSLE, N.B., 2005, Microbial extracellular polymeric substances in marine biogeochemical processes: Current Science, v. 88, p. 45-53.

BOGGS, S., 2006, Principles of Sedimentology and Stratigraphy: Pearson Prentice Hall, New Jersey, 676 p.

BOUMA, A.H., 1962, Sedimentology of Some Flysch Deposits: A Graphic Approach to Facies Interpretation: [Published Ph.D. (Doctoral dissertation)], Elsevier, 168p.

CAMPBELL, R.B., MOUNTJOY E.W., AND YOUNG F.G., 1973, Geology of McBride map-area, British Columbia: Geological Survey of Canada, Paper v. 72, 104 p.

CANTERO, M.I., CANTELLI, A., PIRMEZ, C., BALACHANDAR, S., MOHRIG, D., HICKSON, T.A., YEH, T., NARUSE, H., AND PARKER, G., 2011, Emplacement of massive turbidites linked to extinction of turbulence in turbidity currents: Nature Geoscience, v. 5, p. 42–45. https://doi.org/10.1038/ngeo1320.

CLARE, M.A., CLARKE, J.H., TALLING, P.J., CARTIGNY, M.J., AND PRATOMO, D.G., 2016, Preconditioning and triggering of offshore slope failures and turbidity currents revealed by most detailed monitoring yet at a fjord-head delta: Earth and Planetary Science Letters, v. 450, p. 208-220.

CLARK, J.D., AND PICKERING, K.T., 1996, Architectural elements and growth patterns of submarine channels: application to hydrocarbon exploration: American Association of Petroleum Geologists Bulletin, v. 80, p. 194-220.

CLEMENCEAU, G.R., COLBERT J., AND EDENS D., 2000, Production results from levee-overbank turbidite sands at Ram/Powell Field, deepwater Gulf of Mexico, *in* Weimer, P., Slatt, R.M., Coleman, J., Rosen, N.C., Nelson, H., Bouma, A.H., Styzen, M.J., and Lawrence, D.T., eds., Deep-Water Reservoirs of the World, Gulf Coast Section of the Society for Sedimentary Geology Foundation 20th Annual Research Conference, p. 241-251.

COCHRANE, D.J., NAVARRO, L., AND ARNOTT, R.W.C., 2019, Sedimentological and geochemical evolution of an Ediacaran mixed carbonate-siliciclastic continental slope system, Windermere Supergroup, southern Canadian Cordillera, British Columbia, Canada: Precambrian Research, v. 327, p. 47-67.

COLPRON, M., LOGAN, J.M., AND MORTENSEN, J.K., 2002, U-Pb zircon age constraint for late Neoproterozoic rifting and initiation of the lower Paleozoic passive margin of western Laurentia: Canadian Journal of Earth Sciences, v. 39, p. 133-143.

CRONIN, B.T., HURST, A., CELIK, H., AND TURKMEN, I., 2000, Superb exposure of a channel, levee and overbank complex in an ancient deep-water slope environment: Sedimentary Geology, v. 132, p. 205–216.

DADE, W.B., SELF, R.L., PELLERIN, N.B., MOFFET, A., JUMARS, P.A., AND NOWELL, A.R.M., 1996, The effects of bacteria on the flow behavior of clay-seawater suspensions: Journal of Sedimentary Research, v. 66, p. 39-42.

DAMUTH, J.E., KOWSMANN, R.O., FLOOD, R.D., BELDERSON, R.H., AND GORINI, M.A., 1983, Age relationships of distributary channels on Amazon deep-sea fan: implications for fan growth pattern: Geology, v. 11, p. 470-473.

DAMUTH, J.E., FLOOD, R.D., KOWSMANN, R.O., BELDERSON, R.H., AND GORINI, M.A., 1988, Anatomy and growth pattern of Amazon deep-sea fan as revealed by long-range sidescan sonar (GLORIA) and high-resolution seismic studies: American Association of Petroleum Geologists Bulletin, v. 72, p. 885–911.

DEPTUCK, M.E., STEFFENS, G.S., BARTON, M., AND PIRMEZ, C., 2003, Architecture and evolution of upper fan channel-belts on the Niger Delta slope and in the Arabian Sea: Marine and Petroleum Geology, v. 20, p. 649-676.

DORRELL, R.M., BURNS, A.D. AND MCCAFFREY, W.D., 2015, The inherent instability of leveed seafloor channels: Geophysical Research Letters, v. 42, p. 4023-4031.

DROZ, L., MARSSET, T., ONDREAS, H., LOPEZ, M., SAVOYE, B., AND SPY-ANDERSON, F. L., 2003, Architecture of an active mud-rich turbidite system: The Zaire Fan (Congo–Angola

margin southeast Atlantic) Results from ZaïAngo 1 and 2 cruises: American Association of Petroleum Geologists Bulletin, v. 87, p. 1145-1168.

DURINGER, P., PAICHELER, J. C., AND SCHNEIDER, J. L., 1991, Un courant d'eau continu peut-il générer des turbidites? Résultats d'expérimentations analogiques: Marine Geology, v. 99, p. 231-246.

ENGLERT, R.G., HUBBARD, S.M., COUTTS, D.S., AND MATTHEWS, W.A., 2018, Tectonically controlled initiation of contemporaneous deep-water channel systems along a Late Cretaceous continental margin, western British Columbia, Canada: Sedimentology, v. 65, p. 2404-2438.

EVENCHICK, C.A., PARRISH, R.R., AND GABRIELSE, H., 1984, Precambrian gneiss and late Proterozoic sedimentation in north-central British Columbia: Geology, v. 12, p. 233-237.

EYSTER, A., FERRI, F., SCHMITZ, M.D., AND MACDONALD, F.A., 2018, One diamictite and two rifts: Stratigraphy and geochronology of the Gataga Mountain of northern British Columbia: American Journal of Science, v. 318, p. 167-207.

FLOOD, R.D., MANLEY, P.L., KOWSMANN, R.O., APPI, C.J., AND PIRMEZ, C., 1991, Seismic facies and late Quaternary growth of Amazon submarine fan, *in* Weimer, P., and Link, M.H., eds., Seismic Facies and Sedimentary Processes of Submarine Fans and Turbidite Systems Springer, New York, NY, p. 415-433.

FLOOD, R.D., AND PIPER, D.J., 1997, Amazon Fan sedimentation: the relationship to equatorial climate change, continental denudation, and sea-level fluctuations: *in* Flood, R.D., Piper, D.J.W., Klaus, A., and Peterson L. C., eds., Proceedings of the Ocean Drilling Program, Scientific Results, National Science Foundation, v. 155, p. 653-675.

GENNESSEAUX, M., GUIBOUT, P., AND LACOMBE, H., 1971, Enregistrement de courants de turbidité dans la vallée sous-marine du Var (Alpes-Maritimes): Comptes Rendus de l'Académie des Sciences, v. 273, p. 2456-2459.

HANSEN, L.A., CALLOW, R.H., KANE, I.A., GAMBERI, F., ROVERE, M., CRONIN, B.T., AND KNELLER, B.C., 2015, Genesis and character of thin-bedded turbidites associated with submarine channels: Marine and Petroleum Geology, v. 67, p. 852-879.

HANSEN, L., CALLOW, R., KANE, I., AND KNELLER, B., 2017, Differentiating submarine channel related thin-bedded turbidite facies: outcrop examples from the Rosario Formation, Mexico: Sedimentary Geology, v. 358, p. 19-34.

HAY, A.E., 1987a, Turbidity currents and submarine channel formation in Rupert Inlet, British Columbia 1. Surge observations: Journal of Geophysical Research, v. 92, p. 2875–2881.

HAY, A.E., 1987b, Turbidity currents and submarine channel formation in Rupert Inlet, British Columbia 2. The roles of continuous and surge-type flow: Journal of Geophysical Research, v. 92, p. 2883–2900.

HESSE, R., AND DALTON, E., 1995, Turbidite channel/overbank deposition in a Lower Devonian orogenic shale basin, Fortin Group of Gaspe Peninsula, Northern Appalachians, Canada: Journal of Sedimentary Research, Section B: Stratigraphy and Global Studies, v. 65, p. 44–60.

HISCOTT, R.N., HALL, F.R., AND PIRMEZ, C., 1997, Turbidity-current overspill from the Amazon Channel: texture of the silt/sand load, paleoflow from anisotropy of magnetic susceptibility and implications for flow processes, *in* Flood, R.D., Piper, D.J.W., Klaus, A., and Peterson, L.C., eds., Proceedings of the Ocean Drilling Program, College Station, Texas, v. 155, p. 53-78.

HO, V.L., DORRELL, R.M., KEEVIL, G.M., BURNS, A.D., AND MCCAFFREY, W.D., 2018, Pulse propagation in turbidity currents: Sedimentology, v. 65, p. 620-637

HODGSON, D.M., DI CELMA, C.N., BRUNT, R.L., AND FLINT, S.S., 2011, Submarine slope degradation and aggradation and the stratigraphic evolution of channel–levee systems: Geological Society of London, Journal, v. 168, p. 625-628.

INGRAM, R.L., 1954, Terminology for the thickness of stratification and parting units in sedimentary rocks: Geological Society of America, Bulletin, v. 65, p. 937-938.

JOBE, Z.R., SYLVESTER, Z., PARKER, A.O., HOWES, N., SLOWEY, N., AND PIRMEZ, C., 2015, Rapid adjustment of submarine channel architecture to changes in sediment supply: Journal of Sedimentary Research, v. 85, p. 729-753.

JOHNSON, J.E., PAULL, C.K., NORMARK, W., AND USSLER, W., 2006, The extent and recurrence of Holocene turbidity currents in Monterey Canyon and fan channel, offshore California (abstract): American Geophysical Union Fall Meeting, OS14A-06.

JOPLING, A.V., AND WALKER, R.G., 1968, Morphology and origin of ripple-drift cross-lamination, with examples from the Pleistocene of Massachusetts: Journal of Sedimentary Petrology, v. 38, p. 971-984.

KANE, I.A., KNELLER, B.C., DYKSTRA, M., KASSEM, A., AND MCCAFFREY, W.D., 2007, Anatomy of a submarine channel-levee: an example from Upper Cretaceous slope sediments, Rosario Formation, Baja California, Mexico: Marine and Petroleum Geology, v. 24, p. 540-563.

KANE, I.A., AND HODGSON, D.M., 2011, Sedimentological criteria to differentiate submarine channel levee subenvironments: exhumed examples from the Rosario Fm. (Upper

Cretaceous) of Baja California, Mexico, and the Fort Brown Fm. (Permian), Karoo basin, S. Africa: Marine and Petroleum Geology, v. 28, p. 807-823.

KELLY, R.W., DORRELL, R.M., BURNS, A.D., AND MCCAFFREY, W.D., 2019, The structure and entrainment characteristics of partially confined gravity currents: Journal of Geophysical Research: Oceans, v. 124, p. 2110-2125.

KENDALL, B.S., CREASER, R.A., ROSS, G.M., AND SHELBY, D., 2004, Constraints on the timing of Marinoan snowball Earth glaciation by ^{187}Re-^{187}Os dating of a Neoproterozoic, post-glacial black shale in Western Canada: Earth and Planetary Science Letters, v. 222, p. 729-740.

KENDRICK, J.W., 2000, Turbidite reservoir architecture in the northern Gulf of Mexico deepwater: insights from the development of Auger, Tahoe, and Ram/Powell Fields, *in* Weimer, P. Slatt, R.M., Coleman, J., Rosen, N.C., Nelson, H., Bouma, A.H., Styzen, M.J., and Lawrence, D.T., eds., Deep-Water Reservoirs of the World: Gulf Coast Section SEPM 20th Annual Research Conference, p. 450–468.

KHAN, Z.A., AND ARNOTT, R.W.C., 2011, Stratal attributes and evolution of asymmetric inner- and outer-bend levee deposits associated with an ancient deep-water channel-levee complex within the Isaac Formation, southern Canada: Marine and Petroleum Geology, v. 28, p. 824-842.

KHAN, Z.A., ARNOTT, B., AND PUGIN, A., 2011, An alternative model of producing topography in the crest region of deep-water levees: American Association of Petroleum Geologists, Bulletin, v. 95, p. 2085-2106.

KHAN, Z., 2012, Origin and architecture of deep-water levee deposits: insight from the ancient rock record and experiments [Ph.D. Thesis]: University of Ottawa, 300 p.

KOMAR, P.D., 1985, The hydraulic interpretation of turbidites from their grain sizes and sedimentary structures: Sedimentology, v. 32, p. 395-407.

KOSTASCHUK, R., NASR-AZADANI, M.M., MEIBURG, E., WEI, T., CHEN, Z., NEGRETTI, M.E., BEST, J., PEAKALL, J., AND PARSONS, D.R., 2018, On the causes of pulsing in continuous turbidity currents: Journal of Geophysical Research: Earth Surface, v. 123, p. 2827-2843.

LAMBERT, A.M., KELTS, K.R., AND MARSHALL, N.F., 1976, Measurements of density underflows from Walensee, Switzerland: Sedimentology, v. 23, p. 87-105.

LARUE, D.K., AND PROVINE, K.G., 1988, Vacillatory turbidites, Barbados: Sedimentary Geology, v. 57, p. 211-219.

LAU, Y.L., AND KRISHNAPPAN, B.G., 1992, Size distribution and settling velocity of cohesive sediments during settling: Journal of Hydraulic Research, v. 30, p. 673-684.

LOWE, D.R., 1979, Sediment gravity flows: Their classification and some problems of application to natural flows and deposits: Society of Economic Paleontologists and Mineralogists, Special Publication, v. 27, p. 75-82.

LOWE, D.R., 1982, Sediment gravity flows II, depositional models with special reference to the deposits of high-density turbidity currents: Journal of Sedimentary Petrology, v. 52, p. 279–297.

MANLEY, P.L., PIRMEZ, C., BUSCH, W., AND CRAMP, A., 1997, Grain-size characterization of Amazon Fan deposits and comparison to seismic facies units, *in* Flood, R.D., Piper, D.J.W., Klaus, A., and Peterson L. C., eds., Proceedings of the Ocean Drilling Program, Scientific Results, National Science Foundation, v. 155, p. 35-52.

MANLEY, P.L., AND FLOOD, R.D., 1988, Cyclic sediment deposition within Amazon deep-sea fan: American Association of Petroleum Geologists, Bulletin, v. 72, p. 912-925.

MCDONOUGH, M.R., AND PARRISH, R.R., 1991, Proterozoic gneisses of the Malton Complex, near Valemount, British Columbia: U-Pb ages and Nd isotopic signatures: Canadian Journal of Earth Sciences, v. 28, p. 1202-1216.

MIDDLETON, G.V., AND HAMPTON M. A., 1973, Sediment gravity flows: mechanics of flow and deposition, *in* Middleton, G.V., andBouma, A.H., eds., Turbidites and Deep-water Sedimentation: SEPM Pacific Section Short Course, Anaheim, California, p. 1–38.

MIDDLETON, G.V., AND HAMPTON, M.A., 1976, Subaqueous sediment transport and deposition by sediment gravity flows *in* Stanley, D.J., and Swift, D.J.P., eds., Marine Sediment Transport and Environment Management:New York, Wiley, p. 197-218.

MIKKELSEN, N., MASLIN, M., GIRAUDEAU, J., AND SHOWERS, W., 1997, Biostratigraphy and sedimentation rates of the Amazon Fan, *in* Proceedings of the Ocean Drilling Program, Scientific Results, v. 155.

NAVARRO, L., AND ARNOTT, R.W.C., 2020, Stratigraphic record in the transition from basin floor to continental slope sedimentation in the ancient passive-margin Windermere turbidite system: Sedimentology, v. 67, p. 1710-1749.

NAVARRO, L., KHAN, Z., AND ARNOTT, R.W.C., 2007, Depositional architecture and evolution of a deep-marine channel-levee complex: Isaac Formation (Windermere Supergroup), Southern Canadian Cordillera, *in* Nilsen, T.H., Shew, R.D., Steffens, G.S., and Studlick, J.R.J., eds., Atlas of Deep-water Outcrops, American Association of Petroleum Geologists, Studies in Geology, v. 56, CD-ROM.

NICHOLS, G., 2009, Sedimentology and Stratigraphy, 2nd Edition: Blackwell, Oxford, 411 p.

NORMANDEAU, A., BOURGAULT, D., NEUMEIER, U., LAJEUNESSE, P., ST-ONGE, G., GOSTIAUX, L., AND CHAVANNE, C., 2020, Storm-induced turbidity currents on a sediment-starved shelf:

Insight from direct monitoring and repeat seabed mapping of upslope migrating bedforms: Sedimentology, v. 67, p. 1045-1068.

NORMARK, W.R., AND DAMUTH, J.E., 1997, Sedimentary facies and associated depositional elements of the Amazon Fan, *in* Proceedings of the Ocean Drilling Program, Scientific Results v. 155, p. 611-651.

NORMARK, W.R., AND DICKSON, F.H., 1976, Man-made turbidity currents in Lake Superior: Sedimentology, v. 23, p. 815-831.

PACKMAN, A. I., AND JEROLMACK, D., 2004, The role of physicochemical processes in controlling sediment transport and deposition in turbidity currents: Marine Geology, v. 204, p. 1-9.

PICKERING, K. T., 1979, Possible retrogressive flow slide deposits from the Kongsfjord Formation: a Precambrian submarine fan, Finnmark, N. Norway: Sedimentology, v. 26, p. 295-306.

PIPER, D.J.W., AND DEPTUCK, M., 1997, Fine-grained turbidites of the Amazon Fan: facies characterization and interpretation, *in* Flood, R.D., Piper, D.J.W., Klaus, A., and Peterson, L.C., eds., Proceedings of the Ocean Drilling Program, [College Station] Scientific Results, v. 155, p. 79–108.

PIPER, D.J.W., AND NORMARK, W.R., 1983, Turbidite depositional patterns and flow characteristics, Navy submarine fan, California Borderland: Sedimentology, v. 30, p. 681–694.

PIPER, D.J.W., HISCOTT, R.N., AND NORMARK, W.R., 1999, Outcrop-scale acoustic facies analysis and latest Quaternary development of Hueneme and Dume submarine fans, offshore California. Sedimentology, v. 46, p. 47-78.

PIRMEZ, C., AND IMRAN, J., 2003, Reconstruction of turbidity currents in Amazon Channel: Marine and Petroleum Geology, v. 20, p. 823-849.

POSAMENTIER, H.W., AND KOLLA, V., 2003, Seismic geomorphology and stratigraphy of depositional elements in deep-water settings: Journal of Sedimentary Research, v. 73, p. 367-388.

POUDEROUX, H., PROUST, J.N., LAMARCHE, G., ORPIN, A., AND NEIL, H., 2012, Postglacial (after 18 ka) deep-sea sedimentation along the Hikurangi subduction margin (New Zealand): Characterisation, timing and origin of turbidites: Marine Geology, v. 295, p. 51-76.

PRICE, R.A., 2000, The southern Canadian Rockies: Evolution of a foreland thrust and fold belt: Calgary, GeoCanada 2000 (field trip guidebook): Calgary, Canadian Society of Petroleum Geologists, 244p.

PRIOR, D.B., ADAMS, C.E., AND COLEMAN, J.M., 1983, Characteristics of deep-sea channel of middle Mississippi Fan as revealed by a high-resolution survey: Gulf Coast Association of Geological Societies, 33rd Meeting, Transactions, p. 389–394.

PRIOR, D.B., BORNHOLD, B.D., WISEMAN, W.J., AND LOWE, D.R., 1987, Turbidity current activity in a British Columbia fjord: Science, v. 237, p. 1330–1333.

REID, L.F., SIMONY, P.S., AND ROSS, G.M., 2002, Dextral strike-slip faulting in the Cariboo Mountains, British Columbia: a natural example of wrench tectonics in relation to Cordilleran tectonics: Canadian Journal of Earth Sciences, v. 39, p. 953-970.

ROSS, G.M., AND ARNOTT, R.W.C., 2007, Regional geology of the Windermere Supergroup, southern Canadian Cordillera and stratigraphic setting of the Castle Creek study area, Canada, *in* Nilsen, T.H., Shew, R.D., and Studlick, J.R.J., eds., Atlas of Deep-water Outcrops: American Association of Petroleum Geologists, Studies in Geology, v. 56, CD-ROM, 22 p.

SAVOYE, B., COCHONAT, P., AND PIPER, D. J., 1990, Seismic evidence for a complex slide near the wreck of the Titanic: model of an instability corridor for non-channeled gravity events: Marine Geology, v. 91, p. 281-298.

SAVOYE, B., BABONNEAU, N., DENNIELOU, B., AND BEZ, M., 2009, Geological overview of the Angola–Congo margin, the Congo deep-sea fan and its submarine valleys: Deep Sea Research Part II: Topical Studies in Oceanography, v. 56, p. 2169-2182.

SHANMUGAM, G., SPALDING, T.D. AND ROFHEART, D.H., 1993, Traction structures in deep-marine, bottom-current reworked sands in the Pliocene and Pleistocene, Gulf of Mexico: Geology, v. 21, p. 929–932.

SIMMONS, S.M., AZPIROZ-ZABALA, M., CARTIGNY, M.J.B., CLARE, M.A., COOPER, C., PARSONS, D.R., POPE, E.L., SUMNER, E.J., AND TALLING, P.J., 2020, Novel acoustic method provides first detailed measurements of sediment concentration structure within submarine turbidity currents: Journal of Geophysical Research: Oceans, v. 125, doi:10.1029/2019JC015904.

SKENE, K.I., PIPER, D.J., AND HILL, P.S., 2002, Quantitative analysis of variations in depositional sequence thickness from submarine channel levees: Sedimentology, v. 49, p. 1411-1430.

SMITH, M.D., ARNOTT, R.W.C., AND ROSS, G.M., 2014, The Old Fort Point Formation: Redefinition and formal subdivision of a distinctive stratigraphic marker in the Neoproterozoic Windermere Supergroup, southern Canadian Cordillera: Bulletin of Canadian Petroleum Geology, v. 62, p. 1-13.

STANLEY, D.J., 1993, Model for turbidite-to-contourite continuum and multiple process transport in deep marine settings: Examples in the rock record: Sedimentary Geology, v. 82, p. 241-255.

STOW, D.A.V., AND SHANMUGAM, G., 1980, Sequence of structures in fine-grained turbidites: comparison of recent deep-sea and ancient flysch sediments: Sedimentary Geology, v. 25, p. 23–42.

STRAUB, K.M., MOHRIG, D., MCELROY, B., BUTTLES, J., AND PIRMEZ, C., 2008, Interactions between turbidity currents and topography in aggrading sinuous submarine channels: a laboratory study: Geological Society of America, Bulletin, v. 120, p. 368–385.

SUTHERLAND, B.R., BARRETT, K.J., AND GINGRAS, M.K., 2015, Clay settling in fresh and salt water: Environmental Fluid Mechanics, v. 15, p. 147-160.

TAN, X., HU, L., REED, A.H., FURUKAWA, Y., AND ZHANG, G., 2014, Flocculation and particle size analysis of expansive clay sediments affected by biological, chemical, and hydrodynamic factors: Ocean Dynamics, v. 64, p. 143-157.

TERLAKY, V., AND ARNOTT, R.W.C., 2014, Matrix-rich and associated matrix-poor sandstones: avulsion splays in slope and basin-floor strata: Sedimentology, v. 61, p. 1175-1197.

TERLAKY, V., ROCHELEAU, J., AND ARNOTT, R.W.C., 2016, Stratal composition and stratigraphic organization of stratal elements in an ancient deep-marine basin-floor succession, Neoproterozoic Windermere Supergroup, British Columbia, Canada: Sedimentology, v. 63, p. 136-175.

VAN LEUSSEN, W., 2011, Macroflocs, fine-grained sediment transports, and their longitudinal variations in the Ems Estuary: Ocean dynamics, v. 61, p. 387-401.

WALKER, R. G., 1965, The origin and significance of the internal sedimentary structures of turbidites: Yorkshire Geological Society, Proceedings, v. 35, p. 1–32.

WALKER, R.G., 1985, Mudstones and thin-bedded turbidites associated with the Upper Cretaceous Wheeler Gorge conglomerates, California: a possible channel-levee Complex: Journal of Sedimentary Petrology, v. 55, p. 279–290.

WEBER, M.E., WIEDICKE, M.H., KUDRASS, H.R., HÜBSCHER, C., AND ERLENKEUSER, H., 1997, Active growth of the Bengal Fan during sea-level rise and highstand: Geology, v. 25, p. 315-318.

WEIMER, P., SLATT, R.M., DROMGOOLE, P., BOWMAN, M., AND LEONARD, A., 2000, Developing and managing turbidite reservoirs: case histories and experiences: results of the 1998 EAGE/AAPG Research Conference: American Association of Petroleum Geologists, Bulletin, v. 84, p. 453-465.

WENTWORTH, C.K., 1922, A scale of grade and class terms for clastic sediments: The Journal of Geology, v. 30, p. 377-392.

WINTERWERP, J.C., AND VAN KESTEREN, W.G., 2004, Introduction to the Physics of Cohesive Sediment Dynamics in the Marine Environment: Elsevier, Amsterdam, The Netherlands, 466 p.

WOLANSKI, E., GIBBS, R.J., MAZDA, Y., MEHTA, A., AND KING, B., 1992, The role of turbulence in the settling of mud flocs: Journal of Coastal Research, v. 8, p. 35-46.

WYNN, R.B., CRONIN, B.T., AND PEAKALL, J., 2007, Sinuous deep-water channels: genesis, geometry and architecture: Marine and Petroleum Geology, v. 24, p. 341–387.

ZBIK, M.S., SMART, R.S.C., AND MORRIS, G.E., 2008, Kaolinite flocculation structure: Journal of Colloid and Interface Science, v. 328, p. 73-80.

Chapter 4: Organic Matter Deposition and Preservation in Ancient Deep-sea Levee Sediments: Implications for Global Trends in Carbon Burial

4.1 Introduction

Deep-marine fan systems represent significant sinks of organic carbon (e.g., Keil et al. 1997a; Galy et al. 2007; Masiello 2007; Baudin et al. 2010). Carbon that becomes buried in these sediments can be stored over geologic timescales, thereby removing atmospheric carbon dioxide, an important greenhouse gas, and increasing atmospheric oxygen levels (Berner 1982; Berner and Canfield 1989; Berner 1990; France-Lanord and Derry 1997; Hayes et al. 1999; Hayes et al. 2006). This process can have significant impacts on the long-term regulation of global climatic and oceanographic trends, and as such is important to study.

Previous work in both recent (e.g., Keil et al. 1997a; Saller et al. 2006; de Jesus Mendes et al. 2007; Galy et al. 2007; Masiello 2007; Baudin et al. 2010; Stetten et al. 2015; Baudin et al. 2017; Lee et al. 2019; Baudin et al. 2020; Hage et al. 2020) and ancient (e.g., McArthur et al. 2016a; 2016b; McArthur et al. 2017; Hussain et al. 2021) deep-marine fan systems have shown that sediment-gravity flows are highly efficient at transporting organic matter (OM) from the continental shelf into the deep marine, where in some cases it becomes preferentially concentrated in specific sub-environments like channels, lobes, and channel-bounding levees. Deep-marine levees, like those described here, are areally extensive, volumetrically significant stratal elements dominated by fine-grained sediment. Much of that fine-grained sediment, which is dominated by clay often associated with organic matter, is a result of turbidity-current overspill – as turbidity currents travel downslope, fine-grained and light-weight particles like silt, clay, and organic matter become concentrated in the upper part of the flow where they can more

easily escape channel confinement and spill over the levee (Fig. 4.1) (Clark and Pickering 1996; Hiscott et al. 1997; Posamentier and Kolla 2003; Posamentier and Walker 2006; Cunningham and Arnott 2021). Due to their fine-grained nature, extensive size, and high rates of sedimentation, levees are ideal sites for significant carbon accumulation and preservation. Although significant carbon enrichment in levees has been reported in several previous studies, most data come from sediments obtained by drilling deep sea cores (e.g., Clemenceau et al. 2000; Kendrick 2000; Weimer et al. 2000; Saller et al. 2006; Baudin et al. 2010). Ancient outcrop descriptions of preserved OM in deep sea levee strata are rare (e.g., McArthur et al. 2016a; 2016b; McArthur et al. 2017), a disparity that is likely due to their typically poor exposure in the ancient sedimentary record.

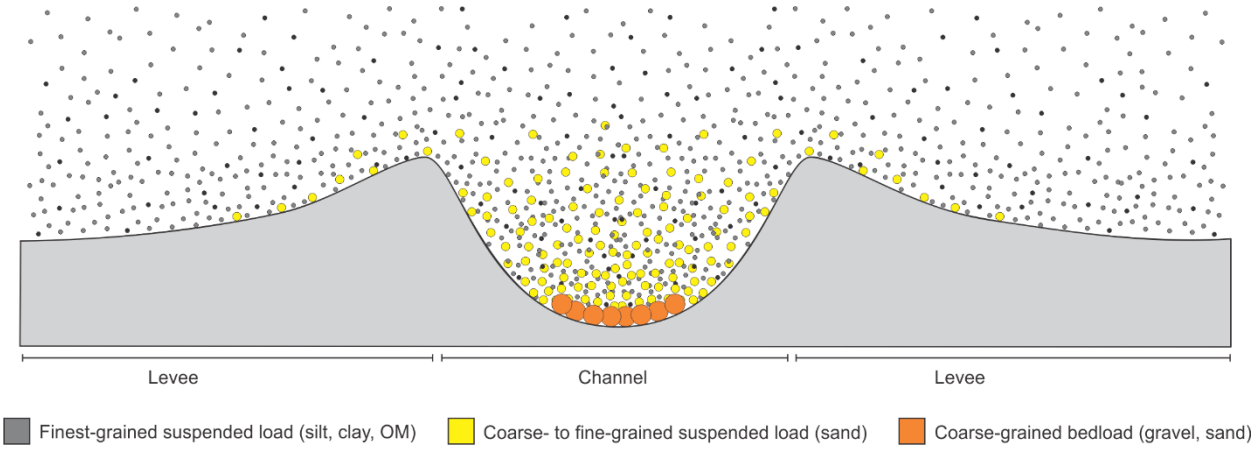

Figure 4.1. *Schematic cross-section of a leveed channel. Coarse, more dense, higher-energy lower part of a turbidity current confined to the channel whereas finer-grained silt, clay, and organic matter are principally carried in the upper part of the flow and therefore more likely to overspill the channel and deposit on levees.*

However, understanding the nature and occurrence of organic matter burial in ancient deep-marine levees is critical to understanding the mechanisms and efficiency by which organic

carbon has been preserved throughout geologic time, and in turn, better constrain models describing global carbon budgets. Here, we provide detailed descriptions and interpretations of organic matter preserved in deep-marine levee deposits of the Neoproterozoic Windermere Supergroup to help fill some of this knowledge gap. Significantly, the data presented here define the common facies associations of organic matter and illustrate the fundamental physical and chemical processes that govern its accumulation and preservation in the rock record.

4.2 Geological Setting

4.2.1 Geological Background

The Windermere Supergroup (WSG) consists of an unconformity-bounded Neoproterozoic succession of mostly metasedimentary rocks associated with the breakup of the Rodinia Supercontinent and subsequent development of a passive continental margin along the western margin of Laurentia (ancestral North America) (Stewart 1972; Ross et al. 1995; Hadlari et al. 2021). In outcrop the WSG stretches more than 4000 km from northwestern Mexico through the western United States and Canada to the Yukon-Alaska border (Ross and Arnott 2007) (Fig. 4.2A). In Mexico, United States and the northern Canadian Cordillera rocks of the WSG comprise continental, marginal-, and shallow-marine to upper-slope strata (Link et al. 1993), whereas in the southern Canadian Cordillera (SCC) a 5-7 km-thick succession of deep marine basin-floor (Kaza Group), continental slope (Isaac Formation), and upper continental slope to shelf (Cunningham and Yankee Belle formations) deposits are superbly exposed (Campbell et al. 1973) and record the progradation of the Laurentian continental margin into the thermally subsiding proto-Pacific Ocean (Fig. 4.2B) (Ross et al. 1995; Ross and Arnott 2007; Hadlari et al. 2021).

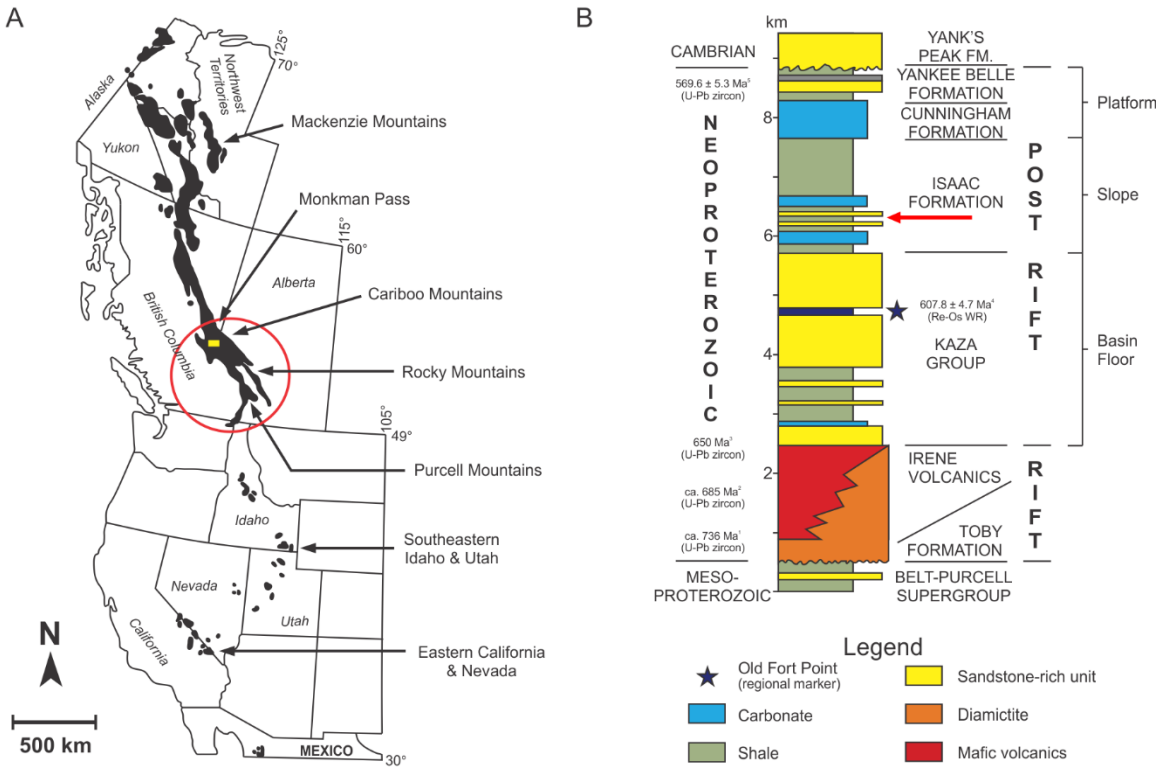

Figure 4.2. *A) Distribution of exposed Windermere Supergroup stratigraphy (black polygons) in western North America. Deep-marine rocks are especially well exposed in the southern Canadian Cordillera (red circle) and at the Castle Creek study area (yellow box). B) General stratigraphy of the Windermere Supergroup in the Cariboo Mountains, east-central British Columbia (Khan 2012). At Castle Creek basin-floor rocks of the Upper Kaza Group are conformably overlain by slope deposits of the lower Isaac Formation. Red arrow indicates the stratigraphic position of strata described here. Radiometric ages are from [1]McDonough and Parrish (1991), [2]Lund et al. (2003), [3]Hadlari et al. (2021), [4]Kendall et al. (2004) and [5]Colpron et al. (2002).*

In the southern Canadian Cordillera age control of the WSG is generally poor and largely constrained by radiometric dates from below and above its bounding unconformities: 736-728 Ma (Evenchick et al. 1984; McDonough and Parrish 1991; Eyster et al. 2018) and 570 +/- 5 Ma (Colpron et al. 2002), respectively. The only depositional age for strata within the WSG in the southern Canadian Cordillera is a rhenium-osmium isochron date of 607.8 +/- 4.7 Ma from organic-rich mudrocks of the Old Fort Point Formation (Kendall et al. 2004; Smith et al. 2014), although a less definitive date is based on the correlation of the ~ 200 m-thick first Issac

carbonate (FIC) (Fig. 4.2B) with deposition immediately preceding the 580 Ma Gaskiers glaciation (Cochrane et al. 2019). Additionally, U-Pb dating of detrital zircons in continental slope deposits sets a maximum depositional age for the WSG at 652 ± 9 Ma (Hadlari et al. 2021). In the Mesozoic to Cenozoic, collision and accretion of allochthonous terranes along the Western margin of Laurentia incorporated rocks of the WSG into the Omineca orogenic belt of the SCC where they experienced multiple phases of deformation and low-grade regional metamorphism (Price 2000; Reid et al. 2002).

4.2.2 Study Area

At the Castle Creek study area in the Cariboo Mountains of British Columbia, Canada (53° 3'0.47"N, 120°25'33.46"W), basin-floor deposits of the Upper Kaza Group are gradationally overlain by continental-slope strata of the Isaac Formation, collectively forming a succession ~ 2.6 km thick and up to 8 km wide (Terlaky et al. 2016; Navarro and Arnott 2020). Bedding is near-vertical (~ 89º) due to its location on the steeply dipping limb of a southwest-verging anticline (Ross and Arnott 2007). Despite lower greenschist metamorphism, primary sedimentary structures and textures are well-preserved, and due to the recent rapid retreat of the Castle Creek glacier, the outcrop is glacially polished and vegetation free, allowing field-based analyses from kilometer- down to millimeter-scale observation and measurement. The Castle Creek study area is divided into four separate sites: Castle Creek North, Castle Creek South, the Hill Section, and the Southeast Drainage (Fig. 4.3); this study focuses on the South and North sites only.

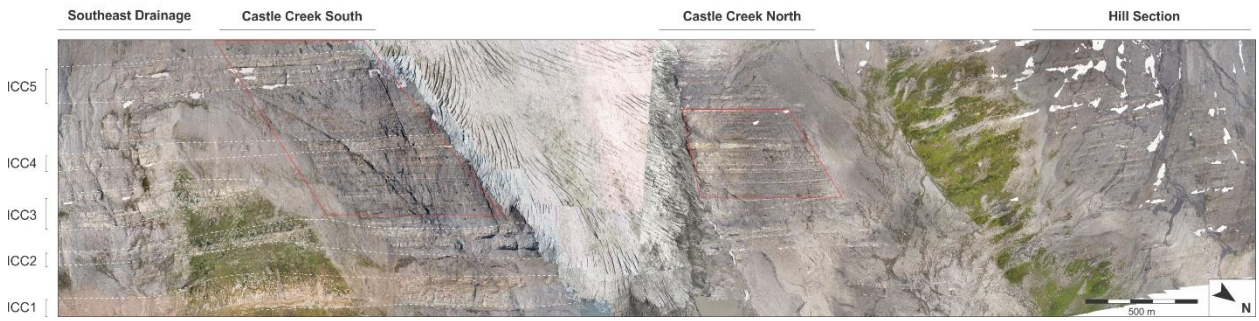

Figure 4.3. *Aerial photomosaic showing slope deposits of the Isaac Formation and the four study areas at Castle Creek: Castle Creek North, Castle Creek South, the Hill Section, and the Southeast Drainage. Isaac Channel Complexes 1 – 5 labeled on the left and outlined with dashed white lines. Levee deposits analyzed in this study are highlighted in red boxes.*

4.2.3 Previous Work

At least seven laterally discontinuous, coarse-grained sandstone and conglomerate units that locally exceed 200 m thick and are interpreted to be leveed slope-channel complexes, have been identified at Castle Creek (Fig. 4.3B). The sedimentology and stratigraphic architecture of the levee deposits associated with two of these channel complexes, namely Isaac Channel Complex 3 (ICC3) and Isaac Channel Complex 4 (ICC4), have been described in detail by previous workers (Navarro et al. 2007; Davis 2011; Khan and Arnott 2011; Khan et al. 2011; Khan 2012; Cunningham and Arnott 2021; Bergen et al. 2022). The channel complexes themselves have also been described in detail by Navarro et al. (2007), Terlaky (2014), Fraino (2020), Bergen et al. (2022), and Fraino et al. (2022), and notably, contain little to no organic material (TOC $\leq$ 0.1%). Similarly, a number of earlier studies had collected geochemical data in levee deposits of the Isaac Formation, but Milczarek (2018) was the first to conduct a systematic sampling program and construct a chemostratigraphic profile from the uppermost part of the FIC below Isaac Channel Complex 1 (ICC1) up through strata of Isaac Channel Complexes 2 and 3 (ICC2 and ICC3, respectively), using major, minor, and trace element composition and

geochemical proxies to analyze trends related to sediment provenance, seawater redox and stratification, and sea level. Ruso (2021) expanded on this work, conducting a geochemical transect from below ICC1 to ICC6 in the South, North, and Hill Section outcrops at Castle Creek to evaluate the effects of ancient climate and eustasy on the development of the continental shelf system. Cochrane et al. (2019) studied the inorganic carbon ($\delta^{13}C_{carb}$) isotopic evolution through the FIC and correlated the observed negative excursion (-6.3 ‰) with the EN2 excursion associated with the 580 Ma Gaskiers glaciation.

These previous studies focused mostly on geochemical trends in the stratigraphy rather than the geochemistry of specific lithologies, and although total organic carbon (TOC) and organic carbon isotopes ($\delta^{13}C_{org}$) of several organic-rich samples were measured by Davis (2011) and Bergen (2017), this study represents the first in-depth analysis of both the physical lithology and the geochemistry of organic-rich strata in levee deposits at Castle Creek.

4.3 Methods

Results presented here are based on observations of levee units from four sites in the Castle Creek study area (levee deposits of ICC3 and ICC4 in both the South and North study areas), encompassing over 250 m of stratigraphy measured vertically and correlated for ~ 2 km along bedding strike. Lithology, grain size, bed thickness, sedimentary structures, and basal contacts were described in mm-scale detail. A total of 56 samples of organic-rich strata were collected and analyzed using a variety of petrographic and geochemical techniques.

4.3.1 Petrography

69 thin sections were prepared from these samples for detailed petrographic description, including grain size, sorting, mineralogy, and microstructure. Petrography was done using an Olympus BX-41 plane, polarized, and reflected light microscope and a JEOL-6610LV scanning-electron microscope (SEM) equipped with an Oxford Inca energy dispersive X-ray spectrometry (EDS) system. SEM-EDS analyses were performed at 15 kV – 20 kV under high vacuum at a working distance of 11 nm, on polished thin sections with a 20-nm-thick carbon coating. In addition, 58 polished thin sections and 3 rock chips were also analysed with SEM-EDS.

4.3.2 Total Organic Carbon and Organic Carbon Isotopes

35 samples of organic-rich strata were analyzed for weight percent of total organic carbon (TOC). Of these, 31 were then analyzed for stable carbon ($\delta^{13}C_{org}$) isotope content. Rock samples collected in the field were broken into chips using a rock hammer. These were then pulverized into a powder using a vibrating pulverizer. To determine TOC, an acid wash was first performed on all samples to remove any inorganic carbonate, which in these samples occurs mostly as carbonate cement. Approximately 500 mg of each powdered sample was weighed and placed in 10 mL beakers into which ~ 7 mL of 20% HCl was added and the solution vigorously stirred to ensure that all the powdered material was thoroughly dispersed in the acid and then left to soak for 24 hours. Samples were then decanted and mixed into distilled water and stirred, allowing the powder to soak, before being set aside to rest for 1.5 hours. The washing procedure was repeated 3 times. After the final wash samples were decanted and the wet powders were placed in an oven and heated at 70ºC for 24 hours.

To determine TOC, approximately 10 mg of each powdered sample was weighed into tin capsules. The capsules were loaded with standards and tungsten oxide, which acts as a combustion catalyst, into an Elementar Vario EL Cube elemental analyzer to measure the percent carbon content (% C) in each sample. In the elemental analyzer, samples were flash combusted with oxygen at ~1800 ºC and then carried by helium through columns of reducing/oxidizing chemicals to produce CO_2 gas. The gas was then trapped within a single "trap and purge" absorption column and released separately, to be detected by the thermal conductivity detector (TCD). The analytical precision (2 sigma) is +/- 0.1%. It is important to note that the effects of greenschist metamorphism would have resulted in the probable loss of ~50 – 80% of the original organic content (Hayes et al. 1983; Smith et al. 2014), resulting in the measured TOC values being significantly lower than the original depositional values.

Organic carbon isotopes were measured using a Thermo Delta Advantage Isotope Ratio Mass Spectrometer (IRMS). Approximately 50 mg of each sample was weighed into tin capsules (ensuring that the amount of carbon in each sample was between 0.02 and 0.2 mg) and loaded into an elemental analyzer connected to the IRMS. As in the previous analysis, samples were then flash combusted at ~1800 ºC and the exsolved gas products carried by helium through columns of oxidizing/reducing chemicals optimised for CO_2. Finally, the gas was separated by a "purge and trap" adsorption column before being sent to the Thermo Conflo III IRMS interface and then the IRMS itself, where the relative abundance of $^{12}C_{org}$ and $^{13}C_{org}$ was measured. Data were normalized using international standards IAEA-CH-6(-10.4‰), NBS-22(-29.91‰), USGS-40(-26.24‰) and USGS-41(37.76‰) and isotopic compositions are reported in permil (‰) relative to the PBS standard. The analytical precision (2 sigma) is +/- 0.2‰.

To confirm that all carbonate that may have been present was removed during the acid wash, measured TOC and $\delta^{13}C_{org}$ values were plotted against each other. A positive correlation would indicate the presence of residual carbonate, which would wrongly increase both the measured $\delta^{13}C_{org}$ and TOC values. However, the plotted values showed no trend, verifying that all carbonate was removed.

4.3.3 Carbonate Isotopes

9 samples of highly carbonate-cemented interbeds were selected for $\delta^{13}C_{carb}$ analysis. Samples were first broken into small chips using a rock hammer. Chips were then pulverized into fine powder. Powdered samples were weighed into exetainers, treated with 0.1 mL of phosphoric acid, and flushed with helium. They were then placed in a bath at 50 ºC for 24 hours. Measurements were performed with a Thermo Finnigan Delta XP and Gas Bench II. Data were normalized using international standards NBS-18, NBS-19, and LVSEC and isotopic compositions are reported in permil (‰) relative to the PBS standard. Analytical precision (2 sigma) is +/- 0.1‰.

4.3.4 Terminology

For clarity, a summary of the terminology used in this paper is first outlined. Descriptions of bed thickness use the classification scheme of Ingram (1954): very thick-bedded (> 100 cm), thick-bedded (30 – 100 cm), medium-bedded (10 – 30 cm), thin-bedded (3 – 10 cm), and very thin-bedded (1 – 3 cm). Grain sizes are categorized using the Wentworth grain-size classification

scale (Wentworth 1922). Turbidites are described according to the terminology of Bouma (1962) and are divided into five divisions comprising a complete classical turbidite:

T_a: poorly sorted, structureless sandstone, often with a scoured base. The term *structureless* describes strata that lack evidence of traction-transport deposition

T_b: planar-laminated sandstone, typically finer-grained than the Ta division

T_c: ripple cross-laminated sandstone, commonly finer-grained than T_b

T_d: well to subtly planar-laminated silt and mud

T_e: pelagic and hemipelagic mud

Turbidites rarely contain all five divisions and instead typically comprise only part of the sequence.

4.4 Results

4.4.1 Organic-rich Facies

Two organic-rich facies have been recognized in the Castle Creek North and South study areas: 1) organic-rich mudstone; and 2) organic-rich sandstone. Collectively, these facies constitute ~ 4 – 5 % of the measured levee stratigraphic thickness and are described next.

4.4.1.1 Facies 1: Organic-rich mudstone

Facies 1 (F1) beds constitute ~ 15 % of the organic-rich beds in the study areas. Beds range in thickness from 1 – 8 cm, are well to subtly thinly planar laminated, and typically stack to form units that are several tens of centimeters thick. F1 strata are black and extremely fissile

and consist mainly of clay-sized grains with lesser silt (Fig. 4.4). Laminations consist of alternating < 1 – 4 mm-thick, parallel bands of light grey siltstone or clayey siltstone and black bands of claystone or silty claystone. Laminae are sharply or diffusely bounded, and framboidal pyrite is abundant. TOC in these beds range from 0.4% to 1.8%.

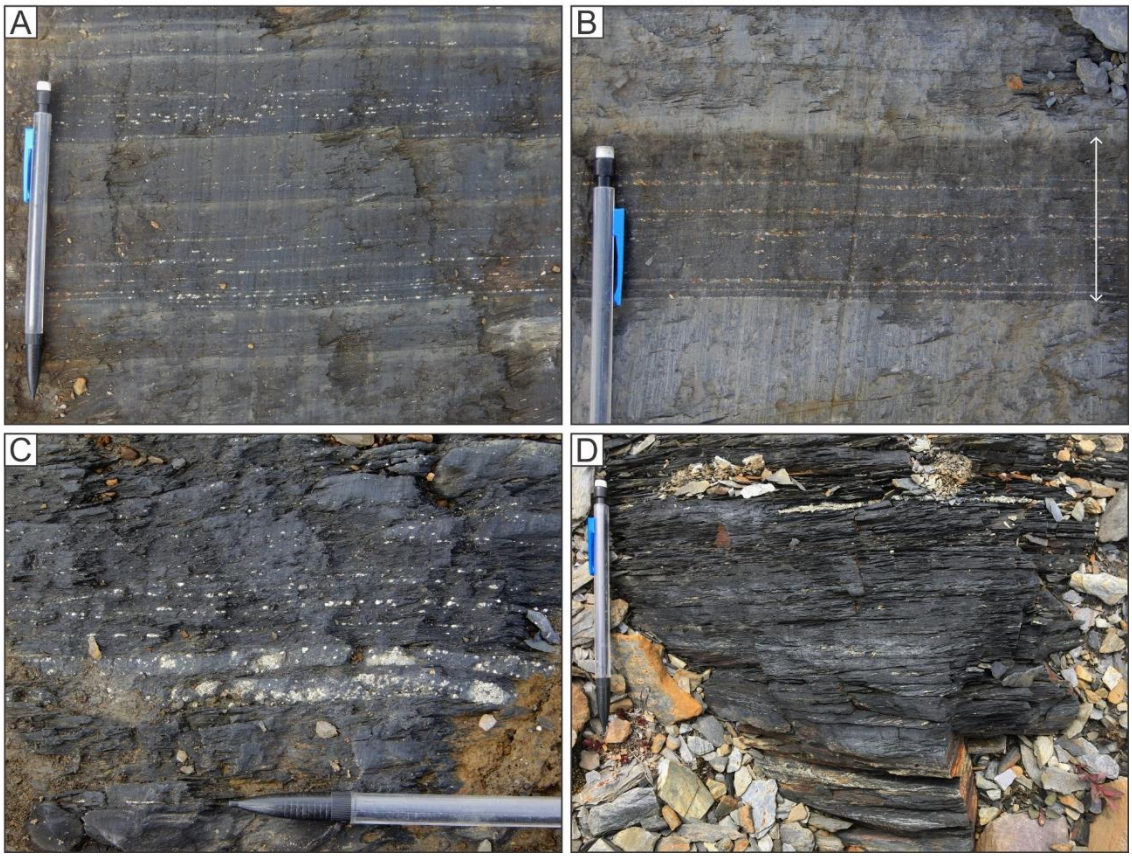

Figure 4.4. *A) Outcrop photo of thinly laminated, organic-rich mudstone (F1). Framboidal pyrite is concentrated along silt-rich laminae. B) Organic-rich mudstone bed (white arrows) bounded above and below by organic-poor mudstone beds. Framboidal pyrite, abundant within the OM-rich bed, is notably absent in the under- and overlying OM-poor beds. C) Fissile, OM-rich mudstone with abundant framboidal pyrite. D) Medium-bedded, highly fissile, OM-rich mudstone. Pencil is 15 cm long.*

4.4.1.2 Facies 2: Organic-rich sandstone

F2 beds constitute the majority (85%) of organic-rich beds in the study areas. They are much thicker than typical levee beds at Castle Creek (2 – 15 cm) (see also Khan and Arnott

2011; Cunningham and Arnott 2021; Bergen et al. 2022), ranging in thickness from 30 – 140 cm, and contain organic carbon contents that vary from 0.6 – 4.0%. Moreover, beds that underlie and overlie F2 strata are not only thinner but also comparatively more OM-poor (TOC values of 0.4 – 0.5%). The basal part of F2 beds is 5 – 30 cm thick and consists of planar-stratified, orange sandstone equivalent to the T_b division of a classical turbidite. Thin (mm-thick) intercalated black bands are common in the upper part of this division. Above the basal sandstone division, strata consist of distinctively alternating bands of black and orange sandstone informally termed "tiger-striped" (Fig. 4.5, 4.6). Bands are sharply bounded and range in thickness from 0.2 – 30 cm. Black bands generally thicken (0.2 – 15 cm) and become more abundant upwards. Orange bands in the middle part of F2 beds are planar-stratified and only rarely ripple cross-stratified. Beds are generally capped by an uppermost layer of orange, ripple- (T_c) and much less commonly planar- (T_b) stratified, fine-grained sandstone, usually overlain by a several-mm-thick thin mud cap (T_{de}).

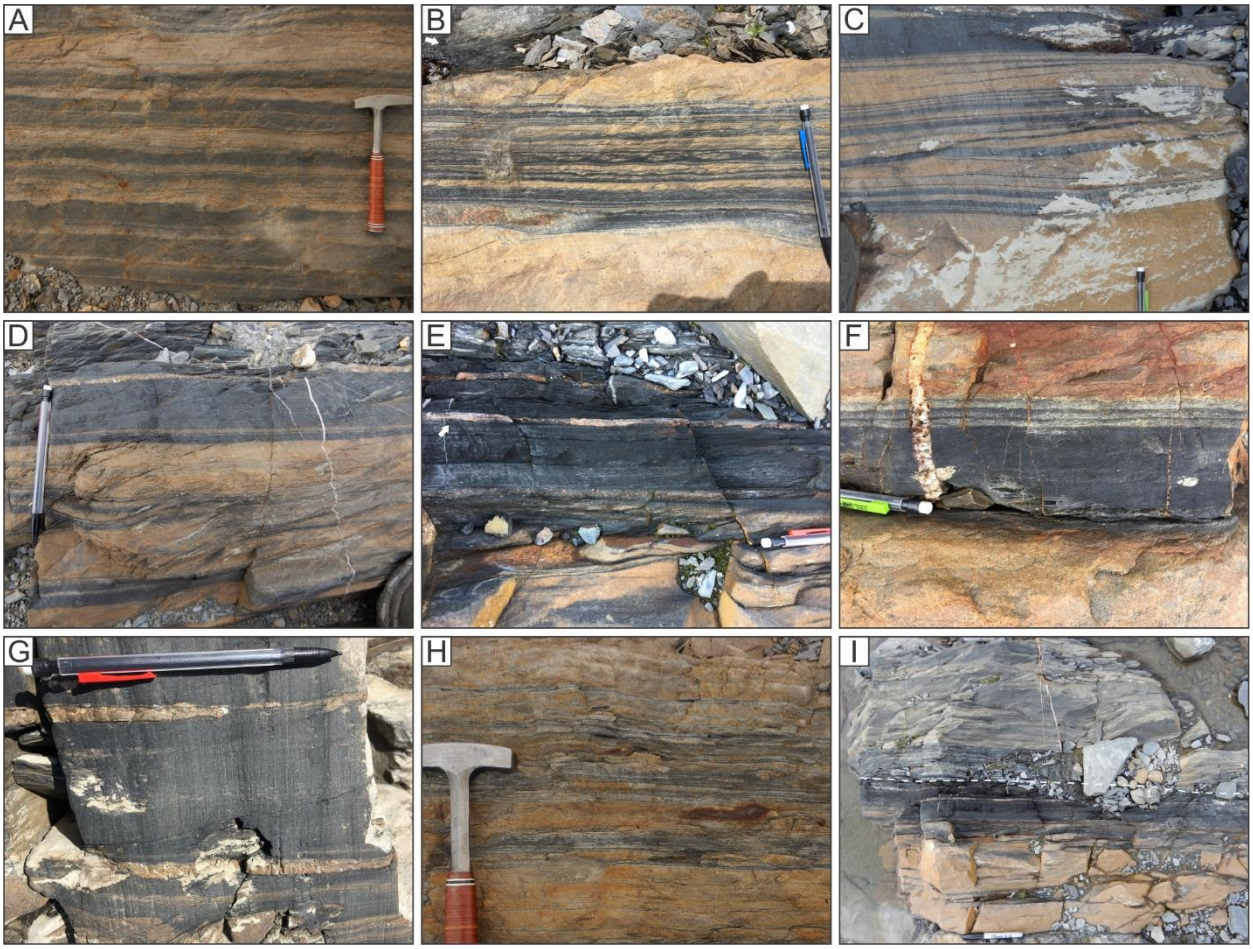

Figure 4.5. *Outcrop photos of OM-rich mudstone and "tiger-stripe" sandstone. Pencil is 15 cm, rock hammer is 34 cm. A) Thick-bedded, planar- and cross-stratified OM-rich sandstone. B) Thinly banded, planar- and cross-stratified OM-rich sandstone sandwiched between thicker orange sandstone bands – basal orange band is planar-stratified (Tb) capped by a single ripple formset (Tc), whereas the upper orange band is ripple cross-stratified (Tc). Note the abundant small-scale load and flame structures along the base of the thin orange bands. Overlying the upper orange sandstone band is grey, OM-poor mudstone (indicated by arrow). C) OM-rich sandstone bed with a thick basal T_b division overlain by a succession of thin, planar-stratified tiger-stripe bands. D) Planar-stratified, OM-rich sandstone with thick black band at the top. E) Thick, black, OM-rich sandstone band with single, orange cemented band (indicated by arrow). F) Massive to planar-stratified, black, matrix-rich sandstone band bounded above and below by thicker, orange, cemented, planar-stratified sandstone bands. G) Black OM-rich sandstone intercalated with thin, orange, cemented bands. H) Thick, planar-stratified OM-rich sandstone intercalated with thin, black, matrix-rich bands. I) Thick OM-rich sandstone bed overlain by more typical OM-poor levee mudstone and sandstone – contact indicated by dashed white line. Note the difference in colour between the orange and black OM-rich bed and the beige and light grey OM-poor beds above.*

F2 beds and their constituent internal bands show only a slight thinning trend away from the associated channel (several centimetres of thinning over lateral distances of several hundreds

of meters). In the middle, tiger-stripe part, bands of orange fine-grained sandstone exhibit common load and flame structures along their base (Fig. 4.7) and high intergranular porosity (5 – 35%) filled with ferroan dolomite cement (Figs. 4.8, 4.9A-B). In one sample (SS 3), minor (≤ 3%) siderite is also present. Ferroan dolomite occurs as 10 – 200 μm, subhedral to anhedral or rhombic, pore-filling crystals that commonly show subtle zonation (Fig. 4.9C-D). Where present, siderite occurs as brown rims around dolomite crystals, or as isolated, small (50-100 μm), brown, lozenge-shaped crystals (Fig. 4.9E-F). Black bands consist of dispersed fine-grained quartz sandstone to sandy mudstone with ~ 30 – 60 % matrix content (matrix consisting of clay-sized particles and organic matter, which imparts the distinctive black colour). For simplicity, and irrespective of the amount of matrix, these strata are collectively termed matrix-rich sandstone. Notably, the sand grains in black bands are the same size as those in the adjacent orange bands and changes little upward, although a subtle overall upward fining is observed in some beds. Uncommonly, F2 beds consist only of black, matrix-rich sandstone.

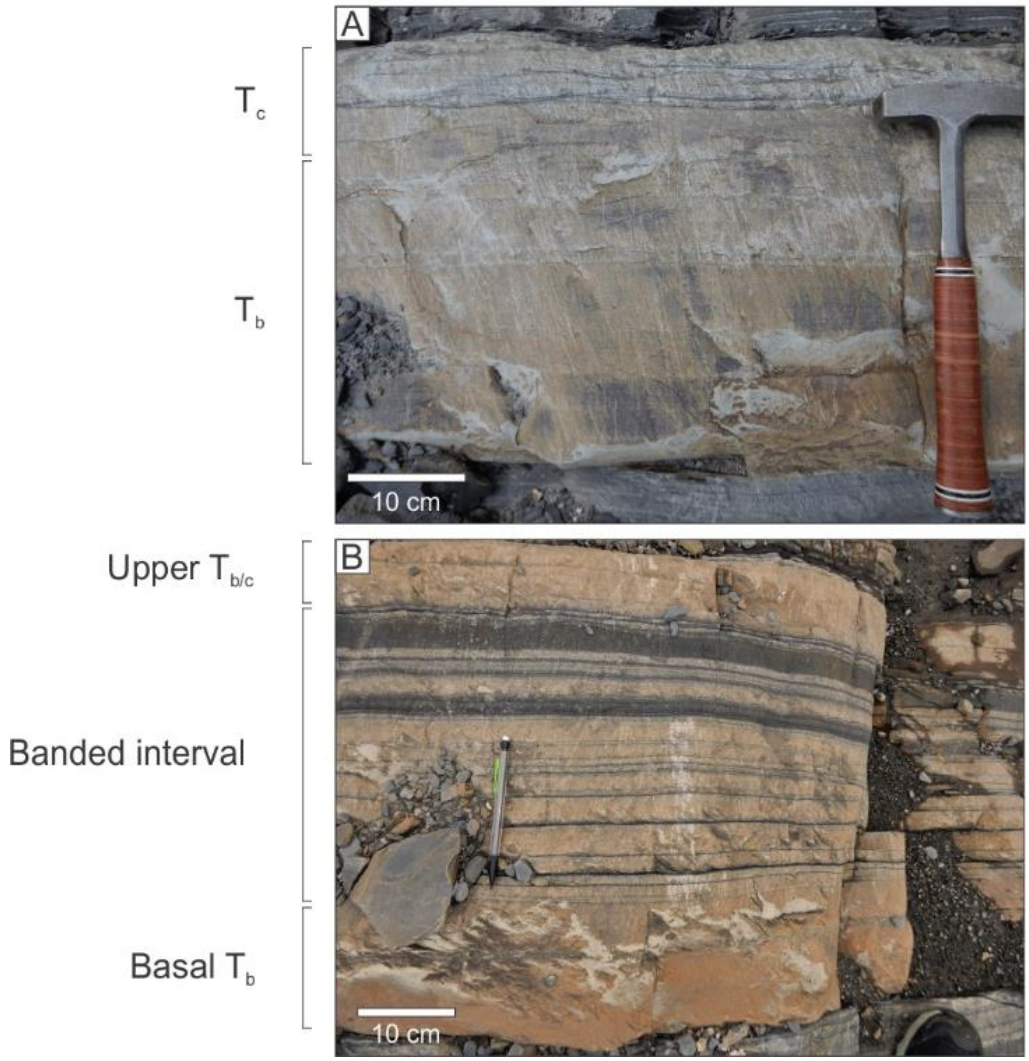

Figure 4.6. *Examples of typical OM-poor (A) and OM-rich (B) T_{bc} turbidites in levee deposits. OM-rich (Facies 2 – F2) are generally thicker than typical levee beds and are extensively cemented, with an intermediate division of alternating black and orange bands (tiger-stripe) between the basal T_b division and upper T_c division.*

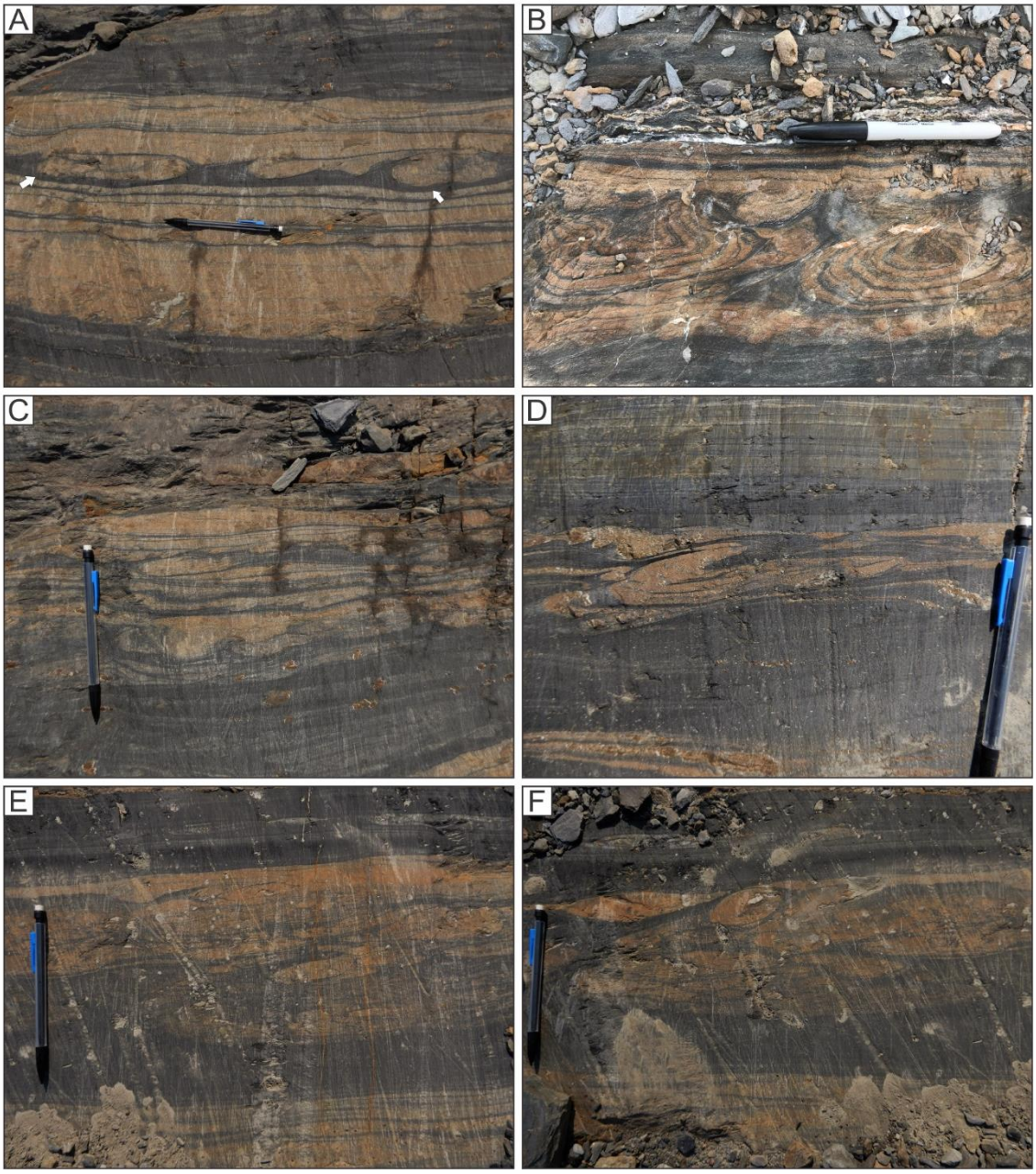

Figure 4.7. *Outcrop photos of soft-sediment deformed strata. Pencil is 15 cm long and the marker is 14 cm long. A) Load casts and flame structures (indicated by white arrows) in the middle bands of an OM-rich sandstone bed. Orange bands are planar- and less commonly ripple cross-stratified. B) OM-rich sandstone bed with convolute lamination that has completely detached and formed "pseudonodules" (sensu Macar 1948). C) Deformed load casts and pseudonodules in OM-rich sandstone. D) Foundered clean sandstone into water-saturated, clay-rich band during or immediately after deposition. E) OM-rich sandstone bed; uppermost sandstone bed shows extensive soft-sediment deformation including flame structures and pseudonodules. F) OM-rich sandstone bed with extensive loading and deformation of the uppermost band of clean sand.*

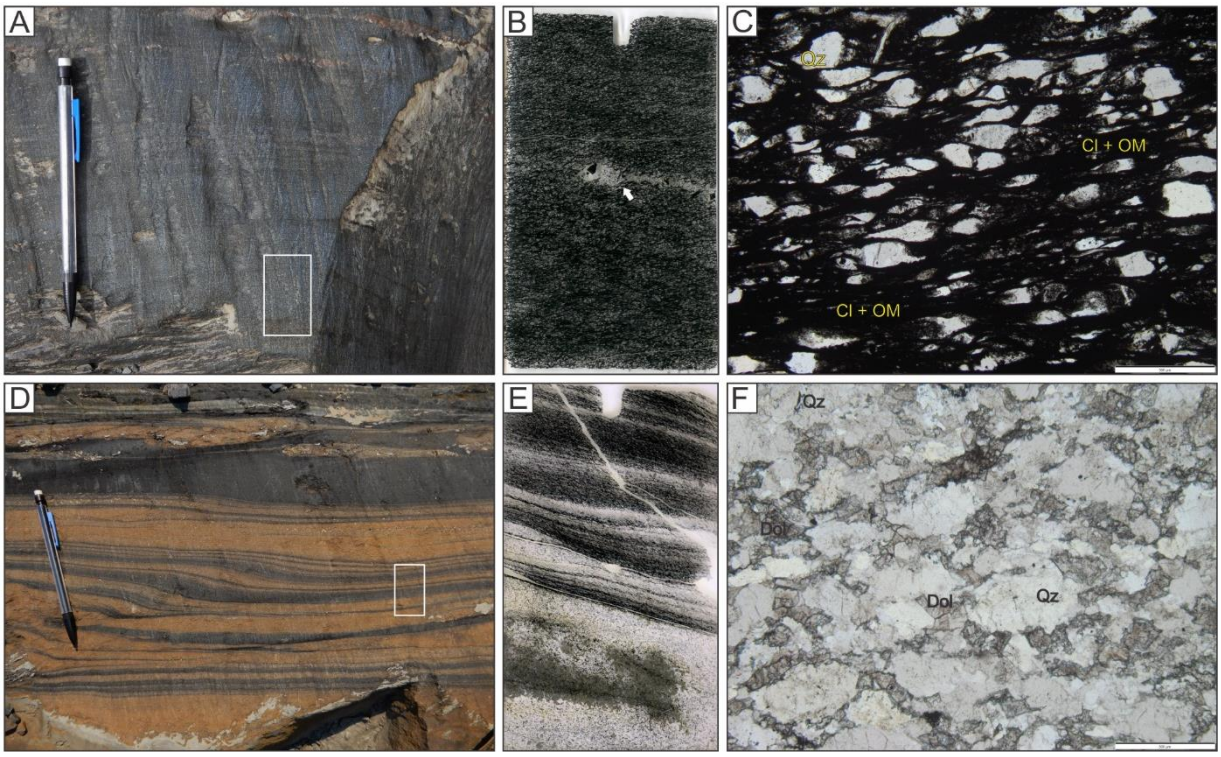

Figure 4.8. *A) Black, clay-rich band of OM-rich sandstone (Facies 2). White box indicates the location of thin section shown in part B. B) Thin section (25 x 45 mm) of the clay-rich band shown in part A. Light band in the middle (white arrow) is a metamorphic quartz vein. C) Plane-polarized photomicrograph of part B. Note the dispersed quartz (Qz) sand grains in an opaque black matrix, which based on electron microscopy, consists of clay (Cl) and organic matter (OM). D) Alternating black, clay-rich and orange highly cemented bands in an organic-rich sandstone. White box indicates location of thin section in part E. E) Thin section showing alternating clay- and sand-rich bands in part D. F) Plane-polarized photomicrograph of a sand-rich band in part B. Note the abundance of pore-filling, rhombic ferroan dolomite (Dol) cement.*

4.4.2 Types of Organic Matter

Due to the fine-grained nature of the organic-rich rocks, scanning-electron microscopy was needed to differentiate mineral grains from organic matter and identify and classify the organic matter. Using this method, three types of OM were identified: 1) nanometer- to micrometer-scale coatings around clay grains; 2) discrete, silt- to sand-sized carbon grains; and 3) sand-sized organomineralic aggregates. The first type is the most abundant and constitutes ~ 92 % of the organic matter observed. This type occurs as thin, black coatings around and

between clay mineral grains (Fig. 4.10A-C) and is the principal type found in organic-rich F2 sandstones (where it occurs in association with the matrix in black bands of matrix-rich sandstone) and constitutes nearly all the OM in organic-rich F1 mudstones. The second type is less common, accounting for ~ 7 % of the organic content observed and consists of amorphous carbon particles that range in size from 10 – 120 μm (Fig. 4.10D-F). This type of organic carbon occurs primarily in the orange cemented bands of F2 strata. The final type is the least common, accounting for only ~1 % of the organic content observed. These grains, termed organomineralic aggregates (OMAs), are generally larger in size than the previous type, ranging from ~ 60 – 150 μm, and consisting of aggregates of organic matter and clay grains (Fig. 4.10G-I). OMAs are observed in both the black, clay-rich bands and the orange, cemented bands of F2 strata in addition to F1 strata.

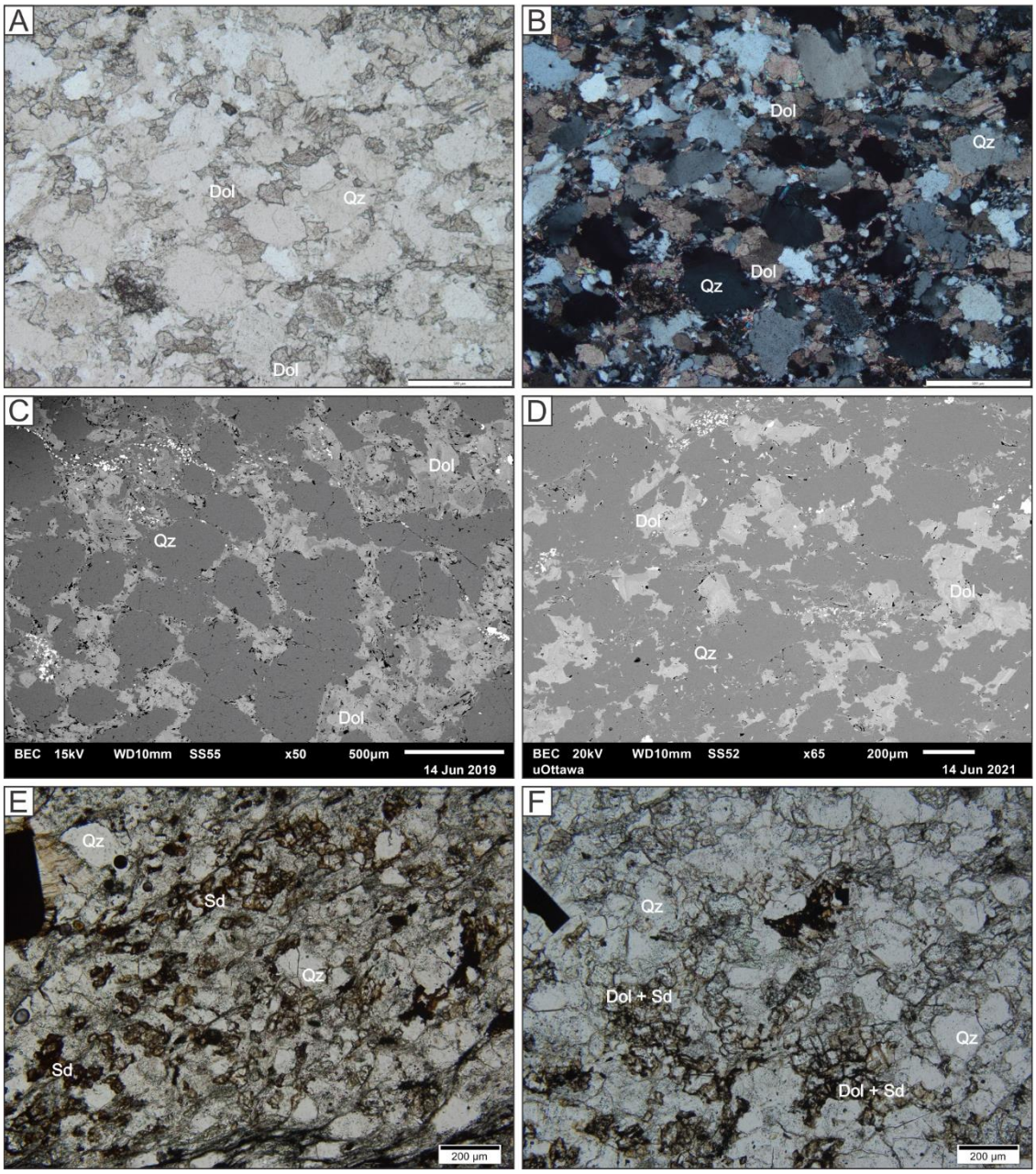

Figure 4.9. *A) Plane-polarized and (B) cross-polarized photomicrographs of fine-grained, orange sandstone with extensive early diagenetic ferroan dolomite cement. C, D) Backscattered electron micrographs of dolomite-cemented (light grey) quartz (dark grey) sandstone. Note the slight lightening of the dolomite crystals from center to rim indicating zonation or multiple phases of growth. E) Quartz sandstone with siderite (Sd) cement that occurs as small, brown, lozenge-shaped crystals. F) Quartz sandstone with subhedral dolomite rimmed with dark brown siderite cement.*

4.4.3 Accessory Minerals

Several additional minerals were commonly observed in association with organic carbon in F1 and F2. Framboidal pyrite is abundant in all organic-rich strata, but particularly in the clay matrix of black bands of F2 beds (Fig. 4.11A-B). Heavily pyritized organomineralic aggregates were also observed, consisting of clay, minor silt, and pyrite framboids (Fig. 4.11E-F). Additionally, amorphous carbonate apatite (collophane) was observed in both F1 and F2 strata and ranges from 50 – 100 μm (Fig. 4.11E), whereas more common authigenic chlorite, especially abundant in clay-rich laminae, ranges from 50 – 500 μm (Fig. 4.11C-D).

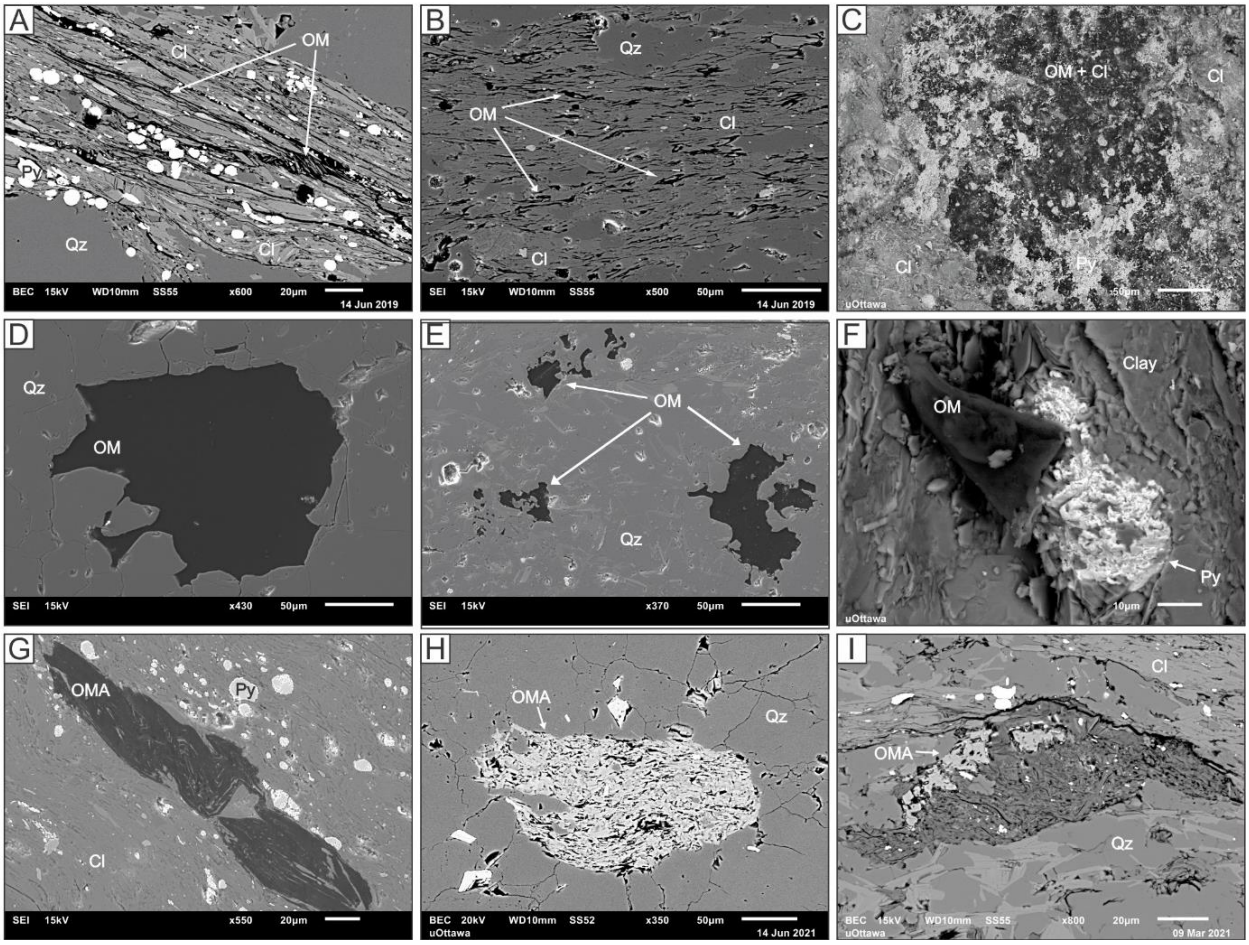

Figure 4.10. *A) Backscattered electron micrograph of a black, clay-rich band in an organic-rich sandstone (perpendicular to bedding). Nano-scale rims of organic matter (OM, black) surround most clay particles (Cl, light grey). B) Secondary electron micrograph of a clay-rich band in an organic-rich sandstone (perpendicular to bedding). C) Backscattered electron micrograph of an organic-rich mudstone (parallel to bedding). Clay particles (dark grey, cloudy to needle-like in appearance) and framboidal pyrite (light grey) surrounded by organic carbon (black). D) Secondary electron micrograph of an amorphous carbon particle in and orange sandstone. E) Secondary electron micrograph of dispersed carbon particles in an orange sandstone band. F) Secondary electron micrograph of a carbon particle and pyrite framboid (py) in an organic-rich claystone. G) Secondary electron micrograph of an organomineralic aggregate (OMA) composed primarily of OM surrounded by pyrite framboids and clay grains. H) Backscattered electron micrograph of an OMA composed primarily of chlorite grains. I) Backscattered electron micrograph of an OMA composed of muscovite, OM, and pyrite surrounded by clay and silt.*

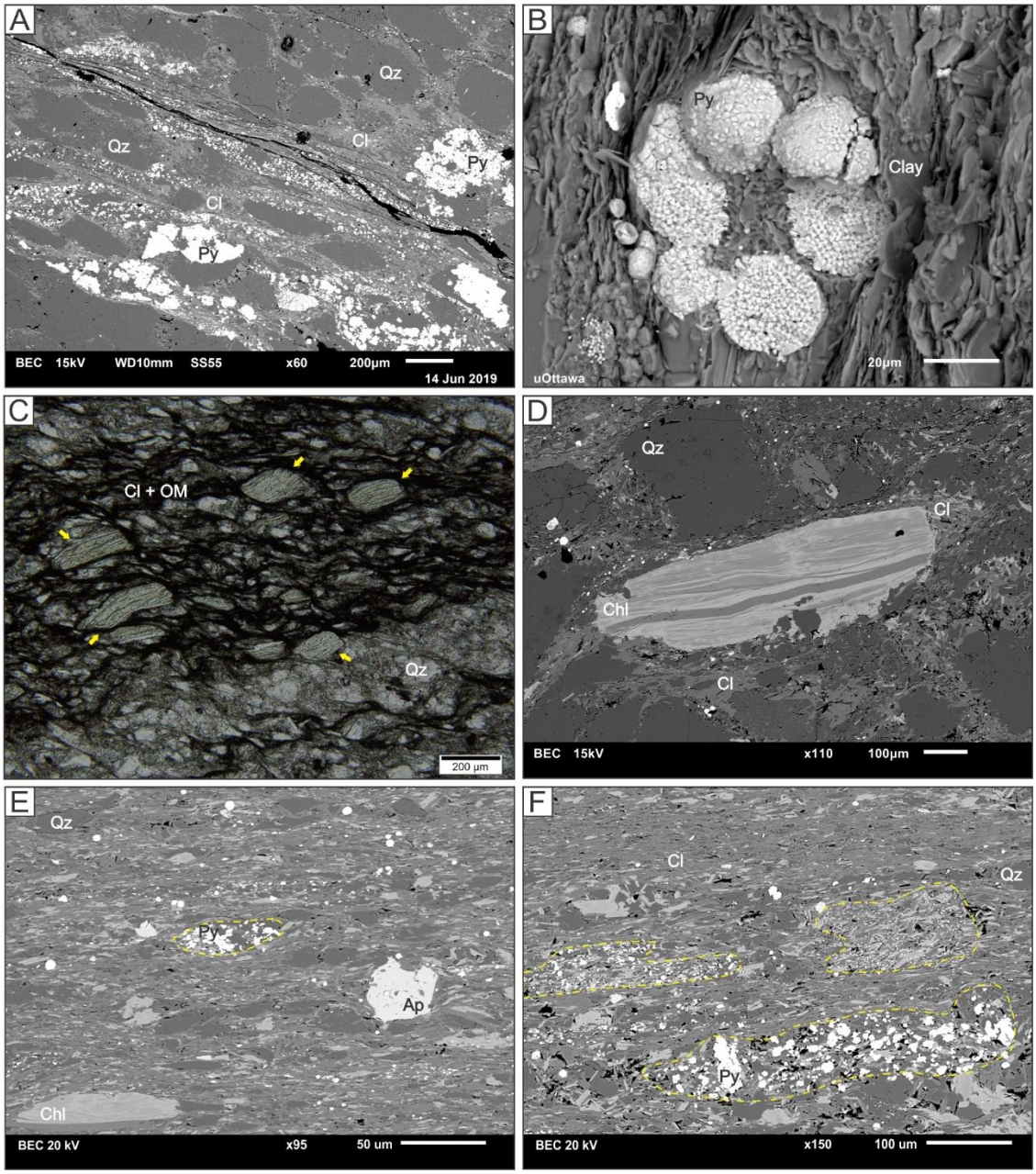

Figure 4.11. *A) Backscattered electron micrograph of a black, clay-rich band in an organic-rich sandstone (perpendicular to bedding). At this scale the OM surrounding individual clay grains cannot be observed (see Fig. 9A) but note the abundance of pyrite (dominantly framboidal) within the clay. B) Secondary electron micrograph of a pyrite framboid within an organic-rich claystone. C) Authigenic chlorite crystals (indicated by yellow arrows) within a clay-rich band of an organic-rich sandstone. D) Backscattered electron micrograph of an authigenic chlorite crystal (Chl) surrounded by clay and quartz grains. E) Backscattered electron micrograph of a clay-rich band of organic-rich sandstone. Note the presence of amorphous carbonate apatite (Ap), authigenic chlorite, and outlined by dashed yellow lines, pyritized organomineralic aggregates. F) Backscattered electron micrograph of three pyritized organomineralic aggregates (outlined by dashed yellow lines) made up of pyrite framboids (white), clay grains (light grey), and silt grains (dark grey).*

4.4.4 Geochemistry

4.4.4.1 Total Organic Carbon (TOC) Content

Previous work at Castle Creek has shown that background TOC values in channel and more typical levee deposits of the Isaac Formation at Castle Creek are ≤ 0.1 % (Davis 2011; Bergen 2017). Geochemical data from the 18 samples analyzed for TOC in this study, plus the unpublished data of Davis (2011), are presented in Table 4.1 and show that TOC in organic-rich facies ranges from 0.2 % to 4.04 %. These values are uncorrected for the effects of lower greenschist metamorphism and probable loss of ~ 50 – 80 % of the original organic carbon content (Hayes et al. 1983; Smith et al. 2014), suggesting that depositional values may have been as high as 20 %.

Sample ID	TOC (%)
CS 34	1.8
CS 1.29	1.5
CN 1X	0.7
CN 1Y	0.6
CN 1Z	0.6
CN 2.19	0.4
AS 0	0.8
Ch2 30	1.0
Ch2 50	0.8
J 0	0.5
J 10	1.0
J 20	0.5
J 27	1.4
J 32	0.4
J 40	1.8
J 50	0.4
COM 7	4.0
TM V	1.5
TM W	3.1
TM X	1.4
TM Y	1.3
TM Z	1.3
TM B	2.1
CN 11	0.4
CN 24	0.4
A 0	1.6
A 40	0.5
*2.1	0.4
*4.1	0.5
*5.5	0.4
*5.24	0.8
*M2.1	0.7
*M2.2	0.6
*M2.4	0.4
*M2.5	0.5

Table 4.1. *Total organic carbon (TOC) in organic-rich beds. Values with an asterisk are from Davis (2011).*

4.4.4.2 Organic Carbon Isotopes ($\delta^{13}C_{org}$)

Measured $\delta^{13}C_{org}$ values in this study are presented in Table 4.2 and reflect the $\delta^{13}C_{org}$ of the primary detrital organic carbon. Values range from -20.3 ‰ to -26.09 ‰. This is consistent with previous work that report $\delta^{13}C_{org}$ values in levee deposits elsewhere at Castle Creek ranging from -18.0 ‰ to -28.5 ‰ (Davis 2011, see also Table 4.2). It is important to note that thermal alteration may have altered the isotopic signature of primary organic carbon (McKirdy and Powell 1974; Hayes 1983; Kaufman et al. 1991; Des Marais 2001), but in this case (burial diagenesis and low-grade metamorphism) would have increased the $\delta^{13}C_{org}$ signatures of these strata by at most a few per mil (Arthur et al. 1983; Hayes 1983; Hayes 1993; Des Marais 2001; Razvazzhaeva et al. 2007; Osterhout et al. 2019), and therefore insufficient to alter the results and interpretations in this study.

Sample ID	$\delta^{13}C_{org}$ (‰)
CS 34	-24.8
CS 1.29	-24.8
CN 1X	-25
CN 1Y	-24.7
CN 1Z	-24.6
CN 2.19	-24.2
AS 0	-24.2
Ch2 30	-23.8
Ch2 50	-13.8
J 0	-23.4
J 10	-23.8
J 20	-24.1
J 27	-22.7
J 32	-24.9
J 40	-24.4
J 50	-26.1
COM 7	-19.3
TM V	-23.3
TM W	-23.9
TM X	-23
TM Y	-23.7
TM Z	-24.2
TM B	-22.7
*2.1	-24.4
*4.1	-24.4
*5.5	-24.2
*5.24	-22.9
*M2.1	-24.6
*M2.2	-24.7
*M2.4	-28.5
*M2.5	-24.2

Table 4.2. *Organic carbon isotope data ($\delta^{13}C_{org}$) from organic-rich beds. Values shown with an asterisk are from Davis (2011).*

4.4.4.3 Carbonate Isotopes ($\delta^{13}C_{carb}$)

$\delta^{13}C_{carb}$ was measured from dolomite cement in the orange bands. Values range from -5.6 ‰ to -9.5 ‰ and are presented in Table 4.3.

Sample ID	$\delta^{13}C_{carb}$ (‰)
TS 3A	-8.1
TS 3B	-8
TS 3C	-8.1
TS 3D	-8.3
SS 3	-9.1
SS 8	-7.9
SS 10	-9.5
A S8	-5.6
CS 28	-9.3

Table 4.3. *Inorganic (carbonate) carbon ($\delta^{13}C_{carb}$) isotope data from organic-rich beds.*

4.5 Discussion

4.5.1 Source of Organic Matter

The organic matter in this study is interpreted to have originated in updip shelfal areas before being remobilized downslope by turbidity currents. Because terrestrial plants had not yet evolved in the Neoproterozoic (Behrensmeyer et al. 1992; Butterfield 2015; Gensel 2021), the potential sources of OM are restricted to marine organisms, including various kinds of ancient algae and bacteria, such as cyanobacteria. However, due to the effects of lower greenschist metamorphism it is not possible to determine with confidence the original molecular composition of the organic matter or resolve fine-scale morphological structural details that could help identify specific organic groups or species.

Likewise, it is not possible to accurately assess the relative contribution of various organic components based solely on stable carbon isotope data. All photosynthetic bacteria, algae, and plants preferentially use light carbon isotopes (^{12}C) in redox reactions to maximize energy generation, and therefore exhibit ^{12}C-enriched isotopic signatures, but the degree of isotopic fractionation is dependent on various metabolic processes and will differ between

different groups (e.g., Arthur et al. 1983; Gearing et al. 1984; Clarke 2015), but with considerable overlap. For example, marine phytoplankton such as cyanobacteria generally have $\delta^{13}C_{org}$ values that range from -10 ‰ to -31 ‰, whereas algae $\delta^{13}C_{org}$ values typically range from -3 ‰ to -23 ‰ (Arthur et al. 1983). The values measured in this study (Table 4.2) range from -18 ‰ to -28.5 ‰, and probably represent a mix of organic carbon sourced from multiple types of marine microorganisms.

Notably, fragments of stromatolites (and oolites) are commonly preserved in mass-transport deposits at Castle Creek (e.g., Arnott et al. 2011), indicating that cyanobacterial production, including stromatolites and bacterial mats, were prevalent in shallower water on the shelf. This, combined with the overall low $\delta^{13}C_{org}$ values measured (average = -24 ‰), suggests that cyanobacteria were probably the dominant source of OM in these sediments, rather than algae. Indeed, both the discrete sand-sized carbon grains and the sand-sized organomineralic aggregates are interpreted to be detrital grains sourced from disaggregated bacterial mats that grew on the continental shelf.

The third type of organic matter, nanometer- to micrometer-scale coatings around clay grains, is interpreted to have originated as freely suspended micro- and nano-scale organic compounds and extracellular polymeric substances (EPS) that made up part of the suspended organic carbon pool in the upper water column over the continental shelf and further offshore. These biologically synthesized substances are produced by microorganisms and constitute a significant portion (up to 40%) of the modern marine carbon pool, and can encapsulate cell surfaces, form hydrated biofilms, or be freely released into suspension (Falkowski et al. 1998; Bhaskar and Bhosle 2005; Cao et al. 2011; Craig et al. 2020). They can also significantly impact the physical dynamics of sediment gravity flows (Dade et al. 1996; Baker et al. 2017; Craig et al.

2020), which as discussed next, has important implications on the transport, deposition, and preservation of sediment and OM in the deep sea.

4.5.2 Transport, Deposition, and Preservation of Organic Matter

The different types of OM observed in this study are interpreted to have different sources as well as different transport and depositional histories. Planar-laminated orange sandstone at the base of F2 beds consists of fine-grained, mostly quartz sand and discrete sand-sized carbon grains and organomineralic aggregates sourced from disaggregated bacterial mats (Davis 2011; Bergen 2017), suggesting that both organic and mineral grains were hydraulically equivalent and transported, most probably initially in suspension, but then deposited together as bed-load particles from depletive turbidity currents travelling down the levee slope. The depositional history of the nanometer- to micrometer-scale carbon associated with clay-sized grains in the black bands, on the other hand, is somewhat more complex.

Biologically synthesized organic substances like EPS are dominated by high-molecular-weight polysaccharides and can interact with clay grains via a number of physicochemical processes, such as polymer bridging, intercalation within swelling clay minerals, ion-dipole interaction, and hydrogen bonding (e.g., Keil et al. 1994; Mayer 1994; Ransom et al. 1997; Salmon et al. 2000; Kennedy et al. 2002; Winterwerp and Van Kesteren 2004; Bhaskar and Bhosle 2005; Cao et al. 2011; Van Leussen 2011; Tan et al. 2014), all of which result in OM becoming intimately associated with mineral surfaces. This association of organic compounds with clay mineral surfaces, both physical and chemical, has been widely shown to stabilize and protect the OM from degradation and remineralization, both in the water column and during deposition and later burial diagenesis (Keil et al. 1994; Mayer 1994; Keil et al. 1997a; Salmon et

al. 2000; Burdige 2007; Kennedy et al. 2014; Hemingway et al. 2019). The adsorption of OM onto clay grains also acts to facilitate flocculation by increasing biological cohesion and the size of discrete cohesive clay grains. These grains, in turn, form a network of interconnected particles that increases effective viscosity and yield strength of the suspension (Dade et al. 1996; Winterwerp and Van Kesteren 2004; Bhaskar and Bhosle 2005; Van Leussen 2011; Tan et al. 2014), which can significantly alter near-bed conditions in sediment gravity flows, and lead to *en-masse* deposition of both organo-clay aggregates and sand (Dade et al. 1996; Baker et al. 2017; Craig et al. 2020; Hussain et al. 2021). It is this phenomenon that is interpreted to result in the distinctive banding of clean, cemented sandstone and OM- and matrix-rich sandstone in "tiger-striped" F2 beds.

As described above, tiger-stripe beds consist of a distinctively banded interval (tiger-stripe) sandwiched between two clean, orange, fine-grained sandstone layers. In the Castle Creek study area these strata are confined to the deposits of levees that bound deep-sea channels and are notably thicker than the typically thinly-bedded, OM-poor levee strata. The significant thickness and OM content of these beds suggests that they were deposited by anomalously large, outsized flows that continuously overspilled the channel (Cunningham and Arnott 2021) and were sourced directly from the shelf, where the OM was being produced in abundance. Levees are somewhat unique in that sediment is derived mostly from the pre-sorted, dilute suspension at the top of channelized flows, which detach from the more dense, higher-energy channel-bound part as they overtop the levee crest and overspill onto the levee. Steep spatial gradients in sediment transport results in flow collapse and rapid particle settling, which in this case is interpreted to deposit the clean, planar-stratified, fine-grained orange sandstone in the lower part of the bed (Fig. 4.12A). The dominance of planar stratification suggests that flow conditions, and

in particular density structure, was not conducive to the development of angular bed forms like ripples or dunes, and instead sediment transport patterns were more or less spatially uniform and a planar bed surface prevailed (e.g., Arnott 2012; Tilston et al. 2015).

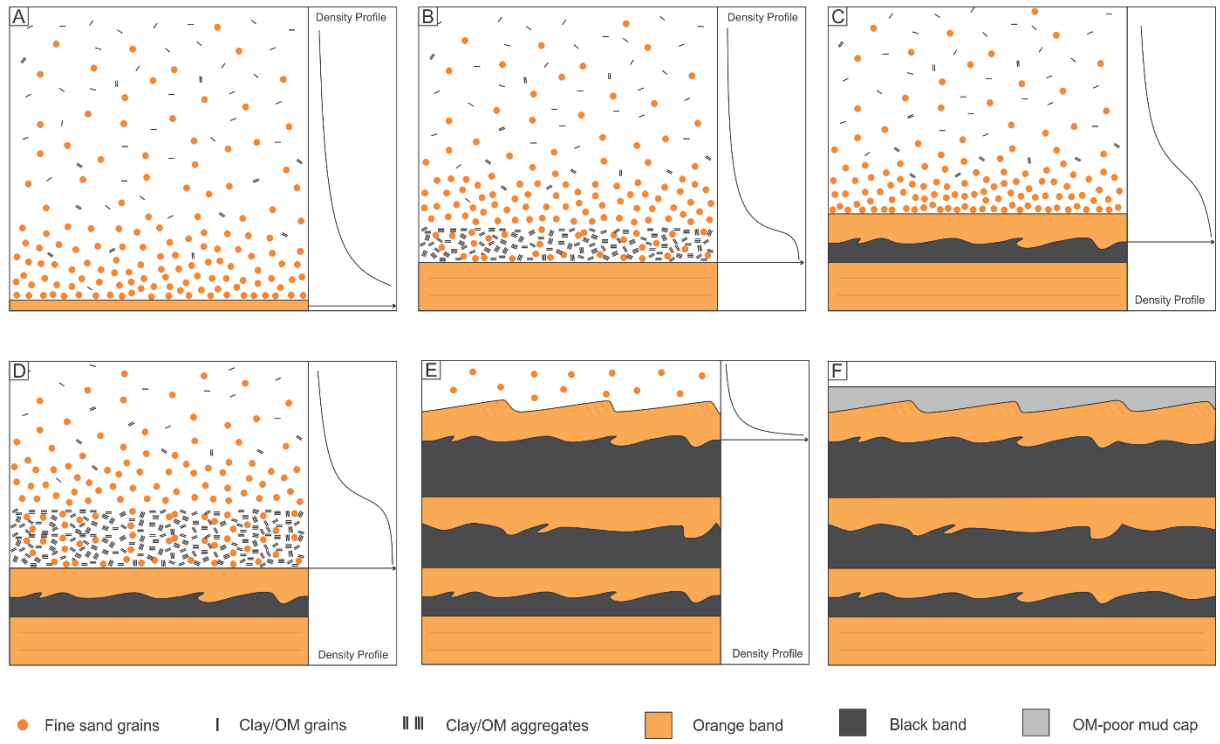

Figure 4.12. *Schematic illustrating the deposition of a banded tiger-striped bed. Density profiles for each stage are shown on the right. A) Fast settling sand grains fall to bed and then are moved as bed load building up the basal planar-stratified orange sandstone band. B) Depleted sand content in near-bed region increases the local mud (OM and clay)-to-sand ratio, increasing viscosity and trapping sand grains until it forms a cohesive plug that freezes and deposits a black, matrix-rich sand layer. C) Settling of sand grains builds up the next clean sand band that founders into the underlying low-density, water-saturated, mud and OM-rich band. D) Like in part B, depleted sand content but elevated mud content increases viscosity and eventually results in the en masse deposition of a black, muddy sand band. Parts C and D are then repeated multiple times. E) Final stage, the flow is fully turbulent and strongly density stratified, promoting the development of current ripples and lastly capped (F) by a thin, organic-poor mudstone (Tde division).*

Further upward, thin, and then increasingly thicker and more abundant matrix-rich bands that make up the distinctively tiger-stripe middle part of the bed, form, and record continued flow deceleration and increased settling of OM and clay-sized particles and aggregates.

However, the distinctive rhythmic intercalation of clean, planar-stratified orange sandstone and black, matrix-rich sandstone in the tiger stripe part of the bed, a motif that closely resembles the banding in the M2 division of deep-water "slurry beds" described by Lowe and Guy (2000), suggests a rhythmic alternation of depositional conditions. Lowe and Guy attribute the banding to repetitive changes in the sedimentary texture and mineralogical composition in the near-bed region of flows enriched in mud. As flow strength wanes sand grains preferentially settle and build up the basal clean sandstone band under turbulent flow conditions. Lower density, more slowly settling mud aggregates begin to accumulate in the very near-bed region, increasing the local mud-to-sand ratio. This build-up of organics and mud increases the cohesion, shear strength, and viscosity in the near-bed layer until it forms a cohesive viscous sublayer of mud aggregates and dispersed sand beneath the overriding turbulent flow. Eventually, compaction caused by sand settling from the overlying flow and accumulating on top of the muddy layer causes the cohesive plug-like flow to collapse and deposit *en-masse*. This process then repeats with clean sand being deposited when turbulent forces dominate in the near-bed region and matrix-rich sandstones deposited when cohesive forces dominate (Fig. 4.13).

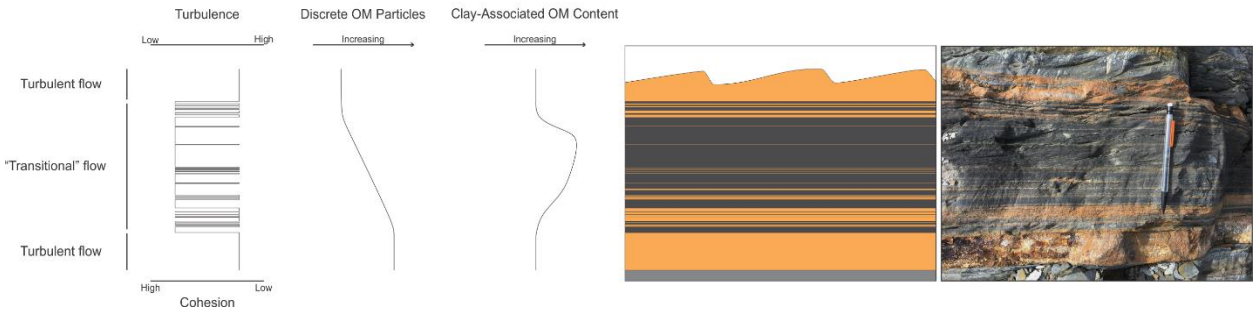

Figure 4.13. *Schematic showing the relative strength of turbulent and cohesive forces during the deposition of a single banded (tiger-stripe) OM-rich sandstone. Outcrop photograph and a simplified schematic highlighting each band shown on right. Plots showing changes in relative turbulence, clay-associated OM content, and number of discrete OM particles during deposition are shown on left.*

A similar, but slightly different explanation builds on the concept of transitional flows in mud-rich open-channel flows, described first by Wang and Plate (1996), and more recently advanced by Baas et al. (2009, 2011, 2016), and Baker and Baas (2020). According to Wang and Plate transitional flows have low to moderate Reynolds numbers and simultaneously exhibit both laminar and turbulent flow conditions, but in different parts of the flow – specifically, laminar conditions immediately above the bed overlain by a turbulent region and capped by a non-shearing plug. Interestingly, in the intervening region between the lower laminar and upper turbulent layers Wang and Plate note the irregular alternation of laminar and turbulent flow conditions – a phenomenon described by their "intermittency factor" (see their figure 3 and compare figures 4 and 5). Baas and Best (2004) and Baas et al. (2009) expand on this and attribute turbulence generation to an internal free-shear layer that develops between the lower part of the flow with its steep velocity gradient and the negligibly developed gradient in the overlying plug. In the case of tiger stripes, bands of clean, parallel-stratified, orange fine-grained sand are interpreted to have been built up of sediment that fell from suspension and then was transported along the bed when turbulence extended very close to the bed (Fig. 4.12B). Moreover, the lack of a strongly stratified density structure in the near-bed region prevented angular bed forms (ripples/dunes) from developing, and instead bed-surface sediment transport remained more less uniform, forming planar stratification on the bed (e.g., Arnott 2012; Tilston et al. 2015).

The preferential settling of sand particles from the near-bed region proportionately increased the abundance of OM and clay-size particles and aggregates, which despite high shear, promoted particle-particle interaction and the development of an increasingly more interconnected particle network (Fig. 4.12C). The corresponding increase in effective viscosity

and yield strength resulted in an upward thickening of the basal laminar sublayer and upward displacement of the zone of turbulence generation (see also Wang and Plate 1996; Baas et al. 2009). Eventually a threshold yield strength in the very near-bed region was exceeded leading to gelling and *en-masse* deposition of a black, matrix-rich band (Fig. 4.12C). This process was then repeated multiple times (Fig. 4.12D, E). The upward thickening and increased abundance of black matrix-rich sandstone bands records depletive depositional conditions during a single sedimentation event and the progressive increase in the proportionate abundance of OM in the suspension. This resulted in increased particle interaction and development of a more extensive particle network that deposited thicker and more frequent black matrix-rich bands. The final stage of deposition is marked by a return to mostly clean, orange, fine-grained sandstone, but this time is mostly ripple-cross-stratified. This suggests that most of the cohesive sediment had been removed from the near-bed region and full-depth turbulent conditions reinstated. Collectively, these conditions may be a consequence of the development of a strongly stratified density profile that would have lowered the height of the mixing layer developed near the velocity maximum, which then added to turbulence being generated lower in the flow (see above) to suspend any residual near-bed clay and organic rich matter and transfer it higher in the flow. Moreover, such a density profile promoted the inception and growth of current ripples on the bed (Arnott 2012; Tilston et al. 2015) (Fig. 4.12F).

Notably, the tiger stripes described here differ from heterolithic strata formed by transitional flows in other studies. For example, Baas et al. (2016) and Baker and Baas (2020) describe heterolithic strata deposited by rapidly decelerated mixed sand-mud flows that consist of stacked sand/mud couplets and an associated suite of distinct bedforms and sedimentary structures, including sandy current ripples, large current ripples, low-amplitude bed waves and

low-angle cross-lamination, and washed-out ripples. More specifically, flow deceleration was accompanied by a progressive change from sandy current ripples under turbulent conditions, followed by large current ripples, and finally low-amplitude bed waves as the near-bed region became more enriched in mud and cohesive forces came to dominate. Although strata in this study are also interpreted to form from decelerating, mixed flows, they contain no such bedforms or cross-lamination. These differences may occur because the flows in this study did not undergo the same one-way transition from turbulent to transitional to laminar. Instead, turbulent conditions, which prevailed during early deposition, were re-established as the flow waned after an intervening episode of transitional flow. Additionally, higher mud content and/or the presence of more abundant OM in the Baker and Baas and Baas examples may have increased the cohesive forces and sustained a more plug-like near-bed density structure throughout the entire depositional event, and as a consequence inhibited the development of angular bed forms.

Notably also, the common (and often extreme) soft-sediment deformation and loading of the clean bands into the matrix-rich bands confirm that deposition of clean bands occurred while the underlying, mud-rich bands were still water-saturated and unconsolidated. This, combined with the lack of a turbiditic mud cap (representing pelagic and hemipelagic fallout) above each light-dark couplet, suggests that the entire stack of light-dark band couplets represents deposition from a single flow (i.e., turbidity current) event comprising multiple individual light-dark couplets.

A similar process of turbulence suppression caused by flocculation and “gelling” of the flow has been suggested to explain the deposition of high TOC, muddy sandstones (Hussain et al. 2021). They also postulated that the rapid emplacement of these thick units can act to protect the OM from post-depositional oxic degradation. This hypothesis is supported by this study,

where the highest TOC contents occur in matrix-rich sandstones rather than organic-rich mudstones, which are instead interpreted to have been deposited by thin, fine-grained, more dilute, lower energy turbidity currents. The presence of diffuse parallel lamination in the mudstone beds suggests that traction transport was still, at least episodically, active rather than purely suspension-settling deposition, and that these beds are equivalent to the T_d division of classical Bouma turbidites (Stow and Bowen 1978). It is also important to note that sedimentation rates on levees are typically high (e.g., Kane et al. 2007, Khan et al. 2011), which could further enhance OM preservation relative to other sub-environments like slope channels and basin-floor depositional lobes. However, the dominance of OM associated with clay mineral surfaces in this study (93%) does suggest that protection of OM by its association with a mineral substrate is essential in its preservation. Accordingly, it is likely a combination of mineral protection and rapid burial promoted the preservation of organic carbon observed here.

4.5.3 Diagenesis of Organic-Rich Strata

The lithology and geochemistry of carbonate cement in the OM-rich strata described here differ significantly from cements in more typical slope strata, which are dominated by iron-poor calcite with $\delta^{13}C_{carb}$ values near 0‰ (Cochrane et al. 2019; Kehew and Arnott 2020). These more typical calcite cements are interpreted to represent primary precipitation from seawater. The distinctive mineral assemblage (ferroan dolomite, pyrite, collophane, and authigenic chlorite) that occurs in organic-rich facies, in contrast, is interpreted to result from progressive diagenesis of the organic matter, which is a reactive, unstable constituent in the sediments. Reactions involving the degradation of organic OM can begin soon after deposition and act to alter the chemical composition of the associated pore fluids (Hesse 1990). With increasing depth and

temperature different diagenetic processes occur, giving rise to various biodiagenetic zones (Fig. 4.14). In order of increasing depth, these zones are 1) bacterial oxidation; 2) bacterial sulphate reduction; 3) bacterial fermentation and methanogenesis; and 4) thermal decarboxylation (Irwin et al. 1977; Curtis 1978; Morad 1998; Mazzullo 2000; Hesse and Schacht 2011).

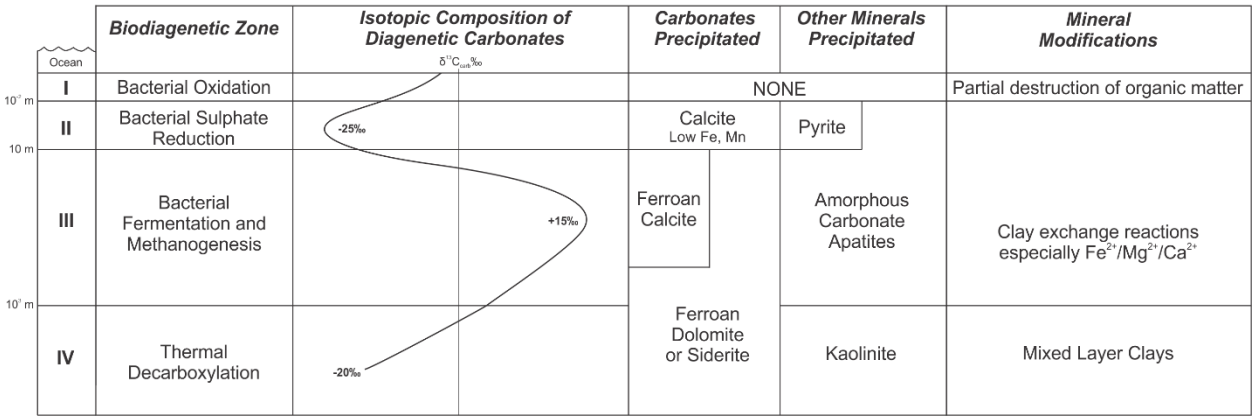

Figure 4.14. *Diagenetic zones in progressively more deeply buried organic-rich marine sediments (after Curtis 1978 and Mazzullo 2000).*

In the strata described here, framboidal pyrite would have been the first diagenetic mineral to form as reducing conditions, indicative of Zone 2, were established. Here, sulphate reducing bacteria participate in organic matter degradation and produce hydrogen and sulphides, which then react with ferrous iron (Fe^{2+}) to form iron sulphides (including pyrite):

$$2CH_2O + SO_4^{2-} \rightarrow 2HCO_3^- + H_2S$$

$$Fe^{2+} + H_2S \rightarrow FeS + 2H^+$$

$$FeS + H_2S \rightarrow H_2 + FeS_2 \text{ (pyrite)}$$

Previous sulphur isotope analyses of rocks from the Isaac Formation by Ross et al. (1995) show depleted signatures suggestive of bacterial reduction of seawater sulfate. Phosphatic compounds such as collophane (amorphous carbonate apatite) may also begin to precipitate at this stage,

with phosphorous sourced from the OM (Curtis 1978). Both reactions produce bicarbonate with a carbonate isotopic composition similar to the original organic carbon source (i.e., ~ -25‰) (Curtis 1978; Kelts and McKenzie 1982; Mazzullo 2000; Meyer 2004; Clarke 2015). This would have increased pore water alkalinity and promoted the precipitation of carbonate cement (Hesse 1990; Boetius et al. 2000). However, early diagenetic carbonate cements are typically iron-poor calcites with strongly depleted (-25‰) $\delta^{13}C$ values (Curtis, 1978), which contrasts the less depleted (-5.6 to -9.5‰) values in ferroan dolomite cements reported here. Instead, these cements most probably formed later at slightly higher burial temperatures and depths, and incorporate bicarbonate produced from both deeper-burial decarboxylation and bacterial fermentation.

Bacterial fermentation of the OM would occur first, producing methane highly depleted in ^{13}C (e.g. -50‰ to -100‰) and bicarbonate highly enriched in ^{13}C (+15‰) (Bottinga 1969; Curtis 1978; Arthur et al. 1983; Mazzullo 2000; Meyer 2004). At this stage, ferrous iron (Fe^{2+}) concentrations begin to increase in porewater due to the lack of sulphide to remove the iron by forming pyrite. In addition, clay mineral reactions, and in particular the smectite-illite transformation, releases Fe^{2+}, Mg^{2+}, and Ca^{2+} into the porewater (Boles 1978; Boles and Franks 1979). With further burial and increase in temperature, decarboxylation of OM will begin and produce bicarbonate with ^{13}C isotopic signatures (-20‰) resembling those in the original organic material (Curtis 1978; Mazzullo 2000). Fe^{2+}, Mg^{2+}, and Ca^{2+} in porewater will react with the bicarbonate produced in these two stages and form ferroan dolomite and siderite cements (Boles 1978; Curtis 1978; Kelts and McKenzie 1982; Mazzullo 2000). Stable inorganic carbon isotopes in these cements range from -5.3‰ to -9.5‰, suggesting the mixing of bicarbonate produced by bacterial fermentation (+15‰) and decarboxylation (-20‰), which based on a simple mass

balance calculation suggests ~ 55 - 65% of the bicarbonate was derived from decarboxylation and 35 - 45% from bacterial fermentation. Finally, authigenic chlorite is interpreted to have formed at temperatures of ~165 °C from the reaction of kaolinite clay with excess Fe^{2+} and Mg^{2+} in the pore fluid (Boles 1978; Boles and Franks 1979; Curtis 1978).

However, the isotope values measured in this study are bulk values, and therefore a mix of the different phases of dolomite growth (i.e. zoned dolomite), which may reflect a more complex diagenetic history. Likewise, mixing of the siderite and ferroan dolomite cements in sample SS 3 may also reduce the significance of the measured $\delta^{13}C_{org}$ value. Further work is needed to fully isolate and evaluate each phase of cement growth within these strata.

4.5.4 Deep-Marine Levees as Efficient Organic Carbon Sinks

Organic matter in marine sediments plays an important role in the global carbon cycle. Organic carbon that becomes sequestered in these sediments is protected from remineralization and becomes preserved over geologic timescales, which serves to remove atmospheric carbon dioxide, and in turn promote the accumulation of oxygen (Fig. 4.15) (Berner and Canfield 1989; Berner 1990; Keil et al. 1994; Hedges and Keil 1995; Burdige 2005; Masiello 2007; Hemingway et al. 2019). It is therefore important to understand both the spatial distribution of organic carbon sinks and the processes that foster its accumulation and preservation.

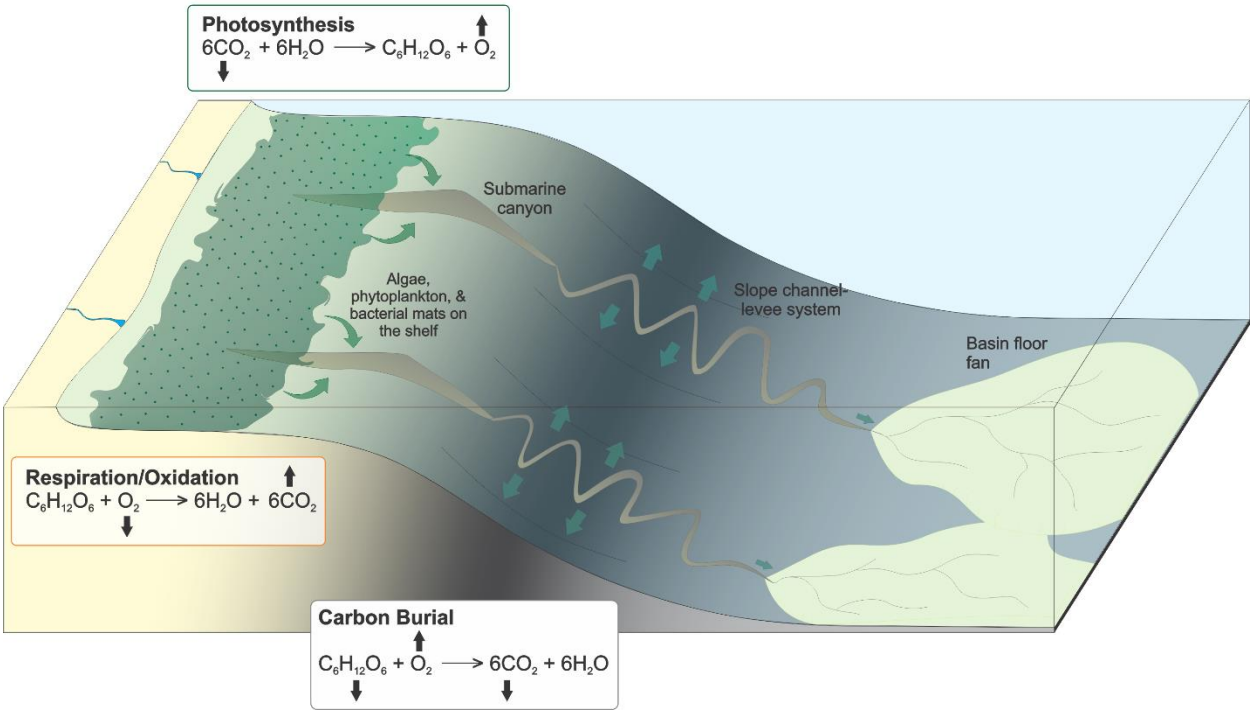

Figure 4.15. *Depositional model showing a shelf to basin floor turbidite system. Shown also is the origin, transport, and deposition of organic material (OM), and the relative impacts of photosynthesis, oxidation, and carbon burial on the carbon budget. Black arrows in the rectangles indicate which products are being consumed (down) or released (up) in each process. Much of the OM resedimented downslope by turbidity currents is preferentially lost (green arrows) to the levees that bound continental slope channels. Residual OM is then transferred to the basin floor where it is diluted by more abundant mineral matter.*

At the Castle Creek study site, levees are the only architectural element that contain significant amounts of OM. This is probably due to the unique flow conditions that occur on levees, and the nature of the OM itself. As previously discussed, ~ 92% of the OM is intimately associated with clay-sized particles that generally is concentrated in the upper parts of turbidity currents where it is prone to overspill onto the levee. Now detached from the channel-bound part of the flow the current over the levee rapidly depletes and leads to significant sedimentation. Within the channel, the more dense, higher energy part of the flow exhibits more progressive deceleration during a single transport event, which tends to prevent low-density and/or small mass particles from interacting and forming larger particle networks and causing any remaining

OM to remain as discrete particles that are flushed through the system to the basin floor where they become diluted by hydraulically similar, but much more abundant, mineral grains.

This work shows that large amounts of OM can be buried in deep-marine levee deposits and, importantly, preserved over hundreds of millions of years. When the substantial thickness and geographical expanse of levees and levee deposits are considered collectively, it follows that they represent significant reservoirs of buried organic carbon. This, then, challenges the common assumption that much of the organic carbon in deep-marine sediments is pelagic in origin and that depleted oxygen, or complete anoxia, in bottom waters is necessary for widespread carbon preservation (e.g., Tissot and Welte 1978; Demaison and Moore 1979). Instead, much OM may be concentrated in sediments that were resedimented by turbulent sediment gravity flows and transported into the deep sea. Adsorption onto clay grains and physical sheltering (through the formation of organo-clay aggregates), in addition to rapid burial in channel-margin levees, allowed OM to be preserved despite the prevalence of well-oxygenated bottom waters (as documented by Milczarek 2018). Accordingly, these results demonstrate the importance of deep-marine levees and depositional processes on organic carbon fluxes on continental margins and emphasize the need to further study and quantify the impact of deep-marine levees in theoretical models of global carbon budgets.

4.5.5 Trends in Carbon Burial over Geologic Time

Although this study has shown that considerable amounts of organic matter can be buried in deep-sea levee systems, and in turn impact global carbon fluxes, OM burial in the Neoproterozoic is not entirely representative of modern systems. Firstly, oceans in the Neoproterozoic were highly enriched in phosphorous (as phosphate) compared to their modern

counterparts (e.g., Papineau 2010; Planavsky et al. 2010; Drummond et al. 2015; Horton 2015; Cox et al. 2016; Laakso et al. 2020). This phosphorus, which is generally believed to be sourced from the weathering of continental crust (Papineau 2010; Planavsky et al. 2010; Horton 2015; Cox et al. 2016), is an essential nutrient that regulates rates of primary productivity, and therefore the rate that atmospheric CO_2 is converted into organic matter (Follmi 1996). The abundance of this essential, but often limiting nutrient in the Neoproterozoic oceans would have promoted organic carbon production, and even if only fractionally preserved, increased the net amount of buried organic carbon. Additionally, because terrestrial plants had not yet evolved in the Neoproterozoic, organic matter was exclusively of marine origin. However, recent studies of modern systems have shown that terrestrial organic matter constitutes a significant portion of the organic content in levee and other deep-marine sediments. For example, Saller et al. (2006), Galy et al. (2007), Baudin et al. (2010), Lee et al. (2019), and Hage et al. (2020) report that > 70% of the organic matter in recent and modern deep-water fan systems is of terrestrial origin. Furthermore, much of this terrestrial organic matter is wood or leaf debris that occurs as coarse detrital particles in sandy turbidites in channel and lobe deposits (Saller et al. 2006; Baudin et al. 2020; McArthur et al. 2016a; Hage et al. 2020). This has several important implications. Marine organic matter is generally more reactive than terrestrial organic matter, and as such is more easily remineralized (e.g., Burdige 1991; Aller et al. 1996; Prahl et al. 1997; Burdige 2005). Because the mechanisms and efficiency by which terrestrial and marine organic matter are buried and preserved can differ significantly, changes in the production rate and relative input of each through geologic time would likely have had a profound effect on the global carbon cycle, and accordingly, atmospheric and climatic conditions. To understand how carbon burial in

marine sediments affects the global carbon cycle, it is therefore important to understand the controls on carbon burial and preservation throughout geologic time.

Changes in production rate and relative input of terrestrial and marine OM would have been dependent on many factors, including the existing biodiversity, glacial cycles and sea level fluctuations, and tectonic cycles. For example, fluctuations in sea level exert a direct control on shelf width, which in turn affects primary productivity — wide, shallow shelves promote increased productivity (e.g., Berger 2001; Davies et al. 2011; James and Jones 2016; Ren et al. 2017). Importantly, fluctuations in sea level are particularly accentuated during icehouse periods, such as the Neoproterozoic, when the amplitude of eustatic changes is greatly increased relative to greenhouse periods (Blum and Womack 2009; Sømme et al. 2009; Sweet and Blum 2016). Reduced amplitude of eustatic change during greenhouse times can allow fluvial systems, especially those with high sediment flux, to remain connected to the deep sea even during highstand conditions, which would further enhance the delivery of terrestrial OM into the deep sea (Keil et al. 1997b; Burdige 2005; Sweet and Blum 2016). During icehouse periods, on the other hand, the increased amplitude of eustatic fluctuations typically results in continental fluvial systems being separated from the deep sea by a wide continental shelf during highstands (Blum and Womack 2009; Sømme et al. 2009; Sweet and Blum 2016; Fraino et al. 2022). This suggests that during the Proterozoic, when marine OM was the single source of organic carbon, icehouse transgressive to the early/middle part of the falling stage systems tracts would provide optimal conditions for OM production and burial in the deep marine.

Tectonics have also been shown to play an important role in organic carbon delivery and burial. Along tectonically active margins, like the modern-day Himalayas, high erosion rates in the hinterland result in high sediment and terrestrial OM flux to the coast (Zhang et al. 2001,

Galy et al. 2007; Masiello 2007). Although much of the sediment produced by this erosion is sequestered in terrestrial and shallow coastal systems (e.g., Clift and Jonell 2021), enough makes it to the deep marine to result in high sedimentation rates and high rates of OM burial and preservation (France-Lanord and Derry 1997; Masiello 2007), and notably in channel-bounding levees (Galy et al. 2007). Future studies should focus on examining how these factors have shaped organic carbon flux to the deep sea throughout geologic time in order to advance our understanding of the global carbon cycle and improve the evaluation of present and future carbon fluxes.

4.6 Conclusions

Observations from continental slope levee deposits of the Neoproterozoic Windermere Supergroup have shown that depositional processes in levees can result in the concentration and enrichment of sedimentary marine organic matter (OM). When the significant thickness and wide geographical extent of levee deposits are considered, it follows that they represent significant geological reservoirs of organic carbon. Although occurring in mudstones, OM is more common in matrix-rich sandstones, and mostly in the form of micro- to nano-scale carbon associated with clay grains. Higher spatial gradients in sediment transport over levees compared to those in the coeval channels results in rapid collapse of turbulent suspensions as they overspill the levee crest resulting in elevated rates of net sedimentation. These conditions, in addition to the general fine-grained, and at times organic rich nature of the overspill, promotes aggregation of OM and clay particles and leads to rapid suspension settling. In strata described here, deposition begins under turbulent conditions with the formation of a planar-stratified T_b division sandstone. This, then, is succeeded by an interval of transitional flow where near-bed hydraulic

conditions irregularly fluctuate between turbulent and non-turbulent flow and deposit the distinctively interstratified black OM-rich and clean orange bands. Later, fully turbulent flow conditions resume and deposit the uppermost unit of OM-poor, mostly ripple cross-stratified sandstone capped by OM-poor mud (T_{cde} divisions).

High rates of sedimentation on levees compared to coeval channels, enhanced by rapid deposition from clay- and OM-rich turbidity currents, coupled with additional protection of OM by its association with clay mineral surfaces, prevent its destruction by oxidation or respiration, thereby effectively sequestering significant amounts of carbon in the sediment and therein a sink for atmospheric CO_2. Significantly, this preservation can occur without bottom-water anoxia. However, carbon burial and preservation in deep-sea sediments can be influenced by many other factors, including biodiversity, glacial cycles, global sea level fluctuations, and tectonic cycles. Improving our knowledge of how these factors have affected the mechanisms and efficiency by which organic carbon has been preserved throughout geologic history will help evaluate past and present global carbon fluxes and improve our understanding of the global carbon cycle.

4.7 References

ALLER, R.C., BLAIR, N.E., XIA, Q., AND RUDE, P.D., 1996, Remineralization rates, recycling, and storage of carbon in Amazon shelf sediments: Continental Shelf Research, v. 16, p. 753-786.

ARNOTT, R.W.C., 2012, Turbidites, and the case of the missing dunes: Journal of Sedimentary Research, v. 82, p. 379-384, doi:10.2110/jsr.2012.29.

ARNOTT, R.W.C., WALLACE, K. AND LAURIN, J., 2011, Stratal architecture and temporal evolution of a passive margin mass-transport deposit, Neoproterozoic Isaac Formation, Cariboo Mountains, British Columbia, Canada, *in* Mass-Transport Deposits in Deepwater Settings, eds. R.C. Shipp, P. Weimer and H.W. Posamentier, SEPM Special Publication, v. 96, 532 p., doi:10.2110/sepmsp.096.221

ARTHUR, M. A., ANDERSON, T. F., KAPAN I. R., VEIZER, J., AND LAND, L. S., 1983, Stable isotopes in sedimentary geology: SEPM Short Course No. 10, 554.

BAUDIN, F., DISNAR, J.R., MARTINEZ, P., AND DENNIELOU, B., 2010, Distribution of the organic matter in the channel-levees systems of the Congo mud-rich deep-sea fan (West Africa). Implication for deep offshore petroleum source rocks and global carbon cycle: Marine and Petroleum Geology, v. 27, p. 995-1010.

BAUDIN, F., STETTEN, E., SCHNYDER, J., CHARLIER, K., MARTINEZ, P., DENNIELOU, B., AND DROZ, L., 2017, Origin and distribution of the organic matter in the distal lobe of the Congo deep-sea fan – A Rock-Eval survey: Deep Sea Research Part II: Topical Studies in Oceanography, v. 142, p. 75-90.

BAUDIN, F., RABOUILLE, C., AND DENNIELOU, B., 2020, Routing of terrestrial organic matter from the Congo River to the ultimate sink in the abyss: A mass balance approach: Geologica Belgica, v. 23, ff10.20341/gb.2020.004.

BEHRENSMEYER, A.K., DAMUTH, J.D., DIMICHELE, W.A., POTTS, R., SUES, H.D. AND WINGS, S.L., 1992, Terrestrial ecosystems through time. evolutionary paleoecology of terrestrial plants and animals, University of Chicago Press, Chicago IL.

BERGEN, A.L., 2017, Vertical and lateral facies architecture of levees and their genetically-related channels, Isaac Formation, Neoproterozoic Windermere Supergroup, Cariboo Mountains, B.C.: Unpublished M.Sc. thesis, Université d'Ottawa/University of Ottawa, 193 p.

BERGEN, A.L., CUNNINGHAM, C.M., TERLAKY, V., AND ARNOTT, R.W.C., 2022, Influence of sediment supply and related channelized-flow density structure on the timing and stratal architecture of deep-marine levee sedimentation: Journal of Sedimentary Research, v. 92, p. 1257-1274.

BERGER, A., 2001, The role of CO2, sea-level and vegetation during the Milankovitch-forced glacial-interglacial cycles, *In* Bengtsson LO, Hammer UC (eds) Geosphere-Biosphere Interactions and Climate. Cambridge University Press, New York, p. 119-146.

BERNER, R.A., 1982, Burial of organic carbon and pyrite sulfur in the modern ocean: its geochemical and environmental significance: American Journal of Science, v. 282, p. 451-473.

BERNER, R.A., 1990, Atmospheric carbon dioxide levels over Phanerozoic time: Science, v. 249, p. 1382-1386.

BERNER, R.A. AND CANFIELD, D.E., 1989, A new modal for atmospheric oxygen over Phanerozoic time: American Journal of Science, v. 289, p. 333-361.

BHASKAR, P.V., AND BHOSLE, N.B., 2005, Microbial extracellular polymeric substances in marine biogeochemical processes: Current Science, v. 88, p. 45-53.

BLUM, M.D., AND HATTER-WOMACK, J., 2009, Climate change, sea-level change, and fluvial sediment supply to deepwater depositional system, *in* Kneller, B., Martinsen, O.J., and McCaffrey, B., eds., External Controls on Deepwater Depositional Systems: SEPM Special Publication 92, p. 15–39.

BOETIUS, A., FERDELMAN, T., AND LOCHTE, K., 2000, Bacterial activity in sediments of the deep Arabian Sea in relation to vertical flux; the biogeochemistry of the deep Arabian Sea: Deep Sea Research Part II: Topical Studies in Oceanography, v. 47, p. 2835, 2875.

BOLES, J.R., 1978, Active ankerite cementation in the subsurface Eocene of Southwest Texas: Contributions to Mineralogy and Petrology, v. 68, p. 13-22.

BOLES, J.R. AND FRANKS, S.G., 1979, Clay diagenesis in Wilcox Sandstones of Southwest Texas; implications for smectite diagenesis on sandstone cementation: Journal of Sedimentary Research, v. 49, p. 55-70.

BOTTINGA, Y., 1969, Calculated fractionation factors for carbon and hydrogen isotope exchange in the system calcite-carbon dioxide-graphite-methane-hydrogen-water vapor: Geochimica et Cosmochimica Acta, v. 33, v. 49-64.

BOUMA, A.H., 1962, Sedimentology of Some Flysch Deposits: A Graphic Approach to Facies Interpretation: [Published Ph.D. (Doctoral dissertation)], Elsevier, 168p.

BURDIGE, D.J., 1991, The kinetics of organic matter mineralization in anoxic marine sediments: Journal of Marine Research, v. 49, p. 727-761.

BURDIGE, D.J., 2005, Burial of terrestrial organic matter in marine sediments: A reassessment: Global Biogeochemical Cycles, v. 19, p. 1-7.

BURDIGE, D.J., 2007, Preservation of organic matter in marine sediments: controls, mechanisms, and an imbalance in sediment organic carbon budgets?: chemical reviews, v. 107, p. 467-485.

BUTTERFIELD, N.J., 2015, Early evolution of the Eukaryota: Palaeontology, v. 58, p. 5-17.

CAMPBELL, R.B., MOUNTJOY E.W., AND YOUNG F.G., 1973, Geology of McBride map-area, British Columbia: Geological Survey of Canada, Paper v. 72, 104 p.

CAO, Y., WEI, X., CAI, P., HUANG, Q., RONG, X., AND LIANG, W., 2011, Preferential adsorption of extracellular polymeric substances from bacteria on clay minerals and iron oxide: Colloids and Surfaces B: Biointerfaces, v. 83, p. 122-127.

CLARK, I. D., 2015, Groundwater geochemistry and isotopes. Boca Raton, Florida, USA: CRC press, 97-119; 169-208.

CLARK, J.D., AND PICKERING, K.T., 1996, Architectural elements and growth patterns of submarine channels: application to hydrocarbon exploration: American Association of Petroleum Geologists Bulletin, v. 80, p. 194-220.

CLEMENCEAU, G.R., COLBERT J., AND EDENS D., 2000, Production results from levee-overbank turbidite sands at Ram/Powell Field, deepwater Gulf of Mexico, in Weimer, P., Slatt, R.M., Coleman, J., Rosen, N.C., Nelson, H., Bouma, A.H., Styzen, M.J., and Lawrence, D.T., eds., Deep-Water Reservoirs of the World, Gulf Coast Section of the Society for Sedimentary Geology Foundation 20th Annual Research Conference, p. 241-251.

CLIFT, P. D., AND JONELL, T. N., 2021, Monsoon controls on sediment generation and transport: Mass budget and provenance constraints from the Indus River catchment, delta and

submarine fan over tectonic and multimillennial timescales: Earth-Science Reviews, v. 220, 103682.

COCHRANE, D.J., NAVARRO, L., AND ARNOTT, R.W.C., 2019, Sedimentological and geochemical evolution of an Ediacaran mixed carbonate-siliciclastic continental slope system, Windermere Supergroup, southern Canadian Cordillera, British Columbia, Canada: Precambrian Research, v. 327, p. 47-67.

COLPRON, M., LOGAN, J.M., AND MORTENSEN, J.K., 2002, U-Pb zircon age constraint for late Neoproterozoic rifting and initiation of the lower Paleozoic passive margin of western Laurentia: Canadian Journal of Earth Sciences, v. 39, p. 133-143.

CRAIG, J.M., BAAS, J.H., AMOS, K.J., STRACHAN, L.J., MANNING, A.J., PATERSON, D.M., HOPE, J.A., NODDER, S.D., AND BAKER, M.L., 2020, Biomediation of submarine sediment gravity flow dynamics: Geology, v. 38, p. 72-76. http://doi.org/10.1130/G46837.1.

CUNNINGHAM, C.M., AND ARNOTT, R.W.C., 2021, Systematic organization of thin-bedded turbidites in ancient deep-marine levees: Possible evidence of rhythmic pulsing in turbidity currents: Journal of Sedimentary Research, v. 91(11), p. 1257-1274. http://doi.org/10.2110/jsr.2020.003.

CURTIS, C.D., 1978, Possible links between sandstone diagenesis and depth-related geochemical reactions occurring in enclosing mudstone: Journal of the Geological Society, v. 135, p. 107-117.

DADE, W.B., SELF, R.L., PELLERIN, N.B., MOFFET, A., JUMARS, P.A., AND NOWELL, A.R.M., 1996, The effects of bacteria on the flow behavior of clay-seawater suspensions: Journal of Sedimentary Research, v. 66, p. 39-42.

DAVIES, M.H., MIX, A.C., STONER, J.S., ADDISON, J.A., JAEGER, J., FINNEY, B., AND WIEST, J., 2011, The deglacial transition on the southeastern Alaska Margin: Meltwater input, sea level rise, marine productivity, and sedimentary anoxia: Paleoceanography: v. 26, p. 1-18. doi:10.1029/2010PA002051.

DAVIS, L., 2011, Architecture of deep-marine interchannel deposits: Isaac Formation, Windermere Supergroup (Neoproterozoic), southern Canadian Cordillera: M.Sc. thesis, Université d'Ottawa/University of Ottawa, 174 p.

DE JESUS MENDES, P.A., THOMSEN, L., HOLSCHER, B., DE STIGTER, H.C., GUST, G., 2007, Pressure effects on the biological degradation of organo-mineral aggregates in submarine canyons: Marine Geology, v. 246, p. 165-175.

DEMAISON, G.J., AND MOORE, G.T., 1980, Anoxic environments and oil source bed genesis: American Association of Petroleum Geologists Bulletin, v. 64, p. 1179-1209.

DES MARAIS, D.J., 2001, Isotopic Evolution of the Biogeochemical Carbon Cycle During the Precambrian: Reviews in Mineralogy and Geochemistry, v.43, p. 555–578, doi:10.2138/gsrmg.43.1.555

EVENCHICK, C.A., PARRISH, R.R., AND GABRIELSE, H., 1984, Precambrian gneiss and late Proterozoic sedimentation in north-central British Columbia: Geology, v. 12, p. 233-237.

EYSTER, A., FERRI, F., SCHMITZ, M.D., AND MACDONALD, F.A., 2018, One diamictite and two rifts: Stratigraphy and geochronology of the Gataga Mountain of northern British Columbia: American Journal of Science, v. 318, p. 167-207.

FALKOWSKI, P.G., BARBER, R.T., AND SMETACEK, V., 1998, Biogeochemical controls and feedbacks on ocean primary production: Science, v. 281, p. 200-206.

FRAINO, P.E., 2020, Spatial and Temporal Stratal Evolution of an Ancient Deep-Marine Channel-Levee Complex, Neoproterozoic Isaac Formation, Windermere Supergroup, British Columbia, Canada [M.Sc. thesis]: University of Ottawa, 211 p.

FRAINO, P.E., ARNOTT, R.W.C., AND NAVARRO, L., 2022, The influence of sediment supply on the stratigraphic evolution of an ancient passive margin deep-marine slope channel system, Windermere Supergroup, British Columbia, Canada: Journal of Sedimentary Research, v. 92, p. 232-256.

FRANCE-LANORD, C., AND DERRY, L.A., 1997, Organic carbon burial forcing of the carbon cycle from Himalayan erosion: Nature, v. 390, p. 65-67.

GALY, V., FRANCE-LANORD, C., BEYSSAC, O., FAURE, P., KUDRASS, H., AND PALHOL, F., 2007, Efficient organic carbon burial in the Bengal fan sustained by the Himalayan erosional system: Nature, v. 450, p. 407-410. https://doi.org/10.1038/nature06273

GEARING, J.N., GEARING, P.J., RUDNICK, D.T., REQUEJO, A.G., AND HUTCHINS, M.J., 1984, Isotopic variability of organic carbon in a phytoplankton-based, temperate estuary: Geochimica et Cosmochimica Acta, v. 48, p. 1089-1098.

GENSEL, P.G., 2021, When did terrestrial plants arise?: Science, v. 373, p. 736-737.

HADLARI, T., ARNOTT, R. W. C., MATTHEWS, W. A., POULTON, T. P., ROOT, K., MADRONICH, L. I., AND SIMMS, A. R., 2021, Provenance of the Incipient Passive Margin of NW Laurentia (Neoproterozoic): Detrital Zircon from Continental Slope and Basin Floor Deposits of the Windermere Supergroup, Southern Canadian Cordillera: Lithosphere, 10 p., doi:10.2113/2021/8356327.

HAGE, S., GALY, V.V., CATIGNY, M.J.B., ACIKALIN, S., CLARE, M.A., GRÖCKE, D.R., HILTON, R.G., HUNT, J.E., LINTERN, D.G., MCGHEE, C.A., AND PARSONS, D.R., 2020, Efficient

preservation of young terrestrial organic carbon in sandy turbidity-current deposits: Geology, v. 48, p. 882-887. https://doi.org/10.1130/G47320.1.

HANSEN, L.A., CALLOW, R.H., KANE, I.A., GAMBERI, F., ROVERE, M., CRONIN, B.T., AND KNELLER, B.C., 2015, Genesis and character of thin-bedded turbidites associated with submarine channels: Marine and Petroleum Geology, v. 67, p. 852-879.

HAYES, J.M., 1983, Practice and principles of isotopic measurements in organic geochemistry, in Organic Geochemistry of Contemporaneous and Ancient Sediments, eds Meinschein W.G., Bloomington, Great Lakes.

HAYES, J. M., 1993, Factors controlling 13C contents of sedimentary organic compounds: principles and evidence: Marine Geology, v. 113, p. 111-125.

HAYES, J. M., KAPLAN, I. R., AND WEDEKING K. W., 1983, Precambrian organic geochemistry; preservation of the record, *in* J. W. Schopf, ed.: Princeton, Princeton Univ. Press.

HAYES, J. M., STRAUSS, H., AND KAUFMAN, A. J., 1999, The abundance of 13C in marine organic matter and isotopic fractionation in the global biogeochemical cycle of carbon during the past 800 Ma. Chemical Geology, 161(1), 103-125.

HAYES, J.M. AND WALDBAUER, J.R., 2006, The carbon cycle and associated redox processes through time: Philosophical Transactions of the Royal Society B: Biological Sciences, v. 361, p.931-950.

HEDGES, J.I., AND KEIL, R.G., 1995, Sedimentary organic matter preservation: an assessment and speculative synthesis: Marine Chemistry, v. 49, p. 81-115.

HEMINGWAY, J.D., ROTHMAN, D.H., GRANT, K.E., ROSENGARD, S.Z., EGLINTON, T.I., DERRY, L.A., AND GALY, V.V., 2019, Mineral protection regulates long-term global preservation of natural organic carbon: Nature, v. 570, p. 228-231. https://doi.org/10.1038/s41586-019-1280-6

HESSE, R., 1990, Early diagentic pore water/sediment interaction: modern offshore basins, *in* I. A. McIlreath, and D. W. Morrow, eds., Diagenesis: Ottawa, Runge Press Ltd., Geological Association of Canada, 277-316.

HESSE, R., & SCHACHT, U., 2011, Early diagenesis of deep-sea sediments. Deep-Sea Sediments. Developments in Sedimentology, Elsevier, Amsterdam, 63, 557-714.

HISCOTT, R.N., HALL, F.R., AND PIRMEZ, C., 1997, Turbidity-current overspill from the Amazon Channel: texture of the silt/sand load, paleoflow from anisotropy of magnetic susceptibility and implications for flow processes, in Flood, R.D., Piper, D.J.W., Klaus,

A., and Peterson, L.C., eds., Proceedings of the Ocean Drilling Program, College Station, Texas, v. 155, p. 53-78.

HUSSAIN, A., HAUGHTON, P.D.W., SHANNON, P.M., MORRIS, E.A., PIERCE, C.S., AND OMMA, J.E., 2021, Mud-forced turbulence dampening facilitates rapid burial and enhanced preservation of terrestrial organic matter in deep-sea environments: Marine and Petroleum Geology, v. 130, 105101. https://doi.org/10.1016/j.marpetgeo.2021.105101

INGRAM, R.L., 1954, Terminology for the thickness of stratification and parting units in sedimentary rocks: Geological Society of America, Bulletin, v. 65, p. 937-938.

IRWIN, H., CURTIS, C., AND COLEMAN, M., 1977, Isotopic evidence for source of diagenetic carbonates formed during burial of organic-rich sediments: Nature, v. 269, p. 209-213.

JAMES, N.P., AND JONES, B., 2016, Origin of carbonate sedimentary rocks. John Wiley & Sons, Ltd., West Sussex, UK.

KANE, I.A., KNELLER, B.C., DYKSTRA, M., KASSEM, A., AND MCCAFFREY, W.D., 2007, Anatomy of a submarine channel-levee: an example from Upper Cretaceous slope sediments, Rosario Formation, Baja California, Mexico: Marine and Petroleum Geology, v. 24, p. 540-563.

KAUFMAN, A.J., HAYES, J.M., KNOLL, A.H., AND GERMS, G.J., 1991, Isotopic compositions of carbonates and organic carbon from upper Proterozoic successions in Namibia: stratigraphic variation and the effects of diagenesis and metamorphism: Precambrian Research, v. 49, p. 301-327.

KEHEW, J., AND ARNOTT, R.W.C., 2020, Litho- and chemostratigraphic analysis of meter-scale cycles in an ancient mixed siliciclastic-carbonate slope system, Windermere Supergroup, Southern Canadian Cordillera, B.C., Canada: Reservoir Magazine, v. 47, p. 8-13.

KEIL, R.G., MONTLUÇON, D.B., PRAHL, F.G., AND HEDGES, J.I., 1994, Sorptive preservation of labile organic matter in marine sediments: Nature, v. 370, p. 549-552.

KEIL, R.G., TSAMAKIS, E., WOLF, N., HEDGES, J.I., AND GOÑI, M., 1997a, Relationships between organic carbon preservation and mineral surface area in Amazon Fan sediments (Holes 932A and 942A): Proceedings of the Ocean Drilling Program, Scientific Results, v. 155, p. 531-538.

KEIL, R.G., MAYER, L.M., WUAY, P.D., RICHEY, J.E., AND HEDGES, J.I., 1997b, Loss of organic matter from riverine particles in deltas Geochimica et Cosmochimica Acta, v. 61, p. 1507-1511.

KELTS, K., AND MCKENZIE, J., 1982, Diagenetic dolomite formation in Quaternary anoxic diatomaceous muds of Deep Sea Drilling Project Leg 64, Gulf of California, *in* Curray,

J.R., Moore, D.G., et al., Initial reports of the Deep Sea Drilling Project, Volume 64: Washington, D.C., U.S. Government Printing Office, p. 553-569.

KENDALL, B. S., CREASER, R. A., ROSS, G. M., AND SELBY, D., 2004, Constraints on the timing of Marinoan "Snowball Earth" glaciation by 187 Re–187 Os dating of a Neoproterozoic, post-glacial black shale in Western Canada: Earth and Planetary Science Letters, 222(3), 729-740.

KENDRICK, J.W., 2000, Turbidite reservoir architecture in the northern Gulf of Mexico deepwater: insights from the development of Auger, Tahoe, and Ram/Powell Fields, in Weimer, P. Slatt, R.M., Coleman, J., Rosen, N.C., Nelson, H., Bouma, A.H., Styzen, M.J., and Lawrence, D.T., eds., Deep-Water Reservoirs of the World: Gulf Coast Section SEPM 20th Annual Research Conference, p. 450–468.

KENNEDY, M.J., PEVEAR, D.R., AND HILL, R.J., 2002, Mineral surface control of organic carbon in black shale: Science, v. 295, p. 657-660.

KENNEDY, M.J., LÖHR, S.C., FRASER, S.A., AND BARUCH, E.T., 2014, Direct evidence for organic carbon preservation as clay-organic nanocomposites in a Devonian black shale; from deposition to diagenesis: Earth and Planetary Science Letters, v. 388, p. 59-70. http://dx.doi.org/10.1016/j.epsl.2013.11.044.

KHAN, Z., 2012, Origin and architecture of deep-water levee deposits: insight from the ancient rock record and experiments. Ph.D. Thesis, University of Ottawa, 300 pp.

KHAN, Z.A., AND ARNOTT, R.W.C., 2011, Stratal attributes and evolution of asymmetric inner- and outer-bend levee deposits associated with an ancient deep-water channel-levee complex within the Isaac Formation, southern Canada: Marine and Petroleum Geology, v. 28, p. 824-842.

KHAN, Z.A., ARNOTT, B., AND PUGIN, A., 2011, An alternative model of producing topography in the crest region of deep-water levees: American Association of Petroleum Geologists, Bulletin, v. 95, p. 2085-2106.

LEE, H., GALY, V., FENG, X., PONTON, C., GALY, A., FRANCE-LANORD, C., AND FEAKINS, S.J., 2019, Sustained wood burial in the Bengal Fan over the last 19 My: Proceedings of the National Academy of Sciences, v. 116, p. 22518-22525.

LINK, P.K., CHRISTIE-BLICK, N., DEVLIN, W.J., ELSTON, D.P., HORODYSKI, R.J., LEVY, M., MILLER, J.M.G., PEARSON, R.C., PRAVE, A., STEWART, J.H., WINSTON, D., WRIGHT, L.A., WRUCKE, C.T., 1993, Middle and Late Proterozoic stratified rocks of the western US Cordillera, Colorado Plateau, and Basin and Range province. *In* Precambrian: Conterminous U.S., The Geology of North America: Geological Society of America Decade of North American Geology Series, v. c-3. Edited by J.C. Reed, Jr. M.E.

Bickford, R.S. Houston, P.K. Link, D.W. Rankin, P.K. Sims, and W.R. Van Schmus, pp. 474-690. https://doi.org/10.1130/DNAG-GNA-C2.463.

LOWE, D.R., AND GUY, M., 2000, Slurry-flow deposits in the Britannia Formation (Lower Cretaceous), North Sea: a new perspective on the turbidity current and debris flow problem: Sedimentology, v. 47(1), p. 31-70.

MACAR, P., 1948, Les pseudo-nodules du Famenien et leur origine: Annales de la Société Géologique de Belgique, v. 72, p. 47–74.

MASIELLO, C.A., 2007, Quick burial at sea: Nature, v. 450, p. 360-361.

MAYER, L.M., 1994, Surface area control of organic carbon accumulation in continental shelf sediments: Geochimica et Cosmochimica Acta, v. 58, p. 1271-1284.

MAZZULLO, S.J., 2000, Organogenic dolomitization in peritidal to deep-sea sediments: Journal of Sedimentary Research, v. 70, p. 10-23.

MCARTHUR, A.D., KNELLER, B.C., WAKEFIELD, M.I., SOUZA, P.A., AND KUCHLE, J., 2016a, Palynofacies classification of the depositional elements of confined turbidite systems: Examples from the Gres d'Annot, SE France: Marine and Petroleum Geology, v. 77, p. 1254-1273.

MCARTHUR, A.D., KNELLER, B.C., WAKEFIELD, M.I., SOUZA, P.A., AND KUCHLE, J., 2016b, Characterization of deep-marine channel-levee complex architecture with palynofacies: An outcrop example from the Rosaria Formation, Baja California, Mexico: Marine and Petroleum Geology, v. 73, p. 157-173.

MCARTHUR, A.D., GAMBERI, F., KNELLER, B.C., WAKEFIELD, M.I., SOUZA, P.A., AND KUCHLE, J., 2017, Palynofacies classification of submarine fan depositional environments: Outcrop examples from the Marnoso-Arenacea Formation, Italy: Marine and Petroleum Geology, v. 88, p. 181-199.

MCDONOUGH, M.R., AND PARRISH, R.R., 1991, Proterozoic gneisses of the Malton Complex, near Valemount, British Columbia: U-Pb ages and Nd isotopic signatures: Canadian Journal of Earth Sciences v. 28(8), p. 1202-1216.

MCKIRDY, D.M., AND POWELL, T.G., 1974, Metamorphic alteration of carbon isotopic composition in ancient sedimentary organic matter: new evidence from Australia and South Africa: Geology, v. 2(12), p. 591-595.

MEYER, L., 2004, Internal architecture of an ancient deep-water, passive margin, basin-floor fan system, Upper Kaza Group, Windermere Supergroup, Castle Creek, British Columbia: M.Sc. thesis, University of Calgary, 188 p.

MILCZAREK, G., 2018, Chemostratigraphic analysis of mudrocks and its implication on provenence and sequence stratigraphy in the Isaac Formation, Windermere turbidite system, Castle Creek, B.C., Canada. Unpublished B.Sc. thesis, University of Ottawa, 59 p.

MORAD, S., 1998, Carbonate cementation in sandstones: controls by patterns of fluid flow and pyscho-chemical, environmental and climatic conditions. *In* Morad, S., Carbonate Cementation in Sandstones, Blackwell Science, 511 p.

NAVARRO, L., AND ARNOTT, R.W.C., 2020, Stratigraphic record in the transition from basin floor to continental slope sedimentation in the ancient passive-margin Windermere turbidite system: Sedimentology, v. 67, p. 1710-1749.

NAVARRO, L., KHAN, Z., AND ARNOTT, R.W.C., 2007, Depositional architecture and evolution of a deep-marine channel-levee complex: Isaac Formation (Windermere Supergroup), Southern Canadian Cordillera, in Nilsen, T.H., Shew, R.D., Steffens, G.S., and Studlick, J.R.J., eds., Atlas of Deep-water Outcrops, American Association of Petroleum Geologists, Studies in Geology, v. 56, CD-ROM.

OSTERHOUT, J.T., CZAJA, A.D., BARTLEY, J.K., AND FRALICK, P.W., 2019, Preservation of carbon isotopes kerogen from thermally altered Mesoproterozoic lacustrine microbialites: Canadian Journal of Earth Sciences, v. 56(10), p. 1017-1026.

POSAMENTIER, H.W., AND KOLLA, V., 2003, Seismic geomorphology and stratigraphy of depositional elements in deep-water settings: Journal of Sedimentary Research, v. 73, p. 367-388.

POSAMENTIER, H.W., AND WALKER, R. G., 2006, Deep-water turbidites and submarine fans: Facies models revisited, SEPM Special Publication 84, Tulsa, Oklahoma, 399-520.

PRAHL, F.G., DE LANGE, G.J., SCHOLTEN, S., AND COWIE, G.L., 1997, A case of post-depositional aerobic degradation of terrestrial organic matter in turbidite deposits from the Madeira Abyssal Plain: Organic Geochemistry, v. 27, p. 141-152.

PRICE, R.A., 2000, The southern Canadian Rockies: Evolution of a foreland thrust and fold belt: Calgary, GeoCanada 2000 (field trip guidebook): Calgary, Canadian Society of Petroleum Geologists, 244p.

RANSOM, B.B.R.H., BENNETT, R.H., BAERWALD, R., AND SHEA, K., 1997, TEM study of in situ organic matter on continental margins: occurrence and the "monolayer" hypothesis: Marine Geology v. 138, p. 1-9.

RAZVOZZHAEVA, E. A., NEMEROV, V. K., & MAKRYGINA, V. A., 2007, Carbon isotope composition of sedimentary rocks in the southern Siberian Platform and surrounding fold systems: Geochemistry International, v. 45(3), p. 261-269.

REID, L.F., SIMONY, P.S., AND ROSS, G.M., 2002, Dextral strike-slip faulting in the Cariboo Mountains, British Columbia: a natural example of wrench tectonics in relation to Cordilleran tectonics: Canadian Journal of Earth Sciences, v. 39, p. 953-970.

REN, H., SIGMAN, D. M., MARTÍNEZ-GARCÍA, A., ANDERSON, R. F., CHEN, M. T., RAVELO, A. C., STRAUB, M., WONG, G.T. AND HAUG, G.H., 2017, Impact of glacial/interglacial sea level change on the ocean nitrogen cycle: Proceedings of the National Academy of Sciences, v. 114, p. E6759-E6766.

ROSS, G.M., AND ARNOTT, R.W.C., 2007, Regional geology of the Windermere Supergroup, southern Canadian Cordillera and stratigraphic setting of the Castle Creek study area, Canada, in Nilsen, T.H., Shew, R.D., and Studlick, J.R.J., eds., Atlas of Deep-water Outcrops: American Association of Petroleum Geologists, Studies in Geology, v. 56, CD-ROM, 22 p.

ROSS, G. M., BLOCH, J. D. AND KROUSE, H. R., 1995, Neoproterozoic strata of the southern Canadian Cordillera and the isotopic evolution of seawater sulfate: Precambrian Research, v. 73, p. 71–99.

RUSO, S., 2021, Stratigraphic architecture and characterization of a Neoproterozoic continental slope system, Windermere Supergroup, east-central British Columbia, Canada. Unpublished M.Sc. thesis, University of Ottawa, 162 p.

SALLER, A., LIN, R., AND DUNHAM, J., 2006, Leaves in turbidite sands: The main source of oil and gas in the deep-water Kutei Basin, Indonesia: American Association of Petroleum Geologists Bulletin, v. 90(10), p. 1585-1608.

SALMON, V., DERENNE, S., LALLIER-VERGÈS, E., LARGEAU, C., AND BEAUDOIN, B., 2000, Protection of organic matter by mineral matrix in a Cenomanian black shale: Organic Geochemistry, v. 31, p. 463-474.

SMITH, M. D., 2009, Stratigraphic and geochemical evolution of the Old Fort Point Formation, southern Canadian Cordillera: The deep-marine perspective of Ediacaran post-glacial environmental change. Unpublished Ph.D. thesis, University of Ottawa.

SMITH, M.D., ARNOTT, R.W.C., AND ROSS, G.M., 2014, The Old Fort Point Formation: Redefinition and formal subdivision of a distinctive stratigraphic marker in the Neoproterozoic Windermere Supergroup, southern Canadian Cordillera: Bulletin of Canadian Petroleum Geology, v. 62, p. 1-13.

SØMME, T. O., HELLAND-HANSEN, W., AND GRANJEON, D., 2009, Impact of eustatic amplitude variations on shelf morphology, sediment dispersal, and sequence stratigraphic interpretation: Icehouse versus greenhouse systems: Geology, v. 37, p. 587-590.

STETTEN, E., BAUDIN, F., REYSS, J.L., MARTINEZ, P., CHARLIER, K., SCHNYDER, J., RABOUILLE, C., DENNIELOU, B., COSTON-GUARINI, J., AND PRUSKI, A., 2015, Organic matter

characterization and distribution in sediments of the terminal lobes of the Congo deep-sea fan: evidence for the direct influence of the Congo River: Marine Geology, v. 369, p. 182–195. https://doi.org/10.1016/j.margeo.2015.08.020

STEWART, J. H.,1972, Initial deposits in the Cordilleran geosyncline: Evidence of a late Precambrian (< 850 my) continental separation: Geological Society of America Bulletin, v. 83, p. 1345-1360, https://doi.org/10.1130/0016-7606(1972)83[1345:IDITCG]2.0.CO;2.

STOW, D. A., AND BOWEN, A. J., 1978, Origin of lamination in deep sea, fine-grained sediments: Nature, v. 274, p. 324-328.

SWEET, M. L., AND BLUM, M. D., 2016, Connections between fluvial to shallow marine environments and submarine canyons: Implications for sediment transfer to deep water: Journal of Sedimentary Research, v. 86, p. 1147-1162, https://doi.org/10.2110/jsr.2016.64.

TAN, X., HU, L., REED, A.H., FURUKAWA, Y., AND ZHANG, G., 2014, Flocculation and particle size analysis of expansive clay sediments affected by biological, chemical, and hydrodynamic factors: Ocean Dynamics, v. 64, p. 143-157.

TERLAKY, V., 2014, Sedimentology, stratigraphy, architecture and origin of deep-water, basin-floor deposits: Middle and upper Kaza Group, Windermere Supergroup, B.C., Canada [Ph.D.
Thesis]: University of Ottawa, Ottawa, ON.

TERLAKY, V., ROCHELEAU, J., AND ARNOTT, R.W.C., 2016, Stratal composition and stratigraphic organization of stratal elements in an ancient deep-marine basin-floor succession, Neoproterozoic Windermere Supergroup, British Columbia, Canada: Sedimentology, v. 63, p. 136-175.

TILSTON, M., ARNOTT, R. W., RENNIE, C. D., AND LONG, B., 2015, The influence of grain size on the velocity and sediment concentration profiles and depositional record of turbidity currents: Geology, v. 43, p. 839-842.

TISSOT, B. P., AND WELTE, D. H., 1978, Sedimentary processes and the accumulation of organic matter. *In* Petroleum Formation and Occurrence: A New Approach to Oil and Gas Exploration, Eds. B.P. Tissot and D.H. Welte, Springer-verlag, Berlin, Heidelberg, p. 55-62.

VAN LEUSSEN, W., 2011, Macroflocs, fine-grained sediment transports, and their longitudinal variations in the Ems Estuary: Ocean dynamics, v. 61, p. 387-401.

WEIMER, P., SLATT, R.M., DROMOOGLE, P., BOWMAN, M., AND LEONARD, A., 2000, Developing and managing turbidite reservoirs: case histories and experiences: results of the 1998 EAGE/AAPG Research Conference: American Association of Petroleum Geologists, Bulletin, v. 84, p. 453-465.

WENTWORTH, C.K., 1922, A scale of grade and class terms for clastic sediments: The Journal of Geology, v. 30, p. 377-392.

WINTERWERP, J.C., AND VAN KESTEREN, W.G., 2004, Introduction to the Physics of Cohesive Sediment Dynamics in the Marine Environment: Elsevier, Amsterdam, The Netherlands, 466 p.

ZHANG, P., MOLNAR, P. AND DOWNS, W., 2001, Increased sedimentation rates and grain sizes 2–4 Myr ago due to the influence of climate change on erosion rates: Nature, v. 410, p. 891–897.

Chapter 5: Controls on the Stratigraphic Distribution of Organic Carbon in Ancient Deep-marine Levees

5.1 Introduction

Deep-marine fan systems have been shown to effectively sequester organic carbon over geologic timescales (e.g., Keil et al. 1997; Galy et al. 2007; Masiello 2007; Baudin et al. 2010, Cunningham and Arnott *accepted*). Burial of this organic material, or more specifically carbon, has important implications on the global carbon cycle and processes like atmospheric oxygen and carbon dioxide content and its influence on climate, in addition to forming important hydrocarbon source rocks. Because of this significance, it is important to study the mechanisms that form organic-rich strata and the factors that control their distribution in the ancient sedimentary record.

Previous studies have shown that turbidity currents efficiently transport organic matter (OM) from continental margins into deep-sea fan systems (Saller et al. 2006; de Jesus Mendes et al. 2007; Galy et al. 2007; Masiello 2007; Baudin et al. 2010; Stetten et al. 2015; Baudin et al. 2017; McArthur et al. 2017; Lee et al. 2019; Baudin et al. 2020; Hage et al. 2020; Hussain et al. 2021; Cunningham and Arnott *accepted*). Although various physical processes act to concentrate this OM in specific fan sub-environments, such as levees, channels, and lobes (Saller et al. 2006; McArthur et al. 2016a; 2016b; McArthur et al. 2017; Hage et al. 2020; Hussain et al. 2021; Cunningham and Arnott *accepted*), its distribution in the stratigraphic record is ultimately controlled by larger-scale environmental factors, including productivity, ocean redox, and detrital clastic sediment flux (e.g., Arthur et al. 1987; Murphy et al. 2000; Tyson 2001; Frimmel et al. 2004; Algeo et al. 2013; Zeng et al. 2015; Chen and Sharma 2016; Zhang et al. 2019; Awan

et al. 2020; Niu et al. 2021). Currently some of these mechanisms are still a matter of debate, and recent work has shown that in many cases it is a combination rather than singular factors that are ultimately responsible for organic matter enrichment. Furthermore, the interplay between these various factors, both physical and chemical, can be highly complex.

In this study, sea level, primary productivity, ocean redox conditions, source rock mineralogy, weathering intensity, and detrital flux were evaluated in a 340 m-thick succession of variously organic-rich ancient continental slope deposits. Significantly, the results demonstrate the effect of each of these factors on organic carbon enrichment and help to elucidate the complex relationships and interactions between them. As such, this work can be applied to the assessment of organic matter accumulation and preservation in future studies.

5.2 Geological Setting

5.2.1 Geological Background

The Windermere Supergroup (WGS) is a Neoproterozoic succession of mostly metasedimentary rocks recording the breakup of the supercontinent Rodinia and subsequent sedimentation along a passive continental margin (Stewart 1972; Ross et al. 1995; Hadlari et al. 2021). In outcrop rocks of the WSG form a linear belt that extends more than 4000 km from northwestern Mexico to the Yukon-Alaska border (Figure 5.1) (Ross and Arnott 2007). Strata of the WSG exposed in Mexico and the western United States are terrestrial to shallow marine in origin (Link et al. 1993), whereas strata in the southern Canadian Cordillera (SCC) consist mostly of siliciclastic deep-marine to shelf deposits, and in the northern Canadian Cordillera carbonate-rich upper slope and shelf facies (Narbonne et al. 1994; Ross et al. 1995). Collectively

this succession records the progradation of the Laurentian continental margin into the thermally subsiding proto-Pacific Ocean (Ross et al. 1995; Ross and Arnott 2007; Hadlari et al. 2021). In the SCC rocks of the WSG are particularly well exposed and form a 5 – 7 km-thick succession of deep-marine basin floor (Kaza Group), slope (Isaac Formation), and upper slope to shelf (Cunningham and Yankee Belle formations, respectively) deposits (Campbell et al. 1973).

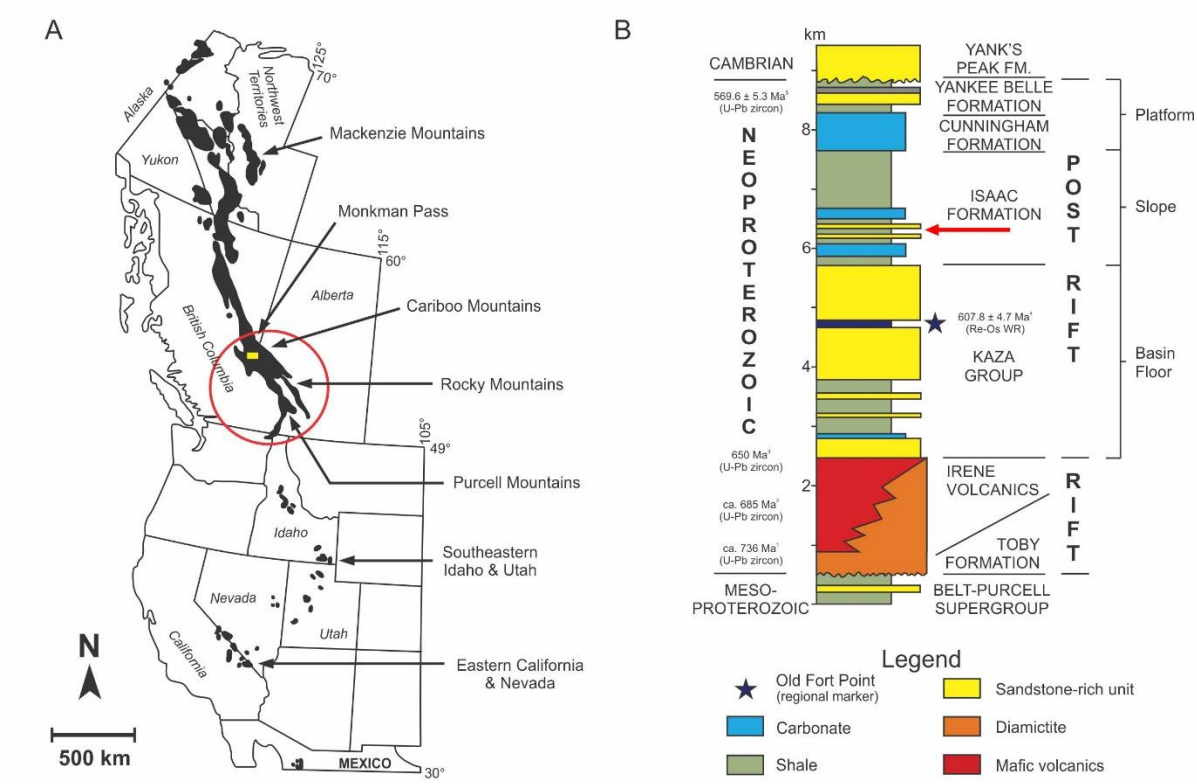

Figure 5.1. *A) Distribution of exposed Windermere Supergroup stratigraphy (black polygons) in western North America. Deep-marine rocks are especially well exposed in the southern Canadian Cordillera (red circle) and at the Castle Creek study area (yellow box). B) General stratigraphy of the Windermere Supergroup in the Cariboo Mountains, east-central British Columbia (Khan 2012). At Castle Creek basin-floor rocks of the Upper Kaza Group are conformably overlain by slope deposits of the lower Isaac Formation. Red arrow indicates the stratigraphic position of strata described here. Radiometric ages are from [1]McDonough and Parrish (1991), [2]Lund et al. (2003), [3]Hadlari et al. (2021), [4]Kendall et al. (2004) and [5]Colpron et al. (2002).*

In the SCC age control is generally poor due to a paucity of datable markers. Age is largely constrained by radiometric dates from below and above its bounding unconformities,

respectively, 736 – 728 Ma (Evenchick et al. 1984; McDonough and Parrish 1991; Eyster et al. 2018) and 570 +/- 5 Ma (Colpron et al. 2002). Dates within the Windermere sedimentary pile are limited to Hadlari et al. (2021) who report a maximum depositional age of 650 Ma based on U/Pb dating of detrital zircons, a Re-Os isochron date of 607.8 +/- 4.7 Ma from organic-rich mudstones of the Old Fort Point Formation (Kendall et al. 2004; Smith et al. 2014), and the correlation of a 200 m-thick carbonate unit informally termed the first Isaac carbonate (FIC) with the onset of the Gaskiers Glaciation at 580 Ma (Cochrane et al. 2019).

During the Mesozoic to early Cenozoic, rocks of the WSG were uplifted and incorporated into the Canadian Cordillera by collision and accretion of allochthonous terranes along the western margin of Laurentia where they underwent multiple phases of deformation and low-grade metamorphism (Price 2000; Reid et al. 2002). This deformation also resulted in significant shortening of the system. Although the WSG is currently exposed over ~ 35,000 km^2 in the SCC, if palinspastically reconstructed, represents a system of at least 80,000 km^2, and therefore dimensionally comparable to modern turbidite systems like the Mississippi, Congo, and Amazon deep-sea fans, and makes it one of the largest ancient deep-marine turbidite systems (Ross and Arnott 2007).

5.2.2 Study Area

Deep-marine sedimentary rocks of the Kaza Group (basin floor) and Isaac Formation (continental slope) crop out at the Castle Creek study area in the Cariboo Mountains of British Columbia, Canada, where they form a conformable succession ~ 2.6 km thick and up to 8 km wide (Terlaky et al. 2016; Navarro and Arnott 2020). Due to its location on the steeply dipping limb of a regionally extensive anticline bedding is near-vertical (~89°) and recent deglaciation

has resulted in a glacially polished, vegetation-free outcrop that locally is obscured by glacial ice and debris (Figure 5.2A). Despite lower-greenschist metamorphism, primary sedimentary structures are well-preserved, allowing for millimeter-scale observation and measurement. Although this metamorphism altered the primary clay minerals to muscovite and chlorite, based on the provenance of the sediment kaolinite is believed to have been the dominant clay mineral in the Isaac Formation at the time of deposition.

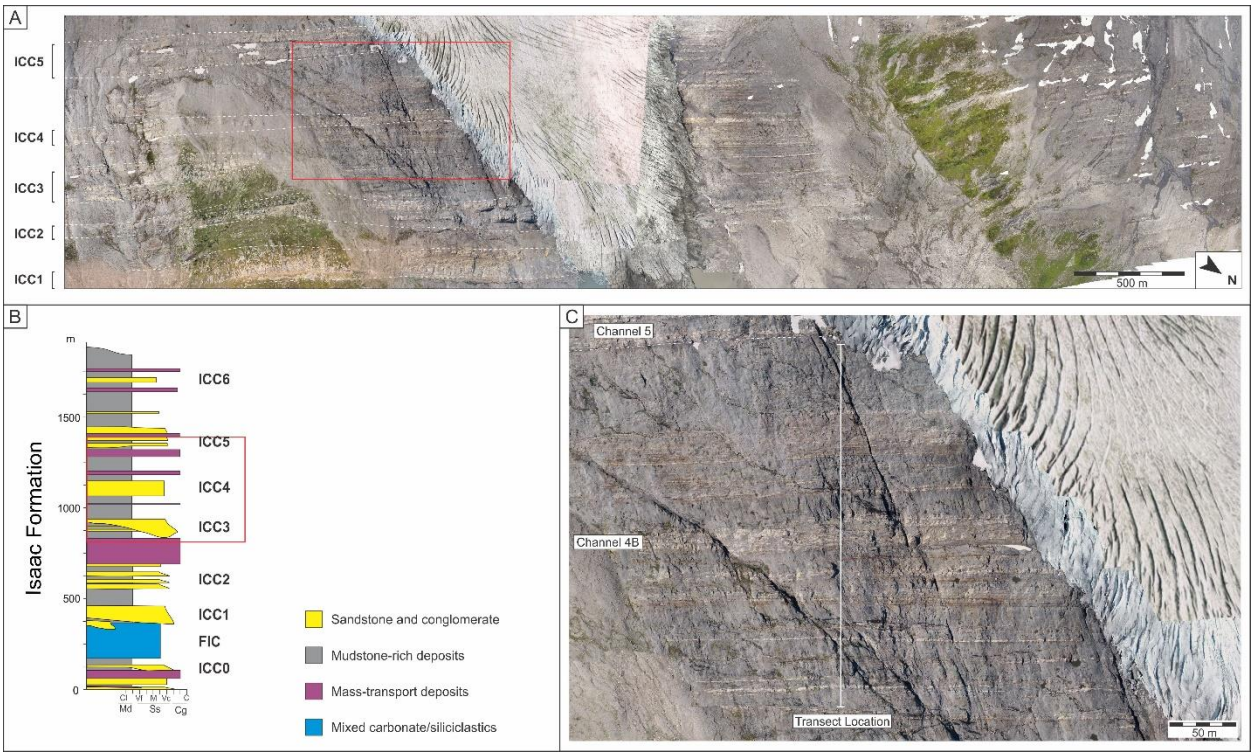

Figure 5.2. *A) Aerial photomosaic showing slope deposits of the Isaac Formation at Castle Creek, with Isaac Channel Complex Sets 1 – 5 labelled on the left and outlined with white dashed lines. The study area for this paper is highlighted by a red box (see C). B) Stratigraphic column of the Isaac Formation strata exposed at Castle Creek. The study interval is highlighted by a red box. C) Aerial photomosaic of the study area, with the transect location indicated by a white line.*

5.2.3 Previous Work

The Isaac Formation at Castle Creek has been shown to comprise at least seven coarse-grained, laterally discontinuous units that range up to over 200 m in thickness and are interpreted to represent slope-channel complex sets bounded by finer-grained overbank deposits, namely levee deposits (Figure 5.2B). The sedimentology and stratigraphic architecture of these channel-levee complex sets have been described in detail in previous work (Navarro et al. 2007; Schwarz and Arnott 2007; Davis 2011; Khan and Arnott 2011; Khan et al. 2011; Khan 2012; Bergen 2017; Fraino 2020; Ruso 2021; Cunningham and Arnott 2021; Fraino et al. 2022; Bergen et al. 2022).

Several geochemical analyses have also been conducted in slope deposits of the Isaac Formation using a variety of methods, including elemental analysis, total organic carbon (TOC), and stable isotopes. Notably, TOC values from slope channel deposits, as well as from basin floor deposits, are characteristically low ($\leq 0.1\%$, uncorrected for lower greenschist metamorphism), whereas levee deposits have notably higher organic content (average TOC is 0.5%). Cochrane et al. (2019) examined the inorganic carbon ($\delta^{13}C_{carb}$) isotopic evolution of the first Isaac carbonate and correlated the observed trends with the onset of the 580 Ma Gaskiers glaciation. Kehew and Arnott (2020) combined elemental analysis with TOC and inorganic carbon isotopes to further study the FIC and characterize sea level trends throughout. Chemostratigraphic profiles from the FIC to Isaac Channel Complex Set 3 (ICC3) and from Isaac Channel Complex Set 1 (ICC1) to Isaac Channel Complex Set 6 (ICC6) were compiled by Milczarek (2018) and Ruso (2021), respectively. These studies used major, minor, and trace element composition and various geochemical proxies, combined with stratigraphic architecture, to reconstruct ancient sea level patterns and evaluate the effects of eustasy on the development of

the continental shelf and deep-marine system. Sea level reconstructions from ICC1 to ICC5 were also produced by Fraino (2020) using detailed analysis of the stratal architecture of channel fill deposits.

Detailed physical and geochemical characterization of organic-rich levee deposits at the Castle Creek study area have also been performed (Cunningham and Arnott *accepted*). However, to date no study has evaluated the distribution of organic-rich strata in levee strata, or the controls on its deposition and preservation.

5.3 Methods

5.3.1 Outcrop

Fieldwork was conducted at the Castle Creek study site during the summers of 2018, 2019, and 2021. Detailed bed-by-bed stratigraphic logs (10-130 m long) were measured in levee deposits of ICC3 and ICC4 and compiled into a single continuous 340 m-long stratigraphic log (Figure 5.2C). Lithology, bed thickness, grain size, sedimentary structures, and basal contacts were described in mm-scale detail. A total of 124 samples were collected for petrographic and geochemical analysis.

5.3.2 Petrography

120 thin sections were prepared from these samples and used to characterize mineralogy, grain size, and microscale structures. Petrography was done using an Olympus BX-41 plane, polarized, and reflected light microscope, and a JEOL-6610LV scanning-electron microscope (SEM) equipped with an Oxford Inca energy dispersive X-ray spectrometry (EDS) system.

SEM-EDS analyses were performed at 15 kV – 20 kV under high vacuum at a working distance of 11 nm on polished thin sections with a 20-nm-thick carbon coating.

5.3.3 Geochemistry

Shale samples were taken every 4 – 10 m along a 340 m vertical transect, totalling 44 samples. Where no shale was present (e.g., sandstone-rich channel deposits of ICC4) the next stratigraphically higher shale bed was sampled instead. Samples were then pulverized using a TM/SLTX mill and prepared for total organic carbon (TOC) and X-ray fluorescence (XRF) analyses. Due to COVID-19 restrictions and closures, all the geochemical data used in this study were taken from previously collected and analyzed samples. Accordingly, not all the samples had the same range of geochemical analyses performed. Future work could re-analyze the samples to eliminate this potential inconsistency.

5.3.3.1 Total Organic Carbon

40 samples were analyzed to determine weight percent of total organic carbon (TOC). An acid wash was first performed on all samples to remove inorganic carbonate, which in these samples occurs mostly as carbonate cement. Approximately 500 mg of each powdered sample was weighed and placed in 10 mL beakers. ~ 7 mL of 20% HCl was added and the solution vigorously stirred to ensure that all the powdered material was thoroughly dispersed in the acid. Samples were then left to soak for 24 hours before being decanted and mixed into distilled water and stirred, allowing the powder to soak, and then set aside to rest for 1.5 hours. The washing

procedure was repeated 3 times. After the final wash samples were decanted and the wet powders placed in an oven and heated at 70 ºC for 24 hours.

To determine TOC approximately 10 mg of each powdered sample was weighed into tin capsules and then loaded with standards and tungsten oxide, which acts as a combustion catalyst, into an Elementar Vario EL Cube elemental analyzer to measure the percent carbon content (% C) in each sample. Samples were flash combusted with oxygen at ~1800 ºC and then carried by helium through columns of reducing/oxidizing chemicals to produce CO_2 gas. The gas was then trapped within a single "trap and purge" absorption column and released separately past a thermal conductivity detector (TCD). The analytical precision (2 sigma) is +/- 0.1%. The values measured here do not account for the effects of greenschist metamorphism, would have resulted in the probable loss of ~50 – 80% of the original organic content (Hayes et al. 1983; Smith et al. 2014). Because of this, the reported TOC values are likely significantly lower than the original deposition values.

5.3.3.2 X-Ray Fluorescence

30 samples were selected for XRF analysis. To calibrate each XRF analysis a Loss on Ignition (LOI) analysis of a 1 g sample heated at 1050 ºC for 1 hour was first carried out to determine post-combustion percent weight loss. Exactly 0.8 g of pulverized sample then was mixed with a lithium-borate solution and fused into a disk that was exposed to incident X-rays in a WDXRF Rigaku 200 supermini. The intensity and type of reflected rays were recorded and graphed using an analytical software; each ray corresponds to a different element that collectively make up the bulk composition of each disk (sample). Shale standards were used to calibrate the measured values of major elements (presented as oxides in mass percent) Na_2O,

MgO, Al_2O_3, SiO_2, P_2O_5, K2O, CaO, TiO_2, MnO, and Fe_2O_3. Element abundance is measured in mass percent. Minor elements, specifically, S, Cr, Cu, Zn, Sr, Y, and Nb, are measured in ppm. An additional 8 samples were also analyzed for V, Ni, Zr, Co, Ba, Ce, Pb, Th, U, and La in ppm. Elemental ratios and proxies were then used to evaluate paleoredox conditions, tectonic setting and provenance, and continental sediment supply.

5.4 Results

5.4.1 Lithostratigraphic Trends

The stratigraphic section measured in this study begins at the base of Isaac Channel-Levee Complex Set 3 (ICC3) and comprises ICC3 levee deposits, sandy channel deposits of Isaac Channel-Levee Complex Set 4A, and levee deposits of Isaac Channel-Levee Complex Set 4B (Figure 5.2C). Immediately underlying the section is a 30 m-thick mass-transport deposit (MTD), which along strike thickens to 110 m and can be correlated across the entire Castle Creek outcrop (e.g. Arnott et al. 2011). The contact between the top of the MTD and the overlying ICC3 levee deposits serves as the stratigraphic datum in this study. The succession is subdivided into three units, termed the Lower (0 – 104 m), Middle (104 – 165 m), and Upper (165 – 340 m). The Lower and Middle units comprise levee deposits of ICC3, whereas the Upper Unit consists of the channel and levee deposits of ICC4.

Detailed studies of the sedimentology and stratigraphic architecture of these strata have been previously conducted by Mussa-Caleca (2008), Khan and Arnott (2011), Khan et al. (2011), Khan (2012), Terlaky (2014), Bergen (2017), Cunningham and Arnott (2021), Bergen et al.

(2022), Ningthoujam et al. (2022) and Cunningham and Arnott (*accepted*). A summary of the facies and architectural elements and their distribution in the succession is presented next.

LEVEE FACIES: Levee deposits are dominated by fine-grained, thin-bedded, upper-division turbidites (Figure 5.3A-B). Distal levee deposits make up most of the succession from 0 m to 170 m and consist of thin- to very-thin-bedded, fine-grained, upper-division turbidites interbedded with rare, thick-bedded, medium- to coarse-grained, lower-division turbidites. Proximal levee deposits can be subdivided into packages consisting of two sharply bounded parts: a 3 – 10 m-thick, coarse-grained lower part consisting mostly of medium- to thick-bedded, coarse-grained, lower-division turbidites intercalated with thin-bedded, fine-grained, upper-division turbidites; and a 3 – 16 m-thick, fine-grained, upper part consisting of thin-bedded, fine-grained, upper-division turbidites intercalated with uncommon medium- to thick-bedded, medium-grained, lower-division turbidites. Each package corresponds to a discrete phase of channel inception and filling. Proximal levee deposits of Isaac Channel Complex Set 4 (ICC4) form a significant part of the succession, from 220 m to 290 m.

Overbank splays, formed when channelized turbidity currents escape confinement or breach the levee, locally punctuate the levee deposits (Figure 5.3C-D). Splay deposits consist of thick-bedded, coarse-grained, lower-division turbidites and matrix-rich sandstone beds and occur from 110 m to 120 m and 129 m to 138 m (Ningthoujam et al. 2022).

CHANNEL FACIES: ICC4 deposits consist mostly of amalgamated medium- to thick-bedded, very coarse- to medium-grained sandstone with common mudstone-clast breccia units (Figure 5.3E-F). Beds are usually normally graded and structureless, although planar stratification, commonly sharply overlying graded, structureless sandstone, is also common. These deposits comprise the interval from 170 to 190 m and are overlain by 30 meters (from 190 m to 220 m) of thin-bedded, very fine-grained, upper-division turbidites that represent channel abandonment and the partial or complete infilling of the deactivated channel by dilute, lower energy turbidity currents (Musa-Caleca 2008).

DEBRITE FACIES: Mass-transport deposits, formed from cohesive sediment-gravity flows (debris flows), consist of mud-matrix-supported conglomerate with dispersed quartz pebbles and, in some cases, carbonate-cemented sandstone, mudstone and carbonate clasts, and range in thickness from 5 m to 60 m (Figure 5.3G-H). Debrites occur throughout the succession, from 80 m to 90 m, 250 m to 255 m, and 290 m to 350 m.

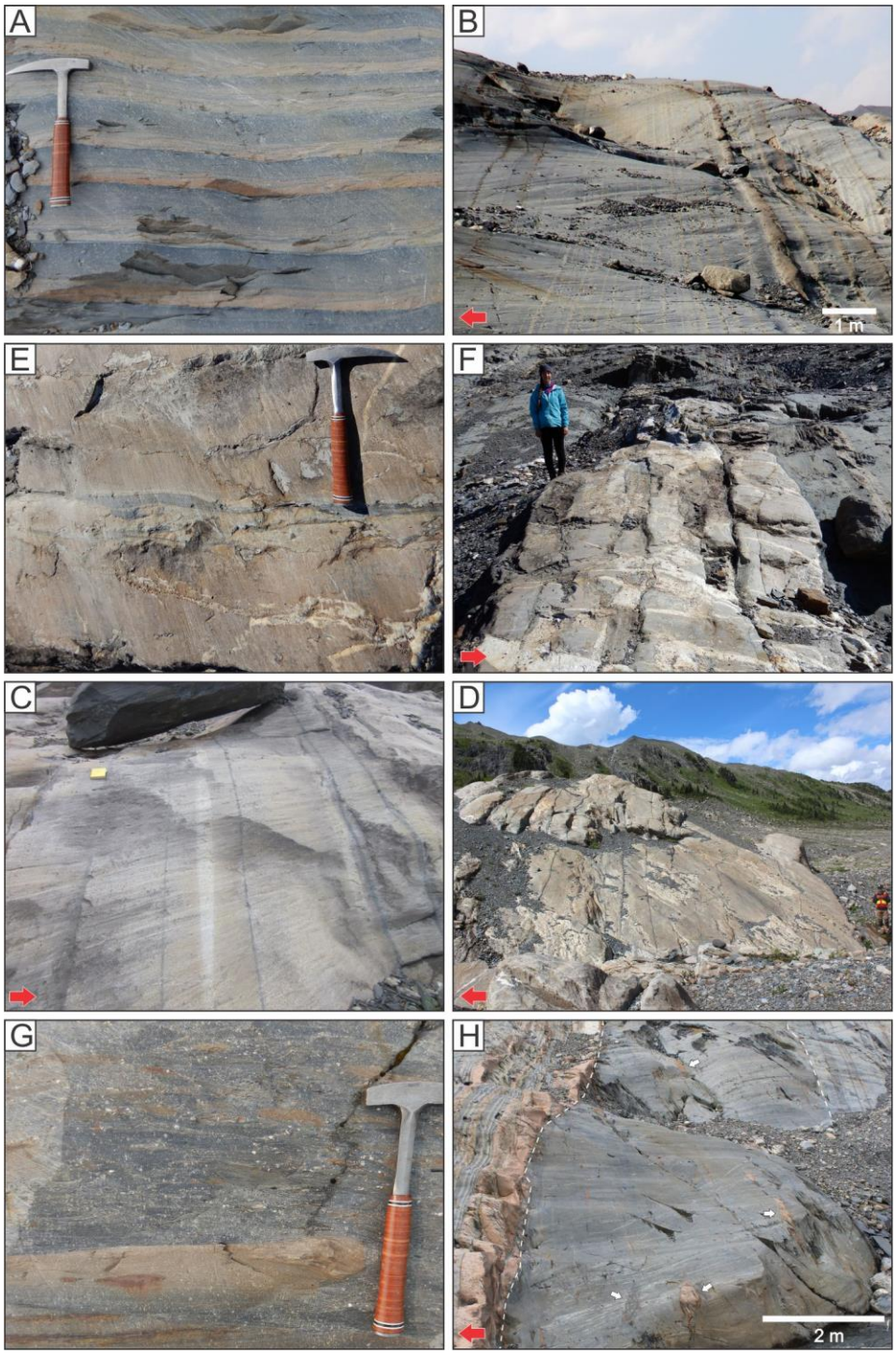

Figure 5.3. *Outcrop photos of levee (A-B), channel (C-D), splay (E-F), and MTD (G-H) strata. Hammer is 32 cm long. Red arrows indicate the direction of younging. A) Thin-bedded, fine-grained, upper-division levee turbidites. B) Stacked thin-bedded levee turbidites intercalated with an uncommon, medium-bedded, lower-division turbidite. C) Thick-bedded, medium-grained, lower-division splay turbidite. D) Sandy splay deposit situated between thin-bedded levee turbidites. E) Thick-bedded, coarse-grained, amalgamated, lower-division channel bed. Yellow notebook (17 cm) for scale. F) Thick channel-fill succession. G) Close-up of a matrix-supported debrite bed with dispersed quartz pebbles and sand-rich intraclasts. H) Debrite deposit overlain by turbidites. White arrows indicate intraclasts.*

ORGANIC-RICH FACIES: Organic-rich facies can be subdivided into two types: OM-rich mudstone and OM-rich sandstone (Figure 5.4) (Cunningham and Arnott *accepted*), both of which are interspersed within more organic-lean levee deposits. OM-rich mudstones are rare and consist of 1 – 8 cm-thick beds of silty, OM-rich claystone, and are observed from 25 m to 30 m, and at 220 m. OM-rich sandstones occur exclusively in levee deposits of ICC3, and in the Middle Unit (104 – 165 m) of the succession. They are medium- to very thick-bedded and planar stratified, and comprise alternating bands of clean (i.e., mud-poor), cemented sandstone and mud-rich sandstone (Cunningham and Arnott *accepted*). OM in these beds occurs primarily as nano-scale coatings on clay particles in the mud-rich bands, but also as uncommon sand-sized organomineralic aggregates and discrete sand-sized amorphous grains (Figure 5.5). Cement in these bands is ferroan dolomite with $\delta^{13}C_{carb}$ values ranging from -5.6 ‰ to -9.5 ‰ and formed from processes related to the burial diagenesis of the organic content (Cunningham and Arnott *accepted*). Although OM-rich sandstones are confined to the Middle Unit, beds do not stack, but rather are interspersed among more typical, thin-bedded, upper-division, less organic-rich turbidites (Figure 5.6).

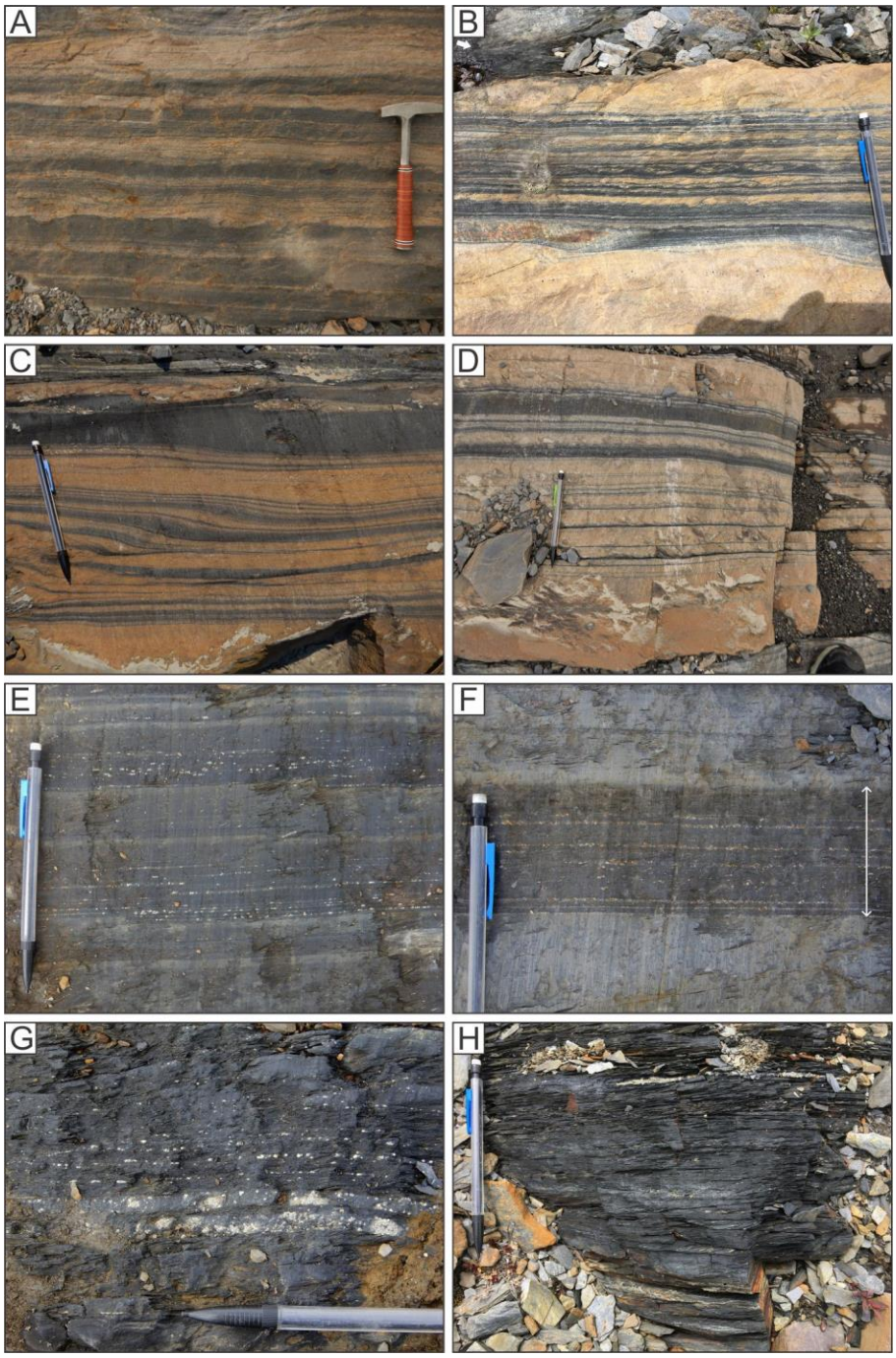

Figure 5.4. *Outcrop photos of OM-rich sandstone (A-D) and OM-rich mudstone (E-H). Pencil is 15 cm long. A) Thick-bedded, planar- and cross-stratified OM-rich sandstone. B) Thinly banded, planar- and cross-stratified OM-rich sandstone sandwiched between thicker orange sandstone bands. C) Alternating black, clay-rich and orange highly cemented bands in an organic-rich sandstone. D) Thick OM-rich sandstone bed. The thickness of black, OM- and mud-rich bands increases upwards. E) Thinly laminated, organic-rich mudstone. Framboidal pyrite is concentrated along silt-rich laminae. F) Organic-rich mudstone bed (white arrows) bounded above and below by organic-poor mudstone beds. Framboidal pyrite, abundant within the OM-rich bed, is notably absent in the under- and overlying OM-poor beds. G) Fissile, OM-rich mudstone with abundant framboidal pyrite. E) Medium-bedded, highly fissile, OM-rich mudstone.*

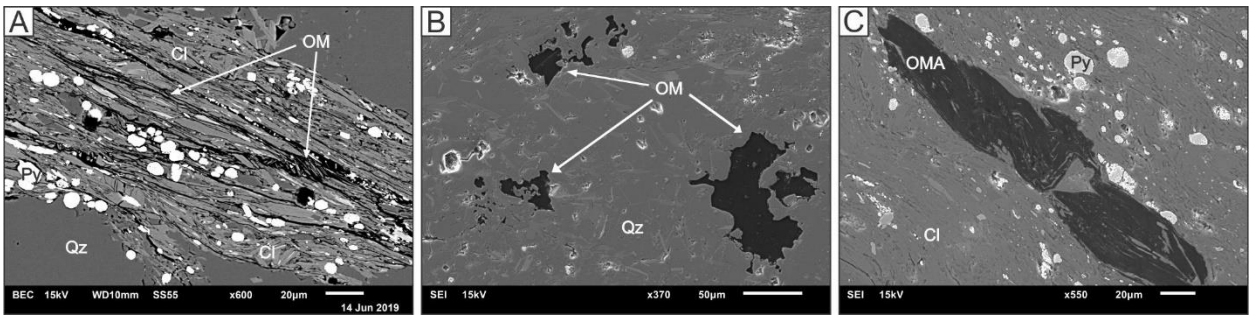

Figure 5.5. *A) Backscattered electron micrograph of a black, clay-rich band in an organic-rich sandstone (perpendicular to bedding). Nano-scale rims of organic matter (OM, black) surround most clay particles (Cl, light grey). B) Secondary electron micrograph of dispersed carbon particles in an orange sandstone band. C) Secondary electron micrograph of an organomineralic aggregate (OMA) composed primarily of OM surrounded by pyrite framboids and clay grains.*

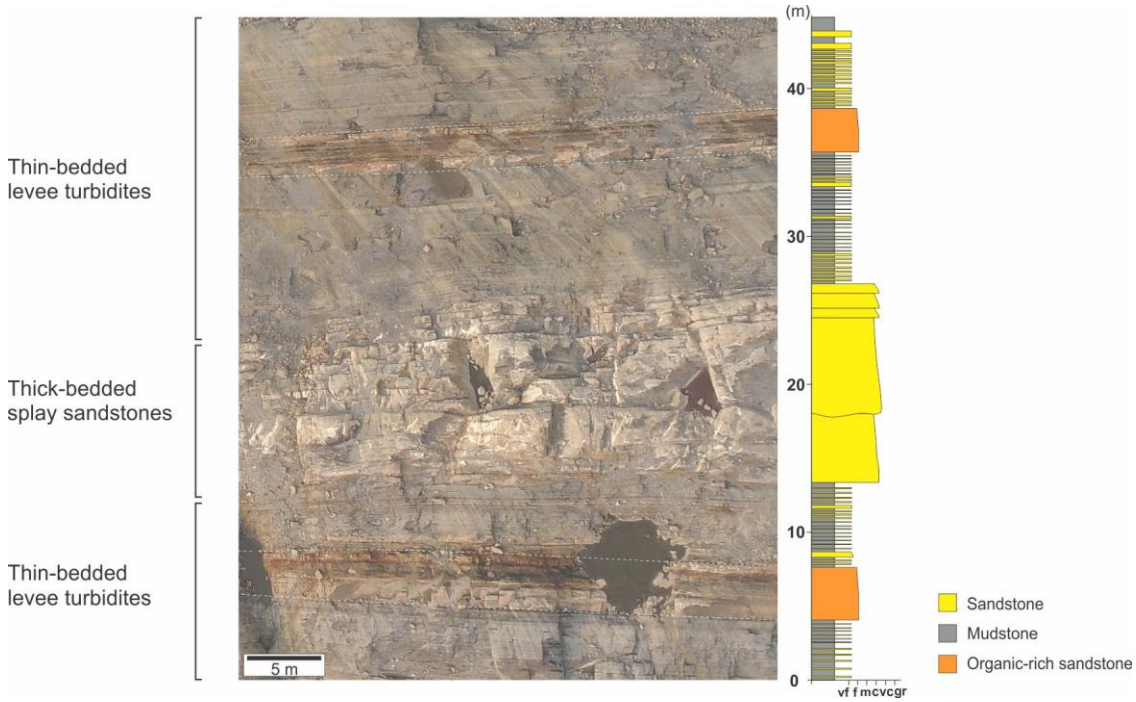

Figure 5.6. *Photo and representative stratigraphic column of relatively organic-poor, thin-bedded levee turbidites intercalated with thick, OM-rich sandstone beds (shown in orange) and a sand-rich splay deposit.*

5.4.2 Total Organic Carbon

TOC values are presented in Table 5.1. TOC trends are also shown in Figure 5.7. TOC ranges from 0.04 – 3.11 %, and with the exception of two TOC peaks at 30 m and 220 m, values are consistently the highest in the Middle Unit. More specifically, in this unit average TOC is 1.25 % and maximum and minimum values are 3.11 % and 0.38 %, respectively, whereas elsewhere (in the Lower and Upper units) average TOC is 0.21 %. The highest peaks (1.31 % – 3.11 %) in the Middle Unit correspond to the distinctive black, organic-rich muddy sandstones and sandy mudstones described earlier. The thin-bedded mudstones in this unit that are more typical of levee strata have lower TOC (0.38 % – 0.53 %), although they are still enriched in OM relative to levee deposits elsewhere in the Castle Creek study area, which typically are < 0.2 %. The other two TOC peaks, at 30 m and 220 m, correspond to thin, isolated OM-rich mudstone beds. Outside the Middle Unit, TOC varies little except for a subtle but progressive upward increase from ~ 0.14 % – 0.24 % at 250 – 280 m, above which TOC declines steadily.

Sample ID	Height	TOC (%)
Ch2 0	0	0.04
Ch2 10	10	0.17
Ch2 20	20	0.13
Ch 30	30	1.03
Ch2 40	40	0.2
Ch2 60	60	0.12
CS 6	76	0.15
CS 12	82	0.16
CS 18	88	0.15
CS 24	94	0.17
CS 30	100	0.16
OM V	104	1.8
J 0	110	0.53
J 10	120	1.04
J 20	130	0.48
OM W	132	3.11
J 27	137	1.36
J 32	142	0.41
OM X	147	1.42
J 40	150	1.84
OM Y	155	1.31
J 50	160	0.38
OM Z	165	1.3
X 0	190	0.14
X 10	200	0.19
X 20	210	0.21
A 0	220	0.79
A 10	230	0.17
A 20	240	0.14
A 30	250	0.14
A 40	260	0.15
A 50	270	0.21
A 60	280	0.24
A 70	290	0.23
A 80	300	0.17
A 90	310	0.16
A 100	320	0.08
A 110	330	0.1
A 120	340	0.13
A 130	350	0.08

Table 5.1. *Total organic carbon (TOC) in mudstones sampled along the stratigraphic column shown in Fig. 5.7.*

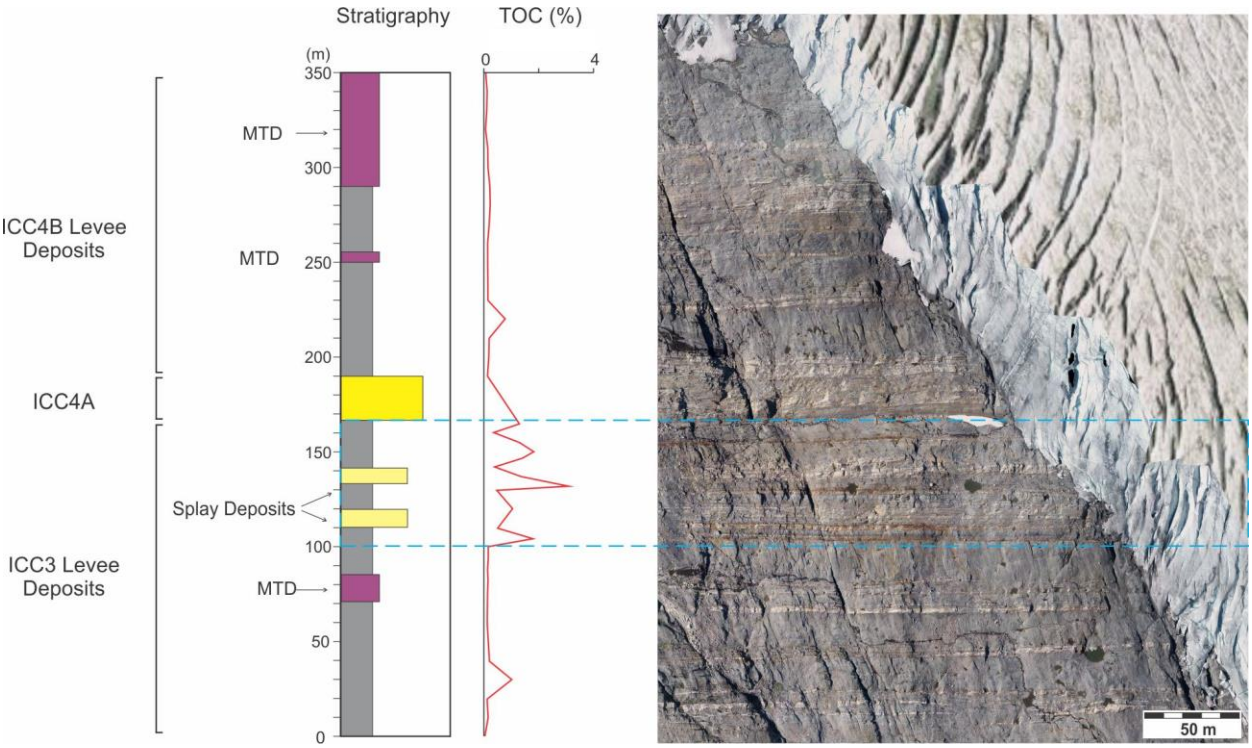

Figure 5.7. *Total Organic Carbon (TOC) trends through the studied stratigraphic interval, shown beside a representative stratigraphic log (left) and photomosaic of the study area (right). The organic-rich Middle Unit is highlighted by blue dashed rectangle.*

5.4.3 X-Ray Fluorescence Analysis

XRF data for 44 samples are presented in Tables 5.2 and 5.3. Major element abundance is presented as oxides in mass % (Table 5.2) (e.g. Rowe et al. 2012; Pietras and Spiegel 2018; Profe et al. 2018; Kabanov et al. 2020) whereas minor element abundance is presented in parts per million (ppm, Table 5.3). These data were used to analyze trends in various environmental proxies, including primary productivity, paleoredox, tectonic setting and provenance, continental sediment input, and weathering indices (see Discussion).

5.4.3.1 Major Elements

SiO_2 (average 56.1%, range from 44.7% to 67.1%) and Al_2O_3 (average 22.2%, range from 16.9% to 30.2%) are the most abundant major oxides, and are inversely related. Samples also have relatively high Fe_2O_3, with an average of 6.7% (range from 3.8% to 9.6%), and MgO that averages 2.3% (range from 1.2% to 3.4%). MnO and CaO are the least abundant major oxides with averages of 0.03% and 0.07% and ranges from 0.003% to 0.09% and 0% to 0.373%, respectively. In many samples, CaO is below detection. The other major oxides, Na_2O, P_2O_5, and TiO_2, collectively account for ~ 2 – 3%.

5.4.3.2 Minor Elements

Zr (average 271ppm), Cr (average 133 ppm), and Sr (average 109 ppm) are the most abundant minor elements, whereas Nb and Cu are the least abundant, with averages of 27.0 ppm and 59 ppm, respectively. 6 samples were analyzed for V, Ni, Co, Ba, Ce, Pb, Th, U, S, and La. S and Ce were the most abundant (averages of 1989 ppm and 116 ppm, respectively) and U and Co were the least abundant (U was below detection in all samples, Co average 8 ppm).

Sample ID	Height	Na_2O	MgO	Al2O3	SiO_2	P_2O_5	K2O	CaO	TiO_2	MnO	Fe_2O_3	LOI	Sub-total
Ch2 0	0	0.676	2.548	22.196	53.858	0.101	4.011	b.d.	1.011	0.039	9.047	6.377	99.864
Ch2 10	10	0.849	2.360	23.089	53.600	0.093	4.153	b.d.	0.923	0.090	9.638	5.102	99.897
Ch2 20	20	1.341	2.775	25.867	49.978	0.117	3.997	b.d.	0.883	0.043	9.023	5.888	99.912
Ch 30	30	1.434	2.869	25.977	50.422	0.128	3.761	b.d.	0.892	0.068	9.283	5.079	99.913
Ch2 40	40	1.787	2.135	26.619	51.904	0.082	3.980	b.d.	0.848	0.058	7.216	5.261	99.89
Ch2 60	60	0.922	3.080	23.762	53.308	0.147	3.956	b.d.	0.927	0.020	9.092	4.675	99.889
CS 0	70	0.763	2.864	21.866	56.155	0.090	5.319	b.d.	0.949	0.019	7.257	4.481	99.763
CS 8	78	0.763	2.834	21.628	56.007	0.122	5.304	b.d.	0.841	0.024	7.241	4.91	99.674
CS 16	86	0.809	3.443	20.061	55.740	0.141	4.657	0.049	0.906	0.069	8.491	5.211	99.577
CS 24	94	0.791	3.142	20.825	57.137	0.140	5.055	b.d.	0.825	0.040	7.238	4.59	99.783
CS 30	100	0.767	3.150	20.036	57.447	0.112	4.718	0.231	0.772	0.060	7.736	4.69	99.719
OM V	104	0.588	1.614	16.884	62.968	0.039	4.602	0.192	0.823	0.015	5.516	6.45	99.691
CS 38	108	0.388	2.790	30.219	44.732	0.422	8.599	0.304	1.259	0.032	5.481	5.614	99.84
J 0	110	0.577	2.252	23.918	53.344	0.510	6.523	0.373	1.025	0.007	5.896	5.261	99.686
J 10	120	0.539	1.620	19.447	61.445	0.080	5.369	b.d.	0.933	0.007	5.193	4.716	99.349
J 20	130	0.582	2.223	24.273	51.881	0.218	6.825	0.040	0.983	0.005	6.539	6.035	99.604
J 27	137	0.443	1.624	22.201	57.239	0.071	6.489	b.d.	1.027	0.003	4.373	6.297	99.767
J 32	142	0.599	1.472	25.160	49.248	0.160	7.441	b.d.	1.291	0.003	6.131	7.6	99.105
OM Z	165	0.636	1.458	16.876	67.123	0.023	4.581	0.106	1.003	0.006	3.821	4.02	99.653
X 0	190	0.936	2.856	23.667	54.236	0.083	6.007	b.d.	0.956	0.010	6.696	4.439	99.886
X 10	200	0.826	2.878	21.237	56.215	0.125	5.304	b.d.	0.795	0.073	7.710	4.703	99.866
X 20	210	0.648	2.860	19.155	59.284	0.116	4.738	b.d.	0.810	0.046	7.659	4.22	99.536
A 0	220	0.206	1.643	21.256	58.308	0.043	6.347	b.d.	1.092	0.004	5.109	5.668	99.676
A 10	230	1.030	2.559	22.550	56.644	0.201	5.699	0.018	0.926	0.012	6.020	4.215	99.874
A 20	240	0.596	1.699	25.225	53.622	0.079	7.363	b.d.	1.357	0.005	4.485	4.954	99.385
A 40	260	0.533	1.740	23.401	57.226	0.427	6.789	0.295	1.266	0.006	3.927	4.134	99.744
A 50	270	1.040	2.780	20.387	60.207	0.119	5.056	b.d.	0.977	0.006	5.598	3.528	99.698
A 60	280	0.618	2.221	22.406	56.215	0.221	6.023	0.049	0.957	0.005	6.652	3.923	99.29
A.70	290	0.484	1.846	22.007	55.415	0.390	6.266	0.328	1.406	0.004	6.264	5.146	99.556
A 80	300	0.619	2.424	22.476	57.095	0.172	5.939	0.068	1.051	0.015	5.841	4.112	99.812
A 90	310	0.928	2.334	21.348	58.165	0.139	5.235	0.259	0.942	0.019	6.454	3.95	99.773
A 100	320	0.759	2.163	19.547	60.480	0.107	4.935	b.d.	0.861	0.035	6.212	4.488	99.587
A 110	330	0.716	2.216	20.160	60.384	0.147	5.121	0.064	0.977	0.040	5.982	4.057	99.864
A 120	340	0.777	2.458	19.787	57.293	0.165	4.917	b.d.	0.873	0.046	8.213	5.089	99.618
A 130	350	0.824	2.481	20.420	58.735	0.107	4.924	0.238	0.945	0.039	7.010	3.96	99.683

Table 5.2. *Major element abundance in mass percent. "b.d." refers to "below detection".*

Sample ID	Height	Cr	Cu	Zn	Rb	Sr	Y	Zr	Nb	V	Ni	Co	Y	Ba	Ce	Pb	Th	U	S	La
Ch2 0	0	168	73	104	0	134	41	332	25											
Ch2 10	10	178	112	108	0	160	42	233	25											
Ch2 20	20	168	161	117	0	248	41	132	23											
Ch 30	30	154	134	113	0	268	52	132	22											
Ch2 40	40	190	72	98	0	317	44	122	21											
Ch2 60	60	161	87	110	0	192	48	196	22											
CS 0	70	108	44	103	0	84	46	285	26											
CS 8	78	125	45	109	0	84	58	225	25											
CS 16	86	111	59	113	0	90	52	259	26											
CS 24	94	108	44	87	0	87	52	183	26											
CS 30	100	127	129	86	79	80	61	207	4	105	109	16	61	286	134	9	17	0	1275	86
OM V	104	158	149	72	81	55	54	314	13	126	114	28	54	0	76	79	10	0	1682	81
CS 38	108	187	21	72	0	131	89	322	33											
J 0	110	144	37	102	0	121	82	319	34											
J 10	120	107	67	58	0	68	57	315	28											
J 20	130	151	30	93	0	97	66	256	32											
J 27	137	125	11	42	0	73	70	348	31											
J 32	142	130	19	32	0	103	76	384	36											
OM Z	165	114	57	48	99	62	61	516	23	110	48	0	61	14	38	13	13	0	2148	92
X 0	190	143	41	74	0	86	53	264	29											
X 10	200	124	69	92	0	83	57	180	29											
X 20	210	103	87	90	0	76	53	227	28											
A 0	220	123	39	42	0	69	64	281	32	130	66	0	39	258	96	48	18	0	4528	31
A 10	230	149	56	66	0	95	64	217	27											
A 20	240	121	38	58	0	81	91	531	39											
A 40	260	112	22	53	0	101	93	301	39											
A 50	270	103	50	92	0	69	57	276	30											
A 60	280	105	52	90	0	91	66	235	32											
A.70	290	156	22	58	0	102	83	380	40											
A 80	300	127	38	75	0	92	78	273	34											
A 90	310	115	26	99	122	70	60	241	11	86	70	0	60	350	156	46	28	0	691	111
A 100	320	103	21	68	0	83	56	220	25											
A 110	330	105	33	77	0	91	63	264	33											
A 120	340	95	64	84	0	91	48	240	30											
A 130	350	168	61	94	122	74	65	268	13	105	79	3	65	193	195	11	14	0	1613	94

Table 5.3. *Minor element abundance in parts per million (ppm).*

5.5 Discussion

5.5.1 Primary Productivity

Being Neoproterozoic, and therefore before the advent of terrestrial plants, the potential sources of organic matter in this study are limited to marine organisms such as algae and bacteria (Behrensmeyer et al., 1992; Butterfield, 2015; Gensel, 2021). Although TOC itself can be considered a proxy for primary productivity, abundance of various trace metals, which are important metabolic nutrients, can also serve as useful proxies (Algeo and Maynard 2004; Calvert and Pedersen 2007; Algeo et al. 2011; Schoepfer et al. 2015; Niu et al. 2021). Here, we use the ratios of P, Cu, and Ni to Al to assess paleoproductivity (Figure 5.8). Each of these elements show a large positive excursion indicating increased productivity between 100 m and 110 m. This coincides with a peak in TOC and the occurrence of the anomalously organic-rich Middle Unit in which organic carbon occurs dominantly in the thick-bedded, banded mud-rich sandstone beds described earlier. Notably also, these proxies display smaller peaks in several other intervals, namely 10 – 30 m, 200 – 230 m, and 260 – 290 m. The first two of these smaller peaks correspond to the TOC peaks at 30 m and 220 m, respectively, and coincide with isolated, thin, organic-rich mudstone beds. The third corresponds to thin-bedded mudstones with slightly elevated TOC values, although they are not visibly organic-rich. This correlation suggests that increased primary productivity did play a significant role in episodes of organic matter enrichment on the Windermere continental slope.

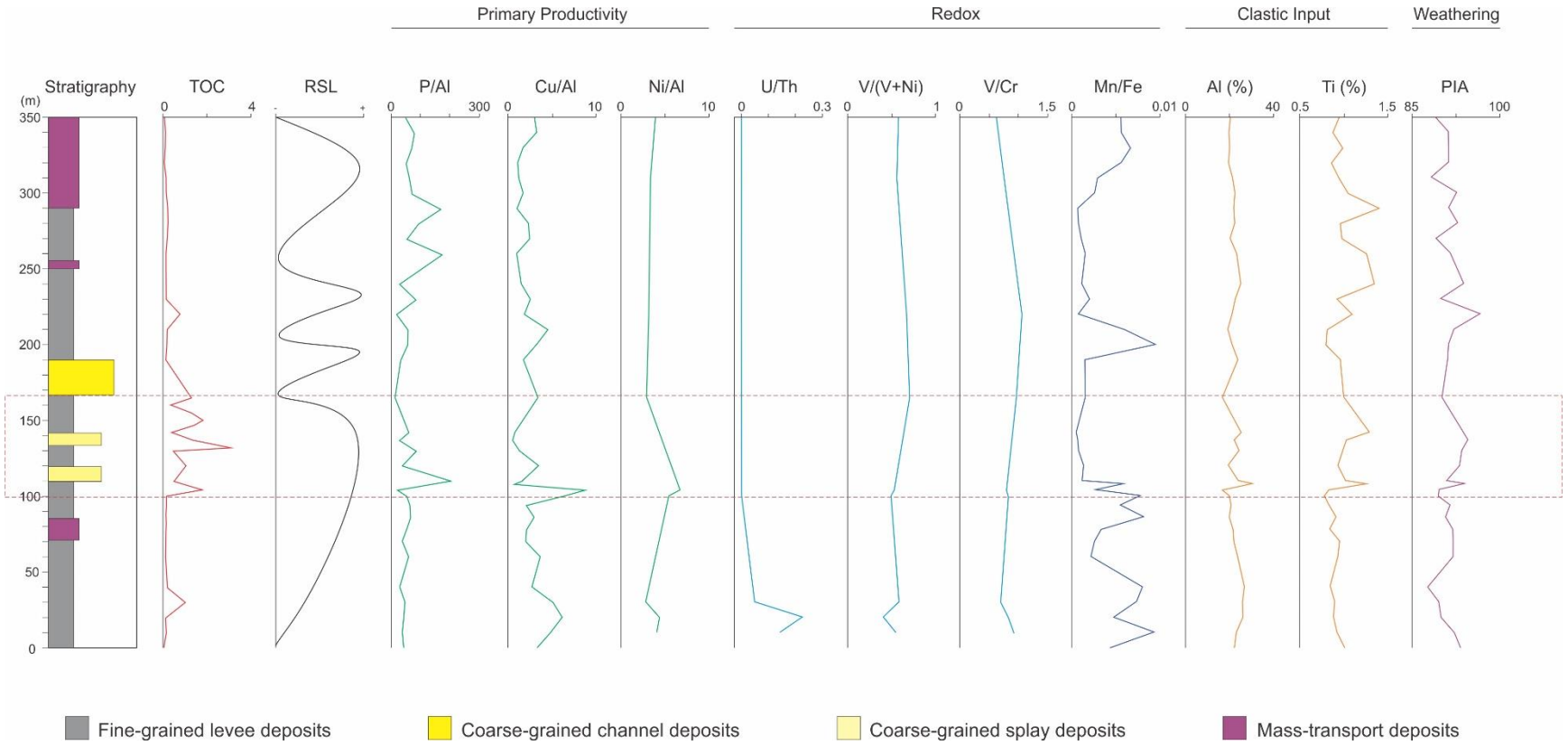

Figure 5.8. *Vertical variations in total organic carbon (TOC), relative sea level, and multiple paleoenvironmental proxies in the measured succession at Castle Creek. The organic-rich Middle Unit is highlighted in red dashed rectangle.*

5.5.2 Sea Level

Many previous studies have noted a correlation between periods of high sea level and marine organic carbon enrichment (e.g., Arthur et al. 1987; Frimmel et al. 2004; Omura and Hoyanagi 2004; Götz et al. 2005; Dong et al. 2017; Liu et al. 2019). Reconstructions of sea level position during deposition of slope deposits in the Isaac Formation have previously been proposed by Fraino (2020) and Ruso (2021) (Figure 5.8). Fraino et al. (2022) used the stratigraphic architecture of channel complexes to estimate sea level position, noting systematic changes in channel fill patterns (specifically, bottom-up versus laterally accreting) that were interpreted to be tied to changes in the granulometric makeup of the sediment supply. These changes, in turn, were linked to the state of the continental shelf and the relative input of shelf-sequestered relict and palimpsest sediment and hinterland sediment supply, which ultimately was controlled by positions of relative sea level. The work by Ruso (2021) supports and expands on the sea level trends proposed by Fraino (2020) and Fraino et al. (2022). Ruso (2021) conducted extensive geochemical analyses of slope deposits at the Castle Creek study site and used various proxies (e.g., strontium (Sr) for carbonate and zirconium (Zr) for siliciclastic sediment) to model the sequence stratigraphy of the succession and subdivide the stratigraphic column in systems tracts. Based on these data and the relative sea level curves of Fraino (2020), the OM-enriched Middle Unit, as well as the OM-rich mudstone bed at 220 m, were deposited during times of elevated relative sea level.

5.5.3 Paleoredox Conditions

Several geochemical proxies have been established to identify oxic, dysoxic, and anoxic conditions in ancient ocean basins (e.g., Ernst 1970; Rogers and Adams 1969; Lewan and

Maynard 1982; Jones and Manning 1994; Wei 2012; Algeo and Liu 2020). Three of these proxies are used here: U/Th, V/(V + Ni), and V/Cr (Figure 5.8). These proxies use the ratios of redox sensitive elements (V and U) to detrital-associated elements (Cr, N, Th). In general, increasing values indicate decreasing oxygen levels, although the threshold for oxic/anoxic conditions varies (see Table 5.4). Results show that irrespective of proxy, conditions were oxic throughout the succession. Additionally, the V/(V + Ni) and V/Cr ratios show an increasing-upward trend from the base to ~ 200 m, followed by a decreasing-upward trend in the uppermost part of the succession, suggesting lower oxygen levels, though still oxic, during deposition of the Middle, organic-rich part. The U/Th ratio, however, has the highest values near the base of the succession, but above 104 m near zero values suggest the most oxygenated conditions in bottom waters (i.e., in the Middle and Upper units).

Proxy	Oxic	Dysoxic	Anoxic
U/Th	< 0.75	0.75 - 1.25	> 1.25
V/(V+Ni)	< 0.84		> 0.84
V/Cr	< 2	2 - 4.25	> 4.25

Table 5.4. *Various paleoredox proxies and their oxic/anoxic thresholds of Jones and Manning (1994).*

Several studies have also used the Mn/Fe ratio to estimate redox conditions in sediments (e.g., Engstrom and Wright 1984; Calvert and Pedersen 2007; Naeher et al. 2013; Makri et al. 2021). Although this ratio provides only a semi-quantitative estimate, as there is no distinct threshold for oxic or anoxic conditions, it can still be used to estimate increasing or decreasing oxygen levels (Naeher et al. 2013). A lower Mn/Fe ratio suggests lower oxygen concentration because Mn is more rapidly reduced than Fe under anoxic conditions, and accordingly is preferentially released. Mn/Fe trends in this study are shown in Figure 5.8. With the exception of a large spike at 200 m, the lowest values, and therefore lowest oxygen concentration, occurs in

the interval from 110 m to 290 m, which is consistent with estimates based on V/Cr and V(V + Ni) ratios (see above). Because organic matter rapidly degrades in the presence of oxygen, dysoxic to anoxic ocean conditions are generally considered favourable, if not required, for the preservation of organic carbon (e.g., Tissot and Welte, 1978; Demaison and Moore, 1979; Arthur et al. 1987; Smith and Bustin 1998). Furthermore, many models suggest that during the Neoproterozoic the oceans were strongly stratified, and that the deep marine was anoxic (e.g., Smith 2009; Canfield 1998; Hurtgen et al. 2002; Canfield et al. 2008). However, data presented here suggests that oxic conditions prevailed over at least the continental slope at this time, and that in spite of these conditions significant organic carbon was efficiently buried and preserved. Nevertheless, it is possible that somewhat lower oxygen concentration during deposition of the Middle, OM-rich part may have contributed to enhanced preservation of organic carbon.

5.5.4 Tectonic Setting and Provenance

The ratio of SiO_2 and K_2O/Na_2O in sediments is related to tectonic setting and commonly used to differentiate active from passive margin environments (Middleton 1960; Roser and Korsch 1986). Along passive margins, sediment is sourced from compositionally mature, quartz-rich, and tectonically stable source areas (e.g., mature mudstones and sandstones, cratonic granites, etc.) and as a consequence are enriched in SiO_2 and K_2O relative to active margins. A plot of SiO_2 vs K_2O/Na_2O of samples in this study (n = 35) is shown in Figure 5.9. Samples cluster in the passive margin field, with the exception of three outliers that lie along the active continental margin/passive continental margin boundary. These three samples occur at the bottom of the studied succession, specifically at 20 m, 30 m, and 40 m above the base.

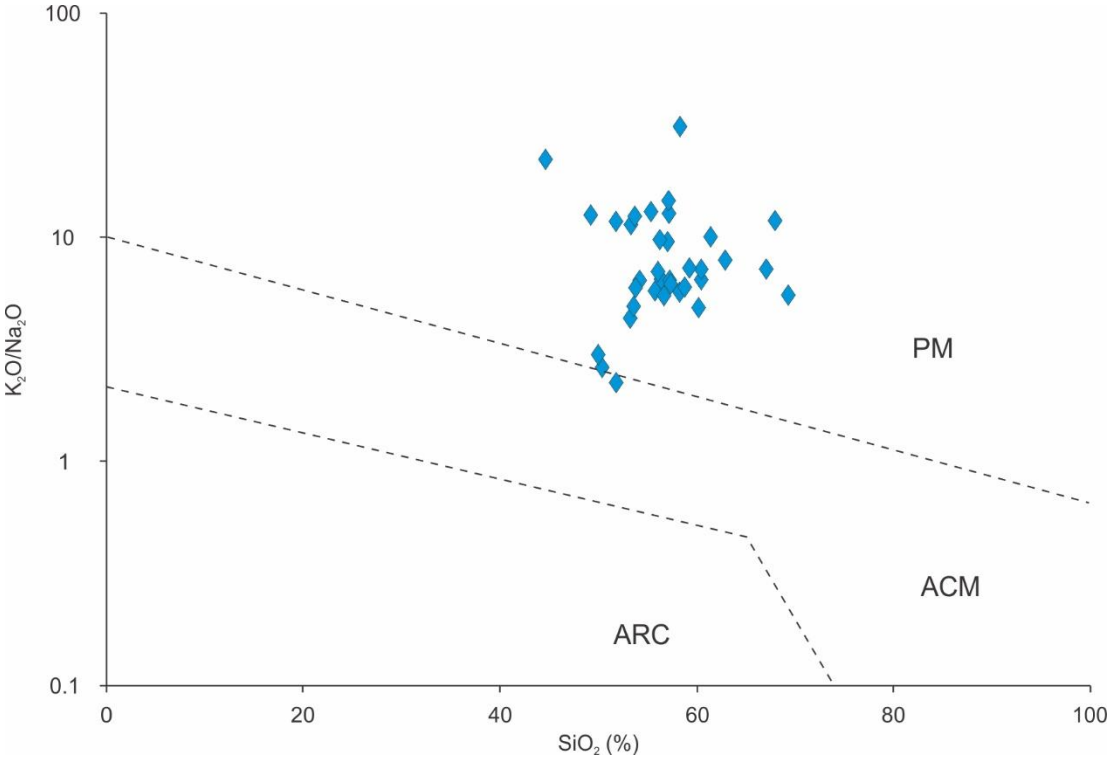

Figure 5.9. *Samples from this study plot predominantly in the passive margin field of the SiO_2 vs K_2O/Na_2O diagram (after Roser and Korsch 1986).*

The TiO_2/Zr ratio was used to estimate the composition of the weathered source rock (Figure 5.10) (Zaid 2016). Except for the three anomalous samples, which plot close to the intermediate field, all other samples indicate a felsic provenance.

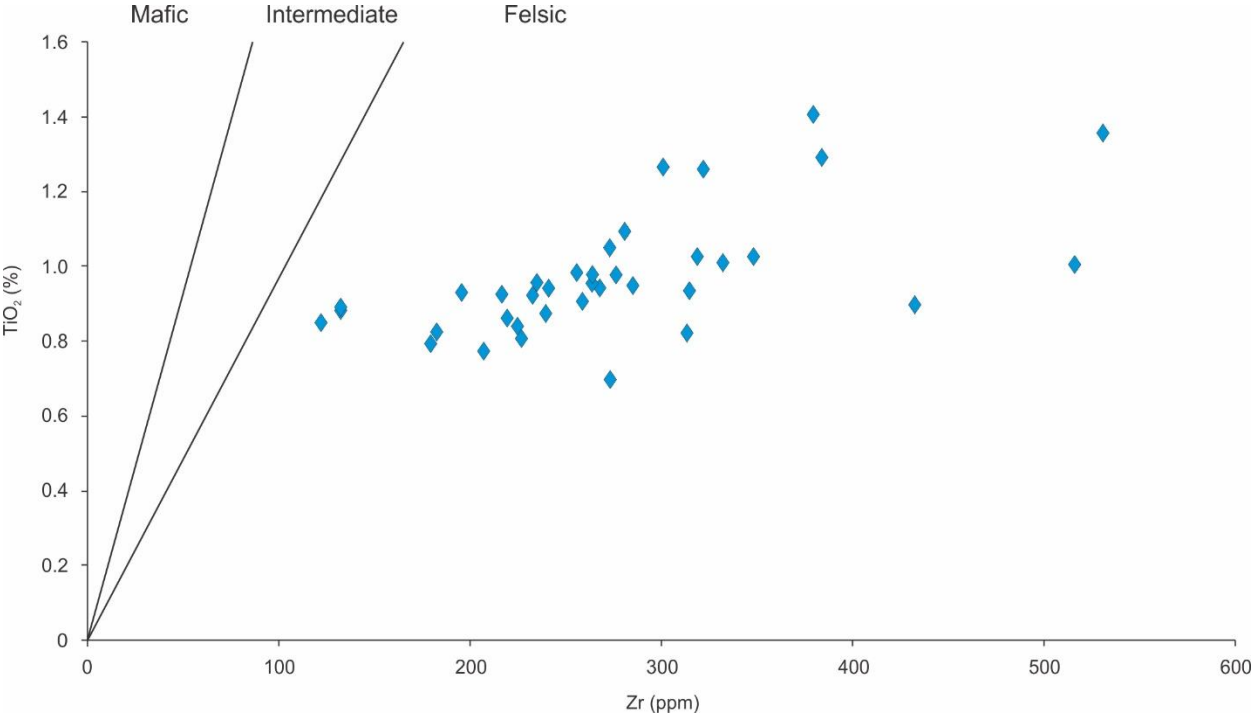

Figure 5.10. *Data points from the rocks in this study plot in the felsic field of Zr vs. TiO_2 chart (after Paulick and McPhie, 1999).*

Tectonic setting and provenance can play an important role in organic carbon deposition, principally by controlling the mineralogical make-up of sediments transported into the deep sea. In particular, organic matter in marine sediment adsorbs to clay mineral surfaces, which then protects it from degradation and remineralization (Keil et al. 1994; Mayer 1994; Keil et al. 1997; Salmon et al. 2000; Burdige 2007; Kennedy et al. 2014; Hemingway et al. 2019). The degree of adsorption is controlled by clay mineral type, and principally surface area-to-volume ratio, which in decreasing order of effectiveness is smectite, illite and then kaolinite (Cao et al. 2011). However, rocks in this study have experienced lower greenschist-level metamorphism that has altered primary clay minerals to metamorphic chlorite and muscovite, thereby complicating the assessment of the clay mineral assemblage at the time of deposition.

Because original clay mineralogy cannot be determined directly, tectonic setting and provenance proxies were used to investigate the potential for changes in detrital mineralogy based on the type and environment of the source rock. Source rock type is of interest to this study because when weathered, mafic rocks produce more smectite than felsic rocks, which produce more kaolinite (e.g., Zijlstra et al. 1985; Jeong 1998; Schroeder and West 2005; Babu et al. 2021). Because of this, changes in source rock composition could indicate changes in the relative input of smectite and kaolinite, and in turn, the amount of carbon adsorption and preservation. However, the lack of apparent change in the tectonic setting and provenance suggests that the mineralogical composition was likely to have changed little, and therefore had negligible influence on the anomalous concentration of organic matter in the middle part of the succession. This is supported by detrital zircon work by Ross and Bowring (1990), and more recently Hadlari et al. (2021), which shows no geographical or stratigraphic change in sediment provenance in the Windermere turbidite system.

5.5.5 Weathering and Terrigenous Clastic Input

The degree of source-rock chemical weathering was estimated using XRF elemental data to calculate the Plagioclase Index of Alteration (PIA) (Figure 5.8). This index is based on the ratio of aluminum, which is highly stable, to calcium and sodium, which are more easily removed during weathering, to estimate the intensity of chemical weathering. It is similar to the Chemical Index of Alteration (CIA) (Nesbitt and Young 1982), but importantly the PIA corrects for the addition of K2O into mudstones during K-metasomatism, in which aluminous clays like kaolinite are altered to illite and plagioclase is altered to K-feldspar (Fedo et al. 1995). The formula for the index is:

PIA = (Al2O3 – K2O)/ (Al2O3 + CaO + Na2O – K2O) *100 (Fedo et al. 1995)

Results show that the PIA ranges from 88 – 98, suggesting that sediment was sourced from a hinterland that had undergone intense, prolonged weathering, such as in a humid, tropical climate (Nesbitt and Young 1982; Tao et al. 2017). This is consistent with paleogeographic reconstructions that place the WSG near the equator during the Neoproterozoic (Li et al. 2013).

Although the data are somewhat variable, several trends can be identified. At the base of the succession an initial decrease in the intensity of weathering is followed by a steady increase, with the most weathered sediment in the intervals from 110 – 140 m and 210 – 220 m. The first of these intervals corresponds to the OM-rich Middle Unit, and the second to an isolated OM-rich mudstone in the Upper Unit, indicating a potential positive correlation between the degree of weathering and the amount of OM accumulation. This is discussed in more detail below.

Terrigenous input is assessed using the major elements Al and Ti, owing to their abundance in silicate rocks and chemical stability (Lu et al. 2019; Yang et al. 2020; Niu et al. 2021), and is shown in Figure 5.8. Although the data vary, two intervals show elevated values suggesting increased terrigenous flux: 108 – 142 m, and 240 – 290 m. The first of these intervals (108 – 142 m) coincides with the Middle Unit, suggesting that increased terrigenous input, as well as increased weathering (see above), may have had a positive effect on organic matter deposition and preservation.

Although many studies have shown that increased terrigenous input can be associated with low TOC due to the dilution of organic material by clastic sediment (e.g., Dong et al. 2017; Niu et al. 2021), high rates of weathering and continental runoff can also supply important nutrients, like nitrogen and phosphorus that regulate primary productivity (St. Pierre et al. 2021). This may have been especially relevant during the Neoproterozoic, when retreating continental

glaciers left an expansive reservoir of easily erodible sediment potentially containing significant amounts of essential nutrients and subsequently transported it basinwards. Periods of elevated runoff may have even generated large algal blooms along the coast, further increasing the production of organic material (e.g., Wrightstone 2011; Zhang et al. 2019). Additionally, the clay minerals delivered to the coast along with essential nutrients would also have provided abundant surfaces for organic compound adhesion, thus facilitating their transport into the deep sea and later preservation.

It is also possible that the increased terrigenous input resulted in increased turbidity and eutrophication in shallow coastal waters, reducing light penetration and preventing carbonate production. Carbonate units present elsewhere in the study area, such as the 200 m-thick first Isaac carbonate (FIC), although also deposited during a period of generally elevated relative sea level, may instead reflect periods of lower terrigenous input, with accordingly lower water turbidity, generally oligotrophic conditions, and better light penetration, making conditions more conducive to carbonate production.

5.5.6 Carbon-enriched Flow Events

Although the Middle Unit (104 – 165 m) is enriched in TOC the organic carbon is not uniformly distributed. Most of the OM is concentrated in a small number of medium- to thick-bedded, clay-rich, lower- to upper-division turbidites that average 1.65 % TOC. Separating these beds are thin-bedded, upper-division turbidites more typical of levee deposits in the studied stratigraphic interval and generally elsewhere in the greater Castle Creek study area (Figure 5.6). The average TOC in thin beds in the Middle Unit is 0.45 %, which, although higher than elsewhere in the full stratigraphic column (average 0.21 %), is still significantly lower than in the

thick-bedded OM-rich turbidites. This suggests that although basin conditions throughout this interval were generally more conducive to the production, accumulation, and preservation of organic carbon, most of the deposition was associated with episodic delivery by anomalously large, sand- and OM-enriched flows.

There are several possible explanations for the origin of such flows. Carbon enrichment in these turbidity currents may have been enhanced by local algae blooms, which would have served to cause a sudden increase in organic matter content in shelf sediments prior to downslope remobilization (Zhang et al. 2019). Also, large storms, which can last many hours to days with sustained high winds and wave height, have been documented to trigger large, sustained turbidity currents sourced from remobilized shelf sediments (Normandeau et al. 2020), and could be responsible for the deposition of these beds. Another potential cause could be large flood events possibly related to monsoons or other intense rainfall events, or from voluminous seasonal snowmelt. During Icehouse conditions, like in the Neoproterozoic, glacial outburst floods caused by extreme discharge from glacial lakes or subglacial reservoirs (e.g., Shaw and Gilbert 1990; Tweed and Russell 1999; Russell et al. 2006; Veh et al. 2019; Weckwerth et al. 2019), are also a possible cause of anomalously large, flood-triggered turbidity currents.

However, although anomalously thick, sand-rich beds occur (uncommonly) in the generally organic-poor levee deposits of Lower and Upper units, they are notably more common in the Middle Unit, where they are also enriched in OM as previously described. This suggests that the frequency of large flow events may be linked to primary productivity on the shelf, and that the accumulation of organic matter itself is in some way responsible for triggering these outsized, shelf-derived flows. High primary productivity in shallow shelfal waters would result in high rates of organic matter fallout through the water column and rapid accumulation on the

seafloor. As OM settles, particles typically aggregate and form networks of interconnected cohesive organic particles with abundant pore volume (Dade et al. 1996; Winterwerp and Van Kesteren 2004; Bhaskar and Bhosle 2005; Van Leussen 2011; Tan et al. 2014). Although the biological cohesion may act to temporarily bind and stabilize this accumulating sediment, rapid sedimentation of OM may lead to gravitational instability, particularly along the edges of submarine canyons and at the shelf-slope break, and result in episodic seafloor failure. This could create anomalously large surge-like flows enriched in OM that travel downslope and continuously overspill channel margins, forming the thick, OM-rich beds described here. These episodic events not only deplete the shelf of OM and other kinds of available unconsolidated sediment, but apparently reduce the slope gradient, and results in the more typical smaller, OM-poor turbidity currents. The abrupt and single-bed occurrence of OM-rich strata also suggests that the buildup of OM-rich strata and seafloor stabilization was rapid and of only limited duration.

Additionally, the high sedimentation rates during these outsized flow events likely played a significant role in the preservation of OM post-deposition. Previous work at Castle Creek by Cunningham and Arnott (*accepted*) found that levees are the only architectural element that contain significant amounts of OM, which is interpreted to result from the unique flow conditions that occur on levees and the nature of the OM itself. Because the majority of OM at this site is intimately associated with clay-sized particles, it is generally concentrated in the upper parts of turbidity currents and therefore more likely to overspill onto the levee, especially during anomalously large flow events. Once detached from the channel-bound part of the flow the current over the levee rapidly collapses and depletes, leading to high rates of sedimentation, whereas in the channel the more dense, higher energy part of the flow exhibits more progressive

deceleration. This gradual deceleration tends to prevent low-density and/or small mass particles from interacting and forming larger aggregates, causing any remaining OM to remain as discrete particles that are flushed through the system to the basin floor where they become diluted by hydraulically similar, but much more abundant, mineral grains (Cunningham and Arnott *accepted*).

5.5.7 Summary Model and the Role of Climate in Organic Matter Enrichment

Based on the earlier discussion, primary productivity, ocean redox conditions, sea level, degree of weathering, and terrigenous input are all factors that control the distribution of organic carbon in deep-marine levee deposits. However, optimal conditions for any one individual factor alone are not enough to alter the rate of OM enrichment in the basin; this instead requires the "perfect storm" of events where all the above factors align to create the ideal environment for both organic carbon production and accumulation. Therefore, although individual factors may have repeatedly reached optimal conditions during deposition of the studied succession, there is only one interval that contains elevated OM—the Middle Unit, in which all factors apparently aligned simultaneously. Notably also, the fact that OM preservation occurred despite oxic bottom waters suggests that source conditions, rather than basin conditions, are the most important for OM enrichment.

Importantly, sea level, weathering, and terrigenous input are themselves dependent on external factors, but primarily climate. The Neoproterozoic was characterized by three possibly global glaciations; Sturtian (715 – 680 Ma), Marinoan (650 – 632 Ma), and Gaskiers (580 Ma) (e.g., Godderis et al. 2003; Halverson et al. 2004; Fairchild and Kennedy 2007; Li et al. 2013; Lan et al. 2014; Rooney et al. 2015; Prave et al. 2016). Cochrane et al. (2019) correlated the first

Isaac carbonate (FIC), a 200 m-thick carbonate unit that occurs ~ 300 m stratigraphically below the studied interval, with slope deposition immediately prior to the Gaskiers glaciation. Based on this stratigraphic relationship, it appears likely that the strata described here were deposited sometime during the interglacial period that followed the end of the late Ediacaran Gaskiers glaciation. Additionally, in the case of this study, the recent glaciation may have formed a degraded landscape with an abundant supply of glacially eroded, fine-grained sediment for organic matter to adsorb to. This coincided with the breakup of Rodinia and development of extensive continental margins with large turbidite systems.

During interglacial periods, such as the one that followed the Gaskiers glaciation, the study area's equatorial paleogeographic location would result in a warm, tropical climate with high rainfall – an interpretation supported by consistently elevated weathering indices. Warm temperatures and enhanced solar radiation near the equator would also have promoted the growth of marine phytoplankton. Interglacials would also have been associated with large-scale melting of continental ice, increasing terrestrial runoff. The increased runoff from melting glacier ice and higher precipitation rates, both a direct result of the warm interglacial climate, would have simultaneously raised sea level and continental nutrient fluxes to the oceans. Collectively, these conditions were ideal for maximizing organic carbon generation, accumulation, and preservation. The enrichment of OM in this interval is particularly significant given that TOC values from late Neoproterozoic strata are generally very low (Sperling and Stocky 2018), similar to strata in the organic-poor parts of the succession.

However, it is important to emphasize that in this study the organic matter is exclusively of marine origin. Because of this, and as discussed earlier, elevated primary productivity was essential for OM enrichment. Following the evolution of terrestrial plants in the Late Silurian

(Behrensmeyer et al. 1992; Butterfield 2015; Gensel 2021) however, it may have been possible for significant OM enrichment to occur in the deep marine without such high levels of marine primary productivity if instead there was abundant terrestrial OM being supplied to the system. This phenomenon has been documented in several modern systems, where studies have found that the majority of OM is terrestrial in origin (e.g., Galy et al. 2007; Baudin et al. 2010; Hage et al. 2020; Hage et al. 2022). Terrestrial OM is also found by these studies to be more highly concentrated in sand-rich channel and lobe elements than in fine-grained levee and overbank environments, which is probably due to terrestrial OM commonly occurring as coarse, detrital wood or leaf particles instead of clay-bound EPS, like marine OM (Saller et al. 2006; Galy et al. 2007; Baudin et al. 2010; Lee et al. 2019; Hage et al. 2020; Hage et al. 2022; Cunningham and Arnott *accepted*).

Because of this, much terrestrial OM is generally more hydraulically similar to sand grains, and therefore tends to be transported and deposited with the sand fraction from a turbidity current. Because marine OM consists dominantly of EPS that can adsorb onto clay mineral grains, it is transported with the finer-grained fraction of turbidity currents and is therefore more likely to be concentrated in mud-dominated settings, such as levees (Cunningham and Arnott *accepted*). Marine OM can also be transported much farther through the system to overbank and distal basin settings compared to large, waterlogged terrestrial OM particles, which are more likely to remain confined within the channel and ultimately deposited in more distal depositional lobes (Baudin et al. 2010; Hage et al. 2022). This difference in transport behaviour could explain why levees are the only architectural element at the Castle Creek study site that contain significant amounts of OM (Cunningham and Arnott *accepted*). It is therefore important to specify that the factors discussed in this paper are necessary for marine OM enrichment and that

further work is needed is needed to characterize how the processes of marine and terrestrial OM enrichment may differ, although that is beyond the scope of this paper.

5.6 Conclusions

Detailed physical and geochemical examination of a 340 m-thick succession of ancient continental slope strata, consisting mostly of levee deposits, has shown that organic carbon is primarily confined to a single 60 m-thick interval. Organic-rich strata are not distributed uniformly within this interval, but instead occur principally in anomalously thick, mud-rich, lower- to upper-division sandstone turbidites interspersed with comparatively organic-poor, thin-bedded, upper-division turbidites. Where present, organic matter occurs mostly as micro- to nano-scale carbon sorbed onto the surface of clay grains.

Various geochemical proxies were used to examine the factors controlling the stratigraphic distribution of OM in this succession and the complex interplay between them. Results suggest that intense continental weathering, high terrigenous input, and elevated sea level served to increase primary productivity over the shelf, which coupled with somewhat lowered near-bed oxygenation conditions over the deeper-water continental slope, combined to enhance organic matter production, accumulation and preservation - conditions that coincided with the deposition of the Middle Unit. Further, the results suggest that this alignment of various factors is in fact necessary for significant marine OM enrichment, which can only occur during such a "perfect storm" of events when all environmental conditions are optimal. Because these conditions are all fundamentally controlled by climate, organic carbon enrichment in the deep-marine can be considered climate-driven.

This study helps to elucidate the role of various paleoenvironmental factors in deep-marine organic matter enrichment and may serve as a model for future studies of organic carbon accumulation and preservation in both modern and ancient systems. Future work could examine the carbon distribution and geochemical trends of levee successions elsewhere to determine whether the influence of these factors varies in systems of different age, tectonic setting, and make-up of the organic material.

5.7 References

ALGEO, T. J., AND LIU, J., 2020, A re-assessment of elemental proxies for paleoredox analysis: Chemical Geology, v. 540, 119549.

ALGEO, T.J., AND MAYNARD, J.B., 2004, Trace-element behavior and redox facies in core shales of Upper Pennsylvanian Kansas-type cyclothems: Chemical Geology, v. 206, p. 289-318.

ALGEO, T.J., KUWAHARA, K., SANO, H., BATES, S., LYONS, T., ELSWICK, E., HINNOV, L., ELLWOOD, B., MOSER, J. AND MAYNARD, J.B., 2011, Spatial variation in sediment fluxes, redox conditions, and productivity in the Permian–Triassic Panthalassic Ocean: Palaeogeography, Palaeoclimatology, Palaeoecology, v. 308, p. 65-83.

ALGEO, T.J., HENDERSON, C.M., TONG, J., FENG, Q., YIN, H. AND TYSON, R.V., 2013, Plankton and productivity during the Permian–Triassic boundary crisis: an analysis of organic carbon fluxes: Global and Planetary Change, v. 105, p. 52-67.

ARNOTT, R.W.C., WALLACE, K. AND LAURIN, J., 2011, Stratal architecture and temporal evolution of a passive margin mass-transport deposit, Neoproterozoic Isaac Formation, Cariboo Mountains, British Columbia, Canada, *in* Mass-Transport Deposits in Deepwater Settings, eds. R.C. Shipp, P. Weimer and H.W. Posamentier, SEPM Special Publication, v. 96, 532 p., doi:10.2110/sepmsp.096.221

ARTHUR, M.A., SCHLANGER, S.T. AND JENKYNS, H.C., 1987, The Cenomanian-Turonian Oceanic Anoxic Event, II. Palaeoceanographic controls on organic-matter production and preservation: Geological Society, London, Special Publications, v. 26, p. 401-420.

AWAN, R.S., LIU, C., GONG, H., DUN, C., TONG, C. AND CHAMSSIDINI, L.G., 2020, Paleo-sedimentary environment in relation to enrichment of organic matter of Early Cambrian black rocks of Niutitang Formation from Xiangxi area China: Marine and Petroleum Geology, v. 112, p. 104057.

BABU, S.S., RAO, V.P., SATYASREE, N., RAMANA, R.V., MOHAN, M.R. AND SAWANT, S., 2021, Mineralogy and geochemistry of the sediments in rivers along the east coast of India: Inferences on weathering and provenance: Journal of Earth System Science, v. 130(2), p.1-24.

BAUDIN, F., DISNAR, J.R., MARTINEZ, P., AND DENNIELOU, B., 2010, Distribution of the organic matter in the channel-levees systems of the Congo mud-rich deep-sea fan (West Africa).

Implication for deep offshore petroleum source rocks and global carbon cycle: Marine and Petroleum Geology, v. 27, p. 995-1010.

BAUDIN, F., STETTEN, E., SCHNYDER, J., CHARLIER, K., MARTINEZ, P., DENNIELOU, B., AND DROZ, L., 2017, Origin and distribution of the organic matter in the distal lobe of the Congo deep-sea fan – A Rock-Eval survey: Deep Sea Research Part II: Topical Studies in Oceanography, v. 142, p. 75-90.

BAUDIN, F., RABOUILLE, C., AND DENNIELOU, B., 2020, Routing of terrestrial organic matter from the Congo River to the ultimate sink in the abyss: A mass balance approach: Geologica Belgica, v. 23, ff10.20341/gb.2020.004.

BEHRENSMEYER, A.K., DAMUTH, J.D., DIMICHELE, W.A., POTTS, R., SUES, H.D. AND WINGS, S.L., 1992, Terrestrial ecosystems through time. evolutionary paleoecology of terrestrial plants and animals, University of Chicago Press, Chicago IL.

BERGEN, A.L., 2017, Vertical and lateral facies architecture of levees and their genetically-related channels, Isaac Formation, Neoproterozoic Windermere Supergroup, Cariboo Mountains, B.C.: Unpublished M.Sc. thesis, Université d'Ottawa/University of Ottawa, 193 p.

BERGEN, A.L., CUNNINGHAM, C.M., TERLAKY, V., AND ARNOTT, R.W.C., 2022, Influence of sediment supply and related channelized-flow density structure on the timing and stratal

architecture of deep-marine levee sedimentation: Journal of Sedimentary Research, v. 92, p. 1257-1274.

BHASKAR, P.V., AND BHOSLE, N.B., 2005, Microbial extracellular polymeric substances in marine biogeochemical processes: Current Science, v. 88, p. 45-53.

BURDIGE, D.J., 2007, Preservation of organic matter in marine sediments: controls, mechanisms, and an imbalance in sediment organic carbon budgets?: chemical reviews, v. 107, p. 467-485.

BUTTERFIELD, N.J., 2015, Early evolution of the Eukaryota: Palaeontology, v. 58, p. 5-17.

CALVERT, S.E., AND PEDERSEN, T.F., 2007, Elemental proxies for palaeoclimatic and palaeoceanographic variability in marine sediments: Interpretation and application C. Hillaire-Marcel, A. De Vernal (Eds.), Developments in Marine Geology, Elsevier, p. 567-644

CAMPBELL, R.B., MOUNTJOY E.W., AND YOUNG F.G., 1973, Geology of McBride map-area, British Columbia: Geological Survey of Canada, Paper v. 72, 104 p.

CANFIELD, D.E., 1998, A new model for Proterozoic ocean chemistry: Nature, v. 396, p. 450-453.

CANFIELD, D.E., POULTON, S.W., KNOLL, A.H., NARBONNE, G.M., ROSS, G., GOLDBERG, T. AND STRAUSS, H., 2008, Ferruginous conditions dominated later Neoproterozoic deep-water chemistry: Science, v. 321, p. 949-952.

CAO, Y., WEI, X., CAI, P., HUANG, Q., RONG, X., AND LIANG, W., 2011, Preferential adsorption of extracellular polymeric substances from bacteria on clay minerals and iron oxide: Colloids and Surfaces B: Biointerfaces, v. 83, p. 122-127

CHEN, R. AND SHARMA, S., 2017, Linking the Acadian Orogeny with organic-rich black shale deposition: Evidence from the Marcellus Shale: Marine and Petroleum Geology, v. 79, p. 149-158.

COCHRANE, D.J., NAVARRO, L., AND ARNOTT, R.W.C., 2019, Sedimentological and geochemical evolution of an Ediacaran mixed carbonate-siliciclastic continental slope system, Windermere Supergroup, southern Canadian Cordillera, British Columbia, Canada: Precambrian Research, v. 327, p. 47-67.

COLPRON, M., LOGAN, J.M., AND MORTENSEN, J.K., 2002, U-Pb zircon age constraint for late Neoproterozoic rifting and initiation of the lower Paleozoic passive margin of western Laurentia: Canadian Journal of Earth Sciences, v. 39, p. 133-143.

CUNNINGHAM, C.M., AND ARNOTT, R.W.C., 2021, Systematic organization of thin-bedded turbidites in ancient deep-marine levees: Possible evidence of rhythmic pulsing in

turbidity currents: Journal of Sedimentary Research, v. 91(11), p. 1257-1274. http://doi.org/10.2110/jsr.2020.003.

CUNNINGHAM, C.M., AND ARNOTT, R.W.C., *accepted,* Organic matter deposition and preservation in ancient deep-sea levee sediments: Implications for global trends in carbon burial: Sedimentology.

DADE, W.B., SELF, R.L., PELLERIN, N.B., MOFFET, A., JUMARS, P.A., AND NOWELL, A.R.M., 1996, The effects of bacteria on the flow behavior of clay-seawater suspensions: Journal of Sedimentary Research, v. 66, p. 39-42.

DAVIS, L., 2011, Architecture of deep-marine interchannel deposits: Isaac Formation, Windermere Supergroup (Neoproterozoic), southern Canadian Cordillera: M.Sc. thesis, Université d'Ottawa/University of Ottawa, 174 p.

DE JESUS MENDES, P.A., THOMSEN, L., HOLSCHER, B., DE STIGTER, H.C., GUST, G., 2007, Pressure effects on the biological degradation of organo-mineral aggregates in submarine canyons: Marine Geology, v. 246, p. 165-175.

DEMAISON, G.J., AND MOORE, G.T., 1980, Anoxic environments and oil source bed genesis: American Association of Petroleum Geologists Bulletin, v. 64, p. 1179-1209.

DONG, T., HARRIS, N.B. AND AYRANCI, K., 2018, Relative sea-level cycles and organic matter accumulation in shales of the Middle and Upper Devonian Horn River Group, northeastern British Columbia, Canada: Insights into sediment flux, redox conditions, and bioproductivity: GSA Bulletin, v. 130, p. 859-880.

ENGSTROM, D.R., AND WRIGHT, H.E., 1984, Chemical stratigraphy of lake sediments as a record of environmental change *in* E.Y. Haworth, J.W.G. Lund (Eds.), Lake Sediments and Environmental History, Leicester University Press, Leicester, pp. 11-67

ERNST, T.W., 1970, Geochemical Facies Analysis. Elsevier, Amsterdam, 152 pp.

EVENCHICK, C.A., PARRISH, R.R., AND GABRIELSE, H., 1984, Precambrian gneiss and late Proterozoic sedimentation in north-central British Columbia: Geology, v. 12, p. 233-237.

EYSTER, A., FERRI, F., SCHMITZ, M.D., AND MACDONALD, F.A., 2018, One diamictite and two rifts: Stratigraphy and geochronology of the Gataga Mountain of northern British Columbia: American Journal of Science, v. 318, p. 167-207.

FAIRCHILD, I.J. AND KENNEDY, M.J., 2007, Neoproterozoic glaciation in the Earth System: Journal of the Geological Society, v. 164(5), p. 895-921.

FEDO, C.M., WAYNE NESBITT, H. AND YOUNG, G.M., 1995, Unraveling the effects of potassium metasomatism in sedimentary rocks and paleosols, with implications for paleoweathering conditions and provenance: Geology, v. 23, p. 921-924.

FRAINO, P.E., 2020, Spatial and Temporal Stratal Evolution of an Ancient Deep-Marine Channel-Levee Complex, Neoproterozoic Isaac Formation, Windermere Supergroup, British Columbia, Canada [M.Sc. thesis]: University of Ottawa, 211 p.

FRAINO, P.E., ARNOTT, R.W.C., AND NAVARRO, L., 2022, The influence of sediment supply on the stratigraphic evolution of an ancient passive margin deep-marine slope channel system, Windermere Supergroup, British Columbia, Canada: Journal of Sedimentary Research, v. 92, p. 232-256.

FRIMMEL, A., OSCHMANN, W. AND SCHWARK, L., 2004, Chemostratigraphy of the Posidonia Black Shale, SW Germany: I. Influence of sea-level variation on organic facies evolution: Chemical Geology, v. 206, p. 199-230.

GALY, V., FRANCE-LANORD, C., BEYSSAC, O., FAURE, P., KUDRASS, H., AND PALHOL, F., 2007, Efficient organic carbon burial in the Bengal fan sustained by the Himalayan erosional system: Nature, v. 450, p. 407-410. https://doi.org/10.1038/nature06273

GENSEL, P.G., 2021, When did terrestrial plants arise?: Science, v. 373, p. 736-737.

GODDÉRIS, Y., DONNADIEU, Y., NÉDÉLEC, A., DUPRÉ, B., DESSERT, C., GRARD, A., RAMSTEIN, G. AND FRANÇOIS, L.M., 2003, The Sturtian 'snowball'glaciation: fire and ice: Earth and Planetary Science Letters, v. 211, p.1-12.

GÖTZ, A.E., SZULC, J. AND FEIST-BURKHARDT, S., 2005, Distribution of sedimentary organic matter in Anisian carbonate series of S Poland: evidence of third-order sea-level fluctuations: International Journal of Earth Sciences, v. 94, p. 267-274.

HADLARI, T., ARNOTT, R. W. C., MATTHEWS, W. A., POULTON, T. P., ROOT, K., MADRONICH, L. I., AND SIMMS, A. R., 2021, Provenance of the Incipient Passive Margin of NW Laurentia (Neoproterozoic): Detrital Zircon from Continental Slope and Basin Floor Deposits of the Windermere Supergroup, Southern Canadian Cordillera: Lithosphere, 10 p., doi:10.2113/2021/8356327.

HAGE, S., GALY, V.V., CATIGNY, M.J.B., ACIKALIN, S., CLARE, M.A., GRÖCKE, D.R., HILTON, R.G., HUNT, J.E., LINTERN, D.G., MCGHEE, C.A., AND PARSONS, D.R., 2020, Efficient preservation of young terrestrial organic carbon in sandy turbidity-current deposits: Geology, v. 48, p. 882-887. https://doi.org/10.1130/G47320.1.

HAGE, S., GALY, V.V., CARTIGNY, M.J., HEEREMA, C., HEIJNEN, M.S., ACIKALIN, S., CLARE, M.A., GIESBRECHT, I., GRÖCKE, D.R., HENDRY, A. AND HILTON, R.G., 2022, Turbidity currents can dictate organic carbon fluxes across river-fed fjords: An example from Bute

Inlet (BC, Canada): Journal of Geophysical Research: Biogeosciences, p.e2022JG006824.

HALVERSON, G.P., MALOOF, A.C. AND HOFFMAN, P.F., 2004, The Marinoan glaciation (Neoproterozoic) in northeast Svalbard: Basin Research, v. 16(3), p.297-324.

HEMINGWAY, J.D., ROTHMAN, D.H., GRANT, K.E., ROSENGARD, S.Z., EGLINTON, T.I., DERRY, L.A., AND GALY, V.V., 2019, Mineral protection regulates long-term global preservation of natural organic carbon: Nature, v. 570, p. 228-231. https://doi.org/10.1038/s41586-019-1280-6

HURTGEN, M.T., ARTHUR, M.A., SUITS, N.S. AND KAUFMAN, A.J., 2002, The sulfur isotopic composition of Neoproterozoic seawater sulfate: implications for a snowball Earth?: Earth and Planetary Science Letters, v. 203, p. 413-429.

HUSSAIN, A., HAUGHTON, P.D.W., SHANNON, P.M., MORRIS, E.A., PIERCE, C.S., AND OMMA, J.E., 2021, Mud-forced turbulence dampening facilitates rapid burial and enhanced preservation of terrestrial organic matter in deep-sea environments: Marine and Petroleum Geology, v. 130, 105101. https://doi.org/10.1016/j.marpetgeo.2021.105101

JEONG, G.Y., 1998, Formation of vermicular kaolinite from halloysite aggregates in the weathering of plagioclase: Clays and Clay Minerals, v. 46(3), p.270-279.

JONES, B. AND MANNING, D.A., 1994, Comparison of geochemical indices used for the interpretation of palaeoredox conditions in ancient mudstones: Chemical Geology, v. 111, p. 111-129.

KABANOV, P., VANDENBERG, R., PELCHAT, P., CAMERON, M., AND DEWING, K., 2020, Lithostratigraphy of Devonian basinal mudrocks in frontier areas of northwestern Canada augmented with ED-XRF technique: Arktos, v. 6(1), p. 39-52.

KEHEW, J., AND ARNOTT, R.W.C., 2020, Litho- and chemostratigraphic analysis of meter-scale cycles in an ancient mixed siliciclastic-carbonate slope system, Windermere Supergroup, Southern Canadian Cordillera, B.C., Canada: Reservoir Magazine, v. 47, p. 8-13.

KEIL, R.G., MONTLUÇON, D.B., PRAHL, F.G., AND HEDGES, J.I., 1994, Sorptive preservation of labile organic matter in marine sediments: Nature, v. 370, p. 549-552.

KEIL, R.G., TSAMAKIS, E., WOLF, N., HEDGES, J.I., AND GOÑI, M., 1997, Relationships between organic carbon preservation and mineral surface area in Amazon Fan sediments (Holes 932A and 942A): Proceedings of the Ocean Drilling Program, Scientific Results, v. 155, p. 531-538.

KENDALL, B. S., CREASER, R. A., ROSS, G. M., AND SELBY, D., 2004, Constraints on the timing of Marinoan “Snowball Earth” glaciation by 187 Re–187 Os dating of a Neoproterozoic, post-glacial black shale in Western Canada: Earth and Planetary Science Letters, 222(3),

729-740.

KENNEDY, M.J., LÖHR, S.C., FRASER, S.A., AND BARUCH, E.T., 2014, Direct evidence for organic carbon preservation as clay-organic nanocomposites in a Devonian black shale; from deposition to diagenesis: Earth and Planetary Science Letters, v. 388, p. 59-70. http://dx.doi.org/10.1016/j.epsl.2013.11.044.

KHAN, Z., 2012, Origin and architecture of deep-water levee deposits: insight from the ancient rock record and experiments. Ph.D. Thesis, University of Ottawa, 300 pp.

KHAN, Z.A., AND ARNOTT, R.W.C., 2011, Stratal attributes and evolution of asymmetric inner- and outer-bend levee deposits associated with an ancient deep-water channel-levee complex within the Isaac Formation, southern Canada: Marine and Petroleum Geology, v. 28, p. 824-842.

KHAN, Z.A., ARNOTT, B., AND PUGIN, A., 2011, An alternative model of producing topography in the crest region of deep-water levees: American Association of Petroleum Geologists, Bulletin, v. 95, p. 2085-2106.

LAN, Z., LI, X., ZHU, M., CHEN, Z.Q., ZHANG, Q., LI, Q., LU, D., LIU, Y. AND TANG, G., 2014, A rapid and synchronous initiation of the widespread Cryogenian glaciations: Precambrian Research, v. 255, p.401-411.

LEE, H., GALY, V., FENG, X., PONTON, C., GALY, A., FRANCE-LANORD, C., AND FEAKINS, S.J., 2019, Sustained wood burial in the Bengal Fan over the last 19 My: Proceedings of the National Academy of Sciences, v. 116, p. 22518-22525.

LEWAN, M.D. AND MAYNARD, J.B., 1982, Factors controlling enrichment of vanadium and nickel in the bitumen of organic sedimentary rocks: Geochimica et Cosmochimica Acta, v. 46, p. 2547-2560.

LI, Z.X., EVANS, D.A.D., AND HALVERSON, G.P., 2013, Neoproterozoic glaciations in a revised global palaeogeography from the breakup of Rodinia to the assembly of Gondwanaland: Sedimentary Geology, v. 294, p. 219-232.

LINK, P. K., 1993, Middle and late Proterozoic stratified rocks of the western U.S. Cordillera, Colorado Plateau, and Basin and Range Province. *In:* J. C. Reed, Jr., M. E. Bickford, R. S. Houston, P. K. Link, D. W. Rankin, P. K. Sims, and W. R. Van Schmus, eds., Precambrian: Conterminous U. S., The Geology of North America: Geological Society of America Decade of North American Geology Series, v. c-3, p. 474–690.

LIU, B., SCHIEBER, J., MASTALERZ, M. AND TENG, J., 2019, Organic matter content and type variation in the sequence stratigraphic context of the Upper Devonian New Albany Shale, Illinois Basin: Sedimentary Geology, v. 383, p. 101-120.

LU, Y., JIANG, S., LU, Y., XU, S., SHU, Y. AND WANG, Y., 2019, Productivity or preservation? The factors controlling the organic matter accumulation in the late Katian through Hirnantian Wufeng organic-rich shale, South China: Marine and Petroleum Geology, v. 109, p.22-35.

LUND, K., J. N. ALEINIKOFF, K. V. EVANS, AND C. M. FANNING, 2003, SHRIMP U-Pb geochronology of Neoproterozoic Windermere Supergroup, central Idaho: Implications for rifting of western Laurentia and synchroneity of Sturtian glacial deposits: Geological Society of America Bulletin, v. 115, p. 349–372.

MAKRI, S., WIENHUES, G., BIGALKE, M., GILLI, A., REY, F., TINNER, W., VOGEL, H. AND GROSJEAN, M., 2021, Variations of sedimentary Fe and Mn fractions under changing lake mixing regimes, oxygenation and land surface processes during Late-glacial and Holocene times: Science of the total environment, v. 755, p. 143418.

MASIELLO, C.A., 2007, Quick burial at sea: Nature, v. 450, p. 360-361.

MAYER, L.M., 1994, Surface area control of organic carbon accumulation in continental shelf sediments: Geochimica et Cosmochimica Acta, v. 58, p. 1271-1284.

MCARTHUR, A.D., KNELLER, B.C., WAKEFIELD, M.I., SOUZA, P.A., AND KUCHLE, J., 2016a, Palynofacies classification of the depositional elements of confined turbidite systems:

Examples from the Gres d'Annot, SE France: Marine and Petroleum Geology, v. 77, p. 1254-1273.

MCARTHUR, A.D., KNELLER, B.C., WAKEFIELD, M.I., SOUZA, P.A., AND KUCHLE, J., 2016b, Characterization of deep-marine channel-levee complex architecture with palynofacies: An outcrop example from the Rosaria Formation, Baja California, Mexico: Marine and Petroleum Geology, v. 73, p. 157-173.

MCARTHUR, A.D., GAMBERI, F., KNELLER, B.C., WAKEFIELD, M.I., SOUZA, P.A., AND KUCHLE, J., 2017, Palynofacies classification of submarine fan depositional environments: Outcrop examples from the Marnoso-Arenacea Formation, Italy: Marine and Petroleum Geology, v. 88, p. 181-199.

MCDONOUGH, M.R., AND PARRISH, R.R., 1991, Proterozoic gneisses of the Malton Complex, near Valemount, British Columbia: U-Pb ages and Nd isotopic signatures: Canadian Journal of Earth Sciences v. 28(8), p. 1202-1216.

MIDDLETON, G.V., 1960, Chemical composition of sandstones: Geological Society of America Bulletin, v. 71, p. 1011-1026.

MILCZAREK, G., 2018, Chemostratigraphic analysis of mudrocks and its implication on provenence and sequence stratigraphy in the Isaac Formation, Windermere turbidite

system, Castle Creek, B.C., Canada. Unpublished B.Sc. thesis, University of Ottawa, 59 p.

MURPHY, A.E., SAGEMAN, B.B. AND HOLLANDER, D.J., 2000, Eutrophication by decoupling of the marine biogeochemical cycles of C, N, and P: A mechanism for the Late Devonian mass extinction: Geology, v. 28, p. 427-430.

MUSSA-CALECA, M., 2008, Architecture and depositional history of a Neoproterozoic deepwater slope channel complex in a passive margin setting: Isaac Formation, Windermere Supergroup, southern Canadian Cordillera. Unpublished M.Sc. thesis, University of Ottawa, Ottawa, 128 p.

NAEHER, S., GILLI, A., NORTH, R.P., HAMANN, Y. AND SCHUBERT, C.J., 2013, Tracing bottom water oxygenation with sedimentary Mn/Fe ratios in Lake Zurich, Switzerland: Chemical Geology, v. 352, p. 125-133.

NARBONNE, G.M., KAUFMAN, A.J. AND KNOLL, A.H., 1994, Integrated chemostratigraphy and biostratigraphy of the Windermere Supergroup, northwestern Canada: Implications for Neoproterozoic correlations and the early evolution of animals Geological Society of America Bulletin, v. 106, p. 1281-1292.

NAVARRO, L., AND ARNOTT, R.W.C., 2020, Stratigraphic record in the transition from basin floor to continental slope sedimentation in the ancient passive-margin Windermere turbidite system: Sedimentology, v. 67, p. 1710-1749.

NAVARRO, L., KHAN, Z., AND ARNOTT, R.W.C., 2007, Depositional architecture and evolution of a deep-marine channel-levee complex: Isaac Formation (Windermere Supergroup), Southern Canadian Cordillera, in Nilsen, T.H., Shew, R.D., Steffens, G.S., and Studlick, J.R.J., eds., Atlas of Deep-water Outcrops, American Association of Petroleum Geologists, Studies in Geology, v. 56, CD-ROM.

NESBITT, H. AND YOUNG, G.M., 1982, Early Proterozoic climates and plate motions inferred from major element chemistry of lutites: Nature, v. 299, p. 715-717.

NINGTHOUJAM, J., WEARMOUTH, C., AND ARNOTT, R.W.C., 2022, Stratal characteristic and depositional origin of two-part (Mud-poor overlain by mud-rich) and associated deep-water strata: Components in a lateral depositional continuum related to particle settling in negligibly sheared mud-rich suspensions: Journal of Sedimentary Research v. 92(6): p. 503–529. doi: https://doi.org/10.2110/jsr.2021.053

NIU, X., LIU, Y., YAN, D., HU, M., LIU, Z., WEI, X. AND ZUO, M., 2021, Constraints on the organic matter accumulation of lower Cambrian Niutitang shales in the middle Yangtze region, south China: Lithosphere, v. 2021(Special 1), p. 6684574.

NORMANDEAU, A., BOURGAULT, D., NEUMEIER, U., LAJEUNESSE, P., ST-ONGE, G., GOSTIAUX, L., AND CHAVANNE, C., 2020, Storm-induced turbidity currents on a sediment-starved shelf: Insight from direct monitoring and repeat seabed mapping of upslope migrating bedforms: Sedimentology, v. 67, p. 1045-1068.

OMURA, A. AND HOYANAGI, K., 2004, Relationships between composition of organic matter, depositional environments, and sea-level changes in backarc basins, central Japan: Journal of Sedimentary Research, v. 74, p. 620-630.

PIETRAS, J. T., AND SPIEGEL, E. B., 2018, XRF-based Chemostratigraphy Between and Across Two Disconformities in the Ordovician Trenton Group and Utica Shale of Central New York, USA: Journal of Sedimentary Research, v. 88(3), p. 365-384.

PRAVE, A.R., CONDON, D.J., HOFFMANN, K.H., TAPSTER, S. AND FALLICK, A.E., 2016, Duration and nature of the end-Cryogenian (Marinoan) glaciation: Geology, v. 44, p.631-634.

PRICE, R.A., 2000, The southern Canadian Rockies: Evolution of a foreland thrust and fold belt: Calgary, GeoCanada 2000 (field trip guidebook): Calgary, Canadian Society of Petroleum Geologists, 244p.

PROFE, J., WACHA, L., FRECHEN, M., OHLENDORF, C., AND ZOLITSCHKA, B., 2018, XRF scanning of discrete samples–A chemostratigraphic approach exemplified for loess-paleosol sequences from the Island of Susak, Croatia: Quaternary International, v. 494, p. 34-51.

REID, L.F., SIMONY, P.S., AND ROSS, G.M., 2002, Dextral strike-slip faulting in the Cariboo Mountains, British Columbia: a natural example of wrench tectonics in relation to Cordilleran tectonics: Canadian Journal of Earth Sciences, v. 39, p. 953-970.

ROGERS, J.J.W. AND ADAMS, J.A.S., 1969, Abundances in rock forming minerals (I), uranium minerals (II). *In*: K.H. Wedepohl (Editor), The Handbook of Geochemistry, Sect. 92-D. Springer, Berlin, pp. 92-D1-92-D2.

ROONEY, A.D., STRAUSS, J.V., BRANDON, A.D. AND MACDONALD, F.A., 2015, A Cryogenian chronology: Two long-lasting synchronous Neoproterozoic glaciations: Geology, v. 43(5), p.459-462.

ROSER, B.P. AND KORSCH, R.J., 1986, Determination of tectonic setting of sandstone-mudstone suites using SiO2 content and K2O/Na2O ratio: The Journal of Geology, v. 94, p. 635-650.

ROSS, G.M., AND ARNOTT, R.W.C., 2007, Regional geology of the Windermere Supergroup, southern Canadian Cordillera and stratigraphic setting of the Castle Creek study area, Canada, in Nilsen, T.H., Shew, R.D., and Studlick, J.R.J., eds., Atlas of Deep-water Outcrops: American Association of Petroleum Geologists, Studies in Geology, v. 56, CD-ROM, 22 p.

ROSS, G. M., BLOCH, J. D. AND KROUSE, H. R., 1995, Neoproterozoic strata of the southern Canadian Cordillera and the isotopic evolution of seawater sulfate: Precambrian Research, v. 73, p. 71–99.

ROSS, G.M. AND BOWRING, S.A., 1990, Detrital zircon geochronology of the Windermere Supergroup and the tectonic assembly of the southern Canadian Cordillera: The Journal of Geology, v. 98, p. 879-893.

ROWE, H., HUGHES, N., AND ROBINSON, K., 2012, The quantification and application of handheld energy-dispersive x-ray fluorescence (ED-XRF) in mudrock chemostratigraphy and geochemistry: Chemical geology, v. 324, p. 122-131.

RUSO, S., 2021, Stratigraphic architecture and characterization of a Neoproterozoic continental slope system, Windermere Supergroup, east-central British Columbia, Canada. Unpublished M.Sc. thesis, University of Ottawa, 162 p.

RUSSELL, A.J., ROBERTS, M.J., FAY, H., MARREN, P.M., CASSIDY, N.J., TWEED, F.S. AND HARRIS, T., 2006, Icelandic jökulhlaup impacts: implications for ice-sheet hydrology, sediment transfer and geomorphology: Geomorphology, v. 75, p. 33-64.

SALLER, A., LIN, R., AND DUNHAM, J., 2006, Leaves in turbidite sands: The main source of oil and gas in the deep-water Kutei Basin, Indonesia: American Association of Petroleum Geologists Bulletin, v. 90(10), p. 1585-1608.

SALMON, V., DERENNE, S., LALLIER-VERGÈS, E., LARGEAU, C., AND BEAUDOIN, B., 2000, Protection of organic matter by mineral matrix in a Cenomanian black shale: Organic Geochemistry, v. 31, p. 463-474.

SCHOEPFER, S.D., SHEN, J., WEI, H., TYSON, R.V., INGALL, E. AND ALGEO, T.J., 2015, Total organic carbon, organic phosphorus, and biogenic barium fluxes as proxies for paleomarine productivity: Earth-Science Reviews, v. 149, p. 23-52.

SCHROEDER, P.A. AND WEST, L.T., 2005, Weathering profiles developed on granitic mafic and ultramafic terrains in the area of Elberton, Georgia: Georgia Geological Society Guidebook, v. 25, p.55-80.

SCHWARZ, E. AND ARNOTT, R.W.C., 2007, Anatomy and evolution of a slope channel-complex set (Neoproterozoic Isaac Formation, Windermere Supergroup, southern Canadian Cordillera): implications for reservoir characterization: Journal of Sedimentary Research, v. 77, p. 89-109.

SHAW, J. AND GILBERT, R., 1990, Evidence for large-scale subglacial meltwater flood events in southern Ontario and northern New York State: Geology, v. 18, p. 1169-1172.

SMITH, M. D., 2009, Stratigraphic and geochemical evolution of the Old Fort Point Formation, southern Canadian Cordillera: The deep-marine perspective of Ediacaran post-glacial environmental change. Unpublished Ph.D. thesis, University of Ottawa.

SMITH, M.G. AND BUSTIN, R.M., 1998,. Production and preservation of organic matter during deposition of the Bakken Formation (Late Devonian and Early Mississippian), Williston Basin: Palaeogeography, Palaeoclimatology, Palaeoecology, v. 142, p.185-200.

SMITH, M.D., ARNOTT, R.W.C., AND ROSS, G.M., 2014, The Old Fort Point Formation: Redefinition and formal subdivision of a distinctive stratigraphic marker in the Neoproterozoic Windermere Supergroup, southern Canadian Cordillera: Bulletin of Canadian Petroleum Geology, v. 62, p. 1-13.

SPERLING, E.A., AND STOCKEY, R.G., 2018, The temporal and environmental context of early animal evolution: Considering all the ingredients of an "explosion": Integrative and Comparative Biology, v. 58, p. 605-622.

ST PIERRE, K.A., HUNT, B.P., TANK, S.E., GIESBRECHT, I., KORVER, M.C., FLOYD, W.C., OLIVER, A.A. AND LERTZMAN, K.P., 2021, Rain-fed streams dilute inorganic nutrients but subsidise organic-matter-associated nutrients in coastal waters of the northeast Pacific Ocean: Biogeosciences, v. 18, p. 3029-3052.

STETTEN, E., BAUDIN, F., REYSS, J.L., MARTINEZ, P., CHARLIER, K., SCHNYDER, J., RABOUILLE, C., DENNIELOU, B., COSTON-GUARINI, J., AND PRUSKI, A., 2015, Organic matter characterization and distribution in sediments of the terminal lobes of the Congo deep-sea fan: evidence for the direct influence of the Congo River: Marine Geology, v. 369, p. 182–195. https://doi.org/10.1016/j.margeo.2015.08.020

STEWART, J. H.,1972, Initial deposits in the Cordilleran geosyncline: Evidence of a late Precambrian (< 850 my) continental separation: Geological Society of America Bulletin, v. 83, p. 1345-1360, https://doi.org/10.1130/0016-7606(1972)83[1345:IDITCG]2.0.CO;2.

TAN, X., HU, L., REED, A.H., FURUKAWA, Y., AND ZHANG, G., 2014, Flocculation and particle size analysis of expansive clay sediments affected by biological, chemical, and hydrodynamic factors: Ocean Dynamics, v. 64, p. 143-157.

TAO, H., SUN, S., WANG, Q., YANG, X., JIANG, L., 2014, Petrography and geochemistry of lower carboniferous greywacke and mudstone in Northeast Junggar, China: Implications for provenance, source weathering, and tectonic setting, Journal of Asian Earth Sciences, v. 87, p. 1-25.

TERLAKY, V., 2014, Sedimentology, stratigraphy, architecture and origin of deep-water, basin-floor deposits: Middle and upper Kaza Group, Windermere Supergroup, B.C., Canada [Ph.D.

Thesis]: University of Ottawa, Ottawa, ON.

TERLAKY, V., ROCHELEAU, J., AND ARNOTT, R.W.C., 2016, Stratal composition and stratigraphic organization of stratal elements in an ancient deep-marine basin-floor succession, Neoproterozoic Windermere Supergroup, British Columbia, Canada: Sedimentology, v. 63, p. 136-175.

TISSOT, B. P., AND WELTE, D. H., 1978, Sedimentary processes and the accumulation of organic matter. *In* Petroleum Formation and Occurrence: A New Approach to Oil and Gas Exploration, Eds. B.P. Tissot and D.H. Welte, Springer-verlag, Berlin, Heidelberg, p. 55-62.

TWEED, F.S. AND RUSSELL, A.J., 1999, Controls on the formation and sudden drainage of glacier-impounded lakes: implications for jökulhlaup characteristics: Progress in Physical Geography, v. 23, p. 79-110.

TYSON, R.V., 2001, Sedimentation rate, dilution, preservation and total organic carbon: some results of a modelling study: Organic Geochemistry, v. 32, p. 333–339.

VAN LEUSSEN, W., 2011, Macroflocs, fine-grained sediment transports, and their longitudinal variations in the Ems Estuary: Ocean dynamics, v. 61, p. 387-401.

VEH, G., KORUP, O., VON SPECHT, S., ROESSNER, S. AND WALZ, A., 2019, Unchanged frequency of moraine-dammed glacial lake outburst floods in the Himalaya: Nature Climate Change, v. 9, p. 379-383.

WECKWERTH, P., WYSOTA, W., PIOTROWSKI, J.A., ADAMCZYK, A., KRAWIEC, A. AND DĄBROWSKI, M., 2019, Late Weichselian glacier outburst floods in North-Eastern Poland: Landform evidence and palaeohydraulic significance. Earth-Science Reviews, v. 194, p. 216-233.

WEI, H. Y., 2012, Productivity and redox proxies of palaeo-oceans: An overview of elementary geochemistry: Sedimentary Geology and Tethyan Geology, v. 32(2), p. 76-88.

WINTERWERP, J.C., AND VAN KESTEREN, W.G., 2004, Introduction to the Physics of Cohesive Sediment Dynamics in the Marine Environment: Elsevier, Amsterdam, The Netherlands, 466 p.

WRIGHTSTONE, G.R., 2011, March. Bloomin'Algae! How paleogeography and algal blooms may have significantly impacted deposition and preservation of the Marcellus Shale: GSA Abstracts with Programs, v. 43, p. 51.

YANG, S., HU, W., YAO, S., WANG, X., HE, W., WANG, Y., ZHU, F. AND SUN, F., 2020, Constraints on the accumulation of organic matter in Upper Ordovician-lower Silurian

black shales from the Lower Yangtze region, South China: Marine and Petroleum Geology, v. 120, p.104544.

ZAID, S.M., 2016, Geochemistry of shales from the Upper Miocene Samh Formation, north Marsa Alam, Red Sea, Egypt: implications for source area weathering, provenance, and tectonic setting: Arabian Journal of Geosciences, v. 9, p. 1-15.

ZENG, S., WANG, J., FU, X., CHEN, W., FENG, X., WANG, D., SONG, C. AND WANG, Z., 2015, Geochemical characteristics, redox conditions, and organic matter accumulation of marine oil shale from the Changliang Mountain area, northern Tibet, China: Marine and Petroleum Geology, v. 64, p. 203-221.

ZHANG, J., JIANG, Z., WANG, S. AND KONG, X., 2019, Phytoplankton as main organism in the Eocene organic-rich turbidites of Jiyang Depression, China: Implication for organic matter accumulation mechanism: Energy Sources, Part A: Recovery, Utilization, and Environmental Effects, p.1-11.

ZIJLSTRA, J., MEIJER, E.L. AND BUURMAN, P., 1985, Soil formation on mafic rocks of north Galicia, Spain. 3. Chlorite-smectite transformations in weathered chloritized amphibolite: Netherlands journal of agricultural science, v. 33, p.67-69.

Chapter 6: Influence of Channelized-flow Density Structure on the Stratal Architecture of Deep-marine Levee Deposits

6.1 Introduction

Deep-marine slope channels are commonly flanked by levees (Posamentier and Kolla 2003) that form as flows overspill, augmented locally by inertial run-up and flow stripping. Overspilling flows deposit sediment that forms topographically elevated levees that act to partially confine flow to the channel (Buffington 1952; Piper and Normark 1983; Hay 1987a, 1987b; Clark and Pickering 1996; Hiscott et al. 1997; Skene et al. 2002; Kane and Hodgson 2011; Khan and Arnott 2011; Morris et al. 2014). Generally, it is explicitly stated, or more commonly diagrammatically implied, that channel-levee systems experience an initial phase dominated by erosion and bypass in the channel thalweg and deposition and aggradation along the margins, resulting in major levee development and increasing channel relief through time as levee deposition outpaces in-channel deposition (Normark et al. 1993; Clark and Pickering 1996; Elliott 2000; Sullivan et al. 2004; Straub and Mohrig 2008; Eggenhuisen et al. 2011; Fildani et al. 2013; Hubbard et al. 2014; Jobe et al. 2017). This is followed sometime thereafter by a second phase characterized by extensive channel filling, placing sandy channel-fill beds in direct contact with older, laterally adjacent levee deposits (Piper and Normark 2001; Navarro et al. 2007; Fildani et al. 2013; Hubbard et al. 2014; Jobe et al. 2017). The reasons for this temporal and spatial change in net sedimentation remain poorly understood (Clark and Pickering 1996; Deptuck et al. 2003; Bain and Hubbard 2016; Hansen et al. 2017). In cross section, deep-sea

levees exhibit a characteristic wedge-shaped or "gull-wing" geometry interpreted to be caused by the lateral thinning and fining of beds away from the channel (Skene et al. 2002; Beauboeuf 2004; Kane and Hodgson 2011; Morris et al. 2014; Hansen et al. 2017). Compared to their subaerial counterparts (see, e.g., Cazanacli and Smith 1998), deep-sea levees are significantly wider, a consequence of the reduced density contrast between the overspilling flow and the ambient fluid (Wynn et al. 2007; Kane et al. 2010a); additionally, they are significantly wider than the adjacent channel. For example, in the modern submarine Mississippi fan, the Mississippi Channel is 2 - 4 km wide and 25 - 45 m deep whereas the channel-bounding levees are 50 km wide and up to 200 m high (Wynn et al. 2007). Thus, by volume, levees make up a significant part of deep-water turbidite systems (Prior et al. 1983; Damuth et al. 1988; Hiscott et al. 1997; Deptuck et al. 2003; Beaubouef 2004; Khan and Arnott 2011; Straub et al. 2012; de Leeuw et al. 2018).

Although levees are proven productive hydrocarbon reservoirs, such as the deep-water Ram/Powell Field, Gulf of Mexico (Clemenceau et al. 2000; Weimer et al. 2000), they remain one of the most poorly understood parts of deep-marine sedimentary systems (Kane et al. 2010a; Sylvester et al. 2011). In modern systems their large size and thickness makes capturing their lithological and architectural details difficult. In the ancient sedimentary record fine-grained levee deposits are commonly extensively weathered and poorly exposed (Clark and Pickering 1996; Khan and Arnott 2011; Beaubouef 2004; Macauley and Hubbard 2013; Englert et al. 2018; Hubbard et al. 2020). Therefore, many channel-levee models are typically based on high-resolution seismic images of modern or shallowly buried systems. Although seismic images are useful for determining large-scale channel-levee geometries, outcrop studies are needed to acquire details about the bed-scale architecture of levee deposits that cannot be resolved from

even high-resolution seismic images (e.g., Mutti 1977; Clark and Pickering 1996; Browne and Slatt 2002; Eschard et al. 2003; Beaubouef 2004; Kane et al. 2007; Khan and Arnott 2011; Jobe et al. 2012; Morris et al. 2014; Hansen et al. 2017; Cunningham and Arnott 2021). It is important to note that "levee" is a morphological term that describes areas of positive depositional relief adjacent to channels in modern systems. Nevertheless, the term "levee" has been commonly used in the ancient sedimentary record to describe strata that crop out adjacent to an exposed or inferred genetically related channel deposit (see for example Cronin et al. 2000; Beaubouef 2004; Kane et al. 2007; Navarro et al. 2007; Kane et al. 2010b; Hodgson et al. 2011, Kane and Hodgson 2011; Hansen et al. 2017; Englert et al. 2018; Cunningham and Arnott 2021), and it is in this context that the term "levee" is used here.

This study examines a channel-levee system in the Isaac Formation of the Windermere Supergroup (Neoproterozoic) that is exposed in the Cariboo Mountains of east-central British Columbia, Canada (Fig. 6.1). Strata are vertically dipping, and due to recent deglaciation, are polished, vegetation free, and almost 100% exposed for 125 m vertically and ~ 2.5 km laterally (except for areas covered by moraine and glacier ice). Individual beds and even laminae, in addition to their composite bedsets and laminasets, can be easily discerned and traced continuously along bedding strike. The excellent bedrock exposure provides an ideal opportunity to directly observe details of the lithological and geometric changes in levee deposits that reflect channel initiation and subsequent development and then use these details to develop a depositional model illustrating the along-strike (spatial) and upward (temporal) relationships between channel and levee sedimentation. This model also related the observed trends in stratigraphy to physical flow processes and properties, such as maximum velocity height and density structure.

6.2 Geological Setting and Study Area

The Windermere Supergroup is an unconformity-bounded succession of Neoproterozoic metasedimentary rocks that crops out for more than 4000 km from northwestern Mexico through the southern Canadian Cordillera and farther north to the Yukon-Alaska border (Fig. 6.1; Ross and Arnott 2007). In the southern Canadian Cordillera, the age of the Windermere Supergroup is bracketed by dates of 736-728 Ma (Evenchick et al. 1984; McDonough and Parrish 1991; Eyster et al. 2018) and 570 ± 5 Ma (Colpron et al. 2002). Here, the basal few kilometers of the Windermere Supergroup consist of an intercalated succession of igneous and continental sedimentary rocks formed during rifting along the western margin of Laurentia (ancestral North America). Overlying this is a 5 – 7-km-thick, upward-shoaling pile of deep- to shallow-marine sedimentary rocks related to progradation of the passive Laurentian continental margin into the proto-Pacific Ocean (Fig. 6.1) (Ross et al. 1995; Ross and Arnott 2007).

In the southern Canadian Cordillera, the exposed part of the Windermere turbidite system extends across an area of about 35,000 km2, which if palinspastically restored (assuming ~ 30% shortening by Mesozoic deformation), represents an area of at least 80,000 km2, and therefore is dimensionally similar to the modern Amazon, Congo, and Mississippi turbidite fan systems (Ross and Arnott 2007). At the Castle Creek study area in the northern Cariboo Mountains of east-central British Columbia (Fig. 6.1), basin-floor (Upper Kaza Group) to slope (Isaac Formation) deposits are particularly well exposed on the steeply dipping limb of a southwest-vergent anticline (Fig. 6.2) (Murphy and Rees 1983; Reid et al. 2002). The rocks are metamorphosed to lower greenschist facies and contain a pervasive foliation (Murphy 1987; Ross and Arnott 2007); nevertheless, primary sedimentary structures and textures are well

preserved. The Castle Creek outcrop extends for about 7 km along strike and 2.5 km perpendicular to bedding. Because of recent deglaciation, exposures are free of surface vegetation and are only locally covered by glacial debris and ice. Mudrocks and sandstones are equally well exposed, allowing strata to be physically traced on scales of centimeters to a few kilometers.

At Castle Creek the lower 800 m consists of sheet-like units, up to decameters thick, of massive to normally graded, medium- to very thick-bedded, medium- to coarse-grained sandstone turbidites interbedded with intervals, up to 40 m thick, of very thin- to thin-bedded, fine-grained turbidites (Fig. 6.2). These rocks make up the Upper Kaza Group and have been interpreted to represent depositional lobes deposited by poorly confined flows on the basin floor (Ross et al. 1995; Meyer and Ross 2007; Terlaky et al. 2016; Navarro and Arnott 2020). These strata are then conformably overlain by a 1.6-km-thick succession of mostly fine-grained, thin-bedded turbidites intercalated with laterally discontinuous, coarse-grained, up to 220-m-thick sandstone and conglomerate units interpreted to be continental-slope channel complexes bounded by thinner-bedded, finer-grained levee deposits (Navarro et al. 2007; Khan and Arnott 2011; Khan et al. 2011; Navarro and Arnott 2020). Debrite, slump, and slide deposits that are meters to several decameters thick are common in the Isaac Formation and are consistent with gravitational instability on the continental slope.

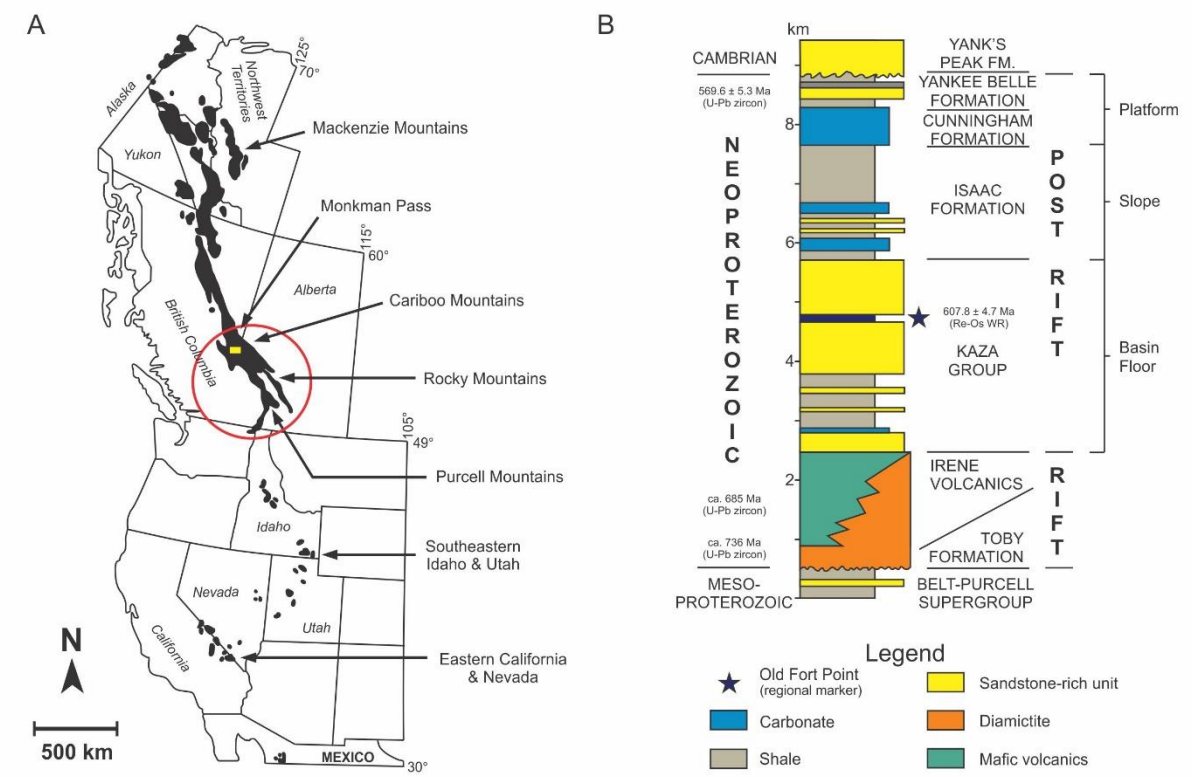

Figure 6.1. *A) Distribution of exposed Windermere Supergroup strata (black) in western North America (modified from Ross 1991). Deep-water Windermere strata are particularly well exposed in the southern Canadian Cordillera (red circle); Castle Creek study area is shown in yellow. B) Stratigraphy of the Windermere Supergroup in the southern Canadian Cordillera (modified from Ross et al. 1995). Radiometric ages are from [1]McDonough and Parrish (1991), [2]Lund et al. (2003), [3]Kendall et al. (2004) and [4]Colpron et al. (2002).*

6.3 Methods

Fieldwork was conducted at three key study areas in the Castle Creek area, referred to as southeast (~ 860 m wide), southern (~ 380 m wide) and northern (~ 190 m wide) study areas. Although these three study areas are separated by moraine (~ 190 m wide) and the Castle Creek Glacier (~ 820 m wide), intercalated debrites allow strata to be confidently correlated across the full width of the study area (~ 2.5 km). Bed-by-bed measurements and detailed sedimentological descriptions of 65 vertical stratigraphic sections, ranging from ~ 2 to ~ 125 m thick, were recorded and mapped (1:500) from all three field areas. Descriptions document stratal thickness,

bedding contacts, grain size, sedimentary structures, and lithology. Important stratal surfaces were then physically walked out in the field and traced onto high-resolution aerial photographs (1:300 - 1:500), which then were combined with the measured stratigraphic data to identify stratal architectures and changes in lithology both along strike and vertically.

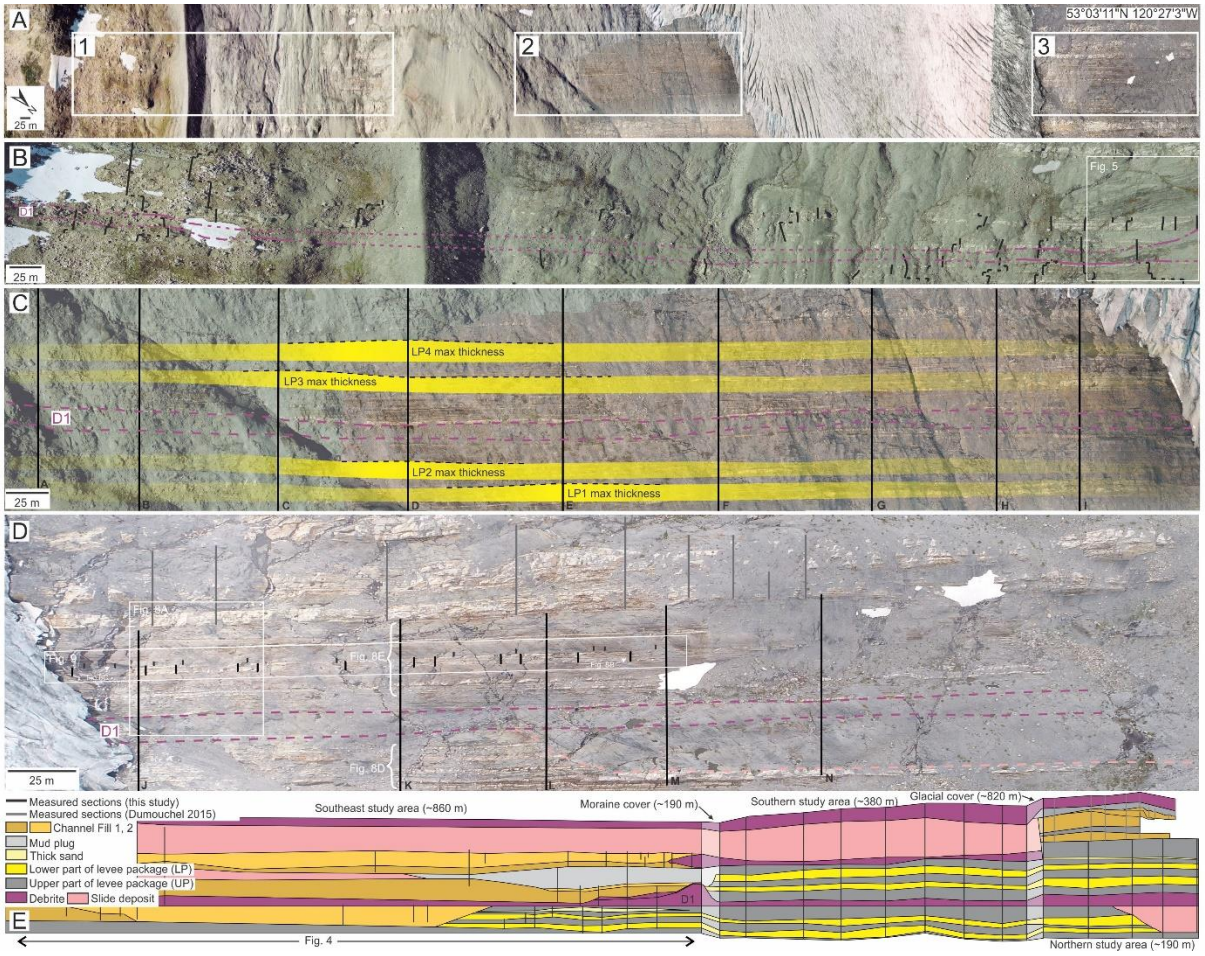

Figure 6.2. *A) Aerial photomosaic showing part of the Castle Creek outcrop and the principal study areas, referred to as southeast (box 1), southern (box 2), and northern (box 3), that were logged and mapped in this study. B) Aerial photomosaic of the southeast study area (box 1 in part A and area shown in Figure 4) with measured stratigraphic logs indicated by black lines. Debrite D1, which is shown also in parts C and D, and is the stratigraphic datum in part E, is highlighted by the dashed purple lines. Location of Figure 5 is indicated by the white polygon. C) Aerial photomosaic of the southern study area (box 2 in part A). Vertical black lines labelled A – I are measured stratigraphic logs, which are presented in detail in Figure 6. Yellow polygons highlight the lower parts of levee packages LP1 to LP4 – position of their maximum thickness indicated by the dashed black lines. D) Northern study area (box 3 in part A). Black lines show location of measured stratigraphic logs J – N (see Figure 6 for details); gray lines are sections measured by Dumouchel (2015). Dashed pink line marks the base of a slide deposit. Shown also is the location of Figures 8 and 9. E) Simplified stratigraphic correlation panel across the full width of the study area showing the channel complex set and associated levee deposits described here. See Figure 7 for the more detailed correlation panel. Stratigraphic datum is debrite D1, which, like other debrites, is exposed in all three study areas (boxes 1 – 3 in part A), thereby allowing strata to be confidently correlated across the moraine and the glacier. The widths of each study area, the moraine, and the glacier are indicated above the line diagram.*

6.4 Facies Descriptions and Interpretations

Sedimentary facies observed in channel and levee deposits at the Castle Creek study area have previously been described in detail (see Khan and Arnott 2011; Khan 2012; Cunningham and Arnott 2021). Three facies were identified in this study: normally graded sandstone lacking traction-transport structures, traction-structured sandstone, and mud-matrix-supported conglomerate. Bed thickness follows the classification scheme of Ingram (1954): very thin-bedded (1 – 3 cm), thin-bedded (3 – 10 cm), medium-bedded (10- 30 cm), thick-bedded (30 – 100 cm), and very thick-bedded (> 100 cm). Grain size is described using the Wentworth grain-size classification scale (Wentworth, 1922). Facies descriptions and interpretations are summarized in Table 6.1.

TABLE 1.—*Lithological description and depositional interpretation of facies observed in channel and levee deposits of this study.*

Facies	Lithology	Bed Thickness	Sedimentary Structures	Bed Contacts	Interpreted Depositional Process	Bouma Sequence Equivalence
F1: normally graded sandstone lacking traction-transport structures	Upper coarse-grained sandstone with granules to medium-grained sandstone capped by 1–2 cm of mudstone. Mudstone intraclasts in the basal part of beds range from 114 cm × 3 cm (large) to 1.5 cm × 1 cm (small).	40–140 cm thick (average = 87 cm)	Normally graded	Typically undulatory; sharp with common soft-sediment-deformation structures (e.g., flames).	Deposited from decelerating, high-density, density-stratified turbulent flows containing granules to clay. Sand-rich basal parts of beds likely deposited under capacity-driven conditions. Lack of tractional sedimentary structures indicates high rates of suspension fallout.	Tade
F2: traction-structured sandstone	Very thin- and thin-bedded strata typically consist of fine- to very fine-grained sandstone and form a 3–27-cm-thick (average = 9 cm) stack of 3–7 non-climbing, ripple-cross-stratified sets. Single non-climbing, ripple-cross-stratified sets are less common. Beds capped by a mudstone 1-2 cm thick. Medium- to thick-bedded strata grade upward from upper medium- to fine-grained sandstone and consist of a basal planar-laminated unit sharply overlain by a small-scale cross-stratified unit overlain by a thin, structureless mudstone unit.	2–326 cm (86% of beds are between 3 and 30 cm)	Planar- and/or ripple cross-stratified	Generally sharp and planar, less commonly undulatory with flame structures.	Competence-driven deposition from turbulent flows consisting of upper-medium sand to clay, but mostly fine-grained sand to clay, suggesting lower rates of fallout, and likely lower sediment concentration than those that deposited F1.	Tbcde/Tbde/ Tcde
F3: mud- matrix-supported conglomerate	Mud-matrix-supported conglomerate with dispersed quartz pebbles and carbonate-cemented sandstone, mudstone, and carbonate clasts	0.5–18 m (typically 4–9 m)	Structureless	Sharp and planar	Deposited by mud-rich cohesive debris flow	N/A

Table 6.1. *Lithological description and depositional interpretation of facies observed in channel and levee deposits of this study.*

6.5 Facies Assemblages: Channel and Extrachannel Deposits

We differentiate channel and extrachannel deposits based on distinctive assemblages of facies 1 and 2 strata (Fig. 6.3). Channel deposits are confined to the southeast study area (Fig. 6.2) and consist of a variety of coarse-grained Facies 1 strata that generally thin upward (very thick- to thin-bedded) and fine upward (very coarse to medium sand), and change from massive to progressively better-graded strata with traction-transport structures in the upper parts of individual beds. In comparison, immediately adjacent strata consist of thin-, medium-, and thick-bedded, typically fine-grained, traction-structured sandstone (Facies 2) that can be divided vertically into packages, each consisting of a sand-rich lower part overlain sharply by a mud-rich upper part. They crop out on the northwestern side of the southeast study area and extend along strike towards the northwest across the southern and northern study areas (Fig. 6.2). As will be discussed below, the consistent lateral changes in facies and vertical stacking patterns of these deposits suggest that they are extrachannel deposits, and more specifically levee deposits that are genetically related to the adjacent channel fills.

Figure 6.3. *A) Facies 1: medium-bedded (26 cm), structureless Tade sandstone. Bed grades upward from upper coarse-grained sandstone with abundant granules to medium-grained sandstone overlain by a thin mudstone cap. B) Facies 2: medium-bedded (28 cm), Tbcde turbidite that grades upward from medium-grained sandstone at its base to silty mudstone at its top. C) Facies 2: multiple thin-bedded (3-8 cm) Tcde turbidites. At their base beds consist of a stack of medium- to fine-grained sets of non-climbing-ripple cross-stratified sandstone (Tc) overlain by interlaminated very fine-grained sandstone and siltstone (Td) capped by mudstone (Te). D) Facies 3: mudstone and quartz clasts dispersed in a silty mudstone matrix. E) Facies 3: boulder-sized carbonate-cemented sandstone clast immediately above the base of a mud-matrix-supported conglomerate. F) Facies 3: oolite clast in a carbonate-clast-rich, mud-matrix-supported conglomerate. G) Facies 3: carbonate-clast-rich, mud-matrix-supported conglomerate containing a stromatolite clast (arrow) and assorted other carbonate fragments.*

6.5.1 Channel Deposits

Numerous classification schemes have been proposed to describe the architectural elements that make up submarine-channel deposits (see, e.g., Mutti and Normark 1987; Normark et al. 1993; Pickering et al. 1995; Abreu et al. 2003; Sprague et al. 2005). In this study the basic element is a discrete channel fill, which comprises the deposits within a negative topographic feature that confined turbidity currents. Channel fills are less than 10 m thick and 200 m wide. A channel complex, in turn, comprises two or more channel fills exhibiting similar lithological and architectural characteristics, and a channel complex set comprises two or more genetically related channel complexes.

The exposed part of the channel complex set in the southeast study area is 70 m thick and 860 m wide. It consists of three channel complexes (CC1 - CC3) intercalated with debrite and slide deposits that in some cases extend across the entire study area (Fig. 6.4). Like their composite channel fills, channel-complex bases are marked by an erosion surface and/or an abrupt increase in grain size.

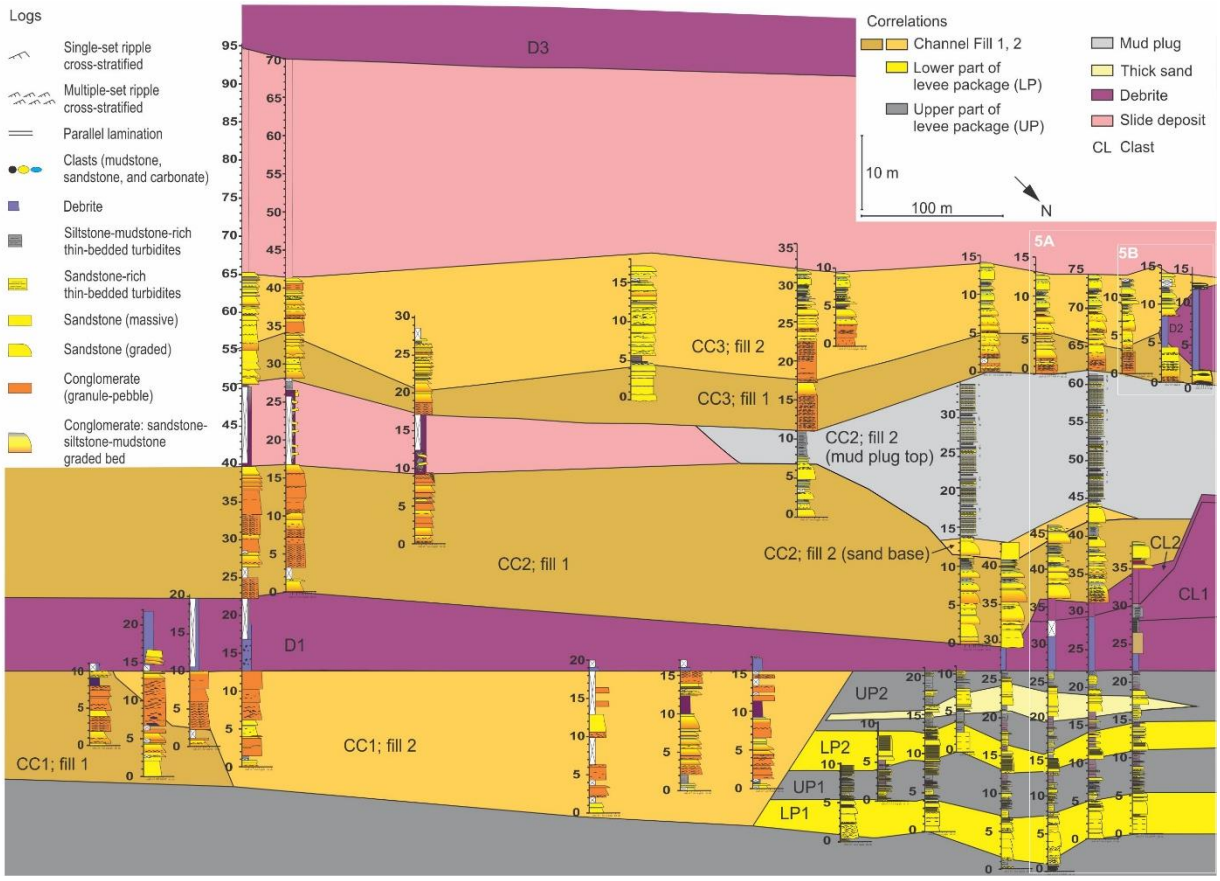

Figure 6.4. *Detailed measured sections and correlation panel showing the channel-complex set exposed in the southeast study area (4X vertical exaggeration) – see Fig. 2 part B for aerial photograph. CC1 to CC3 are channel complexes, D1 to D3 are debrites; stratigraphic datum is the base of D1. Lower (LP) and upper (UP) parts of extrachannel packages crop out adjacent to channel deposits on the northwest side of the panel. CL1 and CL2 are large clasts (rafts) of interstratified siliciclastic mudstone-sandstone (CL1) and carbonate-rich debrite (CL2) supported on the top of debrite D1. The location of photographs in Figure 5 are marked by the white boxes.*

6.5.1.1 Channel Complex 1 (CC1) Description

Channel complex 1 (CC1) erosionally overlies a 10-m-thick succession of fine-grained, thin-bedded, Tcde turbidites (Facies 2). CC1 is up to 18 m thick and comprises two channel fills separated by a sharp erosional surface. The lower channel fill is exposed only in the far southern edge of the southeast study area and is up to 10 m thick. It comprises amalgamated, thin- to very thick-bedded, ungraded and normally graded, coarse- to medium-grained Ta turbidites with

granule to pebble clasts consisting of mudstone, quartz, feldspar, carbonate-cemented sandstone, and limestone.

The upper channel fill deeply scours the lower channel fill and is up to 18 m thick. At its base the fill consists of thin- to very thick-bedded, massive or normally graded strata made up of clast or matrix-supported, coarse-grained sandstone with locally abundant quartz and feldspar pebbles. Mudstone intraclasts, carbonate-cemented sandstone clasts, and limestone clasts are abundant and up to several decimeters long. Clasts are rounded to subangular and are aligned with apparent long axes parallel to the base of the channel. Stratigraphically upward, strata fine to medium- to coarse-grained, massive or graded beds, some of which have planar lamination at their tops.

CC1 is then sharply and locally erosionally overlain by a 10-m-thick, poorly sorted, mudstone-rich debrite (D1). Together these strata form a distinctive stratigraphic marker that can be traced across the width of the entire study area.

6.5.1.2 Channel Complex 2 (CC2) Description

Channel complex 2 (CC2) has an erosional base and sharply overlies or onlaps debrite D1 (Fig. 6.5A). CC2 is up to 35 m thick and comprises two channel fills. The lower fill consists of an upward and laterally (toward the northwest) fining and thinning stratal assemblage of amalgamated, thin- to thick-bedded, normally graded or massive, upper coarse-grained Ta turbidites. It is sharply overlain by a 10-m-thick slide deposit that is truncated to the northwest by the base of the upper channel fill, which thereafter sharply overlies the lower channel fill. The upper channel fill is up to 23 m thick. The basal 3 m of the upper fill consists of very thick- to

medium-bedded, upper coarse-grained Ta and Tab turbidites with local mudstone clasts. This sand-rich base is then overlain sharply by a thick (20 m) succession of upward thinning medium- to thin-bedded, fine-grained turbidites interpreted to be an abandonment mud plug (Fig. 6.4).

6.5.1.3 Channel Complex 3 (CC3) Description

Channel complex 3 (CC3) has an erosional base, ranges from 12 to 20 m thick, and comprises two channel fills (Fig. 6.5A). The lower fill consists of an upward-fining and -thinning stratal package of amalgamated, mudclast-breccia-rich, medium- to thick-bedded, massive and normally graded, very coarse- to coarse-grained sandstone. At the northwestern end of the study area, most of the fill is deformed near the snout of debrite D2 and the upper 1 m of the fill onlaps the debrite (Fig. 6.5A, B).

In most places the upper channel fill sharply overlies the lower channel fill and consists of an upward-fining and -thinning stratal package of coarse- to medium-grained beds with locally erosional bases that typically preserved mud-rich, medium-grained, planar or cross-stratified bed tops. Near the northwestern edge of the outcrop, the channel fill onlaps and then overlaps D2 (Fig. 6.5A, B). The upper channel fill is then overlain by a thick mass-transport deposit that extends across the width of the study area and consists of a basal 30-m-thick slide deposit overlain by a 7-m-thick debrite (D3).

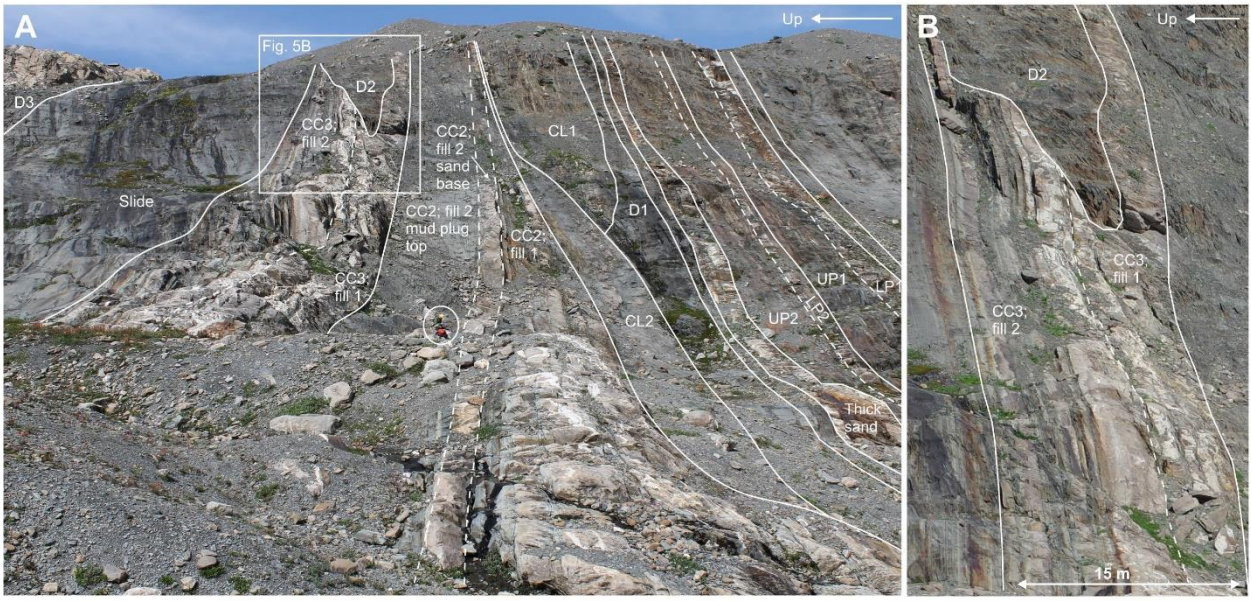

Figure 6.5. *A) Part of the southeast study area where channel complexes (CC1 to CC3) are intercalated with slide and debrite (D1, D2, D3) deposits. Dashed lines mark the contact between the lower and upper parts of an extrachannel package and between the lower and upper fills in a channel complex. Circled person for scale. B) Close-up showing details of area outlined in part A. Most of the lower fill of channel CC3 is deformed near the snout of debrite D2; the upper ~1 m of the fill onlaps the debrite. The upper fill of channel complex 3 onlaps and then overlaps the debrite.*

6.5.2 Extrachannel Deposits

Strata that crop out adjacent to channel complexes 1 to 3 can be traced continuously along strike over 280 m in the southeast study area, 380 m in the southern, and 190 m in the northern study areas (Fig. 6.6, 6.7). Although separated by moraine (~ 190 m wide) and the Castle Creek Glacier (~ 820 m wide), intercalated debrites (F3) allow strata to be correlated across the full width of the study area (2.5 km). The distinctive assemblage of clasts in each debrite allows them to be confidently correlated. In debrite D1 clasts are predominantly quartz pebbles dispersed in a mudstone matrix. It also contains stromatolite and oolite fragments, and meter-scale carbonate-cemented sandstone rafts in the upper part of the deposit. D2 consists mostly of carbonate-cemented sandstone clasts with folded internal stratification and cuspate-

lobate margins. D3 is dominated by quartz pebbles and carbonate-cemented sandstone clasts but lacks the stromatolite and oolite fragments and the rafts observed at the top of D1.

Extrachannel deposits form four packages, 5 - 20 m thick, consisting of strata that are finer and thinner-bedded relative to those in the immediately adjacent channel complexes. The deposits consist of lower (LP) and upper (UP) parts; the contact is marked by a dramatic decrease in bed thickness and grain size (Fig. 6.8A). Strata end abruptly against the margin of channel deposits on the southeastern side of the outcrop and then extend along strike over a distance of at least 1.7 km towards the northwest. Sparse paleoflow (n = 15) data, measured in the troughs of three-dimensional ripples, indicate that levee deposits were deposited by flows generally directed towards the northwest (mean paleoflow is 317°). These flows were formed from the overspill of channels interpreted to have been located to the southeast, and that the trend of the outcrop exposure is oriented oblique to these ancient channel margins.

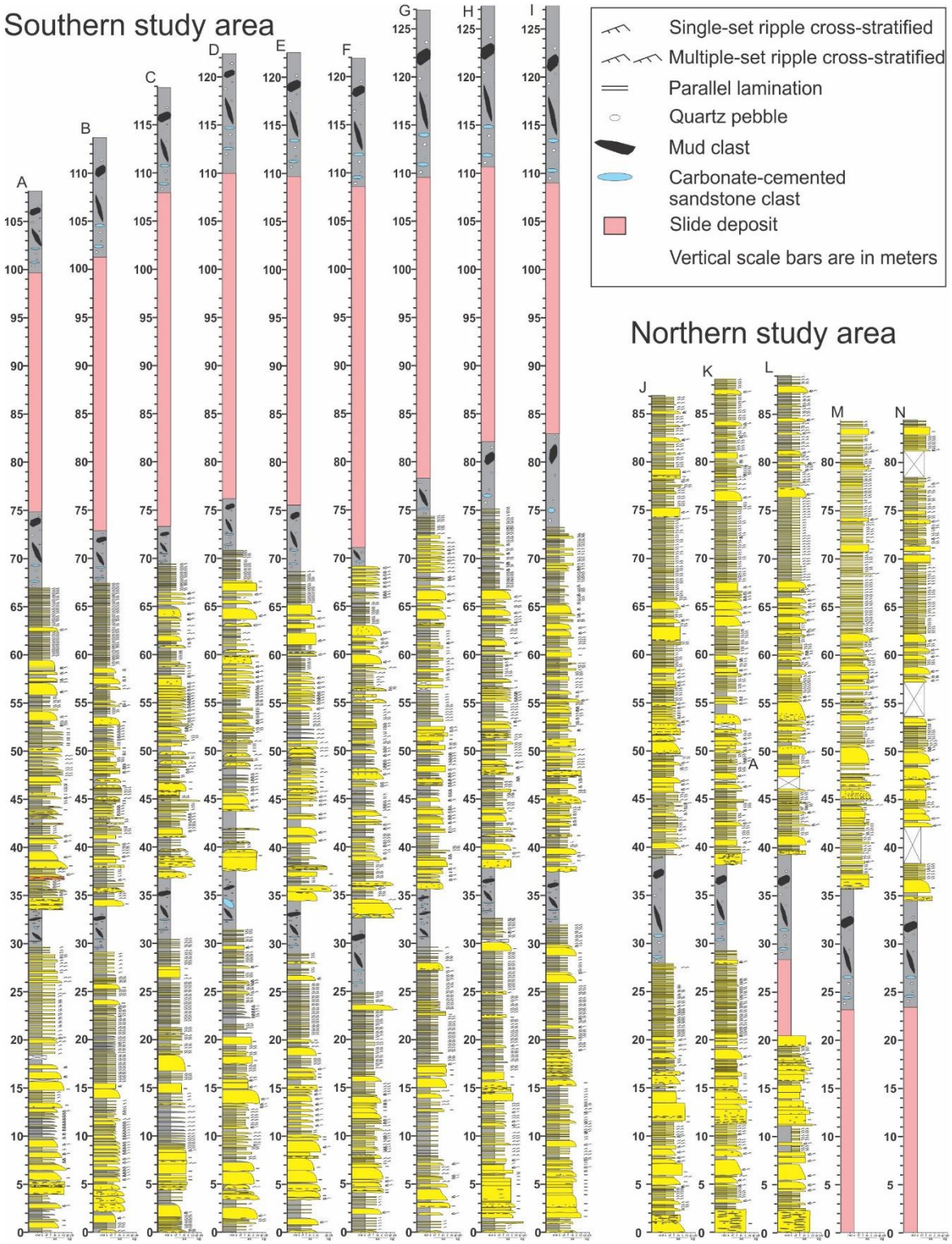

Figure 6.6. *Detailed measured sections of extrachannel deposits exposed in the southern and northern study areas. Letters near the top of each log correspond to the letters in Figures 2 and 7.*

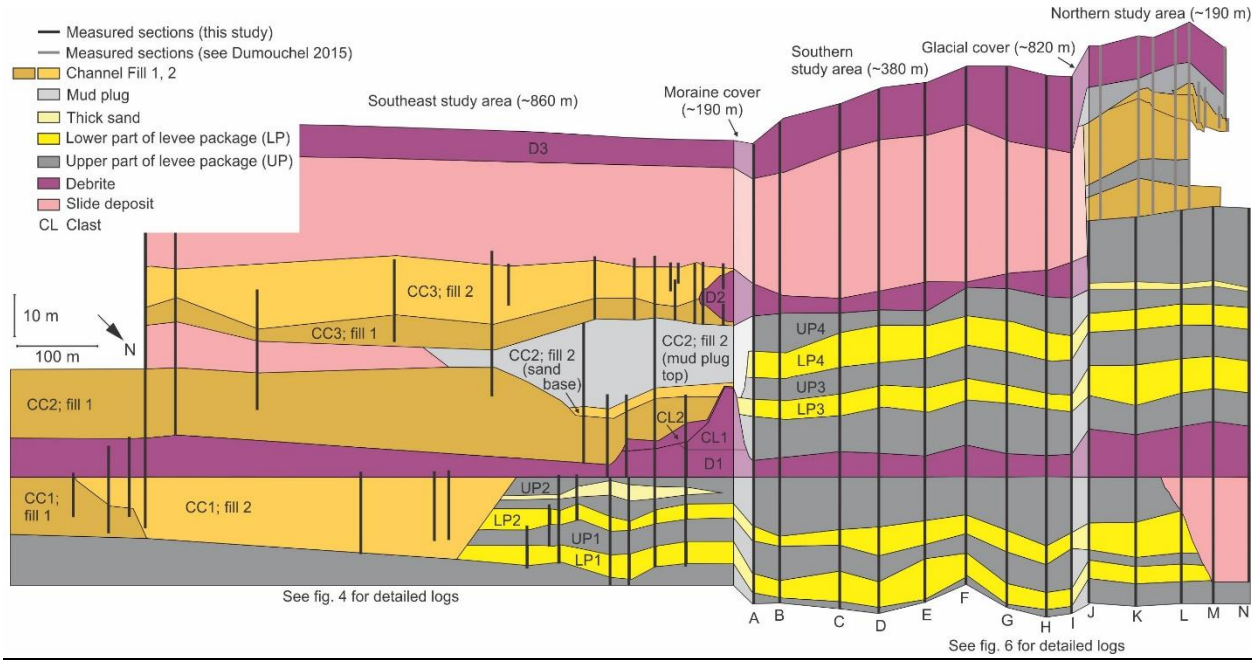

Figure 6.7. *Correlation panel showing the channel-complex set and extrachannel deposits (4X vertical exaggeration) with the base of debrite D1 as stratigraphic datum. Intercalated debrites (D1 and D3) allow strata to be confidently correlated across the full width of the study area (~ 2.5 km). CC1-CC3 are channel complexes 1-3, LP 1-4 are the lower part of extrachannel packages and UP 1-4 are the upper part of extrachannel packages. CL1 and CL2 are large clasts (rafts) of interstratified siliciclastic mudstone-sandstone (CL1) and carbonate-rich debrite (CL2) supported on the top of debrite D1. Refer to Figure 2 to link this correlation panel to the three study areas. Refer to Figure 4 for detailed logs measured in the southeast study area and to Figure 6 for detailed logs measured in the southern and northern study areas.*

6.5.2.1 Extrachannel Deposits Adjacent to Exposed Channel Deposits Description

The lower parts of packages are 3 - 10 m thick and consist mostly of medium- to thick-bedded, upper medium- to coarse-grained, lower-division (Tbcde) turbidites intercalated with very thin- to thin-bedded, fine-grained, upper division (Tcde) turbidites (Fig. 6.8B, 6.9). These strata exhibit a distinctive thickening and then thinning trend laterally away from the margins of the channel deposits; similar observations were reported previously in levee deposits of Isaac channel 3 by Khan and Arnott (2011) and Khan et al. (2011). More specifically, it is the medium- to thick-bedded, upper medium- to coarse-grained Tb and Tbc turbidites that exhibit

this trend, and collectively control the thickness trends in the lower part of each package (Fig. 6.10). Individual beds thicken for the first 560 - 660 m away from the channel-deposit margin, causing the thickness of the lower part to increase on average by 62%. Upon reaching their maximum thickness, beds then thin, with the total thickness of the lower part decreasing by 60% but over a distance of 175 - 275 m. Also away from the channel-deposit margin, but over distances of about 300 - 450 m, thick-bedded very coarse-grained Ta and Tab turbidites thin and transition progressively to upper medium-grained Tbcd turbidites and then thin-bedded, fine-grained Tcd turbidites, or in rare cases, pinch out altogether (Fig 6.11).

In contrast, the intercalated very thin- to thin-bedded, fine-grained, upper-division turbidites show negligible lateral change in thickness, grain size, or sedimentary structures; much of the bed thickness being composed of a single set or multiple set (2 or 3) ripple cross-stratified layer (Tc). In rare cases, very thin- to thin-bedded, fine-grained, upper-division turbidites thicken away from the channel-deposit margin and transition into medium- to thick-bedded, medium-grained Tbcd turbidites (Fig. 6.11). Typically, this transition begins 500 – 600 m away from the channel-deposit margin; closer to the channel deposit margin these beds show negligible changes in thickness and grain size. Collectively, the percentage of total sandstone thickness relative to total stratal thickness in the lower part of a package decreases, although unevenly, from ~ 90% adjacent to channel deposits to ~ 62% along a horizontal distance of 700 m.

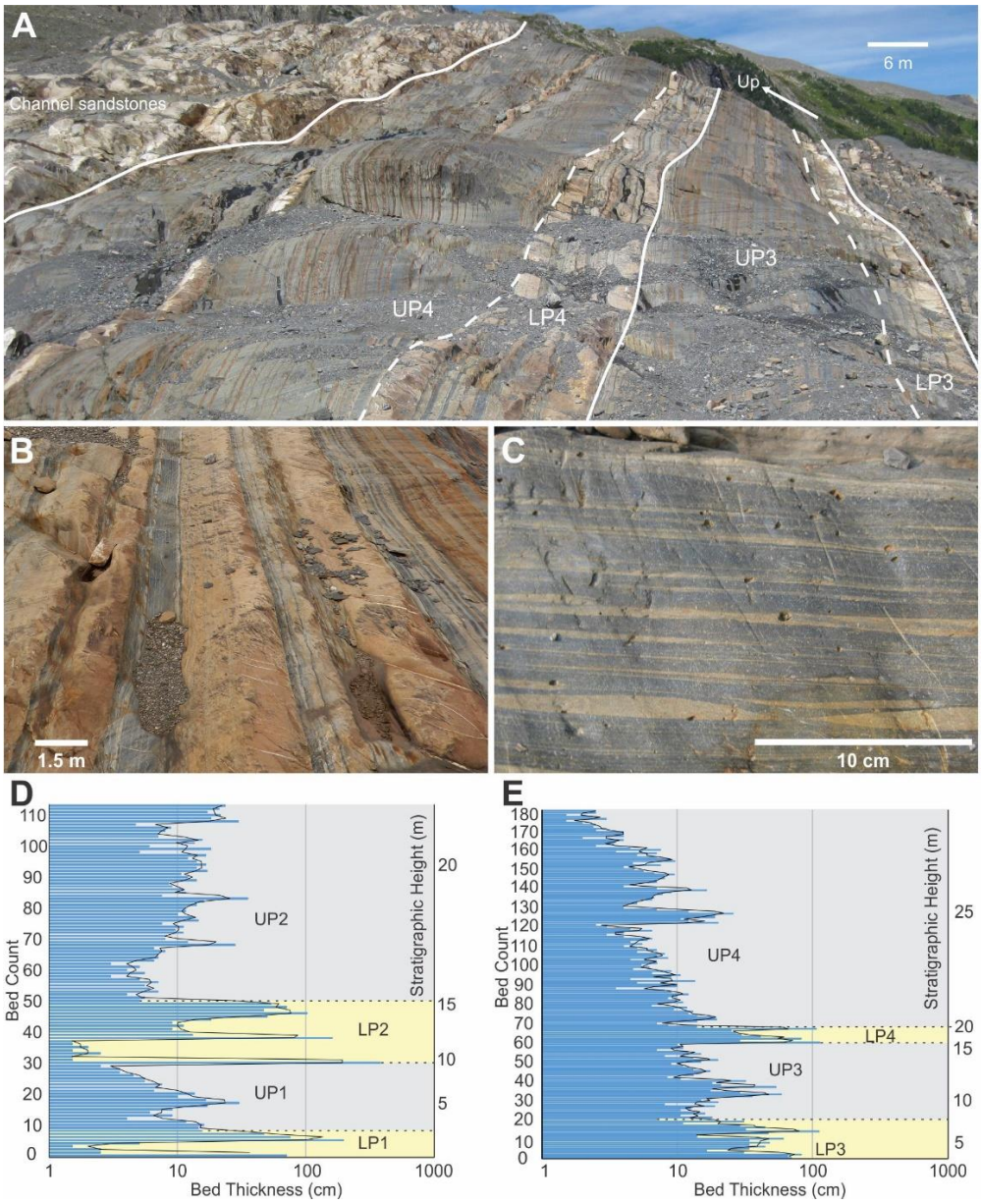

Figure 6.8. *A) In this study four 5 – 20-m-thick stratal packages comprising a lower (LP) and upper (UP) part are observed; the base of the upper part marked by a sudden and striking decrease in bed thickness and grain size. Packages 3 and 4 in the northern study area are shown here (see Fig. 2, parts A and D, for the location of the northern study area). B) Turbidites in the lower part (LP) of a package consist mostly of medium- to thick-bedded, upper medium- to coarse-grained, lower-division turbidites intercalated with very thin- to thin-bedded, fine-grained, upper-division turbidites. C) Turbidites in the upper part (UP) of a package consist mostly of very thin- to thin-bedded, fine-grained, upper-division turbidites intercalated with uncommon medium- to thick-bedded, upper medium-grained, lower-division turbidites. D) Bed thickness data of 114 beds that make up packages 1 and 2, and E) 181 beds that make up packages 3 and 4 in the northern study area. See Fig. 2, part D, for location of measured sections. The contact between the LP and UP part of each package (dashed black lines) is sharp and marked by a sudden and striking decrease in bed thickness. Note that bed thickness is displayed using a logarithmic scale. Solid black vertical trendline represents a two-bed moving average.*

The upper parts of packages are 3 - 16 m thick and consist mostly of very thin- to thin-bedded, fine-grained, upper-division turbidites intercalated with uncommon medium- to thick-bedded, upper medium-grained, lower-division turbidites (Figs. 6.8C, 6.9). Unlike the lower part of the package, the upper part thins and then thickens away from the channel-deposit margin, typically being thinnest where the lower package is thickest (Fig. 6.10). Much of this change in thickness is attributed to changes in the thickness of individual fine-grained, thin-bedded, multiple-set (3 or 4) Tcde turbidites, which for the first 600 - 700 m away from the channel-deposit margin thin on average by 7 cm but then thicken by 2 cm over the next 140 - 240 m. Significantly, grain-size changes are negligible. Similarly, the thickness and grain size of very thin-bedded, fine-grained, single-set Tcde turbidites changes little, although slight thinning and fining along distances of several hundreds of meters is common.

Uncommon medium-bedded, upper medium-grained Tbcd turbidite interbeds typically show negligible change in thickness and grain size for the first 200 - 400 m away from the channel-deposit margin, but then gradually fine and thin for the next several hundred meters and transition to thin- to very-thin bedded, medium- or fine-grained Tcde turbidites (Fig. 6.11), beyond which they show negligible change. As in the lower packages, rare very thin- to thin-bedded Tcde turbidites in the upper packages thicken away from the channel deposit margin and transition into medium- to thick-bedded, medium-grained Tbcd turbidites. This transition occurs several hundreds (~ 300 – 500) of meters away from the channel deposit margin. The percentage of sandstone relative to total thickness in the upper part of packages decreases unevenly from 54% to 36% over the first 350 m away from the channel-deposit margin but then changes little thereafter.

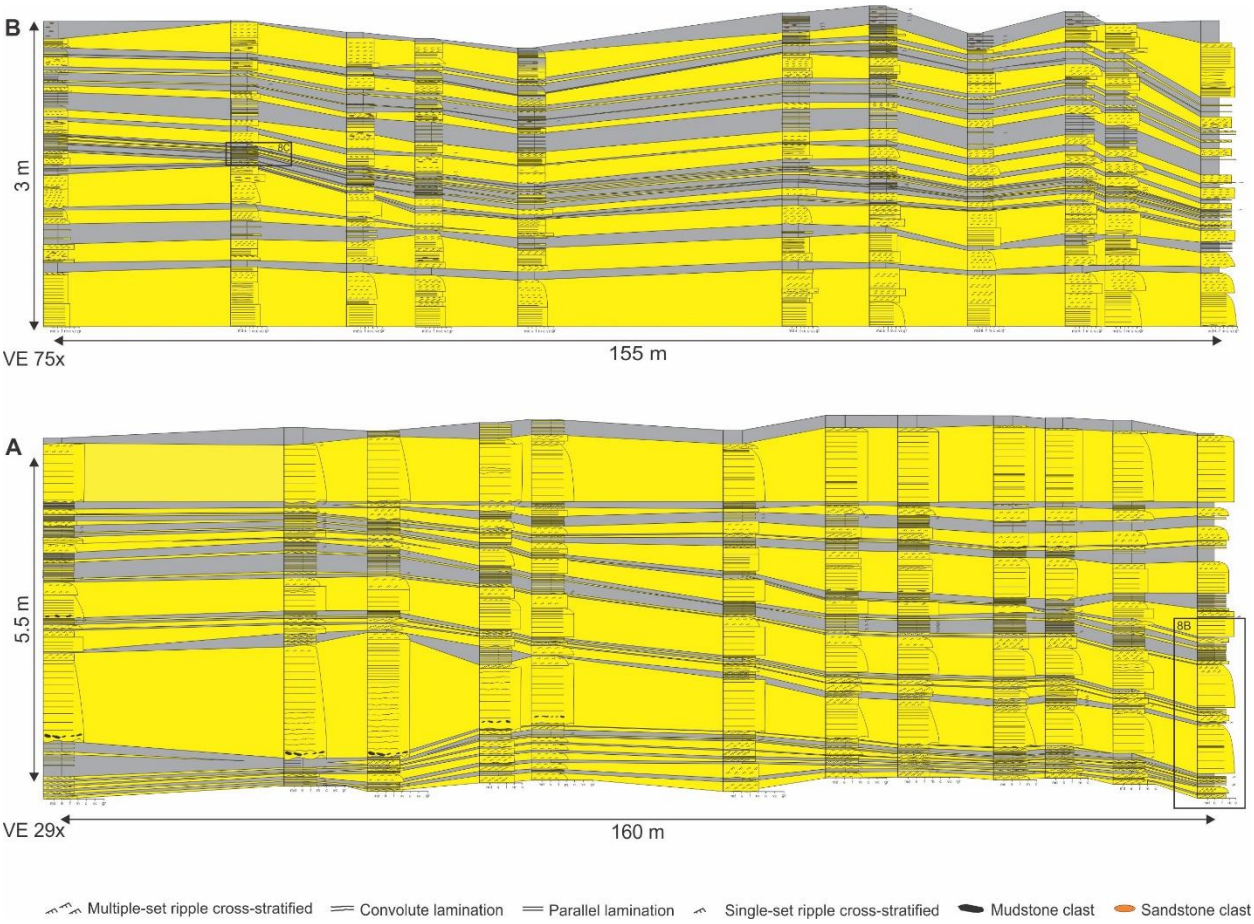

Figure 6.9. *Detailed measured sections spaced 5-20 m apart and correlation panels to document small-scale lateral changes in individual beds in the lower (A) and upper (B) parts of levee package 4 in the northern study area. Note that outcrop conditions allowed all beds to be continuously traced across the full width of the cross section or to their pinch-out. Refer to Fig. 2 part D for cross-section location and to Fig. 8 part A for close-up photograph of levee package 4.*

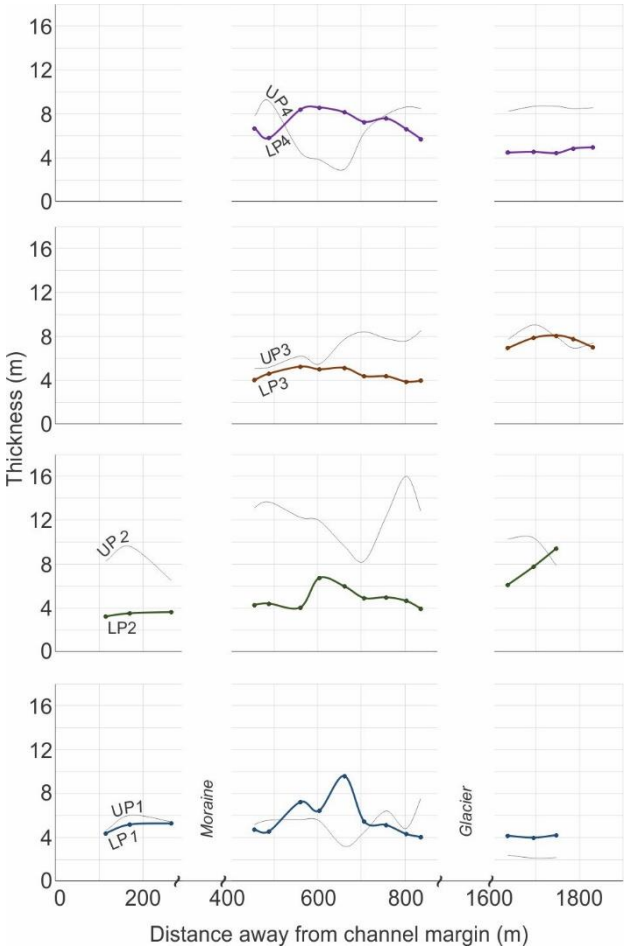

Figure 6.10. *Lateral thickness changes in the lower (colored) and upper (gray) parts of packages 1-4 across the full width of the study area. Locations of measured sections are indicated by dots. Medium- to thick-bedded, upper medium- to coarse-grained Tb and Tbc turbidites in the lower parts (LP) thicken over the first 560 - 660 m away from the channel margin and then thin over the next 175-275 m; collectively they control the thickness trends of the LPs. The upper parts (UP) thin and then thicken away from the channel margin, typically being thinnest where the lower package is thickest. Here it is the thickness of individual fine-grained, thin-bedded, multiple (3 - 4) set Tcde turbidites that collectively control the thickness trends of the UPs.*

6.5.2.2 Extrachannel Deposits Lacking Exposed Channel Deposits Description

The four packages of extrachannel deposits described above can be correlated across the glacier to the northern study area where they are exposed across a lateral distance of up to 190 m. Here they are not bounded on any side by channel deposits. The lower parts of packages consist of thick-bedded, very coarse- to coarse-grained Tbc turbidites intercalated with very thin-bedded, lower medium- to fine-grained Tc turbidites. The lower part of packages is 4 - 9 m thick and

changes little along strike, with the exception being the lower part of package 2, which thins by 3 m along a distance of 110 m towards the glacier (Fig. 6.10). Individual Tbc turbidites, on the other hand, do show lateral changes in thickness, with ~ 50% of them thinning towards the glacier (southeast) and the other 50% either thickening or showing no change in thickness. Some Tbc turbidites that thin also fine towards the glacier. Intercalated very thin-bedded, lower medium- to fine-grained Tcde turbidites show negligible along-strike change in thickness or grain size. The average sandstone to total lower package percentage remains about 82% across the width of the study area.

The upper parts of packages consist of very thin- and thin-bedded, fine-grained Tcde turbidites intercalated with uncommon medium- to thick-bedded, upper medium-grained Tbc turbidites. Thickness, which ranges from 2 to 10 m, and grain size changes little across the study area. Again, however, the exception is package 2, which thickens as its lower part thins towards the glacier (Fig. 6.10). As described above, it is the systematic change in the thickness of individual multiple-set Tcde turbidites that controls this trend. Average sandstone to total upper package percentage is 45 % and changes little laterally across the study area.

6.5.2.3 Vertical Trends of Extrachannel Deposits

As described and interpreted above, extrachannel deposits form four correlatable stratal packages that can be easily subdivided into lower and upper parts, the transition being sharp and marked by a dramatic decrease in bed thickness (Fig. 6.8D, E), grain size, and sandstone content (Fig. 6.8A). The lower part of packages is 3 - 10 m thick and consists mostly of medium- to thick-bedded, upper medium- to coarse-grained, lower-division turbidites intercalated with very thin- to thin-bedded, fine-grained, upper-division turbidites (Fig. 6.8B, 6.9). The upper parts of

packages are 2 - 16 m thick and consist mostly of very thin- to thin-bedded, fine-grained, upper division turbidites intercalated with medium- to thick-bedded, upper medium-grained, lower division turbidites (Fig. 6.8C, 6.9). Significantly, the thickness of very thin- and thin-bedded turbidites in the upper part typically decreases stratigraphically upward, whereas the thickness of intercalated medium- and thick-bedded turbidites changes little.

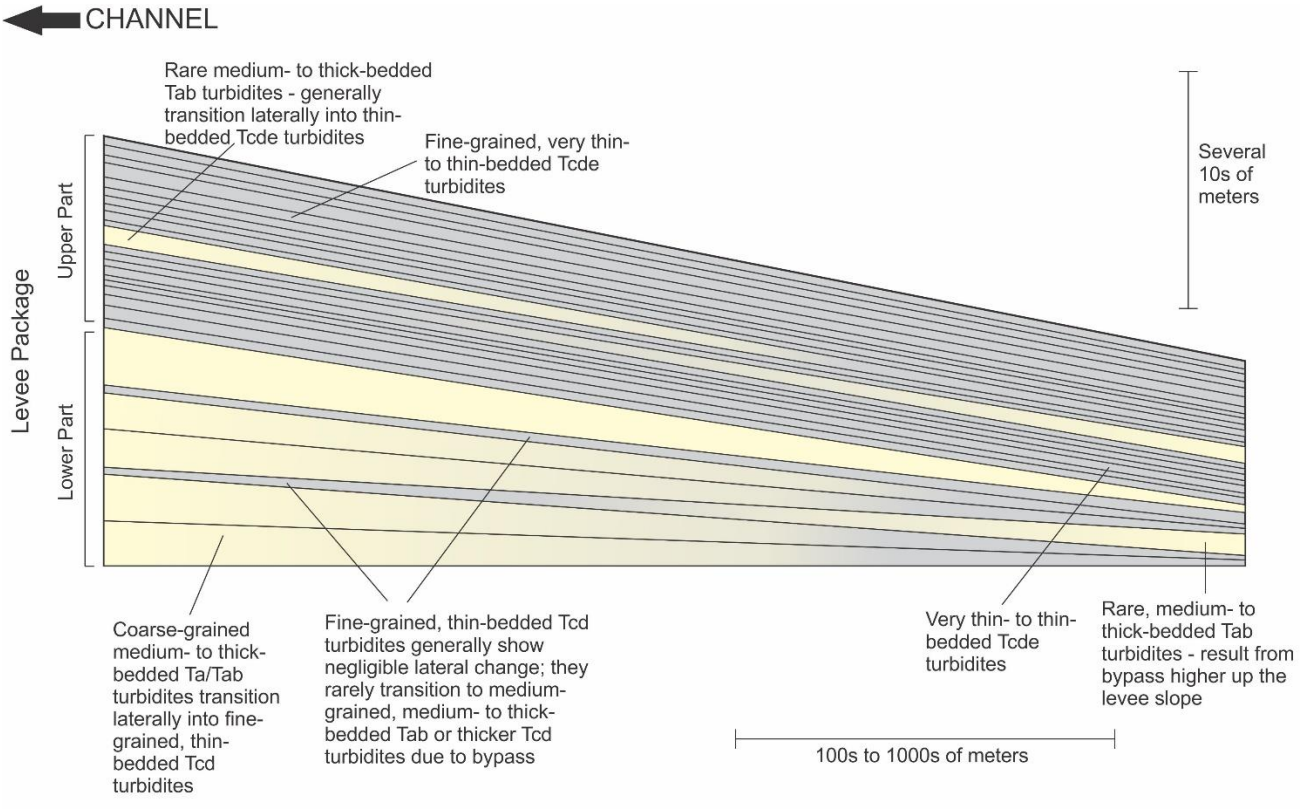

Figure 6.11. *Schematic illustrating the generalized vertical and lateral trends of individual beds in the lower and upper parts of a package beginning at the point of maximum thickness (~ 500 – 600 m from channel margin) and then extending along the direction of flow. Yellow represents sand, and gray is silt and mud.*

6.6 Discussion

6.6.1 Interpretation of Along-Strike Trends in Extrachannel Deposits

The progressive lateral transition over about 450 m (southeast to southern study areas) from coarse-grained Tade (Facies 1) turbidites to finer-grained Tbcde (Facies 2) turbidites in the lower part of packages suggests a rapid but progressive reduction in flow energy, and accordingly, transport capacity and competence. We interpret these extrachannel deposits to be levees based on the consistent and systematic lateral changes in facies and bed thickness from channel deposits that are interpreted to be genetically related, and the ubiquity of multiple-set (3 - 7) ripple cross-stratified sandstone, such as commonly reported from both modern (Hiscott et al. 1997; Piper and Deptuck 1997) and ancient (Walker 1985; King et al. 1994; Kane et al. 2007; Khan and Arnott 2011; Morris et al. 2014; Hansen et al. 2017) levee deposits. More importantly, the negligible angle of climb of multiple-stacked ripple cross-stratified sets requires flow conditions to be at speeds conducive to ripple inception, growth and migration, and to remain steady over a significant period of time. Flow conditions such as these are more reflective of the continuous overspill of the low-density upper parts of turbidity currents whose high-density, high-energy lower part remained confined to the adjacent channel. The absence of climbing-ripple cross-stratification observed in this study contrasts with observations in many other ancient levee deposits (see, e.g., Walker 1985; King et al. 1994; Browne and Slatt 2002; Eschard et al. 2003; Beaubouef 2004; Jobe et al. 2012; Hansen et al. 2017). Here it is interpreted that the rate of suspended-sediment fallout was never high enough to form ripples with detectable angles of climb.

The second important trend suggesting that these deposits are levees is the systematic along-strike changes in thickness of thick, coarse beds in the lower part of each package. Like

strata in the Rosario Formation, Mexico (Kane et al. 2007), and elsewhere at Castle Creek (Khan and Arnott 2011; Khan et al. 2011), beds in the lower parts of packages exhibit an initial thickening and then thinning away from adjacent channel deposits. To our knowledge, such trends have not been reported from channel deposits in the literature. However, they have been reported from strata interpreted to be levee deposits such as by Kane et al. (2007) and Khan and Arnott (2011); the latter attributing the initial thickening to particle settling lagging changes in flow conditions. More specifically, as flows overspilled the margins of the channel and slowed, particle inertia caused the location of maximum sedimentation rate to be displaced ~ 100 m outward from the channel margin (see also Baas et al. 2004). In the present study, coarse, thick beds in the lower parts of packages exhibit a similar thickening but along a distance of about 560 - 660 m, the greater distance possibly being a consequence of increased obliquity between the strike of the exposure relative to the orientation of the channel deposit margin. Beyond the zone of maximum sedimentation, flows became rapidly depleted of much of their coarse-grained sediment, and hence flow density, and began to wane. As a consequence, beds thinned and fined rapidly. With greater distance these flows then became dominated by more slowly settling particles that deposited thinner, finer-grained turbidites that changed character much more slowly thereafter (see also Khan and Arnott 2011).

Similar trends have been observed in Miocene basin-floor lobe deposits by Malgesini et al. (2015), and measured on horizontal scales of 10 - 40 km, which, therefore, are significantly greater than the several hundreds of meters to several kilometers length scales reported in levee deposits (Flood et al. 1991; Piper and Normark 2001; Browne and Slatt 2002; Skene et al. 2002; Pirmez and Imran 2003; Beaubouef 2004; Kane et al. 2007; Talling et al. 2007; Straub and Mohrig 2008; Khan and Arnott 2011; Hansen et al. 2017; Jobe et al. 2017). Levee packages as a

whole, therefore, typically thin exponentially away from the channel (Skene et al. 2002) and much of the change is attributed to thinning of the sandstone part of individual beds (Pirmez and Imran 2003; Straub and Mohrig 2008; Khan and Arnott 2011; Hansen et al. 2017). This is particularly true of the sand-rich turbidites that constitute much of the lower, proximal parts of levee units (Pirmez and Imran 2003; Straub and Mohrig 2008; Khan and Arnott 2011).

Unlike the lower parts of packages, strata in the upper parts show little along-strike change in character. These strata are interpreted to have been deposited as levee relief increased and only the upper, fine-grained part of currents typically overspilled while the lower, coarse-grained part remained confined to the channel (see vertical interpretation below). However, this does not imply that strata in the upper part of packages show no systematic along-strike change. In the well-exposed southern study area, the thickness of multiple (3 or 4) set Tcde turbidite beds thinned as the underlying lower part of the package thickened to its maximum, beyond which the Tcde turbidites then thickened as the lower part thinned (Fig. 6.10). Although the Tc part and overlying Tde caps of individual beds thicken and thin by only a few centimeters, collectively they act to level the underlying topography created by the thickening and thinning of the lower part of the package (see also Khan et al. 2011). Systematic lateral changes in the thickness of multiple-set Tcde turbidites indicate that as flows moved into topographic lows and expanded, sedimentation rates increased and deposited slightly thicker beds, whereas slightly thinner beds were deposited over topographical highs where flows accelerated.

The thickness and grain size of intercalated medium- and thick-bedded, medium-grained Tbcde turbidites gradually decrease across the study areas towards the northwest; these strata are interpreted to be overbank sheets deposited by uncommon, anomalously large flows whose depositional patterns appear to have been little affected by minor seafloor topography. As these

flows decelerated away from the channel margin, beds progressively fined and thinned as they lost their coarser sediment fraction and transitioned to Tcde turbidites. In contrast, rare fine-grained, very thin- and thin-bedded Tcde turbidites that thicken away from the channel deposit margin towards the northwest are interpreted to result from energetic flows that mostly bypassed the channel-proximal part of the levee. After several hundreds of meters the flows had slowed sufficiently to allow increased deposition and the development of tractional sedimentary structures. Like thick beds in the lower packages that thicken and then thin away from the channel-deposit margin, maximum sedimentation for these flows was displaced outward from the channel margin due to particle inertia and therefore occurred in the more channel-distal part of the levee. These flows are interpreted to be similar to the flows that deposited uncommon medium- to thick-bedded turbidites that thin away from the channel-deposit margin but were simply more dense (higher sediment concentration) and therefore higher velocity at the point of overspill, and so bypassed the innermost several hundreds of meters of the levee. Turbidites that thin away from the channel-deposit margin, on the other hand, were immediately depositional, indicating lower energy relative to those that thicken away from the channel.

6.6.2 Alternative Interpretations of Along-Strike Trends in Extrachannel Deposits

Due to the limitations of the outcrop, and the absence of beds that traverse the contact between the channel fill and adjacent strata, it is not possible to definitively prove that the overbank deposits described and interpreted here are levee deposits that are genetically related to the adjacent channel-fill deposits. The two-dimensional nature of the outcrop and the relative paucity of paleoflow data represent significant challenges in outcrop interpretation, despite the excellent exposure and extensive spatial scale. Because the genetic relationship between the

channel-fill deposits and the extrachannel deposits cannot be proven, alternative interpretations of these extrachannel deposits must be considered.

First, beds that thicken laterally away from the exposed margins of the channel-fill deposit might instead originate from an entirely different channel on the opposite side of the exposure, or they could simply reflect the infill of seafloor topography. However, the paleocurrent direction in these beds is oriented outward from the adjacent channel deposits and is therefore consistent with measurements in levee deposits elsewhere, precluding the possibility that they originated from an unexposed channel on the other side of the exposure. Additionally, the outcrop has been mapped continuously for ~ 2.5 kilometers laterally and evidence for topographical confinement was not observed. Moreover, the common lateral tapering of beds differs from their usual tabular nature in confined settings (e.g., Liu et al. 2018).

Second, if lateral changes in bed thickness were instead related to the infilling of seafloor accommodation, several mechanisms could account for the initial topography, the first of which being the development of sediment waves along the levee flank (e.g., Normark et al. 1980; Migeon 2000, 2001; Fildani et al. 2006). However, we expect that the topography created by this mechanism would be significantly greater than the thickness of individual beds, thereby requiring multiple overspill events to infill the (negative) seafloor topography. Additionally, strata that immediately overlie and underlie beds that thicken away from the channel deposits do not show similar changes in bed thickness, and therefore are not infilling accommodation, suggesting that this interpretation is unlikely.

Another possibility is that the lower, sand-rich part of these extrachannel packages are splay deposits overlain by finer, thinner-bedded levee deposits in the upper part of each package. There are several types of splay elements that form in deep-marine systems, including overbank

splays, avulsion splays, and frontal splays (e.g., Terlaky et al. 2016; Lowe et al. 2019; Navarro and Arnott 2020). Overbank and avulsion splays form on the slope where channelized turbidity currents escape confinement due to overspill or levee breaching, respectively (Grundvåg et al. 2014; Terlaky and Arnott 2014; Angus et al. 2019; Lowe et al. 2019). Frontal splays, also termed terminal lobes, form locally on the slope and more generally at the most down-dip depositional position on the basin floor (Fildani and Normark 2004; Prélat et al. 2009; Prélat et al. 2010; Terlaky et al. 2016; Lowe et al. 2019). Regardless of location, frontal and overbank splays are typically dominated by erosionally based, amalgamated, graded, structureless sandstone (i.e., Bouma Ta turbidites) beds that then fine, thin, and develop tractional sedimentary structures towards their margins. In contrast, strata described here are dominated by ripple cross-stratification, are markedly finer-grained than adjacent channel deposits against which they are truncated, and are interbedded with common thin to very thin, very fine-grained sandstone-mudstone. Avulsion splays, on the other hand, are dominated by distinctively matrix-rich strata (Terlaky and Arnott 2014; Angus et al. 2019; Ningthoujam et al. 2022), which are absent in the strata described here.

Notwithstanding these differences, we acknowledge that given the limitations of the outcrop some number of these alternative interpretations for the sand-rich lower packages cannot be completely discounted. Nevertheless, the abundance of beds composed of multiple-set ripple cross stratification, intercalation of thin, fine-grained beds, and absence of structureless or amalgamated sandstone would appear to be more consistent with deposition of sand-rich levees.

6.6.3 Interpretation of Vertical Trends in Extrachannel Deposits

Vertical trends in levee deposits are related to characteristics of the overspilling flows, including flow thickness, velocity, and vertical sediment-concentration profile, in addition to levee relief (i.e., distance from channel floor to levee crest) (Kane et al. 2007; Khan and Arnott 2011; Khan et al. 2011) and channel curvature (Morris et al. 2014). The vertical packaging observed in levee deposits of this study is interpreted to be related to recurring, systematic changes in these parameters.

Recent experimental work by de Leeuw et al. (2016, 2018) showed that as an initially unconfined turbidity current travels down a featureless slope it deposits two subparallel ridges between which the axis of the flow bypasses. Once initiated, the growth of levees necessitates spatial differences in sediment transport and deposition, specifically lower rates of deposition in the axis compared to the margins of the flow. The sharp contact at the bases of each package, overlain by coarse-grained turbidites, is interpreted to mark the base of the incipient levees (initial ridges) that formed during channel inception and helped to confine the axial parts of subsequent flows that travelled through the now better-defined channel (Fig. 6.12A). During Stage A, negligible levee relief allowed the lower, coarse-grained, dense part of flows to overtop the aggrading levees and deposit thick-bedded, coarse-grained, lower-division turbidites that built up most of the lower parts of packages (Fig. 6.12B). To consistently overspill such coarse sediment, the velocity maximum in the dense, lower parts of the average channelized flows was necessarily above the height of the aggrading levee crests. Intercalated thinner-bedded, finer-grained, upper-division turbidites reflect less energetic, smaller-magnitude channelized flows whose coarse basal part remained confined to the channel and only the upper, fine-grained part overspilled.

With time the levees continued to aggrade and conditions in the channel continued to be dominated by flow bypass with negligible net sedimentation. Eventually, confinement relief exceeded the height of the velocity maximum (de Leeuw et al. 2016), after which time only the upper, fine-grained parts of currents overspilled, while the lower, coarse-grained parts remained confined to the channel (Fig. 6.12C). The sharp contact between the lower and upper parts of each package is interpreted to mark this condition followed by deposition of mostly fine-grained, thin-bedded turbidites intercalated increasingly less commonly upward with thicker, coarser turbidites deposited by uncommon, anomalously large flows.

The velocity maximum, which is interpreted to control the vertical packaging of levee deposits, is more fundamentally controlled by the vertical density profile of the channelized flows. Experimental and theoretical work suggests that turbidity currents consist of two end-member vertical density profiles: 1) a plug-like structure where density changes little upward but then decreases sharply; and 2) a structure where density decreases continuously upward (Sequerios et al. 2010; Tilston et al. 2015; Kneller et al. 2016; Arnott et al. 2021) – note that these different profiles can occur in flows having similar depth-averaged density. One of the major differences between these two end members is the nature of the density structure in the region where the high-density lower part transitions to the lower-density upper part of the current, which principally is controlled by the ratio of the buoyancy flux (a measure of the resistance to mixing) to velocity shear forces (energy source for mixing), and captured in a Richardson gradient number (Ri) (Kneller et al. 2016; Tilston 2017):

$$Ri = -g'/\rho \cdot (\partial\rho/\partial z)/(\langle\langle (\partial u/\partial z) \rangle\rangle \text{^}2)$$

where ρ is the density, u is the velocity, z is height above the bed, and $g' = g(\rho_1 - \rho_2)/\rho$ is the reduced gravity. In the case of a plug-like structure, the sharp decrease in density at the top of the

high concentration basal layer (high $\partial\rho/\partial z$) stabilizes the interface and suppresses mixing, whereas mixing is promoted in flows with a continuous density profile. Another major difference is the height of the velocity maximum, which is elevated substantially above the bed in flows with a plug-like density structure, but is located very near the bed in flows with a continuous density profile (Sequeiros et al. 2010; Tilston et al. 2015; Kneller et al. 2016; Arnott et al. 2021). The contact between the lower and upper parts of each levee package is interpreted to approximate the height of the velocity maximum, which as noted above varies from 3 to 10 m above the base of the package (uncorrected for compaction and tectonic shortening). Such significant heights would most probably be consistent with flows exhibiting a plug-like density structure, and therein flows with suppressed energy consuming interfacial mixing, and as a consequence, maintenance of a dense, high-energy core (i.e., efficient flows; Fig. 6.12B). More notably, the sharp density interface that closely approximates the velocity maximum is also marked by a dramatic decrease in grain size and density of the sediment suspension. In the stratigraphic record, this would be manifested by a sharp decrease in grain size and bed thickness, which is consistent with the contact between the lower and upper parts of each levee package. Accordingly, once the height of the velocity maximum was exceeded by the height of the levee crest only the increasingly finer-grained sediment above the density interface overspilled from average channelized flows (Fig. 6.12C).

At some point during deposition of the upper part of each package, the makeup of the sediment supply changed, specifically becoming more poorly sorted. This allowed larger particles to preferentially settle and the throughgoing currents to become more vertically density stratified. Additionally, it depressed the height of the velocity maximum toward the bed (i.e., the base of the channel) and to an elevation now well below the height of the levee crest. The

progressive upward thinning of thin-bedded, upper-division turbidites in the upper parts of most packages is interpreted to reflect the depression of the velocity maximum and overspill of the even more dilute, fine-grained upper parts of the flows (Fig. 6.12D). Significantly, this density-stratified structure would have suppressed the upward diffusion of bed-generated turbulence (Cantero et al. 2011), which combined with near-bed sediment concentration effects (e.g., Bennett et al. 2014; Tilston et al. 2015) and extensive interfacial mixing, would have enhanced energy loss, and accordingly promoted deposition, at least locally, in the channel (Fig. 6.12D). These depositional conditions were then repeated with the formation of the next channel-levee package (Fig. 6.12E). This, then, suggests that it is ultimately the grain-size makeup of the sediment being supplied to the deep-sea transport system that controls the character of the channelized turbidity currents, which in turn controls the stratal architecture and timing of deposition on the levees, and later in the adjacent channel. Future work, therefore, should focus on identifying the fundamental driver(s) that controls the make up of the sediment supply.

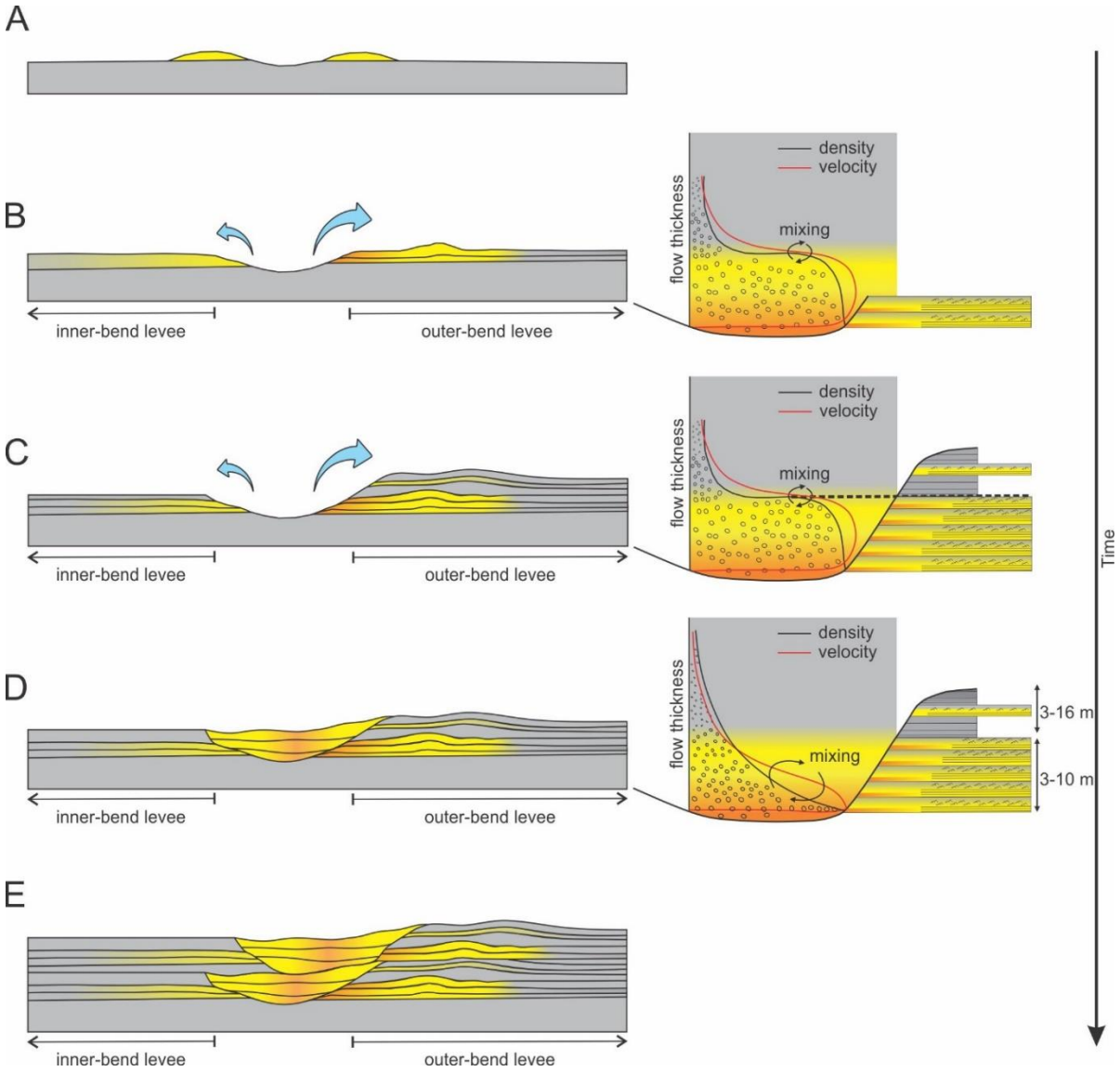

Figure 6.12. *Depositional model for the channel-levee packages observed in this study. A) Incipient conditions. Subparallel ridges deposited by initial turbidity currents form the base of each levee package. B) Coarse-grained and moderately well-sorted channelized flows have a plug-like density structure with negligible vertical stratification and high flow efficiency. The lower, coarse-grained, dense parts of channelized flows overspill the incipient levee ridges and deposit thick-bedded, coarse-grained, lower-division turbidites in the lower part of each package that thicken and then thin away from the channel margins. C) Transition where the relief between the channel floor and the levee crest exceeds the height of the velocity maximum of the average channelized flows. After this transition, which is marked by a sharp contact between the lower and upper parts of a package, only the upper, fine-grained parts of currents overspill while the lower, coarse-grained parts remain confined to the channel. D) A change in the sediment supply results in more poorly sorted, vertically density-stratified channelized flows. The height of the velocity maximum is depressed toward the bed to an elevation well below the height of the levee crest. This is reflected by the progressive upward thinning of thin-bedded, upper-division turbidites in the upper parts of packages. The highly stratified density structure of channelized flows enhances energy loss and promotes deposition in the channel. E) Repetition of the depositional conditions described in parts A-D result in the formation of the next channel-levee package. Refer to Fig. 2C for the location of the "thicker bumps" in outcrop.*

6.6.4 Comparison with Other Systems

Careful comparison between levee deposits of the Isaac Formation and other deep-marine levee systems, both modern and ancient, may provide further insight into the role that the grain-size makeup of the sediment supply plays in levee formation and development. Various characteristics of 12 levee systems (4 modern, 8 ancient) are presented in Table 2. The Amazon fan, as mentioned previously, is similar in scale and tectonic setting to the Windermere, and as such may be a particularly useful analogue. However, levee deposits in the Amazon are significantly wider than those in the Windermere (Damuth et al. 1988; Flood and Piper 1997; Piper and Deptuck 1997; Pirmez and Imran 2003), which might be a consequence of their finer grain size and the inverse relationship between levee width and grain size (e.g., Nakajima and Kneller 2013, Hansen et al. 2015). In terms of thickness, levee deposits in the modern Amazon, like in the Congo and Indus systems, are silt dominated and hundreds of meters thick (Von Rad and Tahir 1997; Babonneau et al. 2002, 2010; Droz et al. 2003), and therefore dramatically thicker than their generally coarser-grained counterparts in the Windermere, even when obvious differences related to physical, chemical, and tectonic compaction are considered (e.g., Khan et al. 2011) (Fig. 6.13).

Another possible contributor to the thickness disparity may be the grain-size makeup of the channelized flows that built up the levees. In systems like the Amazon, the dominance of easily suspended silt with only a minor coarse-grained component may create much thicker, basally plug-like (see above) flows where the velocity maximum (Umax) is positioned substantially higher above the bed compared to flows with a more sizable coarse-grained fraction (Tilston et al. 2015). Overspill from the higher-density lower part of the channelized flow below

Umax would elevate the rate of sedimentation, and in turn, upbuilding of the adjacent levee and levee crest, which in the case of silt-dominated flows with negligible coarse sediment may be several tens of meters above the channel base. Eventually levee growth would exceed the height of Umax, and thereafter, like all other systems, levee growth would proceed at a lower rate from the more dilute upper part of the channelized flow, which in silt-dominated systems would consist of texturally, and therefore acoustically, similar sediment.

Alternatively, the difference in thickness may be related to differences in data acquisition and image resolution of stratal characteristics. Most modern systems are studied using seismic and sonar, with at best widely spaced core control, and due to only minor differences in texture and/or composition in the sedimentary pile, are generally unable to resolve bed-scale changes in lithology, as is possible in outcrop, especially coarser-grained strata. Based on characteristics like abundance of ripple cross-stratification (particularly climbing ripples), mapping contacts to their associated channels, and consistent and systematic lateral changes in facies and bed geometry, several studies in coarser-grained outcrops have identified multiple levee units or packages that generally are of the order of several decameters thick and associated with individual channel fills (e.g., Browne and Slatt 2004; Beaubouef 2004; Pyles et al. 2010; Khan et al. 2011; Hansen et al. 2017; Cochrane et al. 2019). Therefore, due to their more uniform texture, seismic and sonar data sets from finer-grained modern systems may lack the bed-scale resolution necessary to differentiate individual levee packages, and therefore cause those levees to appear to be thicker than their coarser-grained ancient counterparts.

Moreover, the sharp-based, well-defined packages observed in this study are interpreted to be a consequence of systematic temporal changes in the grain-size makeup of the sediment supply. These changes, in turn controlled the density structure of the channelized flows, and

ultimately the observed facies and stratal architecture in adjacent levee deposits. In silt-dominated systems, like the modern Amazon, Bengal, Congo, and Indus, it is likely that there is an insufficient range and/or abundance of different grain sizes, especially sand and coarser sediment, in the sediment supply to alter the density structure of the flows and create recognizable packaging. Nevertheless, it is important to note that the distinctive two-part levee packages described here from the Windermere Supergroup have not been reported from similarly coarse levee deposits in other turbidite systems from the rock record. Although further work is needed to investigate this, it is possible that this apparent disparity is related to differences in tectonic setting.

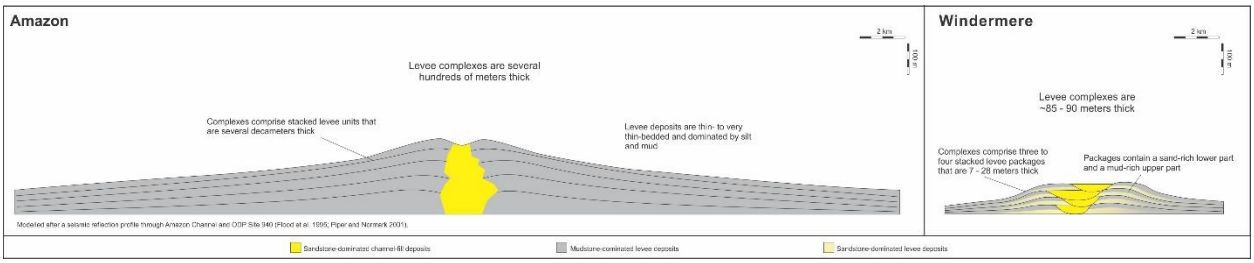

Figure 6.13*. Comparison of levee morphology and composition in the Amazon Fan and the Windermere Fan systems. Yellow represents sand, and gray represents silt and mud. Levees in the Amazon are thicker, wider, and finer-grained than those in the Windermere, and lack the distinctive two-part packages described here.*

Many ancient systems described in the sedimentological literature were deposited in tectonically active basins, for example the Marnosa-Arenacea (Italy -- Mosca and Stefano 1993; Malgesini et al. 2015), Annot Sandstone (France -- Clark and Gardiner 2000; Clark and Stanbrook 2001), Cerro Toro (Chile -- Beaubouef 2004), Rosaria Fm (Mexico -- Kane et al. 2007; Kane and Hodgson 2011; Hansen et al. 2017), Brushy Canyon Fm (Texas -- Beaubouef et al. 2007; Pyles et al. 2010), Kirkgecit Fm (Turkey -- Cronin et al. 2000; Cronin et al. 2007), and Himalia Ridge Fm (Antarctica -- Butterworth and MacDonald 2000), whereas the Windermere

was deposited along a passive continental margin that, at least occasionally, would have had a wide continental shelf, with changes in shelf accommodation controlled principally by eustasy. The observed recurring changes in sediment supply to the deep marine Isaac Formation may be a result of processes unique to this tectonic setting, or more specifically the presence of a continental shelf (i.e., topset), and its influence on the grain-size distribution (i.e., sorting and grain-size makeup) in the sediment supply, and this is a possible explanation for their apparent absence in other systems.

Name	Age	Basin Type	Levee Thickness	Bed Thickness	Levee Grain Size Range	Channel Grain Size Range	# of Levee Units	Levee Width	Nature of Contact with Channel	Ripple Type	Data Source	Relevant Papers
Isaac Fm, Canada (Channel 4)	Neoproterozoic	Passive margin	~ 7 – 25 m	0.5 – 326 cm (majority are 3 – 30 cm)	Very fine – medium sand	Medium sand – pebble conglomerate	4	≥ 2500 m	Channel-fills onlap adjacent levee deposits and post-date levee deposition	Multi-set transition to single-set and starved with increasing distance from channel	Outcrop	This study Cunningham & Arnott (2021)
Isaac Fm, Canada (Channel 3)	Neoproterozoic	Passive margin	12 – 28 m	0.5 – 150 cm (majority are 5 – 15 cm)	Very fine – medium sand	Coarse sand to pebble conglomerate	3	≥ 2500 m	Channel-fills onlap adjacent levee deposits and post-date levee deposition	Multi-set transition to single-set and starved with increasing distance from channel	Outcrop	Navarro et al. 2007 Khan & Arnott 2011 Khan et al. 2011 Cunningham & Arnott (2021)
Isaac Fm, Canada (Channel 2)	Neoproterozoic	Passive margin	~ 3 – > 60 m	1 – 141 cm (average 10 cm)	Very fine – medium sand	Coarse to very coarse sand	4	≥ 2500 m	Channel-fills onlap adjacent levee deposits and post-date levee deposition	Multi-set transition to single-set and starved with increasing distance from channel	Outcrop	Cochrane et al. 2019
Brushy Canyon Fm, Texas	Permian	Intracratonic	~10 m	Avg. 10 cm	Very fine – fine sand	Fine – medium sand to conglomerate	2	1000 – 2000 m	Channel point bars onlap levee deposits	---	Outcrop	Beaubouef et al. 2007 Pyles et al. 2010
Fort Brown Fm, South Africa	Permian	Foreland	30 – 80 m	Proximal sand beds: 20 – 50 cm; distal sand beds: < 10 cm	Medium silt – fine sand	Fine sand	---	10,000 m	Erosional	Climbing transition to single-set and starved with increasing distance from channel	Outcrop	Morris et al. 2014 Figueirdo et al. 2010 Hodgson et al. 2011 Kane & Hodgson 2011 Brunt et al. 2013
Skoorsteenberg Fm, South Africa	Permian	Foreland	---	---	Fine sand	---	---	350 m	Commonly erosional	Climbing	Outcrop	Bouma et al. 2007
Himalia Ridge Fm, Antarctica	Jurassic - Cretaceous	Forearc	40 – 45 m	0.5 – 2 cm	Fine sand	Pebbly sandstone (medium - coarse sand) and conglomerate	---	3000 m	---	Starved and single-set	Outcrop	Butterworth & MacDonald 2007
Cerro Toro Fm, Chile	Cretaceous	Extensional back-arc	30 – 60 m	Tens of cm in proximal region, cm in distal	Fine sand, some medium sand	Pebble – cobble conglomerate, some fine – very coarse sandstone	5	1000 – 1500 m	Channel-fill onlaps levee deposits	Multi-set	Outcrop	Beaubouef 2004
Rosaria Fm, Mexico	Cretaceous	Forearc	100 m (total)	Proximal sand beds: 5 – 20 cm; distal sand beds: avg. 1.5 cm, max 5 cm	Fine sand	Fine – medium sand and pebble – boulder conglomerate	---	2500 m (external) 1000 m (internal)	Channel fills onlap confining levees	Climbing transition to single-set and starved with increasing distance from channel	Outcrop	Kane et al. 2007 Kane & Hodgson 2011 Hansen et al. 2017
Kirkgecit Fm, Turkey	Eocene - Oligocene	Backarc	~ 40 m	0.5 – 4 cm, avg. 0.5 cm	Medium sand	Coarse sand – boulders	---	> 120 m	Channel-fill onlaps adjacent levee deposits and post-dates levee deposition	---	Outcrop	Cronin et al. 2000, Cronin et al. 2007
Mt. Messenger Fm, New Zealand	Miocene	---	~ 10 m	5 – 50 cm	Very fine – fine sand	Medium sand – boulder conglomerate	9	> several 100s of meters	Erosional	Climbing	Outcrop, core	Browne & Slatt 2002
Amazon Channel	Modern	Passive margin	Hundreds of meters	1 – 10 cm, mostly 1 – 3 cm	Very fine silt – very fine sand, mostly silt	Dominantly very fine – medium sand, rare coarse – very coarse sand	~ 20	7000 m	Levees aggrading above active open channels	Starved silt	Seismic, sonar, core	Piper & Deptuck 1997 Damuth et al. 1988 Pirmez & Imran 2003 Flood & Piper 1997 Hiscott et al. 1997 Manley et al. 1997
Bengal Fan	Modern	---	~ 70 m	5 – 40 cm	Medium – coarse silt	Silt, rare very fine - fine sand	---	5000 m	Levees aggrading above active open channels	---	Seismic, sonar, core	Huebscher et al. 1997 Weber et al. 2003 Schwenke et al. 2003 Schwenke et al. 2005
Congo Channel	Modern	Passive margin	250 m	Several cm	Medium silt – very fine sand (dominated by silt)	Fine – medium sand	---	4000 – 25,000 m	Levees aggrading above active open channels	---	Seismic, sonar, core	Babonneau et al. 2002 Babonneau et al. 2010 Droz et al. 2003
Indus Channel	Modern	Foreland	200 m	---	Medium silt – very fine sand	---	---	3000 – 5000 m	Levees aggrading above active open channels	---	Seismic, sonar, core	Von Rad & Tahir, 1997

Table 6.2. *General dimensional and lithological characteristics of modern and ancient levee and associated channel deposits.*

6.7 Conclusions

In this study extrachannel strata interpreted to be levee deposits are divided vertically into four stratal packages. Packages range in thickness from 5 to 20 m and consist of a sand-rich lower part overlain sharply by a mud-rich upper part. The lower part ranges from 3 to 10 m thick and consists mostly of medium- to thick-bedded, upper medium- to coarse-grained, lower-division turbidites intercalated with thin-bedded, fine-grained, upper-division turbidites. Along strike away from the channel deposit margins the thickness of lower division turbidites exhibit a distinctive thickening and then thinning over a few hundreds of meters that results in a similar thickening and thinning of the entire lower part of a package.

The upper parts of packages range from 3 to 16 m thick and consists mostly of thin-bedded, fine-grained, upper-division turbidites intercalated with uncommon medium- to thick-bedded, upper medium-grained, lower-division turbidites. Significantly, the thickness of very thin- and thin-bedded turbidites in the upper part generally decreases stratigraphically upward, whereas the thickness of intercalated medium- and thick-bedded turbidites changes little. Along strike the upper parts of packages thin as the underlying lower parts of the package thicken, and then thicken as the lower parts thin, which acts to level or “heal” the underlying topography. Changes in the thickness of the upper part is a result of variations in the thickness of the ripple cross-stratified part of individual multiple-set Tcde turbidite beds; thickness of the capping Tde layer changes little. Intercalated very thin- to thin-bedded single-set Tcde turbidites in both the lower and upper parts of packages show little or at most slight thinning and fining over along-strike distances of hundreds of meters. In contrast, uncommon medium- and thick-bedded,

lower-division turbidites in the upper part of a package thin and transform into thin- and very thin-bedded upper-division turbidites over distances of several hundreds of meters away from the channel.

The lower part of each levee package is interpreted to represent incipient levee formation and growth that results from continuous overspill of coarse-grained turbidity currents with a plug-like density structure and velocity maximum positioned well above the height of the aggrading levee crest. The thickening and then thinning trend away from the channel-deposit margin is the manifestation of flow inertia and the lag between sedimentation rate and reduction in flow speed. Beyond the zone of maximum sedimentation flows continue to wane, and with lower rates of sedimentation, deposit thinner, finer-grained turbidites that cause a general thinning of the lower parts of packages. The sharp contact between the lower and upper packages marks the point at which relief between the levee crest and channel floor exceeded the height of the velocity maximum of average flows, after which only the uppermost, fine-grained parts of flows could overspill. During deposition of the upper part of each package, changes in the grain-size makeup of the sediment supply caused flows in the adjacent channel to develop a more density-stratified structure. This, in turn, reduced flow efficiency that stratigraphically is marked by a change from conditions of general transport bypass to net in-channel deposition. The changes in granulometric make up of sediment may be related to processes unique to passive-margin continental systems, or more specifically the continental shelf, and therefore account for their apparent absence in other ancient systems.

This study provides another case example to further our understanding of the lithological characteristics and physical origin of the spatial and temporal evolution of levee sedimentation. Future research could attempt to provide a more detailed understanding of deposition associated

with single and successive flow events by further investigating and comparing sedimentological characteristics and stacking patterns of the individual thin-bedded turbidites that dominate levee deposits in outcrop and core, as well as to explore the nature and cause of repetitive changes in sediment supply that govern the depositional trends observed here.

6.7 References

ABREU, V., SULLIVAN M., PIRMEZ C., MOHRIG D., AND MUTTI E., 2003, Lateral accretion packages (LAPs); an important reservoir element in deep water sinuous channels: Marine and Petroleum Geology, v. 20, p. 631–648. https://doi.org/10.1016/j.marpetgeo.2003.08.003

ANGUS, K., ARNOTT, R.W.C., AND TERLAKY, V., 2019, Lateral and vertical juxtaposition of matrix-rich and matrix-poor lithologies caused by particle settling in mixed mud-sand deep-marine sediment suspensions: Sedimentology, v. 66, p. 940-962. https://doi.org/10.1111/sed.12523

ARNOTT, R.W.C., TILSTON, M., FRAINO, P., NAVARRO, L., DUMOUCHEL, G., AND MIKLOVICH, N., 2021, Laterally-accreting sinuous channels and their deposits – the Goldilocks of deep-water slope systems: Journal of Sedimentary Research, v. 91, p. 451-463. doi: 10.2110/jsr.2020.144

BAIN, H.A., AND HUBBARD S.M., 2016, Stratigraphic evolution of a long-lived submarine channel system in the Late Cretaceous Nanaimo Group, British Columbia, Canada: Sedimentary Geology, v. 337, p. 113-132. https://doi.org/10.1016/j.sedgeo.2016.03.010.

BAAS, J.H., VAN KESTEREN, W., AND POSTMA, G., 2004, Deposits of depletive high-density turbidity currents: a flume analogue of bed geometry, structure and texture: Sedimentology, v. 51, p. 1053-1088. https://doi.org/10.1111/j.13653091.2004.00660.x.

BABONNEAU, N., SAVOYE, B., CREMER, M., AND KLEIN, B., 2002, Morphology and architecture of the present canyon and channel system of the Zaire deep-sea fan: Marine and Petroleum Geology, v. 19(4), p. 445-467.

BABONNEAU, N., SAVOYE, B., CREMER, M., AND BEZ, M., 2010, Sedimentary architecture in meanders of a submarine channel: detailed study of the present Congo turbidite channel (ZaiAngo project): Journal of Sedimentary Research, v. 80(10), p. 852-866.

BEAUBOUEF, R.T., 2004, Deep-water leveed-channel complexes of the Cerro Toro Formation, upper Cretaceous, southern Chile: American Association of Petroleum Geologists, Bulletin, v. 88, p. 1471–1500.

BEAUBOUEF, R.T., ROSSEN, C., AND LOVELL, R.W.W., 2007, The Beacon Channel: a newly recognized architectural type in the Brushy Canyon Formation, Texas, USA, in

Nilsen, T., Shew, R., Steffens, G., and Studlick, J., (eds.), Atlas of Deep-Water Outcrops: American Association of Petroleum Geologists, Studies in Geology, v. 56, p. 432-443

BENNETT, S.J., HOU, Y., AND ATKINSON, J.F., 2014, Turbulence suppression by suspended sediment within a geophysical flow: Environmental Fluid Mechanics, v. 14, p. 771-794. https://doi.org/10.1007/s10652-013-9323-2

BOUMA, A.H., DELERY, A.M., AND SCOTT, E.D., 2007, Introduction to deep-water deposits of the Tanqua Karoo, South Africa in Nilsen, T., Shew, R., Steffens, G., and Studlick, J., (eds.), Atlas of Deep-Water Outcrops: American Association of Petroleum Geologists, Studies in Geology, v. 56, p. 302-304.

BROWNE, G.H., AND R.M. SLATT, 2002, Outcrop and behind-outcrop characterization of a late Miocene slope fan system, Mt. Messenger Formation, New Zealand: American Association of Petroleum Geologists, Bulletin,v. 86, p. 841–862. https://doi.org/10.1306/61EEDBB6-173E-11D7-8645000102C1865D

BRUNT, R.L., DI CELMA, C.N., HODGSON, D.M., FLINT, S.S., KAVANAGH, J.P., AND VAN DER MERWE, W.C., 2013, Driving a channel through a levee when the levee is high: An outcrop example of submarine down-dip entrenchment: Marine and Petroleum Geology, v. 41, p. 134-145.

BUFFINGTON E.C., 1952, Submarine natural levees: Journal of Geology, v. 60, p. 473–479. https://doi.org/10.1086/625999

BUTTERWORTH, P.J., AND MACDONALD, D.I., 2007, Channel-levee Complexes of the Fossil Bluff Group, Alexander Island, Antarctica, in Nilsen, T., Shew, R., Steffens, G., and Studlick, J., (eds.), Atlas of Deep-Water Outcrops, Association of Petroleum Geologists, Studies in Geology, v. 56, p. 36-41

CANTERO, M.I., CANTELLI, A., PIRMEZ, C., BALACHANDAR, S., MOHRIG, D., HICKSON, T.A., YEH, T., NARUSE, H., AND PARKER, G., 2011, Emplacement of massive turbidites linked to extinction of turbulence in turbidity currents: Nature Geoscience, v. 5, p. 42–45. https://doi.org/10.1038/ngeo1320.

CAZANACLI, D., AND SMITH, N.D., 1998, A study of morphology and texture of natural levees; Cumberland Marshes, Saskatchewan, Canada: Geomorphology, v. 25, p. 43-55.

CLARK, J.D. AND GARDINER, A.R., 2000, Outcrop analogues for deep-water channel and levee genetic units from the Grès d'Annot turbidite system, SE France, in Weimer, P., Slatt, R.M., Coleman, J., Rosen, N.C., Nelson, H., Bouma, A.H., Styzen, M.J., and Lawrence, D.T., (eds.), Deep-Water Reservoirs of the World: Gulf Coast Section of the Society for Sedimentary Geology (GCSSEPM) Foundation 20th Annual Research Conference, p. 175 – 190.

CLARK, J.D., AND PICKERING, K.T., 1996, Architectural elements and growth patterns of submarine channels: application to hydrocarbon exploration: American Association of Petroleum Geologists, Bulletin, v. 80, p. 194-220.

Clark, J.D., and Stanbrook, D.A., 2001, Formation of large-scale shear structures during deposition from high-density turbidity currents, Grès d'Annot Formation, South-East France, in Clark, J.D., Stanbrook, D.A., McCaffrey, W., Kneller, B., and Peakall, J., Particulate Gravity Currents: Blackwell Publishing Ltd, 2001, pp. 217–232. https://doi.org/10.1002/9781444304275.ch16.

CLEMENCEAU, G.R., COLBERT J., AND EDENS D., 2000, Production results from levee-overbank turbidite sands at Ram/Powell Field, deepwater Gulf of Mexico, in Weimer, P., Slatt, R.M., Coleman, J., Rosen, N.C., Nelson, H., Bouma, A.H., Styzen, M.J., and Lawrence, D.T., eds., Deep-Water Reservoirs of the World: Gulf Coast Section of the Society for Sedimentary Geology (GCSSEPM) Foundation 20th Annual Research Conference, p. 241-251.

COCHRANE, D. J., NAVARRO, L., AND ARNOTT, R. W. C., 2019, Sedimentological and geochemical evolution of an Ediacaran mixed carbonate-siliciclastic continental slope system, Windermere Supergroup, southern Canadian Cordillera, British Columbia, Canada: Precambrian Research, v. 327, p. 47-67.

COLPRON, M., LOGAN, J.M., AND MORTENSEN, J.K., 2002, U-Pb zircon age constraint for late Neoproterozoic rifting and initiation of the lower Paleozoic passive margin of western Laurentia: Canadian Journal of Earth Sciences, v. 39, p. 133-143. https://doi.org/10.1139/e01-069.

CRONIN, B.T., HURST, A., CELIK, H., AND TURKMEN, I., 2000, Superb exposure of a channel, levee and overbank complex in an ancient deep-water slope environment: Sedimentary Geology, v. 132, p. 205–216.

CRONIN, B.T., ÇELIK, H., HURST, A., GUL, M., GÜRBÜZ, K., MAZZINI, A., AND OVERSTOLZ, M., 2007, Slope-channel complex fill and overbank architecture, Tinker Channel, Kirkgecit Formation, Turkey, in Nilsen, T., Shew, R., Steffens, G., and Studlick, J., (eds.), Atlas of Deep-Water Outcrops: Association of Petroleum Geologists, Studies in Geology, v. 56, p. 363-367.

CUNNINGHAM, C.M., AND ARNOTT, R.W.C., 2021, Systematic organization of thin-bedded turbidites in ancient deep-marine levees: Possible evidence of rhythmic pulsing in turbidity currents: Journal of Sedimentary Research, v. 91(11), p. 1257-1274. http://doi.org/10.2110/jsr.2020.003.

DAMUTH, J.E., FLOOD, R.D., KOWSMANN, R.O., BELDERSON, R.H., AND GORINI, M.A., 1988, Anatomy and growth pattern of Amazon deep-sea fan as revealed by long-range side-scan sonar (GLORIA) and high-resolution seismic studies: American

Association of Petroleum Geologists, Bulletin, v. 72, p. 885-911. https://doi.org/10.1306/703C9109-1707-11D7-8645000102C1865D

DE LEEUW, J., EGGENHUISEN, J.T., AND CARTIGNY, M.J., 2016, Morphodynamics of submarine channel inception revealed by new experimental approach: Nature Communications, v. 7, p. 1-7. https://doi.org/10.1038/ncomms10886.

DE LEEUW, J., EGGENHUISEN, J.T., AND CARTIGNY, M.J., 2018, Linking submarine channel–levee facies and architecture to flow structure of turbidity currents: insights from flume tank experiments: Sedimentology, v. 65, p. 931-951. https://doi.org/10.1111/sed.12411.

DEPTUCK, M.E., STEFFENS, G.S., BARTON, M., AND PIRMEZ, C., 2003, Architecture and evolution of upper fan channel-belts on the Niger Delta slope and in the Arabian Sea: Marine and Petroleum Geology, v. 20, p. 649-676. https://doi:10.1016/j.marpetgeo.2003.01.004.

DROZ, L., MARSSET, T., ONDREAS, H., LOPEZ, M., SAVOYE, B., AND SPY-ANDERSON, F. L., 2003, Architecture of an active mud-rich turbidite system: The Zaire Fan (Congo–Angola margin southeast Atlantic) Results from ZaïAngo 1 and 2 cruises: American Association of Petroleum Geologists, Bulletin, v. 87(7), p. 1145-1168.

DUMOUCHEL, I.G., 2015, Stratigraphic Architecture and Depositional History of laterally-accreted channel fills in the Lower Isaac Formation, Windermere Supergroup, British Columbia, Canada, [M.Sc. Thesis]: University of Ottawa, Ottawa, 108 p.

ELLIOTT, T., 2000, Megaflute erosion surfaces and the initiation of turbidite channels: Geology, v. 28, p. 199-122.

EGGENHUISEN, J.T., MCCAFFREY, W.D., HAUGHTON, P.D.W., AND BUTLER, R.W.H., 2011, Shallow erosion beneath turbidity currents and its impact on the architectural development of turbidite sheet system: Sedimentology, v. 58, p. 936-959.

ENGLERT, R.G., HUBBARD, S.M., COUTTS, D.S., AND MATTHEWS, W.A., 2018, Tectonically controlled initiation of contemporaneous deep-water channel systems along a Late Cretaceous continental margin, western British Columbia, Canada: Sedimentology, v. 65, p. 2404-2438. https://doi.org/10.1111/sed.12472.

ESCHARD, R., ALBOUY, E., DESCHAMPS, R., EUZEN, T., AND AYUB, A., 2003, Downstream evolution of turbiditic channel complexes in the Pab Range outcrops; Maastrichtian, Pakistan: Marine and Petroleum Geology, v. 20, p. 691–710. https://doi.org/10.1016/j.marpetgeo.2003.02.004

EVENCHICK, C.A., PARRISH, R.R., AND GABRIELSE, H., 1984, Precambrian gneiss and late Proterozoic sedimentation in north-central British Columbia: Geology, v. 12, p. 233-237. https://doi.org/10.1130/0091-7613(1984)12<233:PGALPS>2.0.CO;2

EYSTER, A., FERRI, F., SCHMITZ, M.D., AND MACDONALD, F.A., 2018, One diamictite and two rifts: stratigraphy and geochronology of the Gataga Mountain of northern British Columbia: American Journal of Science, v. 318, p. 167-207. https://doi.org/10.1139/cjes-2019-0188

FIGUEIREDO, J. J., HODGSON, D. M., FLINT, S. S., AND KAVANAGH, J. P., 2010, Depositional environments and sequence stratigraphy of an exhumed Permian mudstone-dominated submarine slope succession, Karoo Basin, South Africa: Journal of Sedimentary Research, v. 80(1), p. 97-118.

FILDANI, A., AND NORMARK, W.R., 2004, Late Quaternary evolution of channel and lobe complexes of Monterey Fan: Marine Geology, v. 206, p. 199-223.

FILDANI, A., NORMARK, W., KOSTIC, S., AND PARKER, G., 2006, Channel formation by flow stripping: large-scale scour features along the Monterey East Channel and their relation to sediment waves: Sedimentology, v. 53, p. 1265-1287.

FILDANI, A., HUBBARD, S.M., COVAULT, J.A., MAIER, K.L., HUBBARD, B.W., TRAER, M., AND ROWLAND, J.C., 2013, Erosion at inception of deep-sea channels: Marine and Petroleum Geology, v. 41, p. 48-61.

FLOOD, R.D., MANLEY, P.L., KOWSMANN, R.O., APPI, C.J., AND PIRMEZ, C., 1991, Seismic facies and late Quaternary growth of Amazon submarine fan, in Weimer P., and Link M.H., (eds.), Seismic Facies and Sedimentary Processes of Submarine Fans and Turbidite Systems: Springer, New York, NY, p. 415-433. https://doi.org/10.1007/978-1-4684-8276-8_23

FLOOD, R.D., AND PIPER, D.J., 1997, Amazon Fan sedimentation: the relationship to equatorial climate change, continental denudation, and sea-level fluctuations, in Proceedings Ocean Drilling Program Scientific Results, National Science Foundation, p. 653-675.

GRUNDVÅG, S., JOHANNESSEN, E. P., HELLAND-HANSEN, W., AND PLINK-BJÖRKLUND, P., 2014, Depositional architecture and evolution of progradationally stacked lobe complexes in the Eocene Central Basin of Spitsbergen: Sedimentology, v. 62, p. 535-569.

HANSEN, L.A., CALLOW, R.H., KANE, I.A., GAMBERI, F., ROVERE, M., CRONIN, B.T., AND KNELLER, B. C., 2015, Genesis and character of thin-bedded turbidites associated with submarine channels: Marine and Petroleum Geology, v. 67, p. 852-879.

HANSEN, L., CALLOW, R., KANE, I., AND KNELLER, B., 2017, Differentiating submarine channel related thin-bedded turbidite facies: outcrop examples from the Rosario Formation, Mexico: Sedimentary Geology, v. 358, p. 19-34. https://doi.org/10.1016/j.sedgeo.2017.06.009.

HAY, A.E., 1987a, Turbidity currents and submarine channel formation in Rupert Inlet, British Columbia: 1, surge observations: Journal of Geophysical Research, v. 92, p. 2875-2881. https://doi.org/10.1029/JC092iC03p02875

HAY, A.E., 1987b, Turbidity currents and submarine channel formation in Rupert Inlet, British Columbia: 2, the roles of continuous and surge-type flow: Journal of Geophysical Research, v. 92, p. 2883-2900. https://doi.org/10.1029/JC092iC03p02883

HISCOTT, R.N., HALL, F.R., AND PIRMEZ, C., 1997, Turbidity-current overspill from the Amazon Channel; texture of the silt/sand load, paleoflow from anisotropy of magnetic susceptibility and implications for flow processes, in Flood, R.D., Piper, D.J.W., Klaus, A., and Peterson, L.C., eds., Proceedings of the Ocean Drilling Program; College Station, TX, v. 155, p. 53-78.

HODGSON, D.M., DI CELMA, C.N., BRUNT, R.L., AND FLINT, S.S., 2011, Submarine slope degradation and aggradation and the stratigraphic evolution of channel–levee systems: Geological Society of London Journal, v. 168, p. 625-628.

HUBBARD, S.M., COVAULT, J.A., FILDANI, A., AND ROMANS, B.W., 2014, Sediment transfer and deposition in slope channels: Deciphering the record of enigmatic deep-sea processes from outcrop: Geological Society of America, Bulletin, v. 126, p. 857-871.

HUBBARD, S.M., JOBE, Z.R., ROMANS, B.W., COVAULT, J.A., SYLVESTER, Z., AND FILDANI, A., 2020, The stratigraphic evolution of a submarine channel: linking seafloor dynamics to depositional products: Journal of Sedimentary Research, v. 90, p. 673-686. https://doi.org/10.2110/jsr.2020.36.

HÜBSCHER, C., SPIEB, V., BREITZKE, M., AND WEBER, M. E., 1997, The youngest channel-levee system of the Bengal Fan: results from digital sediment echosounder data: Marine Geology, v. 141, p. 125-145.

INGRAM, R.L., 1954, Terminology for the thickness of stratification and parting units in sedimentary rocks: Geological Society of America, Bulletin, v. 65, p. 937-938. https://doi.org/10.1130/0016-7606(1954)65[937:TFTTOS]2.0.CO;2

JOBE, Z.R., LOWE, D., AND MORRIS, W., 2012, Climbing-ripple successions in turbidite systems: depositional environments, sedimentation rates and accumulation times: Sedimentology, v. 59, p. 867–898. https://doi.org/10.1111/j.1365-3091.2011.01283.x

JOBE, Z., SYLVESTER, Z., PITTALUGA, M.B., FRASCATI, A., PIRMEZ, C., MINISINI, D., HOWES, N., AND CANTELLI, A., 2017, Facies architecture of submarine channel deposits on the western Niger Delta slope: Implications for grain-size and density stratification in turbidity currents: Journal of Geophysical Research, Earth Surface, v. 122, p. 473-491

KANE, I.A., AND HODGSON, D.M., 2011, Sedimentological criteria to differentiate submarine channel levee subenvironments: exhumed examples from the Rosario Fm. (Upper Cretaceous) of Baja California, Mexico, and the Fort Brown Fm. (Permian), Karoo basin,S. Africa: Marine and Petroleum Geology, v. 28, p. 807-823. https://doi.org/10.1016/j.marpetgeo.2010.05.009.

KANE, I.A., KNELLER, B.C., DYKSTRA, M., KASSEM, A., AND MCCAFFREY, W.D., 2007, Anatomy of a submarine channel-levee: an example from Upper Cretaceous slope sediments, Rosario Formation, Baja California, Mexico: Marine and Petroleum Geology, v. 24, p. 540-563. https://doi.org/10.1016/j.marpetgeo.2007.01.003.

KANE, I.A., MCCAFFREY, W.D., AND PEAKALL, J., 2010b, On the origin of paleocurrent complexity within deep marine channel levees: Journal of Sedimentary Research, v. 80, p. 54-66

KANE, I.A., MCCAFFREY, W.D., PEAKALL, J., AND KNELLER, B.C., 2010a, Submarine channel levee shape and sediment waves from physical experiments: Sedimentary Geology, v. 223, p. 75-85. https://doi.org/10.1016/j.sedgeo.2009.11.001.

KENDALL, B.S., CREASER, R.A., ROSS, G.M., AND SHELBY, D., 2004, Constraints on the timing of Marinoan snowball Earth glaciation by 187Re-187Os dating of a Neoproterozoic, post- glacial black shale in Western Canada: Earth and Planetary Science Letters, v. 222, p. 729-740. https://doi.org/10.1016/j.epsl.2004.04.004.

KHAN, Z., 2012, Origin and architecture of deep-water levee deposits: insight from the ancient rock record and experiments [Ph.D. Thesis]: University of Ottawa, 300 p.

KHAN, Z.A., AND ARNOTT, R.W.C., 2011, Stratal attributes and evolution of asymmetric inner- and outer-bend levee deposits associated with an ancient deep-water channel-levee complex within the Isaac Formation, southern Canada: Marine and Petroleum Geology, v. 28, p. 824-842. https://doi.org/10.1016/j.marpetgeo.2010.07.009.

KHAN, Z.A., ARNOTT, R.W.C., AND PUGIN, A., 2011, An alternative model of producing levee topography in the crest region of deep-water systems: American Association of Petroleum Geologists, Bulletin, v. 95, p. 2085-2106.

KING, P.R., BROWNE, G.H., SLATT, R.M., WEIMER, P., BOUMA, A.H., AND PERKINS, B., 1994, Sequence architecture of exposed late Miocene basin floor fan and channel-

levee complexes (Mount Messenger Formation), Taranaki Basin, New Zealand, in Weimer, P., Bouma, A.H., and Perkins, B.F. eds., Submarine Fans and Turbidite Systems: Sequence Stratigraphy, Reservoir Architecture and Production Characteristics: Gulf Coast Section SEPM 15th Annual Research Conference, p. 177–192.

KNELLER, B., NASR-AZADANI, M.M., RADHAKRISHNAN, S., AND MEIBURG, E., 2016, Long- range sediment transport in the world's oceans by stably stratified turbidity currents: Journal of Geophysical Research: Oceans, v. 121, p. 8608–8620. https://doi.org/10.1002/2016JC011978.

LIU, Q., KNELLER, B., FALLGATTER, C., VALDEZ BUSO, V., AND MILANA, J.P., 2018, Tabularity of individual turbidite beds controlled by flow efficiency and degree of confinement: Sedimentology, v. 65, p. 2368-2387.

LOWE, D.R., GRAHAM, S.A., MALKOWSKI, M.A., AND BHAGABAN, D., 2019, The role of avulsion and splay development in deep-water channel systems: Sedimentology, architecture, and evolution of the deep-water Pliocene Godavari “A” channel complex, India: Marine and Petroleum Geology, v. 105, p. 81-99.

LUND, K., ALEINIKOFF, J.N., EVANS, K.V., AND FANNING, C.M., 2003, SHRIMP U-Pb geochronology of Neoproterozoic Windermere Supergroup, central Idaho: implications for rifting of western Laurentia and synchroneity of Sturtian glacial deposits: Geological

Society of America, Bulletin, v. 115, p. 349-372. https://doi.org/10.1130/0016-7606(2003)115<0349:SUPGON>2.0.CO;2

MACAULEY, R.V., AND HUBBARD, S.M., 2013, Slope channel sedimentary processes and stratigraphic stacking, Cretaceous Tres Pasos Formation slope system, Chilean Patagonia: Marine and Petroleum Geology, v. 41, p. 146-162. https://doi.org/10.1016/j.marpetgeo.2012.02.004.

MALGESINI, G., TALLING, P.J., HOGG, A.J., ARMITAGE, D., GOATER, A., AND FELLETTI, F., 2015, Quantitative analysis of submarine-flow deposit shape in the Marnoso-Arenacea Formation: what is the signature of hindered settling from dense near-bed layers?: Journal of Sedimentary Research, v. 85, p. 170-191.

MANLEY, P.L., PIRMEZ, C., BUSCH, W., CRAMP, A., FLOOD, R.D., PIPER, D.J.W., KLAUS, A., AND PETERSON, L.C.,, 1997, Grain-size characterization of Amazon Fan deposits and comparison to seismic facies units: Proceedings Ocean Drilling Scientific Program Scientific Results, National Science Foundation, v. 155, p. 35-52.

MCDONOUGH, M.R., AND PARRISH, R.R., 1991, Proterozoic gneisses of the Malton Complex, near Valemount, British Columbia: U-Pb ages and Nd isotopic signatures: Canadian Journal of Earth Sciences, v. 28, p. 1202-1216. https://doi.org/10.1139/e91-108

MEYER, L., AND ROSS, G.M., 2007, Channelized lobe and sheet sandstones of the Upper Kaza Group basin-floor turbidite system, British Columbia, Canada, in Nilsen, T.H., Shew, R.D., and Studlick, J.R.J., (eds.), Atlas of Deep-water Outcrops: American Association of Petroleum Geologists, Studies in Geology 56, CD-ROM, 22 p.

MIGEON, S., SAVOYE, B., AND FAUGERES, J.C., 2000, Quaternary development of migrating sediment waves in the Var deep-sea fan: distribution, growth pattern, and implication for levee evolution: Sedimentary Geology, v. 133, p. 265-293.

MIGEON, S., SAVOYE, B., ZANELLA, E., MULDER, T., FAUGERES, J.C., AND WEBER, O., 2001, Detailed seismic-reflection and sedimentary study of turbidite sediment waves on the Var Sedimentary Ridge (SE France): significance for sediment transport and deposition and for the mechanisms of sediment-wave construction: Marine and Petroleum Geology, v. 18, p. 179-208.

MOSCA, F., AND STEFANO, D., 1993, Organic matter distribution in the flysch deposits of the Marnoso-Arenacea formation, Miocene, northern Appennines, Italy: American Association of Petroleum Geologists mid-continent section meeting, Amarillo, Texas, United States, 10-12 Oct 1993.

MORRIS, E.A., HODGSON, D.M., BRUNT, R.L., AND FLINT, S.S., 2014, Origin, evolution and anatomy of silt-prone submarine external levées: Sedimentology, v. 61, p. 1734-1763. https://doi.org/10.1111/sed.12114.

MULDER, T., AND ALEXANDER, J., 2001, The physical character of subaqueous sedimentary density flows and their deposits: Sedimentology, v. 48, p. 269-299. https://doi.org/10.1046/j.1365-3091.2001.00360.x.

MURPHY, D.C., 1987, Suprastructure/infrastructure transition, east-central Cariboo Mountains, British Columbia: geometry, kinematics and tectonic implications: Journal of Structural Geology, v. 9, p. 13-29. https://doi.org/10.1016/0191-8141(87)90040-X

MURPHY, D.C., AND REES, C.J., 1983, Structural transition and stratigraphy in the Cariboo Mountains, British Columbia: Geological Survey of Canada, Paper, 83–1A, p. 245–252.

MUTTI, E., 1977, Distinctive thin-bedded turbidite facies and related depositional environments in the Eocene Hecho Group (South-central Pyrenees, Spain): Sedimentology, v. 24, p. 107–131. https://doi.org/10.1111/j.1365-3091.1977.tb00122.x

MUTTI, E., AND NORMARK, W.R., 1987, Comparing examples of modern and ancient turbidite systems: problems and concepts, in Leggett, J.R. and Zuffa, G.G. eds., Marine Clastic Sedimentology: Concepts and Case Studies: London, Graham and Trotman, p. 1–37.

NAKAJIMA, T., AND KNELLER, B. C., 2013, Quantitative analysis of the geometry of submarine external levees: Sedimentology, v. 60(4), p. 877-910.

NAVARRO, L., KHAN, Z., AND ARNOTT, R.W.C., 2007, Depositional architecture and evolution of a deep-marine channel-levee complex: Isaac Formation, Southern Canadian Cordillera, in Nilsen, T.H., Shew, R.D., and Studlick, J.R.J., eds., Atlas of Deep-Water Outcrops: American Association of Petroleum Geologists, Studies in Geology 56, CD-ROM, 22 p.

NAVARRO, L., AND ARNOTT, R.W.C., 2020, Stratigraphic record in the transition from basin floor to continental slope sedimentation in the ancient passive-margin Windermere turbidite system: Sedimentology, v. 67, p. 1710-1749. https://doi.org/10.1111/sed.12676.

NORMARK, W.R., HESS, G.R., STOW, D.A.V., AND BOWEN, A.J., 1980, Sediment waves on the Monterey Fan level: Marine Geology, v. 37, p. 1-18.

NORMARK, W.R., POSAMENTIER, H., AND MUTTI, E., 1993, Turbidite systems: state of the art and future directions: Reviews of Geophysics, v. 31(2), p. 91-116.

PICKERING K.T., CLARK J.D., SMITH R.D.A., HISCOTT R.N., RICCI LUCCHI F., AND KENYON N.H., 1995, Architectural element analysis of turbidite systems, and selected topical problems for sand-prone deep-water systems, in Pickering, K.T., Hiscott, R.N., Kenyon, N.H., Ricci Lucchi, F., and Smith R.D.A., eds., Atlas of Deep Water Environments: Dordrecht, Springer, p. 1-10. https://doi.org/10.1007/978-94-011-1234-5_1

PIPER, D.J.W., AND DEPTUCK, M., 1997, Fine-grained turbidites of the Amazon Fan: facies characterization and interpretation, in Flood, R.D., Piper, D.J.W., Klaus, A., and Peterson, L.C., eds., Proceedings of the Ocean Drilling Program, College Station Scientific Results 155, p. 79–108.

PIPER, D.J.W., AND NORMARK, W.R., 1983, Turbidite depositional patterns and flow characteristics, Navy submarine fan, California Borderland: Sedimentology, v. 30, p. 681-694. https://doi.org/10.1111/j.1365-3091.1983.tb00702.x.

PIPER, D.J.W., AND NORMARK, W.R., 2001, Sandy fans: from Amazon to Hueneme and beyond: American Association of Petroleum Geologists, Bulletin, v. 85, p. 1407-1438.

PIRMEZ, C., AND IMRAN, J., 2003, Reconstruction of turbidity currents in Amazon Channel: Marine and Petroleum Geology, v. 20, p. 823-849. https://doi.org/10.1016/j.marpetgeo.2003.03.005.

POSAMENTIER, H.W., AND KOLLA, V., 2003, Seismic geomorphology and stratigraphy of depositional elements in deep-water settings: Journal of Sedimentary Research, v. 73, p. 367-388. https://doi.org/10.1306/111302730367.

PRÉLAT, A., HODGSON, D.M., AND FLINT, S.S., 2009, Evolution, architecture and hierarchy of distributary deep-water deposits: a high-resolution outcrop investigation from the Permian Karoo Basin, South Africa: Sedimentology, v. 56, p. 2132-2154.

PRÉLAT, A., COVAULT, J.A., HODGSON, D.M., FILDANI, A., AND FLINT, S.S., 2010, Intrinsic controls on the range of volumes, morphologies, and dimensions of submarine lobes: Sedimentary Geology, v. 232, p. 66-76.

PRIOR, D.B., ADAMS, C.E., AND COLEMAN, J.M., 1983, Characteristics of deep-sea channel of middle Mississippi Fan as revealed by a high-resolution survey: Gulf Coast Association of Geological Societies Transactions, v. 33, p. 389-394.

PYLES, D.R., JENNETTE, D.C., TOMASSO, M., BEAUBOUEF, R.T., AND ROSSEN, C., 2010, Concepts learned from a 3D outcrop of a sinuous slope channel complex: Beacon Channel Complex, Brushy Canyon Formation, West Texas, USA: Journal of Sedimentary Research, v. 80(1), p. 67-96.

REID, L.F., SIMONY, P.S., AND ROSS, G.M., 2002, Dextral strike-slip faulting in the Cariboo Mountains, British Columbia: a natural example of wrench tectonics in relation to Cordilleran tectonics: Canadian Journal of Earth Sciences, v. 39, p. 953-970. https://doi.org/10.1139/e02-017.

ROSS, G.M., 1991, Tectonic setting of the Windermere Supergroup revisited: Geology, v. 19, p. 1125-1128. https://doi.org/10.1130/00917613(1991)019<1125:TSOTWS>2.3.CO;2.

ROSS, G.M., AND ARNOTT, R.W.C., 2007, Regional geology of the Windermere Supergroup, southern Canadian Cordillera and stratigraphic setting of the Castle Creek study area, Canada, in Nilsen, T.H., Shew, R.D., and Studlick, J.R.J., eds., Atlas of Deep-Water Outcrops: American Association of Petroleum Geologists, Studies in Geology 56, CD-ROM, 22 p.

ROSS, G.M., BLOCH, J.D., AND KROUSE, H.R., 1995, Neoproterozoic strata of the southern Canadian Cordillera and the isotopic evolution of seawater sulfate: Precambrian Research, v. 73, p. 71–99. https://doi.org/10.1016/0301-9268(94)00072-Y.

SCHWENK, T., SPIEß, V., HÜBSCHER, C., AND BREITZKE, M., 2003, Frequent channel avulsions within the active channel–levee system of the middle Bengal Fan—an exceptional channel–levee development derived from Parasound and Hydrosweep data: Deep Sea Research Part II: Topical Studies in Oceanography, v. 50(5), p. 1023-1045.

SCHWENK, T., SPIEß, V., BREITZKE, M., AND HÜBSCHER, C., 2005, The architecture and evolution of the Middle Bengal Fan in vicinity of the active channel–levee system imaged by high-resolution seismic data: Marine and Petroleum Geology, v. 22(5), p. 637-656.

SEQUEIROS, O.E., SPINEWINE, B., BEAUBOUEF, R.T., SUN, T., GARCÍA, M.H., AND PARKER, G., 2010, Characteristics of velocity and excess density profiles of saline underflows and turbidity currents flowing over a mobile bed: Journal of Hydraulic Engineering, v. 136, p. 412-433. https://doi.org/10.1061/(ASCE)HY.1943-7900.0000200.

SKENE, K.I., PIPER, D.J., AND HILL, P.S., 2002, Quantitative analysis of variations in depositional sequence thickness from submarine channel levees: Sedimentology, v. 49, p. 1411-1430. https://doi.org/10.1046/j.1365-3091.2002.00506.x.

SPRAGUE, A.R.G., GARFIELD, T.R., GOULDING, F.J., BEAUBOUEF, R.T., SULLIVAN, M.D., ROSSEN, C., CAMPION, K.M., SICKAFOOSE, D.K., ABREU, V., SCHELLPEPER, M. E., JENSEN, G.N., JENNETTE, D.C., PIRMEZ, C., DIXON, B.T., YING, D., ARDILL, J., MOHRIG, D.C., PORTER, M.L., FARRELL, M.E., AND MELLERE, D., 2005, Integrated slope channel depositional models: the key to successful prediction of reservoir presence and quality in offshore west Africa: Colegio de Ingenenieros Petroleros de México, p. 1-13

STRAUB, K.M., AND MOHRIG, D., 2008, Quantifying the morphology and growth of levees in aggrading submarine channels: Journal of Geophysical Research: Earth Surface, v. 113(F3).

STRAUB, K.M., MOHRIG, D., AND PIRMEZ, C., 2012, Architecture of an aggradational tributary submarine channel network on the continental slope offshore Brunei

Darussalam, in Prather, B.E., Deptuck, M.E., Mohrig, D., Van Hoorn, B., and Wynn, R.B., eds., Application of the Principles of Seismic Geomorphology to Continental-Slope and Base-of-Slope Systems: Case Studies from Seafloor and Near-Seafloor Analogues: SEPM (Society for Sedimentary Geology), Special Publication 99, p. 13-30.

SULLIVAN, M.D., FOREMAN, J.L., JENNETTE, D.C., STERN, D., JENSEN, G.N., AND GOULDING, F.J., 2004, An integrated approach to characterization and modeling of deep-water reservoirs, Diana Field, western Gulf of Mexico, in Grammar, G.M, Harris, P.M., and Eberli, G.P., eds, Integration of Outcrop and Modern Analogs in Reservoir Modeling: American Association of Petroleum Geologists, Memoir 80, pp. 215-234.

SYLVESTER, Z., PIRMEZ, C., AND CANTELLI, A., 2011, A model of submarine channel-levee evolution based on channel trajectories: implications for stratigraphic architecture: Marine and Petroleum Geology, v. 28, p. 716-727. https://doi.org/10.1016/j.marpetgeo.2010.05.012.

TALLING, P.J., AMY, L.A., AND WYNN, R.B., 2007, New insights into the evolution of large volume turbidity currents: comparison of turbidite shape and previous modeling results: Sedimentology, v. 54, p. 737-769.

TERLAKY, V., AND ARNOTT, R.W.C., 2014, Matrix-rich and associated matrix-poor sandstones: avulsion splays in slope and basin-floor strata: Sedimentology, v. 61, p. 1175-1197.

TERLAKY, V., AND ARNOTT, R.W.C., 2016, The control of terminal-splay sedimentation on depositional patterns and stratigraphic evolution in avulsion-dominated, unconfined, deep-marine basin-floor systems: Journal of Sedimentary Research, v. 86, p. 786-799.

TERLAKY, V., ROCHELEAU, J., AND ARNOTT, R.W.C., 2016, Stratal composition and stratigraphic organization of stratal elements in an ancient deep-marine basin-floor succession, Neoproterozoic Windermere Supergroup, British Columbia, Canada: Sedimentology, v. 63, p. 136-175. https://doi.org/10.1111/sed.12222.

TILSTON, M., 2017, The role of particle size and concentration in defining the flow structure of turbidity currents and the morphology of their deposits: insights from computed tomography [Ph.D. Thesis]: University of Ottawa, Ottawa, 148 p.

TILSTON, M., ARNOTT, R.W.C., RENNIE, C.D., AND LONG, B., 2015, The influence of grain size on the velocity and sediment concentration profiles and depositional record of turbidity currents: Geology, v. 43, p. 839-842. https://doi.org/10.1130/G37069.1.

VON RAD, U., AND TAHIR, M., 1997, Late Quaternary sedimentation on the outer Indus shelf and slope (Pakistan): evidence from high-resolution seismic data and coring: Marine Geology, v. 138, p. 193-236.

WALKER, R.G., 1985, Mudstones and thin-bedded turbidites associated with the Upper Cretaceous Wheeler Gorge conglomerates, California; a possible channel-levee Complex: Journal of Sedimentary Petrology, v. 55, p. 279–290. https://doi.org/10.1306/212F869D-2B24-11D7-8648000102C1865D.

WEBER, M. E., WIEDICKE-HOMBACH, M., KUDRASS, H. R., AND ERLENKEUSER, H., 2003, Bengal Fan sediment transport activity and response to climate forcing inferred from sediment physical properties: Sedimentary Geology, v. 155, p. 361-381.

WEIMER, P., SLATT, R.M., DROMGOOLE, P., BOWMAN, M., AND LEONARD, A., 2000, Developing and managing turbidite reservoirs: case histories and experiences: results of the 1998EAGE/AAPG Research Conference: American Association of Petroleum Geologists, Bulletin, v. 84, p. 453-465.

WENTWORTH, C.K., 1922, A scale of grade and class terms for clastic sediments: The Journal of Geology, v. 30, p. 377-392. https://doi.org/10.1086/622910

WYNN, R.B., CRONIN, B.T., AND PEAKALL, J., 2007, Sinuous deep-water channels: genesis, geometry and architecture: Marine and Petroleum Geology, v. 24, p. 341–387. https://doi.org/10.1016/j.marpetgeo.2007.06.001.

Chapter 7: Conclusions

7.1 Overview

Deep-marine levees are geologically significant components of deep-marine turbidite fan systems, but due to their typically fine-grained nature and generally poor exposure in outcrop, to date levee deposits have received considerably less research attention than their coeval channel fills. However, levee deposits of the Neoproterozoic Windermere Supergroup are superbly exposed at the Castle Creek study site in the Cariboo Mountains of east-central British Columbia, allowing for detailed physical and chemical analyses to be performed. In this thesis, standard field techniques such as bed-by-bed stratigraphic logging and correlation were combined with geochemical techniques, including stable carbon isotope analysis, total organic carbon, and X-ray fluorescence, as well as optical and electron microscopy, to examine the physical sedimentology, stratigraphic stacking patterns and stratal architecture, and organic carbon content of ancient levee deposits. The key findings of each chapter are summarized next.

7.2 Summary of Key Findings

7.2.1 Chapter 3

1. Levee deposits at Castle Creek consist mainly of thin-bedded, upper-division turbidites that stack to form sharply bounded bedsets. Beds within each bedset are self-similar in that there is little variation in grain size, bed thickness, T_c and $T_{d/e}$ division thickness, number of sets of ripple cross-lamination per bed, and ripple height, width, and spacing.

2. Bedsets typically comprise 2-10 beds and are interpreted to represent deposition from a single channelized flow event, rather than each bed from separate flow events.
3. Flows that deposit these bedsets are interpreted to be anomalously large, pulsing flows that occur once every several hundred years.

7.2.2 Chapter 4

1. Organic matter (OM) at the Castle Creek study site occurs primarily as micro- to nanometer-thick coatings on clay grains, and principally in clay-rich sandstone rather than mudstone.
2. During deposition abundant OM affects the physical properties and flow mechanics of turbidity currents, forming distinctly banded sandstone beds that differ from typical levee strata in terms of thickness, texture, and sedimentary structures.
3. Post-depositional thermal and microbial degradation of OM results in a distinct diagenetic mineral assemblage of framboidal pyrite, collophane, authigenic chlorite, ferroan dolomite, and siderite.
4. High rates of sedimentation and protection of OM by association with clay mineral surfaces combine to reduce the destruction of OM by oxidation and/or respiration and efficiently sequester significant amounts of carbon in levee deposits.

7.2.3 Chapter 5

1. High sea level, intense continental weathering, and high terrigenous input are all factors that may serve to increase primary productivity on the shallow shelf. However, in order

to have significant carbon enrichment in deep-marine settings, all these factors must coincide in a “perfect storm” that creates ideal conditions for organic matter accumulation and preservation.

2. Because sea level, terrigenous input, and weathering are all strongly influenced by climate, OM enrichment in the deep marine may be considered primarily climate driven.
3. During periods of high productivity on the shelf, OM is primarily transported to the deep marine by anomalously large, surge-like turbidity currents that are thicker than the height of the levee crest and thus continuously overspill onto the levee. The rapid accumulation of OM on the shelf during periods of high primary productivity may be partially responsible for periodically triggering these large flows.

7.2.4 Chapter 6

1. Proximal levee deposits at Castle Creek are subdivided into upper and lower packages. Lower packages consist mainly of medium- to coarse-grained, thick-bedded, lower division turbidites, and upper packages consist mainly of fine-grained, thin-bedded upper division turbidites.
2. Each levee unit (comprising an upper and lower package) is interpreted to be associated with one phase of channel formation and fill, and forms due to cyclic changes in the density structure of channelized flows.
3. The density structure of turbidity currents is controlled by the granulometric makeup of the sediment it contains – cyclic changes in the sediment composition being supplied to the deep sea, therefore, control the density structure of the flows, which in turn control the stratal architecture of the levees.

7.3 Synthesis

Collectively, the data presented in each chapter of this thesis provide significant insight into both the physical and geochemical attributes of levee systems and their formative processes. Results demonstrate that the character of channellized turbidity currents is controlled primarily by their composition, both in terms of granulometric makeup and organic matter content, and that any changes in their character are reflected in the sedimentology and stratal architecture of levee deposits.

During levee inception and early growth, channellized flows are generally moderately well-sorted and sufficiently thick to continuously overspill the channel margin and deposit medium- to thick-bedded, coarse-grained turbidites on the levee (lower packages). However, the majority of levee deposits, especially during the latter part of levee growth, consist of thin-bedded, fine-grained turbidites that stack to form bedsets of self-similar beds. These bedsets were deposited by large, pulsing flows whose sand-rich lower parts remained mostly confined to the channel, except when pulses temporarily increased flow thickness and enabled sand to overspill the levee crest. However, these flows are uncommon with a recurrence interval of every several hundred years, whereas smaller flows, which occur throughout levee development and maybe as frequent as several times a year, remain completely confined within the channel and contribute negligibly to levee growth. Additionally, anomalously large flows that continuously overspill onto the levee may occur more frequently during periods of significantly increased primary productivity on the shelf. Under these conditions, outsized flows transport a significant volume of organic matter from the shelf to the deep marine, where it can then be efficiently sequestered on geologic timescales. The OM in these flows also changes the physical properties

of the flow and deposits characteristically banded, mud-rich turbidites that are distinctly different from typical levee strata.

Such periods of extreme primary productivity are rare in the stratigraphic record (only one interval was observed in this study) and suggests the rare temporal coincidence of multiple paleoenvironmental conditions for ideal organic carbon production, accumulation, and preservation.

This work makes several important contributions to the literature. First, the data presented here challenge the widely accepted notion that each bed equates to one flow in levee deposit and prompts a re-evaluation of some common assumptions regarding the frequency, sedimentation patterns, and preservation potential of individual events in the deep-marine sedimentary record. This study also takes advantage of the exceptional outcrop exposure at Castle Creek to document mm- to km-scale details of levee deposits and link their internal stratigraphy with their depositional processes and larger-scale changes in relative sea level and sediment supply.

Next, this thesis describes organic-rich rock types that to the author's knowledge have not been previously described in the literature and elucidates the fundamental physical and chemical processes that control OM deposition, accumulation, and preservation in deep-marine levees and discusses the wider implications of this for organic carbon burial throughout geologic time. Geochemical attributes and trends of levee strata are also examined in a level of detail that has not previously been done. The data expand our understanding of the external paleoenvironmental factors affecting carbon enrichment and the complex interplay between them, and may serve as a

model for studies elsewhere where the same level of outcrop and geochemical data may not be available.

7.4 Recommendations for Future Research

This work provides an in-depth physical and geochemical analysis of ancient levee deposits at the Castle Creek study site. However, the Windermere Supergroup is not representative of all deep-marine turbidite systems, and as such future work could examine systems of differing ages or tectonic settings in order to compare them to this system. This could include:

- are bedsets of self-similar beds observed in other systems;
- what controls the repetitive changes in sediment supply that form the two-part proximal levee packages described here, and are similar patterns observed elsewhere;
- study how organic carbon flux and characteristics of deposition in the deep sea has changed through geologic time; especially following the advent of terrestrial OM;
- examine whether the same suite of paleoenvironmental factors that control primary productivity in this study affect other systems similarly, and whether this also changed with the evolution of land plants and terrestrial OM input.

Further work could also be conducted at the Castle Creek study site on the levee deposits associated with Isaac Channel Complexes 5 and above. Similar physical and chemical analyses could be conducted to study the evolution of the slope system through time, and to compare and contrast depositional and paleoenvironmental patterns with the levee deposits of Isaac Channel Complexes 3 and 4.